

# Table of Contents

<i>Abstract</i> .....	<i>i</i>
<i>Acknowledgement</i> .....	<i>iii</i>
<i>Table of Contents</i> .....	<i>v</i>
<i>Nomenclature</i> .....	<i>ix</i>
<i>List of Figures</i> .....	<i>xix</i>
<i>List of Tables</i> .....	<i>xxvii</i>
<b>Chapter 1: Introduction</b> .....	<b>- 1 -</b>
<b>1.1 Background</b> .....	<b>- 1 -</b>
<b>1.2 Introduction to IPT Systems</b> .....	<b>- 5 -</b>
1.2.1 Basic Structure and Operating Principle.....	- 5 -
1.2.2 General Features .....	- 6 -
1.2.3 Related Applications.....	- 7 -
<b>1.3 Present Challenges in Power Flow Control of IPT Systems</b> .....	<b>- 11 -</b>
<b>1.4 Objectives and Scope of the Thesis</b> .....	<b>- 14 -</b>
<b>Chapter 2: Overview of Power Flow Control Techniques in IPT Systems</b> .....	<b>- 15 -</b>
<b>2.1 Introduction</b> .....	<b>- 15 -</b>
<b>2.2 Fundamentals of IPT Systems</b> .....	<b>- 16 -</b>
2.2.1 Primary Track Power Supply .....	- 16 -
2.2.2 Secondary Power Pickups .....	- 21 -
<b>2.3 Control of Primary Track Current</b> .....	<b>- 31 -</b>
2.3.1 Magnitude Control of Track Current .....	- 33 -
2.3.2 Operating Frequency Control of Track Current.....	- 35 -
<b>2.4 Existing Power Flow Control Methods of Secondary Power Pickup</b> .....	<b>- 38 -</b>
2.4.1 Voltage Regulator .....	- 38 -
2.4.2 Shorting-Control .....	- 39 -
2.4.3 Dynamic Tuning/Detuning Control .....	- 44 -
<b>2.5 Summary</b> .....	<b>- 49 -</b>
<b>Chapter 3: Directional Tuning/Detuning Control Algorithm (DTDCA)</b> .....	<b>- 51 -</b>
<b>3.1 Introduction</b> .....	<b>- 51 -</b>
<b>3.2 Basic Concept and Control Law of Directional Tuning/Detuning Control</b> <b>Algorithm (DTDCA)</b> .....	<b>- 51 -</b>

<b>3.3</b>	<b>Sampling Frequency and Tuning Step-Size of DTDCA.....</b>	<b>- 61 -</b>
<b>3.4</b>	<b>Standard Procedure of DTDCA.....</b>	<b>- 65 -</b>
<b>3.5</b>	<b>Summary .....</b>	<b>- 68 -</b>
	<b><i>Chapter 4: DTDCA Control of LCL Power Pickup.....</i></b>	<b><i>- 69 -</i></b>
<b>4.1</b>	<b>Introduction .....</b>	<b>- 69 -</b>
<b>4.2</b>	<b>LCL Tuning Power Pickup.....</b>	<b>- 69 -</b>
4.2.1	Basic Structure of LCL Tuning Pickup.....	- 69 -
4.2.2	Characteristics of LCL Tuning Circuit in Steady State .....	- 72 -
4.2.3	Controllable Power Transfer Capacity.....	- 74 -
<b>4.3</b>	<b>Effects of LCL Circuit Parameter Variations on Pickup Output Voltage.....</b>	<b>- 82 -</b>
4.3.1	Operating Frequency Variation.....	- 82 -
4.3.2	Magnetic Coupling Variation .....	- 87 -
4.3.3	Tuning Capacitance Variation .....	- 90 -
4.3.4	Load Variation .....	- 94 -
4.3.5	Choice of $k_{VR}$ and $r_k$ .....	- 97 -
4.3.6	Operating Range of Variable $L_{S2}$ .....	- 100 -
<b>4.4</b>	<b>Implementation of DTDCA Controlled LCL Power Pickup .....</b>	<b>- 102 -</b>
4.4.1	Linear-Mode Saturable Inductor .....	- 102 -
4.4.2	General Structure of Linear-Mode Saturable Inductor Controlled LCL Power Pickup.....	- 105 -
4.4.3	Sampling Frequency for LCL Power Pickup .....	- 106 -
4.4.4	Tuning Step-Size for LCL Power Pickup .....	- 109 -
<b>4.5</b>	<b>Simulation/Experimental Results and Discussion .....</b>	<b>- 110 -</b>
4.5.1	Simulation Study of DTDCA Controlled LCL Power Pickup .....	- 110 -
4.5.2	Experimental Study of DTDCA Controlled LCL Power Pickup .....	- 115 -
4.5.3	Discussion.....	- 120 -
<b>4.6</b>	<b>Summary .....</b>	<b>- 125 -</b>
	<b><i>Chapter 5: Fuzzy Logic DTDCA Control of LCL Power Pickup .....</i></b>	<b><i>- 127 -</i></b>
<b>5.1</b>	<b>Introduction .....</b>	<b>- 127 -</b>
<b>5.2</b>	<b>Fuzzy Logic Controller Design for Tuning Step-Size Automation .....</b>	<b>- 129 -</b>
5.2.1	Fuzzification of Output Voltage Error and Rate of Error .....	- 129 -
5.2.2	Control Rule Base.....	- 132 -
5.2.3	Defuzzification of Output Fuzzy Sets.....	- 134 -
5.2.4	Analytical Structure of Fuzzy Logic Controller.....	- 135 -
5.2.5	Choice of Scaling Factors .....	- 141 -
5.2.6	Standard Procedure of Fuzzy Logic Based (FLB) DTDCA .....	- 144 -
<b>5.3</b>	<b>Simulation and Experimental Results .....</b>	<b>- 146 -</b>

5.3.1	Simulation Study of FLB-DTDCA Controlled LCL Power Pickup .....	- 146 -
5.3.2	Experimental Study of FLB-DTDCA Controlled LCL Power Pickup .....	- 152 -
<b>5.4</b>	<b>Summary .....</b>	<b>- 155 -</b>
<b>Chapter 6: Fuzzy Logic DTDCA Control of Parallel LC Power Pickup .....</b>		<b>- 157 -</b>
<b>6.1</b>	<b>Introduction .....</b>	<b>- 157 -</b>
<b>6.2</b>	<b>Fundamentals of Parallel LC Power Pickup .....</b>	<b>- 158 -</b>
6.2.1	Steady State Characteristics of LC Tuning Circuit .....	- 158 -
6.2.2	Controllable Power Transfer Capacity of Parallel LC Power Pickup .....	- 159 -
<b>6.3</b>	<b>Effects of LC Circuit Parameter Variations on Pickup Output Voltage .....</b>	<b>- 162 -</b>
6.3.1	Operating Frequency Variation.....	- 163 -
6.3.2	Magnetic Coupling Variation.....	- 166 -
6.3.3	Load Variation .....	- 168 -
6.3.4	Choice of $Q_{S_p}$ and $r_k$ .....	- 170 -
6.3.5	Operating Range of Variable $C_s$ .....	- 172 -
6.3.6	Comparison of Output Voltage Variation to Parameters Variation between LC and LCL Tuning Circuits.....	- 173 -
<b>6.4</b>	<b>Implementation of FLB-DTDCA Controlled LC Power Pickup .....</b>	<b>- 176 -</b>
6.4.1	Structure of Switch-Mode Variable Capacitor Controlled LC Power Pickup.....	- 176 -
6.4.2	Selection of $C_{S1}$ and $C_{S2}$ .....	- 177 -
6.4.3	Equivalent Capacitance of $C_{S2}$ .....	- 178 -
6.4.4	Switching Signals for $Q_1$ and $Q_2$ .....	- 180 -
6.4.5	Guideline for Selecting Sampling Frequency of LC Power Pickup .....	- 183 -
<b>6.5</b>	<b>Simulation and Experimental Results .....</b>	<b>- 187 -</b>
6.5.1	Simulation Study of FLB-DTDCA Controlled LC Power Pickup.....	- 187 -
6.5.2	Experimental Study of FLB-DTDCA Controlled LC Power Pickup .....	- 191 -
<b>6.6</b>	<b>Summary .....</b>	<b>- 195 -</b>
<b>Chapter 7: Conclusions and Suggestions for Future Work .....</b>		<b>- 197 -</b>
<b>7.1</b>	<b>General Conclusions .....</b>	<b>- 197 -</b>
<b>7.2</b>	<b>Contributions of This Thesis Work .....</b>	<b>- 202 -</b>
<b>7.3</b>	<b>Suggestions for Future Work .....</b>	<b>- 203 -</b>
<b>References.....</b>		<b>- 205 -</b>
<b>Bibliographies .....</b>		<b>- 217 -</b>
<b>Appendices.....</b>		<b>- 225 -</b>

**Embedded Matlab Functions of SSSA-DTDC and FLB-DTDC Simulations ..... - 225 -**

# Nomenclature

## Acronym

ADC	-	Analog-to-digital converter
AUV	-	Autonomous undersea vehicle
ac	-	Alternating current
BEV	-	Battery electric vehicles
CPT	-	Capacitive power transfer
CSC	-	Control signal conversion
DAC	-	Digital-to-analog converter
DTDCA	-	Directional tuning/detuning control algorithm
dc	-	Direct current
EHF	-	Extremely high frequency
ELF	-	Extremely low frequency
EMI	-	Electromagnetic interference
ESR	-	Equivalent series resistance
emf	-	Electromotive force
FCEV	-	Fuel cell electric vehicles
FLB	-	Fuzzy logic based
FLC	-	Fuzzy logic controller
G1	-	Generation one (current-fed parallel resonant) IPT power supply
G2	-	Generation two (voltage-fed series resonant) IPT power supply
G3	-	Generation three (voltage-fed or current-fed) IPT power supply
HB	-	Hysteresis band
HEV	-	Hybrid electric vehicles
IC	-	Input combination
IPT	-	Inductive power transfer
ISP	-	Internet service provider
LC	-	Inductor-capacitor connection

LCL	-	Inductor-capacitor-inductor connection
LF	-	Low frequency
MF	-	Medium frequency
MMOV	-	Minimum of maximum output voltages
MOSFET	-	Metal oxide silicon field effect transistor
PD	-	Proportional and derivative
PI	-	Proportional and integral
PLECS	-	Piecewise linear electrical circuit simulation
PWM	-	Pulse-width modulation
PZT	-	Lead zirconate titanate
Q	-	Quality factor
RF	-	Radio frequency
SSSA	-	Simple step-size adjustment
TC	-	Tuning curve
TET	-	Transcutaneous energy transmission
T.L/C	-	Tuning inductance or capacitance
ZCD	-	Zero current detection
ZCS	-	Zero current switching
ZVD	-	Zero voltage detection
ZVS	-	Zero voltage switching
2-D	-	Two dimensional
3-D	-	Three dimensional

### **Symbols**

$B_C$	-	Controllable boosting coefficient of LC tuning circuit using variable $C_S$
$B_{C_C}$	-	Controllable boosting coefficient of LCL tuning circuit using variable $C_{S2}$
$B_{C_L}$	-	Controllable boosting coefficient of LCL tuning circuit using variable $L_{S2}$
$C$	-	Capacitor (Farads)
$C_{DC}$	-	DC capacitance (Farads)
$C_{eq}$	-	Equivalent capacitance (Farads)

$C_S$	-	Tuning capacitance of LC power pickup (Farads)
$C_{ST}$	-	Tuning capacitance of LCL power pickup (Farads)
$C_{S1}$	-	Tuning capacitance of LCL power pickup that used to tune to $L_{S1}$ (Farads)
$C_{S2}$	-	Tuning capacitance of LCL power pickup that used to tune to $L_{S2}$ (Farads)
$C_{S\_f}$	-	Fixed tuning capacitance of secondary pickup (Farads)
$C_{S\_v}$	-	Variable or actual tuning capacitance of secondary pickup (Farads)
$C_{S2\_v}$	-	Variable or actual operating Capacitance of $C_{S2}$ (Farads)
$C_{S2\_r\_w_0}$	-	Capacitance of $C_{S2}$ under fully-tuned condition with a resonant frequency equals to $\omega_0$ (Farads)
$C_{ST\_O}$	-	Nominal capacitance of $C_{ST}$ having $C_{S1}$ and $C_{S2}$ selected according to $k_{VR}$ (Farads)
$C_{pi}$	-	Capacitance of $\pi$ network (Farads)
$C_T$	-	Capacitance of T network (Farads)
$C_t$	-	Track tuning capacitance (Farads)
$C_{t\_f}$	-	Fixed track tuning capacitance (Farads)
$C_{t\_v}$	-	Variable track tuning capacitance (Farads)
$D$	-	Duty cycle
$D_{DC}$	-	DC diode
$D_S$	-	Duty cycle of shorting-control switch
$e$	-	Pickup output voltage error
$f$	-	Actual operating frequency (Hz)
$f_d$	-	Drifted resonant tank frequency (Hz)
$f_s$	-	Sampling frequency of controller (Hz)
$f_0$	-	Nominal operating frequency (Hz)
$GE$	-	Scaling factor of error
$GR$	-	Scaling factor of rate of error
$GU$	-	Scaling factor of FLC output
$g_P$	-	Gradient of LCL pickup output power
$g_{P\_L}$	-	Gradient of LCL pickup output power using variable $L_{S2}$

$g_{P\_C}$	-	Gradient of LCL pickup output power using variable $C_{S2}$
$g_V$	-	Gradient of LCL pickup output voltage
$H_I$	-	Current transfer function of power pickup
$H_V$	-	Voltage transfer function of power pickup
$\Delta H$	-	Step-size of controller output signal adjustment
$\Delta h$	-	Step-size of T.L/C (Henrys or Farads)
$I$	-	Current magnitude (Amperes)
$I_{AC}$	-	AC current (Amperes)
$I_{AC\_R}$	-	AC output current of pickup under fully-tuned condition (Amperes)
$I_b$	-	Break-even current (Amperes)
$I_{CS}$	-	Current flowing through $C_S$ (Amperes)
$I_{Ctrl}$	-	DC control current (Amperes)
$I_{C_{DC}}$	-	Current flowing through $C_{DC}$ (Amperes)
$I_L$	-	DC load current of pickup (Amperes)
$I_{L_{DC}}$	-	Current flowing through $L_{DC}$ (Amperes)
$I_P$	-	Primary track current (Amperes)
$I_{PR}$	-	Output current of parallel-tuned pickup (Amperes)
$I_{rect}$	-	Rectified current (Amperes)
$I_S$	-	Secondary pickup current (Amperes)
$I_{SC}$	-	Short-circuit current of pickup coil (Amperes)
$I_{SR}$	-	Output current of series-tuned pickup (Amperes)
$I_{ST}$	-	Current flowing through $C_{ST}$ (Amperes)
$j$	-	Complex operator ( $\sqrt{-1}$ )
$k$	-	Magnetic coupling coefficient
$k_f$	-	Magnetic coupling factor
$k_{IR}$	-	Current boosting factor of pickup under fully-tuned condition
$k_{SV}$	-	Actual required voltage boosting factor of pickup
$k_V$	-	Magnitude of operational voltage boosting factor of LCL pickup
$k_{VR}$	-	Voltage boosting factor of pickup under fully-tuned



	-	condition
$k_{V\_ref}$	-	Operational voltage boosting factor of LCL pickup for achieving $V_{ref}$
$L$	-	Inductor (Henrys)
$L_{AC}$	-	AC inductance (Henrys)
$L_{DC}$	-	DC inductance (Henrys)
$L_{pi}$	-	Inductance of $\pi$ network (Henrys)
$L_S$	-	Self-inductance of secondary pickup coil (Henrys)
$L_{sp}$	-	Self-inductance of splitting transformer (Henrys)
$L_{S1}$	-	Self-inductance of LCL pickup coil (Henrys)
$L_{S2}$	-	Variable tuning inductance of LCL pickup (Henrys)
$L_{S2\_r\_w_0}$	-	Inductance of $L_{S2}$ under fully-tuned condition with a resonant frequency equals to $\omega_0$ (Henrys)
$L_{S2\_startup}$	-	Startup tuning inductance of LCL pickup (Henrys)
$L_{S2\_v}$	-	Variable or actual operating inductance of $L_{S2}$ (Henrys)
$L_T$	-	Inductance of T network (Henrys)
$L_t$	-	Self-inductance of primary current track (Henrys)
$M$	-	Mutual inductance (Henrys)
$N$	-	Number of turns
$n_s$	-	Turns ratio (secondary/primary)
$P$	-	Power (Watts)
$P_{AC}$	-	AC output power of pickup (Watts)
$P_{ACmax\_C}$	-	Maximum AC output power of LCL pickup using variable $C_{S2}$ (Watts)
$P_{ACmax\_L}$	-	Maximum AC output power of LCL pickup using variable $L_{S2}$ (Watts)
$P_{AC\_R}$	-	AC output power of pickup under fully-tuned condition (Watts)
$P_L$	-	DC output power of pickup (Watts)
$P_{max(m)}$	-	Maximum output power of secondary pickup (Watts)
$P_{m\_p}$	-	Maximum output power of parallel-tuned pickup (Watts)
$P_{m\_s}$	-	Maximum output power of series-tuned pickup (Watts)

$P_{ref}$	-	Reference power (Watts)
$Q_p$	-	Quality factor of primary resonant converter
$Q_s$	-	Quality factor of secondary power pickup
$Q_{S_p}$	-	Quality factor of secondary parallel-tuned power pickup
$Q_{S_s}$	-	Quality factor of secondary series-tuned power pickup
$R$	-	Resistance (Ohms)
$R_{AC}$	-	AC equivalent load resistance (Ohms)
$R_{AC_O}$	-	Nominal AC equivalent load resistance (Ohms)
$R_L$	-	DC load resistance (Ohms)
$r$	-	Rate of error
$r_{adj}$	-	Ratio between $L_{S2_v}$ and $L_{S2_r,\omega_0}$ or $C_{S2_v}$ and $C_{S2_r,\omega_0}$
$r_{adj_{cv}}$	-	Required adjusting ratio of $L_{S2}$ for LCL pickup to achieve $V_{ref}$ under tuning capacitor variation
$r_{adj_{cvr}}$	-	Required adjusting ratio of $L_{S2}$ for LCL pickup to fully tune to drifted center frequency of pickup
$r_{adj_{fv}}$	-	Required adjusting ratio of $L_{S2}$ for LCL pickup to achieve $V_{ref}$ under operating frequency variation
$r_{adj_{fvr}}$	-	Required adjusting ratio of $L_{S2}$ for LCL pickup to fully tune to drifted operating frequency
$r_{adj_{ocv}}$	-	Required adjusting ratio of $L_{S2}$ for LCL pickup to achieve $V_{ref}$ under open-circuit voltage variation
$r_{adj_{pvr}}$	-	Required adjusting ratio of $L_{S2}$ for LCL pickup to achieve $V_{ref}$ under integrated effect of considered parameters variation
$r_{adj_{rv}}$	-	Required adjusting ratio of $L_{S2}$ for LCL pickup to achieve $V_{ref}$ under load variation
$r_k$	-	Ratio between $k_{V_{ref}}$ and $k_{VR}$ (or $Q_{S_p}$ ) or $V_{ref}$ and $V_{AC_R}$
$r_{k\_startup}$	-	Ratio between startup voltage and $V_{AC_R}$
$r_{Pmax\_CL}$	-	Ratio between $P_{ACmax_C}$ and $P_{ACmax_L}$
$S_n$	-	Logic signal ( $n = 1, \dots, 7$ )
$T$	-	Time constant (seconds)
$t_n$	-	Sampling time instance (seconds)

$t_s$	-	Circuit settling time (seconds)
$U$	-	Output signal of controller
$\Delta u$	-	Crisp output of FLC
$V$	-	Voltage magnitude (Volts)
$V_{AC}$	-	AC voltage (Volts)
$V_{AC\_cvr\_max}$	-	Maximum output voltage under tuning capacitor variation (Volts)
$V_{AC\_fvr\_max}$	-	Maximum output voltage under operating frequency variation (Volts)
$V_{AC\_ocvr\_max}$	-	Maximum output voltage under open-circuit voltage variation (Volts)
$V_{AC\_R}$	-	AC output voltage of pickup under fully-tuned condition (Volts)
$V_{AC\_rvr\_max}$	-	Maximum output voltage under load variation (Volts)
$V_{Ctrl}$	-	Voltage control signal (Volts)
$V_{DC}$	-	DC voltage (Volts)
$V_F$	-	Forward voltage of diode (Volts)
$V_{GS}$	-	Gate driving voltage of semiconductor device (Volts)
$V_{Hyst-}$	-	Lower bound of hysteresis band (Volts)
$V_{Hyst+}$	-	Upper bound of hysteresis band (Volts)
$V_{IN}$	-	Input voltage (Volts)
$V_L$	-	DC load voltage of pickup (Volts)
$V_{L\_hb}$	-	DC load voltage of pickup having half-bridge rectification (Volts)
$V_{L\_fb}$	-	DC load voltage of pickup having full-bridge rectification (Volts)
$V_{OC}$	-	Open-circuit voltage of pickup coil (Volts)
$V_{OC\_O}$	-	Nominal open-circuit voltage of pickup coil (Volts)
$V_P$	-	Induced voltage in primary track due to $I_S$ (Volts)
$V_{PR}$	-	Output voltage of parallel-tuned pickup (Volts)
$V_{rect}$	-	Rectified voltage (Volts)
$V_{ref}$	-	Reference voltage (Volts)

$V_{\text{ripple}}$	-	Ripple voltage (Volts)
$V_{\text{SR}}$	-	Output voltage of series-tuned pickup (Volts)
$V_{\text{ST}}$	-	Voltage across $C_{\text{ST}}$ (Volts)
$V_{\text{sq}}$	-	Square voltage signal (Volts)
$V_{\text{startup}}$	-	Controller startup voltage (Volts)
$V_{\text{t}}$	-	Track voltage (Volts)
$V_{\text{trig}}$	-	Triangular voltage signal (Volts)
$Z_{\text{P}}$	-	Reflected impedance of $Z_{\text{S}}$ to primary track
$Z_{\text{P}_p}$	-	Reflected impedance of $Z_{\text{S}_p}$ to primary track
$Z_{\text{P}_s}$	-	Reflected impedance of $Z_{\text{S}_s}$ to primary track
$Z_{\text{S}}$	-	Impedance of secondary pickup
$Z_{\text{S}_p}$	-	Impedance of secondary parallel-tuned pickup
$Z_{\text{S}_s}$	-	Impedance of secondary series-tuned pickup
$\alpha$	-	Scaling factor between $\Delta H$ and $\Delta h$
$\alpha_{\text{c}}$	-	Normalized tuning capacitor variation index
$\alpha_{\text{f}}$	-	Normalized operating frequency variation index
$\alpha_{\text{oc}}$	-	Normalized open-circuit voltage variation index
$\alpha_{\text{r}}$	-	Normalized load variation index
$\alpha_{\text{T}}$	-	Integrated variation of $\alpha_{\text{f}}$ and $\alpha_{\text{c}}$ , equals to $\alpha_{\text{f}}^2 \alpha_{\text{c}}$
$\omega$	-	Actual operating angular frequency (radians/s)
$\omega_0$	-	Nominal operating angular frequency (radians/s)
$\varphi$	-	Phase angle
$\beta$	-	Scaling factor for SSSA fine tuning process
$\epsilon$	-	Fine tuning region of DTDCA
$\mu$	-	Membership function

### **Subscripts**

L	-	Large
M	-	Medium
max (m)	-	Maximum
min	-	Minimum
NE	-	Negative error
NR	-	Negative rate

NRZ	-	Negative rate zero
NZ	-	Negative zero
OT	-	Over-tuning
PE	-	Positive error
PR	-	Positive rate
PRZ	-	Positive rate zero
PZ	-	Positive zero
UT	-	Under-tuning
Z	-	Zero

**Superscripts**

‘	-	Primary side
“	-	Secondary side
^	-	Peak value



# List of Figures

Fig. 1-1: Basic structure of a simple CPT system.....	- 4 -
Fig. 1-2: Basic structure of a typical IPT system.....	- 5 -
Fig. 1-3: Wireless charging electric toothbrush.....	- 7 -
Fig. 1-4: Illustration of an inductively powered electric train.....	- 9 -
Fig. 1-5: A TET charging base and an implantable biomedical sensor.....	- 10 -
Fig. 1-6: Relationship between tuning component and output voltage of pickup.....	- 13 -
Fig. 2-1: Current-fed parallel resonant converters.....	- 16 -
Fig. 2-2: Voltage-fed series resonant converter.....	- 18 -
Fig. 2-3: Basic structure of G3 current-fed converter.....	- 20 -
Fig. 2-4: Basic structure of G3 voltage-fed converter.....	- 20 -
Fig. 2-5: Open-circuit voltage and short-circuit current of pickup coil.....	- 21 -
Fig. 2-6: Tuning configurations of secondary power pickup.....	- 23 -
Fig. 2-7: Simplification of a series-tuned circuit.....	- 24 -
Fig. 2-8: Simplification of a parallel-tuned circuit.....	- 24 -
Fig. 2-9: Generalized power pickup circuit with half-wave bridge rectifier.....	- 26 -
Fig. 2-10: Generalized power pickup circuit with full-wave bridge rectifier.....	- 27 -
Fig. 2-11: Power pickup circuit with full-wave bridge synchronous rectifier.....	- 27 -
Fig. 2-12: Voltage and current relationship of diode and MOSFET.....	- 28 -
Fig. 2-13: Structure of primary track current magnitude controlled TET system.....	- 31 -
Fig. 2-14: 2-D charging pad and 3-D charging cage of TET system.....	- 32 -
Fig. 2-15: A simple dc-to-dc buck converter for variable dc input voltage control.....	- 34 -
Fig. 2-16: General structure of frequency control of primary track current.....	- 35 -
Fig. 2-17: Relationship between power and frequency of primary power supply.....	- 36 -
Fig. 2-18: Basic topology of variable frequency push-pull resonant converter.....	- 37 -
Fig. 2-19: Series-tuned power pickup with linear voltage regulation.....	- 38 -
Fig. 2-20: Parallel-tuned power pickup with shorting-control.....	- 39 -
Fig. 2-21: Hysteresis band for switching on/off $S_{SC}$ .....	- 40 -
Fig. 2-22: Power curve of parallel-tuned pickup with different $Q$ factors.....	- 43 -
Fig. 2-23: Power pickup with dynamic tuning/detuning control.....	- 44 -

Fig. 2-24: Configurations of switching capacitor .....	46 -
Fig. 2-25: Simplified dynamic tuning/detuning power pickup model.....	47 -
Fig. 2-26: Relationship between tuning capacitance and output power of pickup .....	48 -
Fig. 3-1: Tracking process of coarse tuning stage in different areas of output voltage tuning curve and corresponding time-domain results.....	53 -
Fig. 3-2: Tracking process of fine tuning stage in different areas of output voltage tuning curve and corresponding time-domain results .....	57 -
Fig. 3-3: Relationship between T.L/C and pickup output voltage.....	61 -
Fig. 3-4: Possible control results after applying SSSA.....	63 -
Fig. 3-5: Flowchart of standard procedure of DTDCA .....	66 -
Fig. 4-1: Basic structure of LCL power pickup .....	70 -
Fig. 4-2: Voltage and current waveforms of LCL power pickup .....	71 -
Fig. 4-3: Simplified model of LCL power pickup circuit.....	72 -
Fig. 4-4: Simplification of fully-tuned LCL pickup circuit.....	73 -
Fig. 4-5: Output power of LCL power pickup using variable $L_{S2}$ under different $k_{VR}$ .	76 -
Fig. 4-6: Gradient of output power using variable $L_{S2}$ under different $k_{VR}$ .....	77 -
Fig. 4-7: Output power of LCL power pickup using variable $C_{S2}$ under different $k_{VR}$ .	79 -
Fig. 4-8: Gradient of output power using variable $C_{S2}$ under different $k_{VR}$ .....	79 -
Fig. 4-9: Gradient of output power using variable $L_{S2}$ or $C_{S2}$ under different $k_{VR}$ .....	79 -
Fig. 4-10: Output voltage behavior of LCL power pickup using variable $L_{S2}$ under operating frequency variations .....	85 -
Fig. 4-11: Adjusting ratio of $L_{S2}$ for LCL power pickup to achieve desired $r_k$ under operating frequency variations .....	87 -
Fig. 4-12: Output voltage behavior of LCL power pickup using variable $L_{S2}$ under magnetic coupling variations .....	89 -
Fig. 4-13: Adjusting ratio of $L_{S2}$ for LCL power pickup to achieve desired $r_k$ under magnetic coupling variations.....	90 -
Fig. 4-14: Output voltage behavior of LCL power pickup using variable $L_{S2}$ under tuning capacitor $C_{ST}$ variations .....	92 -
Fig. 4-15: Adjusting ratio of $L_{S2}$ for LCL power pickup to achieve desired $r_k$ under tuning capacitor $C_{ST}$ variations .....	93 -



Fig. 4-16: Output voltage behavior of LCL power pickup using variable $L_{S2}$ under load variations .....	- 95 -
Fig. 4-17: Gradient of output voltage under different load variations .....	- 96 -
Fig. 4-18: Adjusting ratio of $L_{S2}$ for LCL power pickup to achieve desired $r_k$ under load variations .....	- 97 -
Fig. 4-19: Relationship between output voltage variation and parameter variation under a constant $k_{VR}$ and different $r_k$ .....	- 98 -
Fig. 4-20: Relationship between output voltage variation and parameter variation under a constant $V_{ref}$ and different $k_{VR}$ .....	- 99 -
Fig. 4-21: Testing circuit for obtaining effective core permeability .....	- 103 -
Fig. 4-22: Typical relationship between dc control current and effective inductance of saturable inductor .....	- 104 -
Fig. 4-23: Configuration of dc current controlled saturable inductor .....	- 104 -
Fig. 4-24: General structure of saturable inductor controlled LCL power pickup.....	- 105 -
Fig. 4-25: Model for dc output voltage analysis .....	- 106 -
Fig. 4-26: Current and voltage waveforms under critical conduction condition .....	- 108 -
Fig. 4-27: PLECS model of LCL power pickup .....	- 111 -
Fig. 4-28: Simulink model of DTDCA controlled LCL power pickup.....	- 112 -
Fig. 4-29: Simulation result of a DTDCA controlled LCL power pickup under operating frequency variations .....	- 112 -
Fig. 4-30: Simulation result of a DTDCA controlled LCL power pickup under magnetic coupling variations .....	- 114 -
Fig. 4-31: Simulation result of a DTDCA controlled LCL power pickup under tuning capacitor variations .....	- 114 -
Fig. 4-32: Simulation result of a DTDCA controlled LCL power pickup under load variations .....	- 115 -
Fig. 4-33: Working prototype of LCL power pickup.....	- 116 -
Fig. 4-34: Practical and ideal output voltage tuning curves under load variations with a) $V_{OC} = 2.47$ V, b) $V_{OC} = 2.8$ V, and c) $V_{OC} = 2.15$ V .....	- 117 -
Fig. 4-35: Output voltage waveform of DTDCA controlled LCL power pickup under load variation (5 to 6.5 $\Omega$ ) in the under-tuning region .....	- 118 -

Fig. 4-36: Output voltage waveform of DTDCA controlled LCL power pickup under load variation (6.5 to 3.5 $\Omega$ ) in the under-tuning region.....	- 118 -
Fig. 4-37: Output voltage waveform of DTDCA controlled LCL power pickup under load variation (3.5 to 6.5 $\Omega$ ) in the under-tuning region.....	- 119 -
Fig. 4-38: Output voltage waveform of DTDCA controlled LCL power pickup under magnetic coupling variations in the over-tuning region .....	- 120 -
Fig. 4-39: Output voltage behavior of LCL power pickup under operating frequency/tuning capacitance variations.....	- 121 -
Fig. 4-40: Possible outcomes of tuning attempt .....	- 123 -
Fig. 4-41: Possible locations of operating point using constant $\Delta h_m$ .....	- 124 -
Fig. 5-1: Input membership functions for $e_{IN}$ of FLC.....	- 130 -
Fig. 5-2: Input membership functions for $r_{IN}$ of FLC.....	- 131 -
Fig. 5-3: Output membership functions for $\Delta u$ of FLC .....	- 134 -
Fig. 5-4: Possible input combinations of $e_{IN}$ and $r_{IN}$ .....	- 136 -
Fig. 5-5: Interpolation of $e_{IN}$ , $r_{IN}$ , and FLC output.....	- 139 -
Fig. 5-6: Interpolation of $e_{IN}$ , $r_{IN}$ , and FLC output with: a) $L = 0.5$ , b) $L = 1.0$ , c) $L = 1.5$ , and d) $L = 2.0$ .....	- 142 -
Fig. 5-7: Interpolation of $e_{IN}$ , $r_{IN}$ , and FLC output with: a) $H = 0.25$ , b) $H = 0.5$ , c) $H = 0.75$ , and d) $H = 1.0$ .....	- 144 -
Fig. 5-8: Flowchart of standard procedure of FLB-DTDCA.....	- 145 -
Fig. 5-9: Simulation result of a FLB-DTDCA controlled LCL power pickup under operating frequency variations .....	- 147 -
Fig. 5-10: Simulation result of a FLB-DTDCA controlled LCL power pickup under magnetic coupling variations .....	- 147 -
Fig. 5-11: Simulation result of a FLB-DTDCA controlled LCL power pickup under tuning capacitor variations.....	- 148 -
Fig. 5-12: Simulation result of a FLB-DTDCA controlled LCL power pickup under load variations.....	- 148 -
Fig. 5-13: FLB-DTDCA and SSSA-DTDCA simulation results of a controlled LCL power pickup under operating frequency variations .....	- 149 -
Fig. 5-14: FLB-DTDCA and SSSA-DTDCA simulation results of a controlled LCL power pickup under magnetic coupling variations .....	- 150 -

Fig. 5-15: Possible output voltage conditions for SSSA-DTDCA to have: a) shorter fine tuning period and b) longer fine tuning period ..... - 151 -

Fig. 5-16: Output voltage waveform of controlled LCL power pickup under load variation (5 to 6.5  $\Omega$ ) using: a) FLB-DTDCA and b) SSSA-DTDCA..... - 153 -

Fig. 5-17: Output voltage waveform of controlled LCL power pickup under load variation (6.5 to 3.5  $\Omega$ ) using: a) FLB-DTDCA and b) SSSA-DTDCA..... - 153 -

Fig. 5-18: Output voltage waveform of controlled LCL power pickup under load variation (3.5 to 6.5  $\Omega$ ) using: a) FLB-DTDCA and b) SSSA-DTDCA..... - 153 -

Fig. 5-19: Output voltage waveform of controlled LCL power pickup under load variation (6.5 to 5  $\Omega$ ) using: a) FLB-DTDCA and b) SSSA-DTDCA..... - 153 -

Fig. 5-20: Output voltage waveform of controlled LCL power pickup under magnetic coupling variations using: a) FLB-DTDCA and b) SSSA-DTDCA..... - 154 -

Fig. 6-1: Simplified model of LC power pickup circuit ..... - 158 -

Fig. 6-2: Output voltage response of parallel LC power pickup with respect to the variation of tuning capacitance under different  $Q_{S,p}$ ..... - 161 -

Fig. 6-3: Output current response of parallel LC power pickup with respect to the variation of tuning capacitance under different  $Q_{S,p}$ ..... - 161 -

Fig. 6-4: Power transfer capacity of parallel LC power pickup using variable tuning capacitor under different  $Q_{S,p}$  ..... - 162 -

Fig. 6-5: Output voltage behavior of parallel LC power pickup using variable  $C_S$  under operating frequency variations ..... - 164 -

Fig. 6-6: Adjusting ratio for parallel LC power pickup to achieve desired  $r_k$  under operating frequency variations ..... - 165 -

Fig. 6-7: Output voltage behavior of parallel LC power pickup using variable  $C_S$  under magnetic coupling variations ..... - 166 -

Fig. 6-8: Adjusting ratio for parallel LC power pickup to achieve desired  $r_k$  under magnetic coupling variations ..... - 167 -

Fig. 6-9: Output voltage behavior of parallel LC power pickup using variable  $C_S$  under load variations ..... - 166 -

Fig. 6-10: Adjusting ratio for parallel LC power pickup to achieve desired  $r_k$  under load variations ..... - 169 -

Fig. 6-11: Relationship between output voltage variation and parameter variation under a constant $Q_{S\_p}$ and different $r_k$ .....	- 170 -
Fig. 6-12: Relationship between output voltage variation and parameter variation under a constant $V_{ref}$ and different $Q_{S\_p}$ .....	- 171 -
Fig. 6-13: Comparison of output voltage variation to parameters variation between LC and LCL tuning circuit under a constant $k_{VR}$ or $Q_{S\_p}$ with different $r_k$ .....	- 176 -
Fig. 6-14: Comparison of output voltage variation to parameters variation between LC and LCL tuning circuit under a constant $V_{ref}$ with different $k_{VR}$ or $Q_{S\_p}$ .....	- 176 -
Fig. 6-15: Structure of variable capacitor controlled parallel LC power pickup.....	- 176 -
Fig. 6-16: Proper location of $C_{S1}$ on tuning curve of output voltage.....	- 177 -
Fig. 6-17: Voltages and control signals of ac switched capacitor .....	- 178 -
Fig. 6-18: Relationship between $C_{eq}$ and $D$ of ac switched $C_{S2}$ .....	- 180 -
Fig. 6-19: Conditions of achieving ZVS in $Q_1$ and $Q_2$ .....	- 180 -
Fig. 6-20: Voltage and current waveforms of $C_{S2}$ under full conduction and being switched .....	- 181 -
Fig. 6-21: Waveform of signals used for generating $V_{Ctrl-1}$ and $V_{Ctrl-2}$ .....	- 182 -
Fig. 6-22: Signal generation of: a) $V_{sq}$ and b) $V_{trig}$ .....	- 183 -
Fig. 6-23: Model for dc output voltage analysis of parallel LC power pickup .....	- 184 -
Fig. 6-24: Output response of LCR circuit to a step voltage under different $L_{DC}$ .....	- 185 -
Fig. 6-25: PLECS model of parallel LC power pickup .....	- 187 -
Fig. 6-26: Simulink model of FLB-DTDCA controlled parallel LC power pickup... -	188 -
Fig. 6-27: Simulation result of a FLB-DTDCA controlled LC power pickup under operating frequency variations .....	- 189 -
Fig. 6-28: Simulation result of a FLB-DTDCA controlled LC power pickup under magnetic coupling variations .....	- 190 -
Fig. 6-29: Simulation result of a FLB-DTDCA controlled LC power pickup under load variations.....	- 191 -
Fig. 6-30: Working prototype of parallel LC power pickup.....	- 192 -
Fig. 6-31: Output voltage waveform of FLB-DTDCA controlled LC power pickup under load variations.....	- 192 -
Fig. 6-32: Output voltage waveform of FLB-DTDCA controlled LC power pickup under magnetic coupling variations .....	- 193 -

Fig. 6-33: Voltage waveforms of: a)  $V_{AC}$ , b) switching control signal  $V_{Ctrl-1}$ , and c) switching control signal  $V_{Ctrl-2}$  ..... - 194 -

Fig. 6-34: Voltage waveforms of: a)  $V_{AC}$ , b) voltage across switches  $Q_1$  and  $Q_2$ , and c) voltage across  $C_{S2}$ ..... - 194 -



# List of Tables

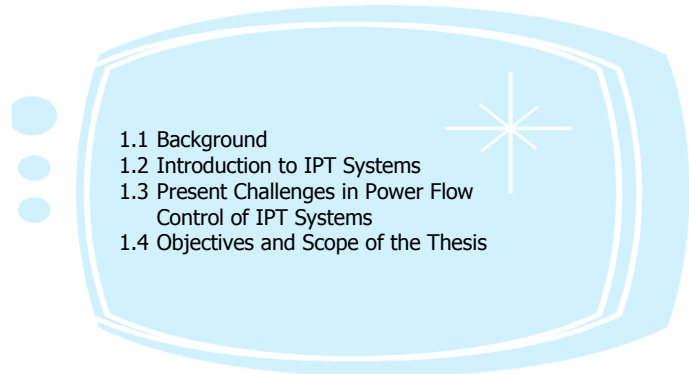
Table 1-1: Contactless/Wireless power transfer options.....	- 3 -
Table 3-1: Results in tracking process of coarse and fine tuning stages.....	- 58 -
Table 3-2: Truth table for determining tuning direction signal $S_4$ .....	- 60 -
Table 3-3: Truth table for $\Delta h$ adjustment determination ( $S_7$ ) .....	- 64 -
Table 5-1: Summarized result of control rule base .....	- 133 -
Table 5-2: Results of evaluating fuzzy control rules $R_1$ to $R_9$ for all ICs whose $e_{IN}$ and $r_{IN}$ are within $[-L, L]$ .....	- 137 -
Table 5-3: Results of evaluating fuzzy control rules $R_1$ to $R_9$ for all ICs whose $e_{IN}$ and $r_{IN}$ are not within $[-L, L]$ .....	- 137 -
Table 5-4: Analytical expressions for crisp output of FLC for ICs $A_1$ to $A_7$ ( $C_1$ to $C_7$ ) and $B_1$ to $B_7$ ( $D_1$ to $D_7$ ) .....	- 138 -
Table 5-5: Analytical expressions for crisp output of FLC for ICs $A_1$ to $A_7$ ( $C_1$ to $C_7$ ) and $B_1$ to $B_7$ ( $D_1$ to $D_7$ ) in classical forms .....	- 140 -
Table 6-1: Truth table for $V_{Ctrl-1}$ and $V_{Ctrl-2}$ generation .....	- 183 -





# Chapter 1

## Introduction



---

### 1.1 Background

By looking at the history of technology developments, it can be seen that a rapid improvement or development of certain technology is normally driven by needs. A typical example of this phenomenon is the wireless internet connection, which has only been made available to people at common public places in recent years. A decade ago, the only way to gain access to the World Wide Web was through telephone lines with a speed up to 56 kbps. Although it was recognized as the most contributive technology in all communication related fields at the time, people were still unsatisfied with slow data exchange rate and therefore drove the research direction to aim at creating faster internet for fulfilling the demands. Few years after, applications of the internet have successfully been extended to various fields, the demands of internet services were therefore no longer focused on the transmission speed but have rapidly moved on to its accessibilities, forced ISPs (Internet Service Providers) to once again change their service direction and made the wireless internet connections available at public places in a very short period of time.

Similar to the revolution of internet connections, power transfer systems have gone through tremendous changes over the last decade. These changes include but not limited to the improvement of power transfer efficiency, circuit topologies, power levels, and most importantly the power transfer methods. It has been known for more than a century that signals and power can both be transferred from one place to another in electromagnetic

forms. The example of internet connection has explicitly shown the two different ways of signal transmission where the signal can either be transmitted using closed circuit with cabling connections, or by wireless without any direct electrical contacts. These two methods can also be applied in the power transfer systems and in fact, have been a common practice in industrial fields, for example, direct power transfer by plugging electrical devices into power sockets, or non-direct power transfer through magnetic coupling in traditional transformers and electrical machines. Although it may seem that the signals and power have shared many commons in their transmission methods and therefore presumably making similar progress of development in the industrial fields, practical constraints and design considerations of the two are still quite different. This has resulted in the development of contactless/wireless power transfer to lag far behind that of signal transfer. Usually a transmission power loss of more than one hundred decibels may be acceptable in a radio system if the information carried by the signal can be recovered at the receiving end [1]. This requires the resonant tuning circuit of the receivers to have a quality factor  $Q$  as high as 100 for achieving proper signal recoveries. On the contrary, in a power transfer system the quality factor  $Q$  has to be designed to be much smaller (around 6 ~ 10) in order to reduce the system sensitivity to parameter variations, as well as the cost, size, and power losses, to meet the load demands. These considerations have inevitably increased difficulties associated with the practical design and implementation of contactless/wireless power transfer systems.

Nowadays the mainstream of power transfer systems is still largely using conductive power transfer based on closed circuits that allow for direct power flow along the conductors. However, it has been found that hard wiring connections may not be suitable for applications such as clean manufacturing plants, underwater vehicles, biomedical implantable devices, etc [2-4]. These kinds of environments normally require power delivery to movable objects with low maintenance and high tolerance to dirt, chemicals, and water. Therefore, contactless/wireless power transfer without direct electrical contact is preferable in these situations.

**Table 1-1: Contactless/Wireless power transfer options**

<b>Features</b>	<b>Energy Harvesting</b>	<b>Capacitive</b>	<b>Inductive</b>
<b>Basic Theories</b>	Wave propagation, Temperature gradient, Acoustics energy, etc.	Distributed electric field	Distributed magnetic field
<b>Typical Techniques</b>	<ul style="list-style-type: none"> <li>• Ambient Electromagnetic Energy Harvesting</li> <li>• Thermoelectric Energy Harvesting</li> <li>• Acoustic Energy Harvesting</li> </ul>	<ul style="list-style-type: none"> <li>• Capacitive Power Transfer (CPT)</li> </ul>	<ul style="list-style-type: none"> <li>• Inductive Power Transfer (IPT)</li> </ul>
<b>Power Level</b>	Low ( $\mu\text{W} \sim \text{mW}$ )	Low (mW) ~ Medium (W)	Low (mW) ~ High (kW)

Table 1-1 shows the available options for achieving contactless/wireless power transfer. As can be seen from the table, the contactless/wireless power transfer technologies are categorized into: energy harvesting, capacitive power transfer (CPT), and inductive power transfer (IPT). The energy harvesting system produces the most environmentally friendly power amongst the three since the electrical power is transferred/converted from ambient-radiation sources, kinetic energy, thermal energy, acoustic energy, etc [5-9]. However, some of these naturally available energy sources are normally not abundant and their availabilities are sometimes uncertain. Moreover, the power flow control, energy gathering and storage techniques needed for this technology are often complicated and difficult which limits this technology to be applied for low power applications such as wireless sensors, wearable electronics, and some mobile devices [10-17].

The capacitive power transfer (CPT) is another way for providing contactless/wireless power to movable objects. Figure 1-1 shows the basic structure of a simple CPT system. CPT is a voltage driven system that uses distributed electric field as power flow path to achieve contactless power transfer. As can be seen, a power source is used for producing high frequency ac voltage to two conductive plates at the primary side of the system. Two other plates at the secondary side are placed within a certain distance from the primary plates such that a loose electric field coupling can be formed and a displacement current can 'flow' through the plates. However, the voltage at the secondary side is usually

unsuitable to be directly used to drive the load. Therefore a power conditioner is normally required to regulate the power into a required form [18].

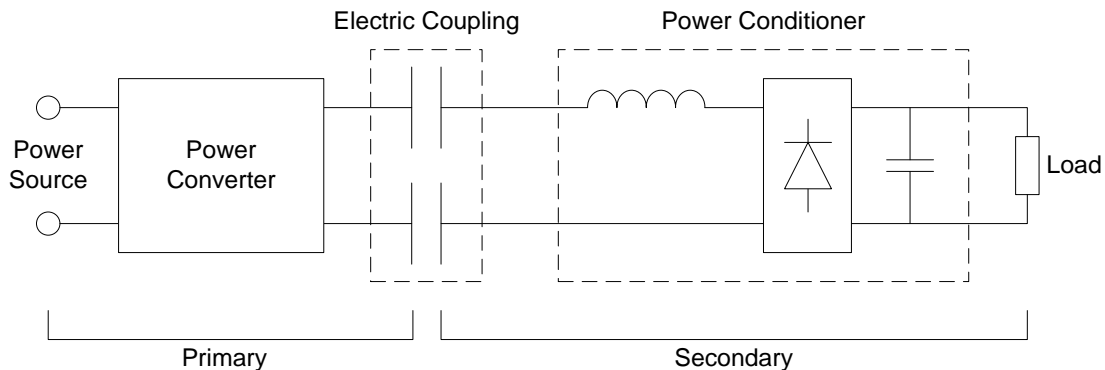


**Fig. 1-1: Basic structure of a simple CPT system**

The CPT system has the advantage of transferring power through metal barriers with low radiated EMI (Electromagnetic Interference). However, because the air has a very low permittivity that is close to  $\epsilon_0$  ( $8.854 \times 10^{-12}$ ) in vacuum, compared to the permeability  $\mu_0$  ( $4\pi \times 10^{-7}$ ), it is much more challenging to design high power CPT systems without very good dielectric materials. Using dielectric materials with high relative permittivity such as PZT (Lead Zirconate Titanate,  $\epsilon_r \approx 2600$ ) makes CPT systems more attractive. But there is a need for more research in this direction before it becomes commercially viable [19].

IPT (Inductive Power Transfer) uses magnetic field as an energy carrying medium for achieving contactless/wireless power transfer. At the beginning, it was considered to be impractical. Transferring power at high levels with low frequencies such as 50 Hz or 60 Hz is nearly impossible, if the primary and secondary side of the system is not tightly coupled as in the traditional transformers. With the rapid development of power semiconductor switching devices and power conversion techniques in the last few decades, the operating frequency can now be raised to a much higher level which enables fast changing rate of the magnetic field. This allows coils of the primary and secondary side to have a much stronger induction effect even they are physically separated. Thus IPT systems has become practically feasible [20].

Among the three options for achieving contactless/wireless power transfer that have been discussed, IPT covers a wider range of power levels, and it has gained many practical applications where direct electrical contact is impossible or inconvenient.

## 1.2 Introduction to IPT Systems

### 1.2.1 Basic Structure and Operating Principle

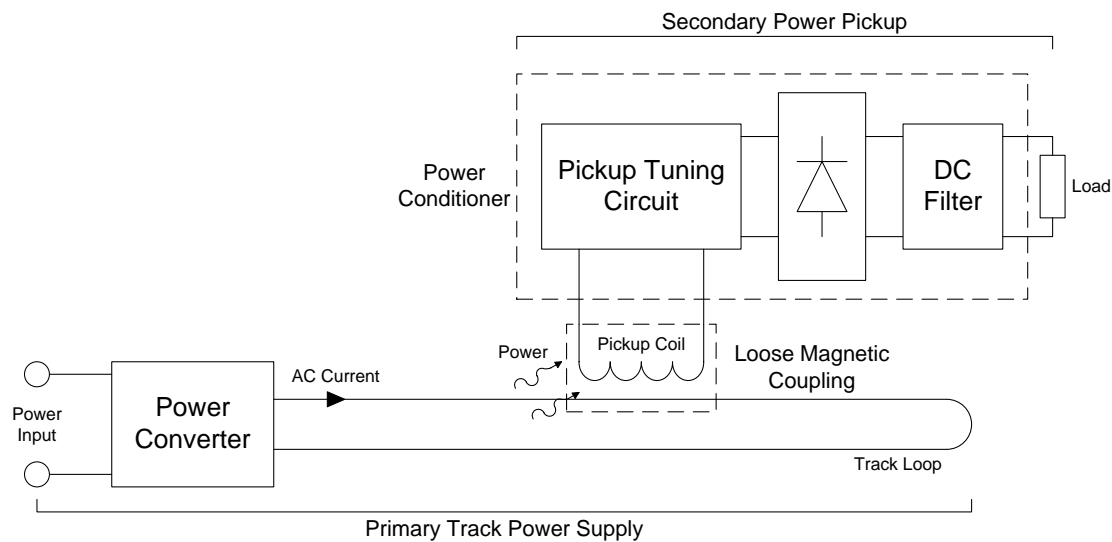


**Fig. 1-2: Basic structure of a typical IPT system**

Figure 1-2 shows the basic structure of a typical IPT system [21]. It can be seen that an IPT system consists of a primary power supply and a secondary power pickup which are electrically isolated from each other. The stationary primary side comprises of a power converter with a track loop. The power converter takes power from a power source to generate a high frequency ac current (normally 10 ~ 100 kHz) with a sinusoidal waveform along the track loop. As such, a magnetic field is created to allow power being transferred from the primary to the secondary through the magnetic coupling between them. The secondary movable power pickup consists of a pickup coil and a power conditioner. By magnetic induction, an emf (electromotive force) is induced in the pickup coil. However, since the primary and secondary side is normally loosely coupled, the induced emf is often too weak to be directly used by the load; therefore a power conditioner is required to regulate the power. The power conditioner can further be separated into an ac tuning part and a dc filtering part by a rectifier. Different tuning configurations such as LC (Inductor-Capacitor) and LCL (Inductor-Capacitor-Inductor) can be applied for boosting up the open-circuit voltage of the pickup coil. For dc applications, the boosted ac voltage after rectification has to be filtered to meet the load requirements.

### **1.2.2 General Features**

IPT provides the following features compared to the traditional power transfer systems:

#### ***Freedom of mechanical movements***

Since the primary current track and the secondary power pickup are loosely coupled, the pickup has much more freedom in mechanical movements. The power pickup is often designed to move in the direction of the track loop to maintain good magnetic coupling (see Fig. 1-2), but 2-Dimensional and 3-Dimensional movements are also needed in some applications such as wireless charging pads and wireless powered animal test cage for biomedical research [22-24].

#### ***Reliable and safe operation***

Since IPT systems transfer power without using direct electrical contact, the two separated parts of the system can independently be enclosed using nonmetal materials. This eliminates possible electric shocks and sparks. Moreover, the system is immune to dirt, dust, water, and chemicals, making it applicable in harsh environments for providing reliable operations.

#### ***Low maintenance***

As the operation of IPT systems does not involve any direct friction like traditional conductive sliding contact power transfer systems, mechanical wears and tears are completely eliminated, which makes it almost maintenance-free.

#### ***Environmentally friendly***

Concerns have been raised regarding to whether by exposure to time-varying magnetic fields could cause harmful effects on human bodies [25-27]. Studies have been undertaken in two major frequency ranges which are the ELF ~ LF (0 ~ 100 kHz) and MF ~ EHF (100 kHz ~ 300 GHz) [28, 29]. Various reports have indicated that human bodies may be affected by high intensity magnetic fields with the result of temperature rise in tissue or body. However, this only happens in microwave range, e.g., broadcasting, telecommunications, radar, and microwave ovens. In a low frequency electromagnetic field range such as 10 ~ 100 kHz (produced in IPT systems), no observable negative biological effects has been found. Therefore IPT is regarded as hazard-free for on-site workers [30, 31].

Furthermore, because the elimination of electrical direct contacts, IPT does not generate any carbon residue during operation as traditional conductive moving contact systems do. This feature also makes the IPT systems environmentally friendly and hence has widely been used in ‘clean rooms’ where semiconductors are manufactured [32].

### ***1.2.3 Related Applications***

The IPT systems have gained many applications owing to its unique contactless/wireless power transfer characteristic and advantageous features aforementioned. To give a general idea for the coverage of IPT systems, some applications are presented and discussed here.

#### ***Electric toothbrush***

Electric toothbrush was initially created for orthodontic patients and claimed to have better performance than manual toothbrushes as it leaves less room for patients to brush insufficiently. There were two different ways for powering the electric toothbrush which are plugging in to a standard wall outlet and run off ac line voltage, or using rechargeable batteries. The first method requires direct cabling connection to a power source and hence, not only limited the portability of device but also created potential electrical hazards in moisturized operating environment such as bathroom. Using rechargeable batteries can allow the device to be operated cordlessly; nevertheless it still requires metal tabs to have direct electrical contact with the charging base.



**Fig. 1-3: Wireless charging electric toothbrush [33]**

An inductive battery charging system was therefore employed to have sealed compartments for preventing water damages and possible electrical hazards associated

with moistures. The charging method operates similarly to IPT systems, but it is much simpler to design since the coupling distance is close and fixed with a fairly low power requirement (2 ~ 4 W). As such, it has now been widely used in various battery charging systems [34-39]. Figure 1-3 shows a wireless charging electric toothbrush.

### ***Electric vehicle***

In the past few decades, vast resources have been invested into developing electric vehicles with intentions to partially or completely replace petrol vehicles for providing emission-free transportations. Different approaches have been implemented, including BEV (Battery Electric Vehicles), FCEV (Fuel Cell Electric Vehicles), and HEV (Hybrid Electric Vehicles) [40, 41]. The BEV and FCEV both have emission-free feature which reduces air pollution. However, the BEV is only applicable in low speed transportation with short driving ranges (100 ~ 200 km) due to its battery management problem, and the FCEV is still at its early development stage with the cost and refueling system as major concerns. The HEV is a hybrid system using both petrol engine and electric motor to drive its wheels. It is commercially available to people and has the advantage of long driving range, better fuel economy, and very low carbon emission. Nevertheless, power management of the HEV is much more complicated compared to vehicles using a single power transmission system; in addition, the HEV requires bulky batteries for electric power storage [42-44].

IPT systems have been implemented in people movers at urban areas as an alternative solution to solve some of the problems associated with the present electric vehicles. An example can be given from an inductively charged electric vehicle which was successfully implemented in 1998 by Wampfler AG, Germany, in association with Auckland UniServices Limited, and the Department of Electrical and Computer Engineering at the University of Auckland. In this project, the electric vehicle charges its batteries by receiving power inductively from a primary charging coil which is buried underground and carrying a current of 80 A at an operating frequency of 12.9 kHz. Power of the vehicle was rated at 30 kW with a total charging current of 200 A for fast battery replenishing (2 ~ 3 minutes) [45]. The electric vehicle is now still being used in Whakarewarewa Thermal Park at Rotorua, New Zealand, and coping well with the harsh operating environment.



Figure 1-4 shows an illustration of an inductively powered electric train, which follows the same principle but runs directly along the rails with a primary track loop. The onboard batteries get continuously charged and therefore do not require a stationary charging process.

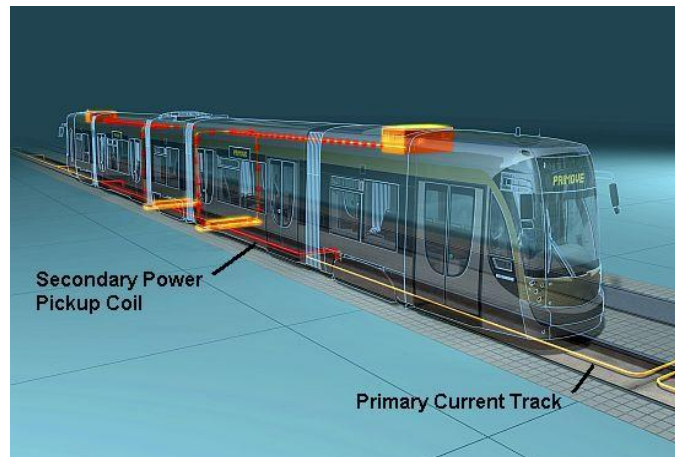


**Fig. 1-4: Illustration of an inductively powered electric train [46]**

Nonintrusive data and power transfer to an AUV (Autonomous Undersea Vehicle) is another good example of IPT systems in the area of electric vehicles. In 1992, an AUV named Odyssey was developed in MIT Sea Grant's AUV Lab under ONR (Office of Naval Research) sponsorship [47]. It was designed to provide marine scientists with access to the ocean at underwater remote sites, using rechargeable batteries to sustain a constant 5 km/hr propulsive speed for 12 hours of operation. Due to the harsh operating environment that the AUV has to constantly deal with, wireless power transfer and communication using IPT systems was considered as a preferred choice and therefore implemented onboard [3, 48-50]. Currently, the adopted IPT system has a power transfer capacity of 200 W with a 10 Mb/s Ethernet for data transmission.

### ***Maglev***

Public transportation such as Maglev (Magnetic Levitation) railways has also been using IPT principles for powering its auxiliary onboard electronics. Inductive power in this application can be easily obtained by receiving power from magnetic fields that were originally generated for levitating the train. A linear power generator is normally used to supply power for the auxiliary onboard electronics with a major concern of its output voltage variation in amplitude and frequency which are in proportion to the speed of

Maglev. Exhaustion of the battery energy occurs when the vehicle runs in lower speed, which may result in shutting down of the Maglev [51]. Solution such as having extra onboard power generated by using harmonic injection method at stator windings has been proposed in solving the problem for onboard power shortage of the Maglev [52]. Different power pickup designs for the Maglev have also been proposed to provide constant power required by the load under all travelling speed [53].

### ***Biomedical implants***

Implantable biomedical devices have found applications in a wide range of medical areas, including pacemakers, monitoring devices, functional electrical stimulators, ventricular assist devices, etc [22, 54-57]. Conventional power transfer method for these devices is through cabling connection with a primary power supply to directly drive the load, or periodically charge up the battery of an implanted device, in order to achieve continuous operation. The current method to achieve this is by piercing wires through the skin (named percutaneous energy transfer) which consequently increases the infection risks [58-60].



**Fig. 1-5: A TET charging base and an implantable biomedical sensor [61]**

Use of the inductive power transfer to replace the original system was therefore suggested, and it is also known as the TET (Transcutaneous Energy Transmission) systems. This kind of application mainly targets at low power range from 50 mW ~ 10 W, and usually need to be compact in size to ease the implantation. Figure 1-5 shows an implantable biomedical sensor developed by Telemetry Research Limited, New Zealand, with a size of 68×15×42mm, and weighted 68 g. The sensor is able to conduct biomedical data

acquisition in the animal body for information such as blood pressure and body temperature, with a wireless transmission range up to 5 meters.

### ***Other applications***

Special applications of IPT systems have also been researched in other areas such as aircraft entertainment system [62], machine tools [63], coalmine power supplies [64], and cordless power stations [65]. However, these areas still require further investigations before the practical systems can be implemented.

## **1.3 Present Challenges in Power Flow Control of IPT Systems**

As the IPT systems are extended to different fields, the need of a suitable power flow control method has become obvious and necessary for applications to meet their specific load requirements.

Like most controllers in other systems, designing the power flow control of IPT systems needs to take aspects such as error tolerance, response speed, overshoot level, simplicity of implementation, robustness, and operating range, etc., into consideration. Other factors that may indirectly affect performance of the system such as power consumption of the controller and EMI (Electromagnetic Interference) also deserve attention. It is normally impossible to have a controller designed to be ideal in all the aspects, therefore trade-offs are often required. Nevertheless, an optimized controller design for specific operating conditions may be available if the relationship between design considerations and system parameters can be well understood.

From experiences accumulated in IPT development, difficulties in controlling the power flow can arise from several factors, which include but not limited to operating frequency drift of the primary power supply, magnetic coupling variations between the primary and secondary coils, load variations, manufacturing tolerance of tuning capacitance, and tuning region variations. Cause and effect of these factors are briefly described below:

### ***Primary frequency drift***

Conventionally, tuning circuit of the secondary power pickup is fine-tuned to match with the primary operating frequency in order to obtain the maximum power transfer capability. However, depending on the design of primary power supplies, certain degree of frequency

drift may exist in practical operations [21]. This results in the tuning circuit of the pickup unable to resonate with the drifted operating frequency, and therefore causes the maximum power transfer capacity to decrease.

### ***Magnetic coupling variations***

As mentioned in Section 1.2.2, the secondary movable load is common to have lateral movements along the primary current track during operations, with the reason being to obtain a fixed magnetic coupling between the primary and the secondary side so as to induce a constant and stable input voltage source (open-circuit voltage of the pickup coil) for the secondary pickup. However in some applications, planar or even spacial movements are also possible [23, 66]. These unconfined movements can cause the open-circuit voltage of the pickup coil to vary and therefore results in the output voltage fluctuation of the pickup.

### ***Load variations***

LC tuning configuration is commonly used in the power pickups of IPT systems. It provides a constant current source to the load under fully-tuned conditions [21]. Since the load is current sourced, the output voltage of the pickup is governed by Ohm's law and varies according to the loading conditions. As the output voltage changes linearly with the loading condition, it may supply insufficient voltage or overvoltage to the load and causes malfunctioning during vast and rapid load changes.

### ***Manufacturing tolerance of tuning capacitance***

In circuit simulation study, ideal components are available and the values can be chosen to be exactly the same as what user defines. However, it does not happen in the real world since there are manufacturing ranges and tolerances. In order to have the center frequency of pickup tuning circuit closely match with the primary operating frequency, high precision and low tolerance to the designated manufacturing range are normally required for tuning components such as a capacitor. But the use of high precision capacitors essentially means adding significant costs into capital and may still require tedious fine tuning process to achieve the desired capacitance value. Due to the above practical issues, it has been found to be troublesome for many manufacturers to do mass production of IPT systems.

### Tuning region variations

In some applications the pickup tuning circuit is controlled to operate in detuning regions instead of staying at the resonance point for meeting the peak load demand [67, 68]. A proportional and integral (PI) controller is normally used in this type of control. However, because one characteristic of PI control is that it can only be designed to track one of the two possible operating points as shown in Fig. 1-6, a safety region close to the resonance point has to be therefore reserved in order to avoid the controller tracking in the wrong direction. This type of control also requires high precision components to keep the tracking process within the designated operating region. Nevertheless, variations in the tuning component caused by self/ambient temperature, pressure, humidity, and aging may still move the tracking process from one region to another, and result in complete failure of the output voltage regulation.

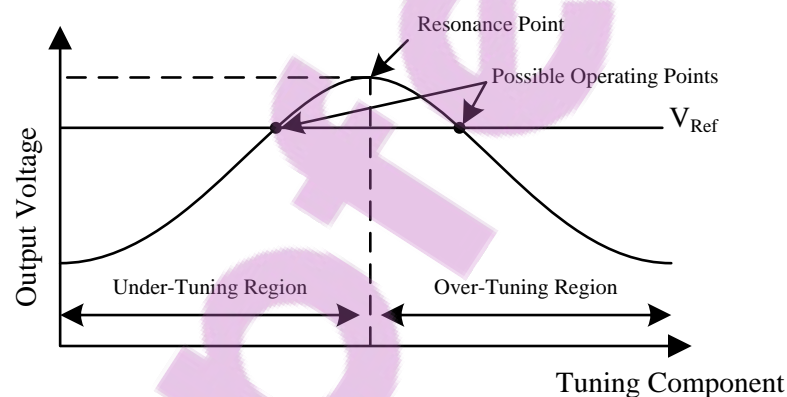


**Fig. 1-6: Relationship between tuning component and output voltage of pickup**

The limiting factors listed above can be easily seen in most applications of the IPT systems. Cost, size, operating range, and power transferring level of the applications are usually restrained to these factors. Different power flow control methods have been proposed in the past to compensate for effects that caused by specific considered parameter variations in order to meet the load requirements [69-71]. The design philosophy of these controllers however, has neglected the fact that multiple parameter variations do exist in the IPT systems, and they often involved with complex and nonlinear behaviors in the integrated effects. This may cause the system to have poor performance or even complete control failure. Therefore, there is a need for a suitable

power flow control method to overcome these limiting factors so as to meet the system load requirements.

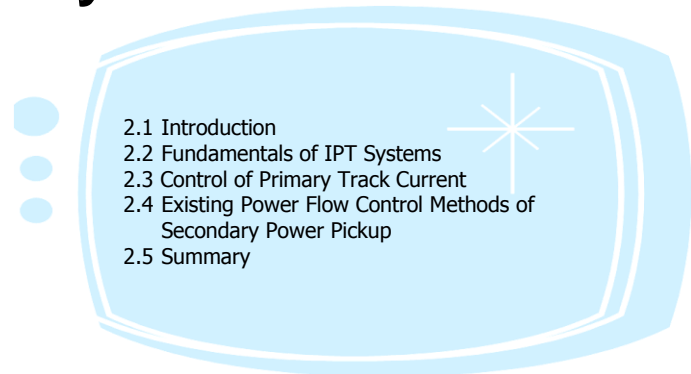
## **1.4 Objectives and Scope of the Thesis**

Depending on the application requirements, power flow control of the IPT systems can either be performed in the primary power converter or the secondary power pickups. For most of the applications, it is preferable to have the control at secondary side since this enables a primary track power supply to drive multiple pickups.

This thesis therefore aims at developing a suitable power flow control method at the secondary power pickup side for general IPT systems. The proposed controller needs to be able to regulate the output voltage under defined worst-case variation of parameters, and deliver sufficient power to the load as required. In addition, the controller is also required to perform full-range tuning for the power pickups to achieve both tuned and detuned operations in the full load range. This feature eliminates the tedious fine tuning process needed for conventional power pickups to achieve high  $Q$  ( $> 10$ ) operation, and therefore makes the IPT systems more cost-effective for mass production with reduced tuning components tolerance requirements.

## Chapter 2

# Overview of Power Flow Control Techniques in IPT Systems



---

## 2.1 Introduction

The IPT systems have gained successful applications in many different fields due to its unique contactless/wireless power transfer characteristic. Similar to other technologies, design considerations such as cost, size, power efficiency, power transfer capability, system stability, and EMI concerns may differ from case to case, depending on the application requirements. This leads research into numerous power flow control techniques for IPT systems. Different assumptions are generally made prior to the design of these controllers so that the system operating conditions can be confined within a specified range of parameter variations. Since the controllers are designed specifically to operate with certain targeted operating conditions, advantages of using these controllers can be presented in some expected aspects but the vulnerabilities to factors that are outside the designed conditions may be inevitable.

In order to have a better understanding of the necessity of power flow control and its state of the art for the IPT systems, this chapter firstly describes the fundamentals of the IPT system with its primary track power supply and secondary power pickups being separately discussed. Then, the chapter outlines the existing power flow control methods in the IPT systems, including their working principles, ideal operating environments, operating constraints, etc.

## 2.2 Fundamentals of IPT Systems

### 2.2.1 Primary Track Power Supply

A good quality track current produced in the primary power supply is essential in the IPT systems since it is used to generate time-varying magnetic fields for the contactless power transfer between the primary and the secondary side. To date, power converters of the IPT systems are in the third generation (G3), having strengths and shortcomings in each generation with comparable overall performance.

#### G1 (First Generation)

The existing IPT primary power converters are categorized as either voltage-fed or current-fed converters, depending on their input sources. The first generation of the primary power supplies is developed based on the current-fed converters, and it has two basic topologies: the full-bridge topology and the push-pull topology [67]. Figure 2-1 (a) and (b) show the current-fed converters based on these two topologies.

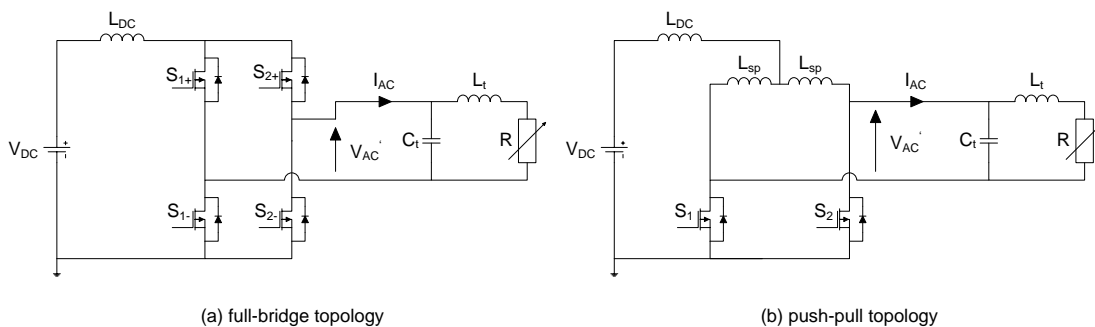


**Fig. 2-1: Current-fed parallel resonant converters**

As can be seen, a dc voltage source  $V_{DC}$  is used in both topologies as the input of the converters, with a large inductor  $L_{DC}$  being connected in series to keep the current nearly constant at high frequencies. Such a configuration provides a voltage controlled current source for the later inverting network without using an actual current source. This makes the control of the current source much easier as it can simply be done by changing the input dc voltage. In the full-bridge inverting network, the switches  $S_{1+}$  and  $S_{1-}$ ,  $S_{2+}$  and  $S_{2-}$ , are complementarily controlled, i.e., when  $S_{1+}$  and  $S_{2-}$  are turned on,  $S_{1-}$  and  $S_{2+}$  are turned off, for injecting current  $I_{AC}$  into the resonant tank. Note that the switching frequency of the inverting network for all IPT track power supplies can either be running at a fixed



frequency or be variably controlled. In the constant frequency control, the switches are forced to run at a predetermined frequency for providing a stable operating frequency to the system. However, the forced operation may impose high voltage and/or current stresses onto the switches and results in high switching losses. In the case of variable frequency control, the switching frequency is allowed to vary with the load and circuit parameters, and hence follows the natural circuit resonance. The advantage of using variable frequency control is that soft-switching for the switches are achievable which improves the power efficiency. But its drawback is that the operating frequency varies slightly under normal operating conditions, and it may shift far away from its nominal value in some extreme situations causing system frequency stability and systems bifurcation problems [21].

In the push-pull inverting network, a phase-splitting transformer is used to replace the  $S_{1+}$  and  $S_{2+}$  in the full-bridge topology. The phase splitting transformer basically divides the dc current in half before it enters the resonant tank. The output ac voltage of the inverting network is expressed by [21, 72]:

$$\hat{V}_{AC}' = \pi V_{DC} \quad (2-1)$$

The above relationship shows that by controlling the average input dc voltage  $V_{DC}$ , the primary ac resonant tank voltage  $V_{AC}'$  can be maintained to regulate the track current.

The resonant tank of a G1 power supply has a capacitor  $C_t$  which is being used to parallel tune to the track inductance  $L_t$  as shown in Fig. 2-1 for compensation purpose, and also to eliminate the possibilities of overvoltage caused by placing two current sources in series.

The nominal primary operating frequency is determined according to  $\omega_0 = 1/\sqrt{L_t C_t}$ . The variable load resistance  $R$  here represents the sum of track resistance and the reflected impedance of secondary power pickups.

In comparison, the push-pull converter is simpler to design as its switches do not require isolated high-side gate drives and can have the negative rail of the dc power supply as a common ground. In addition, the push-pull converter offers a doubled resonant tank voltage compared to the full-bridge converter. This is a very advantageous feature in the IPT systems since a higher track voltage allows the system to drive a longer track for the

same dc voltage supply [21]. Therefore the push-pull converters are more commonly seen in G1 power supplies, owing to its design simplicity and cost effectiveness in terms of the ratio between the dc input voltage and the drivable track length.

The G1 power supplies have many advantages, e.g., 1) it results in good quality track current with low harmonics and radiated EMI; 2) ZVS (Zero-Voltage Switching) can be implemented to have low conduction and switching losses; and 3) magnitude of the track current can be varied without losing ZVS operation through changing the input dc voltage. Nevertheless, it also has drawbacks such as the shorter drivable track length (compared with other generations of the IPT converters having same dc input voltage level), load dependent track current, and load dependent operating frequency [21]. The IPT G3 (Third Generation) power supplies have therefore been developed to overcome the above drawbacks and improve the properties of G1 power supplies. Note that each generation of the IPT power supply is not particularly based on modifications of the previous generation; they are however categorized according to the sequence of being practically used in the industrial fields.

### ***G2 (Second Generation)***

The G2 power supplies were developed based on the voltage-fed converters. Figure 2-2 shows a typical full-bridge voltage-fed series resonant converter in the IPT systems. Note that the G2 power supplies can also be implemented using push-pull topology. However the push-pull topology offers identical features in both the G2 and the G1 power supplies which have been described in the previously section, and therefore, the push-pull implementation of the G2 power supplies is not discussed here.

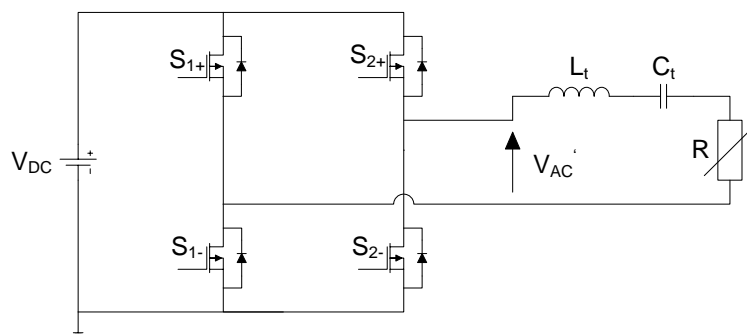


**Fig. 2-2: Voltage-fed series resonant converter**

A dc voltage supply is directly used in the G2 converters as the input power source. Switching strategy of the inverting network here is identical to that of the current-fed full-bridge converters. The output of the inverting network is connected to a series-tuned resonant tank as shown in Fig. 2-2, with at least one inductor being connected to the input of the resonant tank for preventing the possibility of shorting the input voltage source with a voltage-source type of load such as a pure capacitor branch.

Unlike the output ac voltage of G1 inverting network which is determined by the average dc input voltage, switches of the G2 inverting network have the complete control of the resonant tank voltage  $V_{AC}$ . The duty cycle  $D$ , which essentially controls the average injecting current into the resonant tank, is determined by introducing a phase-shift into the switching signals for either  $S_{1+}$  and  $S_{1-}$ , or  $S_{2+}$  and  $S_{2-}$ . This in turn varies the magnitude of  $V_{AC}$ , and thereby regulates the track current. The relationship between the  $V_{AC}$  and the duty cycle  $D$  can be expressed as [21]:

$$\hat{V}_{AC} = \frac{4}{\pi} V_{DC} \cdot \sin\left(\frac{\pi D}{2}\right) \quad (2-2)$$

Some of the important features of the G2 power supplies are: 1) a dc voltage source can directly be used as the input of the converters, which lowers the size, cost, and circuit order for the overall system; 2) the phase-shift control of the switches is much easier to implement than the average dc input voltage control of the G1 power supplies which may require an additional buck converter for varying the input dc voltage. Nevertheless, the input of the resonant tank of a G2 converter normally requires a series tuning circuit, which is not ideal as the resonant tank current has to flow through the switches and may require the switches to have higher power ratings in order to take the full reactive current circulation [21].

### ***G3 (Third Generation)***

The third generation of the IPT primary power supplies is based on modifications of the previous two generations to further improve their converters properties. Two types of G3 primary power supply were separately developed based on the voltage-fed and current-fed converters.

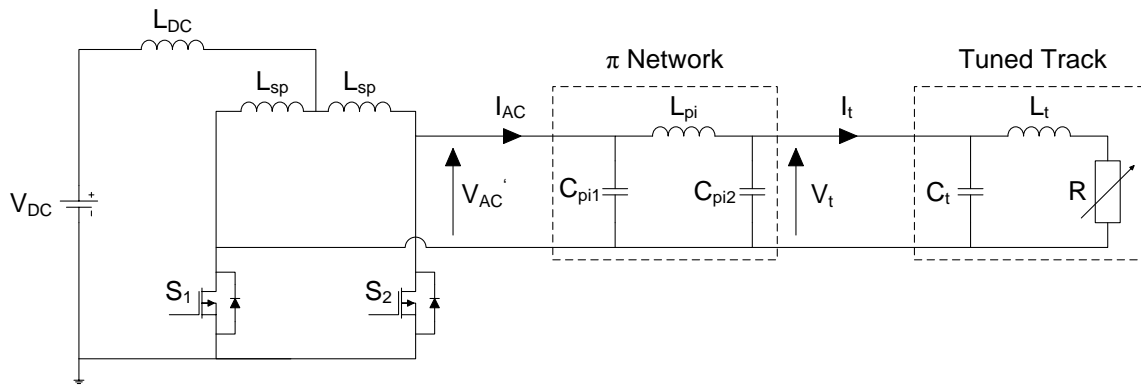


**Fig. 2-3: Basic structure of G3 current-fed converter**

Figure 2-3 shows the basic structure of a G3 current-fed converter. It can be seen that the most significant difference between the G1 and the G3 power supplies is the newly introduced  $\pi$  network. Advantages of using the  $\pi$  network include: 1) compensation of the network so a unity power factor can be obtained; 2) the voltage source can be converted to a current source for a constant track current that is independent of load; 3) it functions as a band-pass filter to have low distortion in the track current [21].

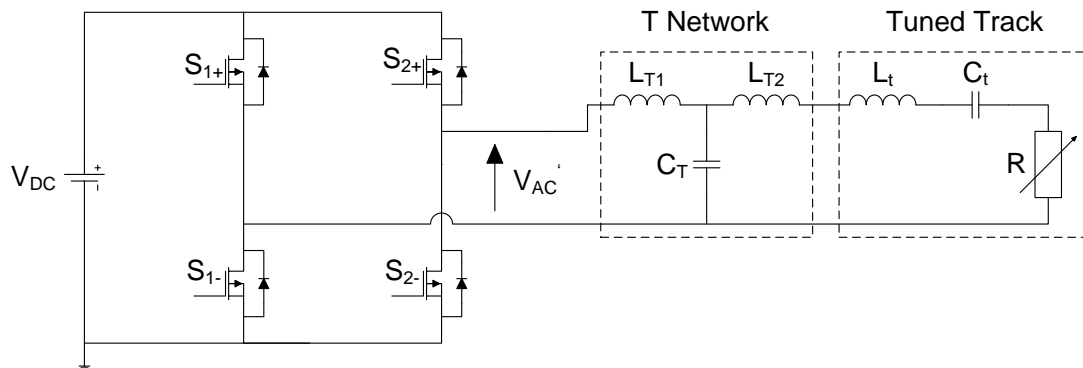


**Fig. 2-4: Basic structure of G3 voltage-fed converter**

With the track fully-tuned to the nominal resonant frequency, the track impedance can be regarded as a pure resistive load. This allows the current-fed resonant tank with a CLC (Capacitor-Inductor-Capacitor)  $\pi$  network to be directly transformed into a voltage-fed resonant tank with a LCL (Inductor-Capacitor-Inductor) T network. Figure 2-4 shows the basic structure of a G3 voltage-fed converter. Since the  $\pi$  and the T networks are dual-circuit, the good features provided in the former can all be inherited by the latter [21].

### 2.2.2 Secondary Power Pickups

The main purpose of power pickups in an IPT system is to receive the power coming from the primary track current through the magnetic coupling between the track and the secondary pickup coil. In practice, the power pickup is designed to deliver the power according to the load demands, with specific power ratings, power efficiency, cost, and size. To design and implement an IPT system that is based on a specified requirement, the following aspects of the power pickup are normally required to be analyzed:

#### Coupling Factor

Figure 2-5 shows the structure of a magnetic coupling between the primary track and the secondary pickup coil.

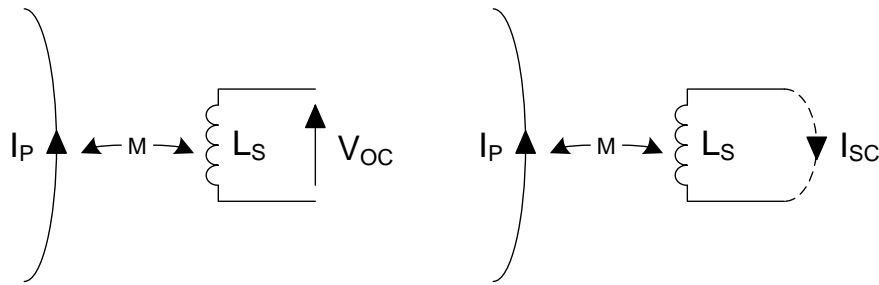


Fig. 2-5: Open-circuit voltage and short-circuit current of pickup coil

The voltage induced in the secondary pickup coil due to the time-varying magnetic fields produced by the primary track current is given by [73]:

$$V_{OC} = j\omega_0 M I_P \quad (2-3)$$

where  $V_{OC}$  is the open-circuit voltage of the pickup coil,  $\omega_0$  is the nominal operating frequency,  $M$  is the mutual inductance between the primary track and the secondary pickup coil, and  $I_P$  is the primary track current. The short-circuit current of the pickup coil can be determined from:

$$I_{SC} = \frac{V_{OC}}{j\omega_0 L_S} \quad (2-4)$$

where  $L_S$  is the inductance of the secondary pickup coil. By substituting (2-3) into (2-4), the short-circuit current can be further expressed as:

$$I_{SC} = \frac{M}{L_s} I_P \quad (2-5)$$

For a traditional inductive power transfer system such as transformers, the degree of magnetic coupling between the primary and the secondary side is measured by a coupling coefficient defined as:

$$k = \frac{M}{\sqrt{L_t L_s}} \quad (2-6)$$

However, considering an IPT application which has a primary track loop with a distance that is normally several times longer than the secondary pickup coil in length, the self-inductance of the pickup coil may only couple to a very small portion of the entire track inductance and therefore, the actual coupling between the two sides may not be properly reflected by the coupling coefficient.

Alternatively, a parameter, termed as the coupling factor, was introduced for a better measure of the IPT systems magnetic coupling and it is defined as [21]:

$$k_f = \frac{N_s I_{SC}}{N_p I_P} = n_s \frac{I_{SC}}{I_P} \quad (2-7)$$

where  $n_s$  is the turns ratio between the secondary pickup coil and the primary track. By rewriting equation (2-4) with respect to  $I_{SC}$ , the relationship between the track current and the short-circuit current of the pickup coil can be presented by [21]:

$$I_{SC} = \frac{k_f}{n_s} I_P \quad (2-8)$$

It can be seen from (2-8) that the secondary current of the IPT systems is inversely proportional to the turns ratio  $n_s$  which is similar to the characteristic of an ideal current transformer, but it is also having a proportional relationship with the coupling factor  $k_f$ . The coupling factor  $k_f$  is usually treated as unity in the transformers since their coupling geometry are fixed with the primary and the secondary being tightly coupled. But it is not true for IPT systems as  $k_f$  varies greatly from 0.1 ~ 0.95.

### Tuning Circuit

In a typical wireless communication system, the receiving end is normally required to be tuned to a certain interested frequency so that the signals carried by this particular channel can be extracted and used. This is no exception to the power pickups in the IPT systems; however instead of the signals, the pickup tuning circuit is tuned to the primary operating frequency so the power transfer capacity can be maximized. Figure 2-6 shows two common pickup tuning configurations which are series and parallel tuning circuits [22, 74-76].

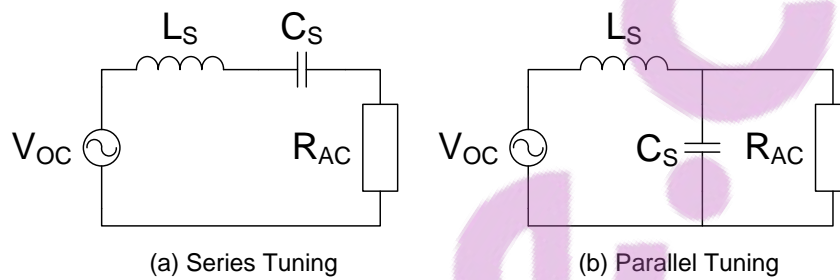


**Fig. 2-6: Tuning configurations of secondary power pickup**

The capacitor  $C_S$  is the tuning capacitor being used to tune to the pickup coil inductance  $L_S$ . The load resistor  $R_{AC}$  here represents the ac load resistance. If a full-bridge rectifier is used to drive a dc load  $R_L$  in a continuous conduction mode, then the equivalent resistance for a voltage source load can be modeled as [77]:

$$R_{AC} = \frac{8}{\pi^2} R_L \quad (2-9)$$

For a current source load it is modeled as [77]:

$$R_{AC} = \frac{\pi^2}{8} R_L \quad (2-10)$$

In the series tuning configuration, the circuit can further be simplified as shown in Fig. 2-7. It can be seen that after the cancellation of the pickup coil inductance and the tuning capacitor under fully-tuned condition, the voltage across the load equals to the open-circuit voltage of the pickup coil. The output voltage of the pickup therefore remains constant regardless of the load variations.

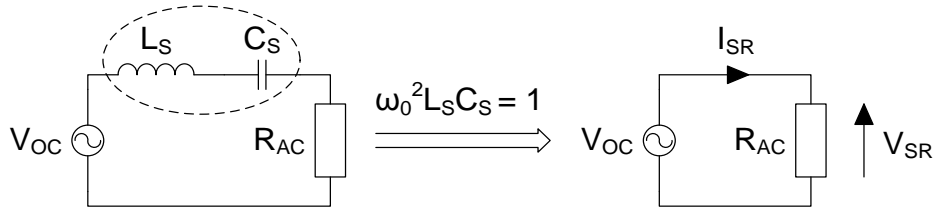


**Fig. 2-7: Simplification of a series-tuned circuit**

The output voltage and load current shown in Fig. 2-7 are given as [21]:

$$V_{SR} = V_{OC}, \quad I_{SR} = Q_{S-s} \cdot I_{SC} \quad (2-11)$$

where the quality factor  $Q_{S-s}$  is given by:

$$Q_{S-s} = \frac{\omega_0 L_S}{R_{AC}} \quad (2-12)$$

The maximum output power of a series-tuned pickup can be calculated by:

$$P_{m-s} = V_{SR} I_{SR} = Q_{S-s} \cdot V_{OC} I_{SC} = \frac{\omega_0 L_S}{R_{AC}} \cdot V_{OC} I_{SC} \quad (2-13)$$

Since the open-circuit voltage is directly used by the load without any voltage boosting, this type of power pickups is suitable for low voltage applications, or used in applications with good coupling to provide sufficient output voltage.

On the other hand, the parallel tuning circuit has gained its popularities in the IPT applications owing to its voltage boosting capability. This feature allows the system to have more freedom in the mechanical movements while still meeting the load requirements. Figure 2-8 shows the simplification of a parallel-tuned circuit.

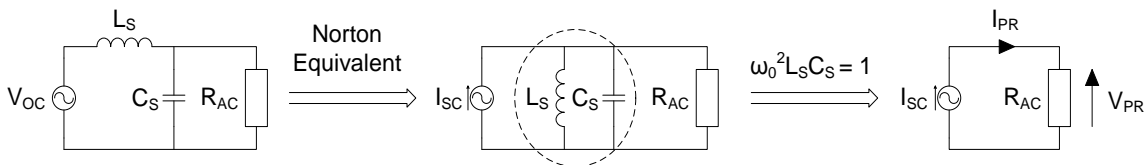


**Fig. 2-8: Simplification of a parallel-tuned circuit**



Contrary to a series-tuned circuit, the load here is directly sourced by the short-circuit current of the pickup coil. The output voltage and load current shown in Fig. 2-8 are given as [78]:

$$V_{PR} = Q_{S-p} \cdot V_{OC}, \quad I_{PR} = I_{SC} \quad (2-14)$$

where the quality factor  $Q_{S-p}$  is:

$$Q_{S-p} = \frac{R_{AC}}{\omega_0 L_S} \quad (2-15)$$

The maximum power of a parallel-tuned power pickup can be obtained by:

$$P_{m-p} = V_{PR} I_{PR} = Q_{S-p} \cdot V_{OC} I_{SC} = \frac{R_{AC}}{\omega_0 L_S} \cdot V_{OC} I_{SC} \quad (2-16)$$

In principle, both the series-tuned and the parallel-tuned circuits are capable of providing unlimited power when their load resistances are approaching to extreme conditions, i.e., approaching short-circuit for the series-tuned pickup and open-circuit for the parallel-tuned pickup. However, when the circuit approaches these extreme conditions, the quality factor will be very large, causing tedious fine tuning requirement because of the significantly increased circuit sensitivity to parameter variations. The quality factor of tuning circuits in practical design is normally limited to be less than 6, and a maximum of 10 to avoid tuning problems associated with the high  $Q$  operation [75].

In order to determine the major system variables that affect the maximum power transfer capacity of an IPT system, both (2-13) and (2-16) can be rewritten as (2-17) by linking the power flow to the magnetic coupling and primary track current [79, 80]:

$$P_m = \frac{\omega_0 I_p^2 M^2 Q_S}{L_S} = \omega_0 I_p^2 Q_S k_f M \frac{N_p}{N_s} \quad (2-17)$$

where  $Q_S$  is the quality factor of the tuning circuit. It can be seen from (2-17) that there are several ways to increase the maximum power transfer capacity in a practical IPT system design. The easiest way is to have a larger ratio in  $M^2/L_S = k_f M N_p/N_s$  [21]. This can

be achieved by having a higher turns ratio between the primary track loop and the secondary coil windings, or a better coupling factor  $k_f$  which is obtained through good coupling geometry and core materials. Moreover, the increase in frequency and magnitude of the track current can also improve the power transfer capacity. However, these two factors need to be cautiously treated as the power losses of the system also increase with them. Since the quality factor  $Q_S$  is normally required to be kept low to avoid the sensitivity problems aforementioned, using high  $Q$  ( $>10$ ) to further improve the power transfer capacity is therefore not recommended in IPT applications with fixed tuning circuits.

### Voltage Rectification

For IPT applications with dc loads, the pickup circuit is required to have rectifiers for ac-to-dc conversion. Two topologies can be used which are the half-wave bridge rectifier topology and the full-wave bridge rectifier topology [67]. Figure 2-9 shows the configuration of a half-wave bridge rectifier in a generalized power pickup circuit.

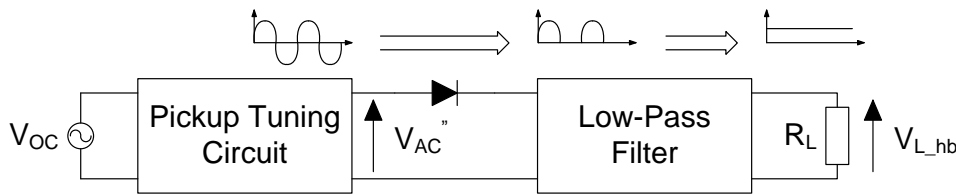


**Fig. 2-9: Generalized power pickup circuit with half-wave bridge rectifier**

If only half a cycle of an ac voltage is rectified, the average dc voltage after the rectification can be expressed as:

$$V_{L\_hb} = \frac{1}{T} \int_0^{\frac{T}{2}} \hat{V}_{AC} \sin(\omega t) dt = \frac{1}{\pi} \hat{V}_{AC} \quad (2-21)$$

where  $T$  is the period of the ac voltage. Since this topology has only used a single diode to perform the voltage rectification, it is therefore very easy to implement. However, as the other half of the ac voltage gets blocked by the diode and cause the circuit to have a longer discharging period, components of the low-pass filter may have to be designed larger for ensuring a smoother dc output [67].

The full-wave bridge rectifier is used if the rectification on a complete ac voltage waveform is desired. Figure 2-10 shows the configuration of a full-wave bridge rectifier in a generalized power pickup circuit.

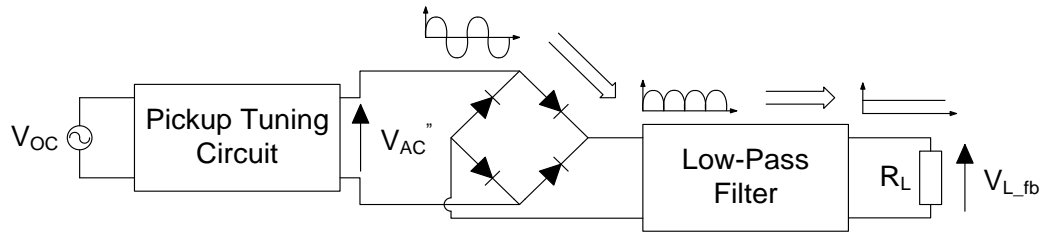


**Fig. 2-10: Generalized power pickup circuit with full-wave bridge rectifier**

The average dc output voltage of this topology is determined by:

$$V_{L\_fb} = \frac{2}{T} \int_0^{\frac{T}{2}} \hat{V}_{AC} \sin(\omega t) dt = \frac{2}{\pi} \hat{V}_{AC} \quad (2-22)$$

It can be seen that the full-wave rectification can give higher voltage at output, but it includes higher power losses due to more diodes being used and has common grounding problem when the controller is applied at the ac tuning side of the pickup circuit with its power supply and feedback signals are coming from dc side of the pickup circuit [67].

To fully use the advantages provided by the full-wave bridge rectifier without having to worry about its drawbacks, the common grounding issues are generally solved by using isolated gate drives. And in order to reduce the conduction losses across the diodes, synchronous rectifiers have been suggested to replace the diode rectifier [81].

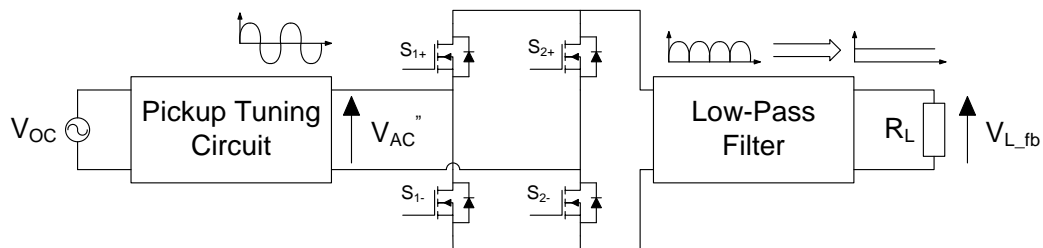


**Fig. 2-11: Power pickup circuit with full-wave bridge synchronous rectifier**

A typical configuration of full-wave bridge synchronous rectifier is shown in Fig. 2-11, and it can be extended to different topologies with some require only two MOSFETs to

achieve the full-wave rectification [82-84]. The synchronous rectifier is also known as the active rectifier since the semiconductor switches, i.e., MOSFETs, which are placed in parallel with freewheeling diodes, are synchronously and actively controlled to perform the voltage rectification. The switching of these MOSFETs is generally controlled during the conducting state of the diodes. When the diodes are forward-biased, the MOSFETs are turned on, and when the diodes are reverse-biased, the MOSFETs are turned off. Thus a rectifying characteristic is obtained without the forward voltage drop being associated with diodes in the on-state.

The reduction in conduction losses is achieved by having a lower forward voltage drop in the MOSFET. Typically a power diode can have a forward voltage drop around 0.7 ~ 1V, which negatively affects the system efficiency, particularly at a low voltage (< 10 V) and high current operation. By using MOSFETs with a low on-resistance, the forward voltage drop can be reduced and this effectively improves the power efficiency. Figure 2-12 shows the voltage and current relationship for both the diode and the MOSFET [85]. The conduction loss of a diode or a MOSFET can be calculated by the product of forward voltage and current. It can be seen that the MOSFET has a lower conduction loss compared with the diode, provided the current flowing through these two is below a certain break-even current  $I_b$ . Modern MOFTETs are made to have very low on-resistance, so practically  $I_b$  can be much larger than the actual operating current.

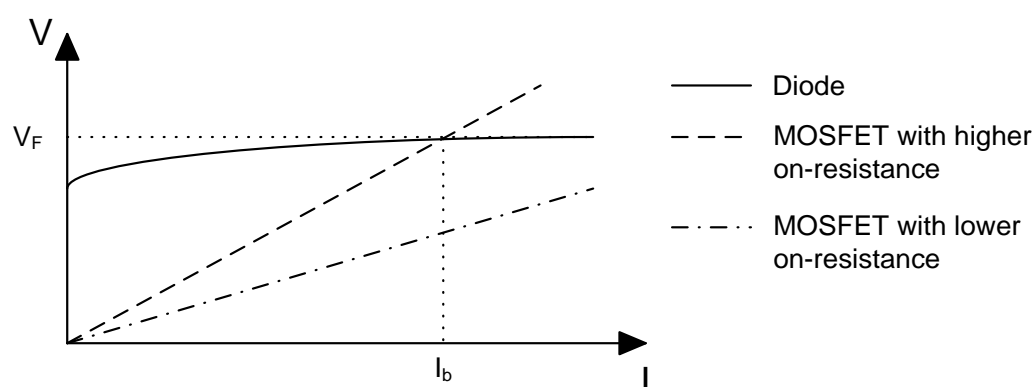


**Fig. 2-12: Voltage and current relationship of diode and MOSFET**

It is clear to see that the adoption of full-wave bridge synchronous rectifier can increase the power pickup efficiency, but it requires current detection of the diodes and isolated gate drives to switch on/off the MOSFETs. These additional components and circuitries

have inevitably complicated the circuit design and increased the size of the power pickup. Furthermore, increase in switching frequency of the MOSFETs and high voltage rating of the load may also result in high switching losses, and cause the power efficiency of synchronous rectification worse than that of the conventional diode scheme. As a result, based on the power rating, system efficiency, size, cost, etc., it is often up to the designer to select a proper rectification method.

### **Pickup Load Modeling**

In order to determine the stability of an IPT system, it is common to have a system model which includes both the primary and the secondary side so a thorough investigation can be carried out. Since the two isolated parts of the system are magnetically coupled to each other, the secondary power pickup can be modeled as a series impedance by reflecting its effects to the primary side. This has been done in many studies to help analyze the load condition and bifurcation of the primary power supply.

For a series-tuned pickup (see Fig. 2-7), the input impedance can be expressed as [21, 86, 87]:

$$Z_{S\_s} = j\omega_0 L_S + \frac{1}{j\omega_0 C_S} + R_{AC} \quad (2-23)$$

By putting (2-23) into rectangular form, it can be rewritten as:

$$Z_{S\_s} = R_{AC} + j\left(\omega_0 L_S - \frac{1}{\omega_0 C_S}\right) \quad (2-24)$$

Under fully-tuned condition, the imaginary part of  $Z_{S\_s}$  is equal to zero so the secondary impedance appears to be a pure resistor and has a value that is equal to the load resistance. The reflected impedance of  $Z_{S\_s}$  to the primary track is given by:

$$Z_P = \frac{V_P}{I_P} \quad (2-25)$$

where  $V_P$  is the induced voltage in the primary track due to the current in the secondary pickup ( $I_S$ ) and can be expressed as:

$$V_p = j\omega_0 M I_s \quad (2-26)$$

Considering  $I_s = V_{OC}/Z_{S-s}$ ,  $V_{OC} = j\omega_0 M I_p$ , and  $V_p = j\omega_0 M I_s$ , equation (2-25) can be rewritten as:

$$Z_p = \frac{\omega_0^2 M^2}{Z_{S-s}} \quad (2-27)$$

By substituting the secondary impedance of a series-tuned power pickup into (2-27), the reflected impedance becomes:

$$Z_{P-s} = \frac{\omega_0^2 M^2}{R_{AC}} \quad (2-28)$$

From (2-28), it can be seen that if a series-tuned pickup is heavily loaded or short-circuited, the reflected impedance will become very large and tends to be infinite, causing low or zero current flowing in the track and eventually blocks the power transfer to other secondary power pickups in a multiple pickups system.

On the other hand with a parallel tuning pickup, a similar approach can also be used to see how a parallel-tuned pickup affects the power transfer of the IPT system when it is coupled to the track. The input impedance of a parallel tuning pickup (see Fig. 2-8) is given by [21]:

$$Z_{S-p} = j\omega_0 L_s + \frac{1}{j\omega_0 C_s + 1/R_{AC}} \quad (2-29)$$

Equation (2-29) can be rewritten in the rectangular form as:

$$Z_{S-p} = \frac{R_{AC}}{1 + (\omega_0 R_{AC} C_s)^2} + j \left( \omega_0 L_s - \frac{\omega_0 R_{AC}^2 C_s}{1 + (\omega_0 R_{AC} C_s)^2} \right) \quad (2-30)$$

Under fully-tuned condition, the reflected impedance of  $Z_{P-p}$  is given by:

$$Z_{P-p} = \frac{M^2 R_{AC}}{L_s^2} - j \frac{\omega_0 M^2}{L_s} \quad (2-31)$$

The real part of  $Z_{P,p}$  is the reflected resistance, and it is proportional to the output load resistance. Contrary to the series-tuned circuit, the power blocking occurs when the pickup is lightly loaded or open-circuited. The negative reactance of the reflected impedance is independent of the load and shows a capacitive load property to the track.

### 2.3 Control of Primary Track Current

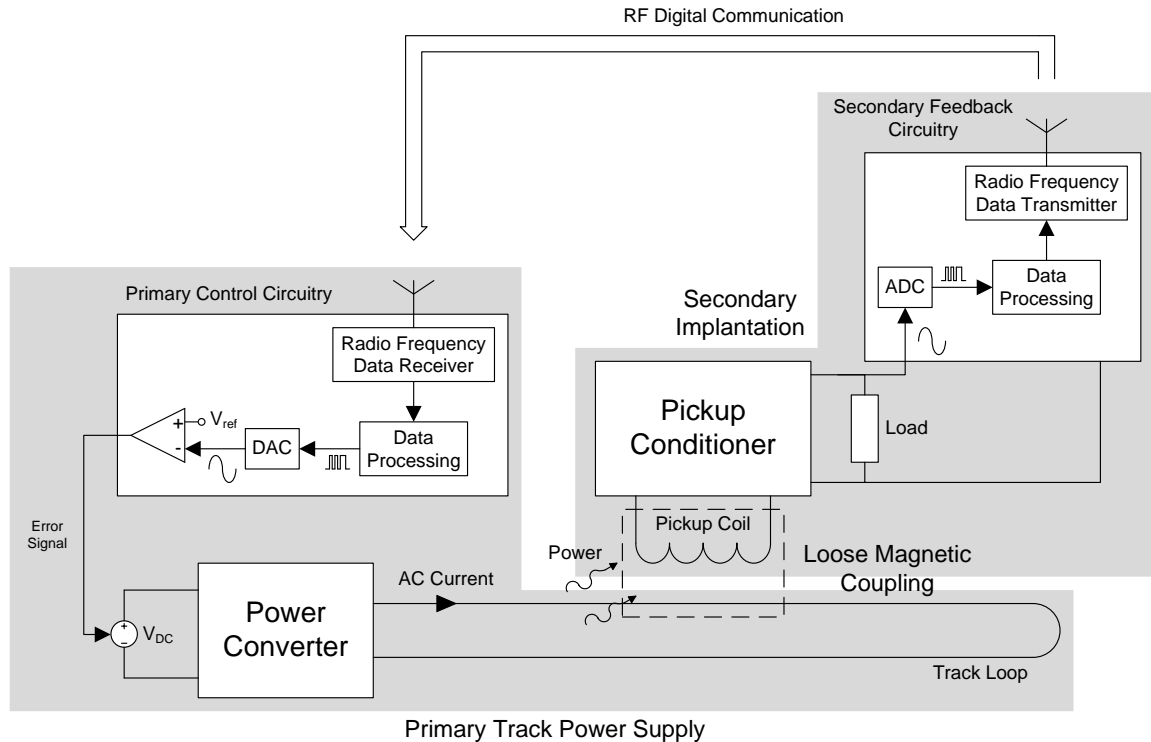


**Fig. 2-13: Structure of primary track current magnitude controlled TET system**

Some IPT applications require the output voltage of the power pickup to be regulated through the control of primary track current. A typical example of this type of application is the TET system which has been discussed in Chapter 1. This is due to the fact that although the power pickups can be individually controlled to enable the system with multiple pickups operation, power losses generated by control actions such as switching and conduction of components may need to be dissipated in the form of heat. The rise in ambient temperature caused by the heat is considered negligible in most applications of the IPT system as long as the heat is able to be dissipated and not accumulated inside the components. However, if the application is to be implanted into an animal body, reduction of heat generation is crucial; otherwise it may cause tissue damage [59, 66, 81]. Figure 2-

13 shows a typical primary track current magnitude controlled TET system. A TET system may involve both 2-D and 3-D movements of the secondary pickup, which makes the system design much more complicated compared to simple monorail applications, because the magnetic coupling between the primary and the secondary side is very weak and changes both in magnitude and direction [72].

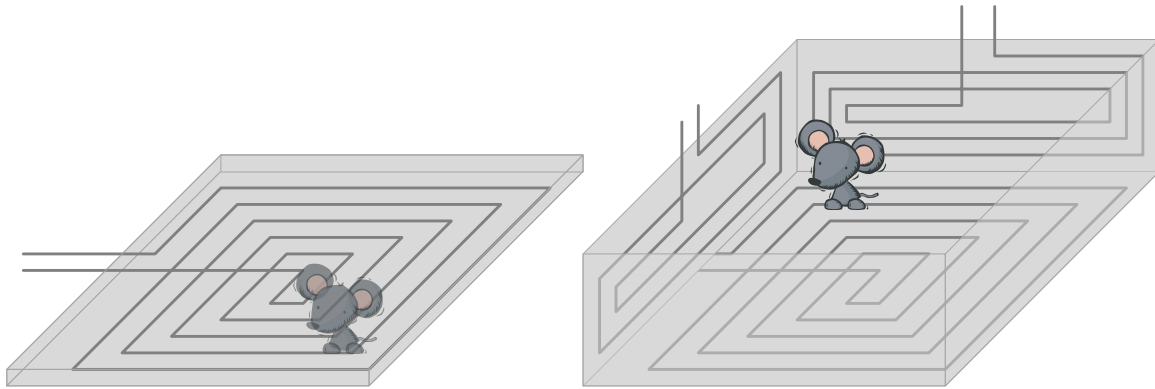


**Fig. 2-14: 2-D charging pad and 3-D charging cage of TET system**

The example shown in Fig. 2-14 gives a fairly good idea on how a power pickup having multi-dimensional movements to cooperate with the primary charging-pad or the primary charging-cage of the TET system. The secondary pickup is normally an implantable device that is implanted into an animal body, and the animal can be at any place within defined areas (normally in the test cage) covered by the magnetic field produced from the primary track current [66]. For monitoring and identification purpose such as body weight, food intake, and physiological parameters related to health and welfare of the individual free moving animal [55], the power pickup is allowed to have much more freedom in mechanical movements and therefore the voltage boosting capability of the parallel tuning circuit is preferred in the TET systems to compensate for the possible output voltage insufficiency. Push-pull topology is normally adopted to reduce the number of switches that have to be used in the primary inverting network, with the track being parallel-tuned to lower the power ratings for the switching devices [66].

There is no major difference between a conventional IPT system and a TET system although an additional RF (Radio Frequency) communication channel between the primary and the secondary side is often present in a TET system. Given that it is preferable for TET systems to have the power flow controller placed at the primary side so



as to reduce the size and heat generation in the implants, the same wireless communication link used for biological data transfer is often used to feedback the secondary output power status to the primary control circuitries so as to change the output power from the primary side accordingly [66, 88].

The secondary feedback circuitry normally consists of an ADC (Analog-to-Digital Converter), a data processing block, and a RF data transmitter. The ADC is used to sample the analog output voltage of the power pickup and then convert it into digital forms so it can be transmitted by the RF data transmitter. The data processing block is mainly for signal processing of the converted data before it is sent out in the air. Note that the sampling frequency and resolution of the ADC can affect the final control result; therefore these two factors need to be carefully selected to ensure a good overall control quality such as minimum steady state error, fast response to output voltage ripples, etc.

At the primary control circuitry side, the secondary feedback signals are received by the RF data receiver and converted back to analog signals through the DAC (Digital-to-Analog Converter). These converted signals are then used to compare with a predetermined voltage reference  $V_{ref}$  (see Fig. 2-13) for generating error signals that will be used for the control of the magnitude or the frequency of track current. The main purpose of controlling the track current is to regulate the power flow so as to maintain the output voltage of the power pickup at a desired level.

### **2.3.1 Magnitude Control of Track Current**

In the track current magnitude control, the control signals are applied to a PWM (Pulse-Width Modulation) controlled variable dc voltage source  $V_{DC}$  which is the input power source to the primary power converter [89]. The variable dc voltage source can be implemented through various ways, such as using a simple dc-to-dc buck converter. Figure 2-15 shows the general structure of a controlled buck converter. By feeding the error signal which is produced from the comparison result of the secondary output voltage feedback signal and the voltage reference  $V_{ref}$ , into a controller, a PWM signal can be generated to switch on/off the MOSFET shown in Fig. 2-15. Note that the controller employed can be of any kind, however, a simple PI (Proportional-Integral) controller is normally used to keep the design simple while providing satisfactory control result.

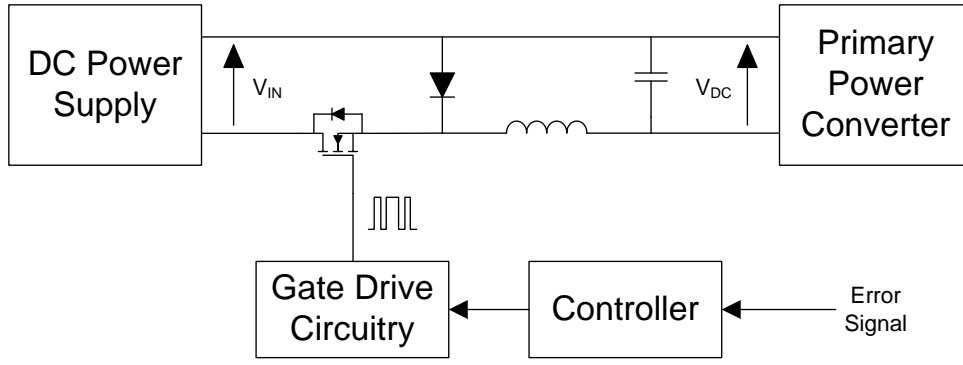


Fig. 2-15: A simple dc-to-dc buck converter for variable dc input voltage control

The output voltage of the buck converter can be obtained by:

$$V_{DC} = D_{PWM} V_{IN} \quad (2-32)$$

where  $D_{PWM}$  is the duty cycle of the PWM signal and  $V_{IN}$  is the constant input voltage to the buck converter. Considering a TET system with a current-fed parallel-tuned primary track, the track current is given by [66]:

$$I_P = \frac{V_{AC}}{j\omega_0 L_t + Z_P} \quad (2-33)$$

Substituting (2-1) and (2-32) into (2-33), the equation of the track current can be rewritten as:

$$I_P = \frac{\pi D_{PWM} V_{IN}}{j\omega_0 L_t + Z_P} \quad (2-34)$$

From (2-34), it can be seen that the track current is directly controlled by the duty cycle of the PWM signal. And since the open-circuit voltage and short-circuit current of the pickup coil are both proportional to the track current according to (2-3) and (2-5), the power pickup with either a voltage source output (which equals to the open-circuit voltage), or current source output (which equals to the short-circuit current), can thus be controlled by the PWM signal.

### 2.3.2 Operating Frequency Control of Track Current

The second way of regulating the pickup output voltage through the primary control is by frequency control of the track current. As it has been previously explained, the nominal operating frequency of the primary resonant tank is determined by the track inductance and the tuning capacitance. If the equivalent tuning capacitance can be varied to allow the resonant tank having different resonant frequencies, the power delivered from the primary track power supply to the secondary power pickup can be consequently controlled through this tuning/detuning process. This frequency control method can be illustrated by Fig. 2-16.

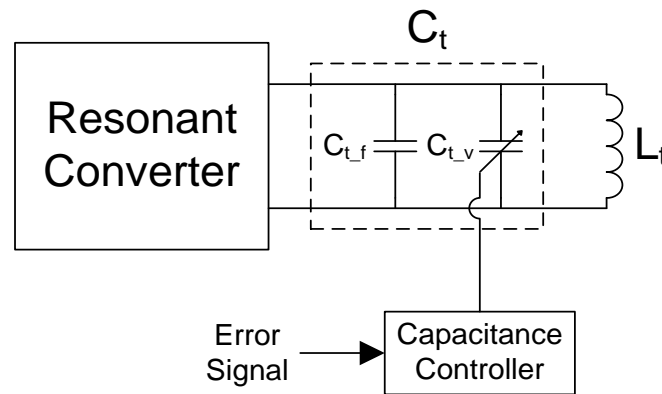
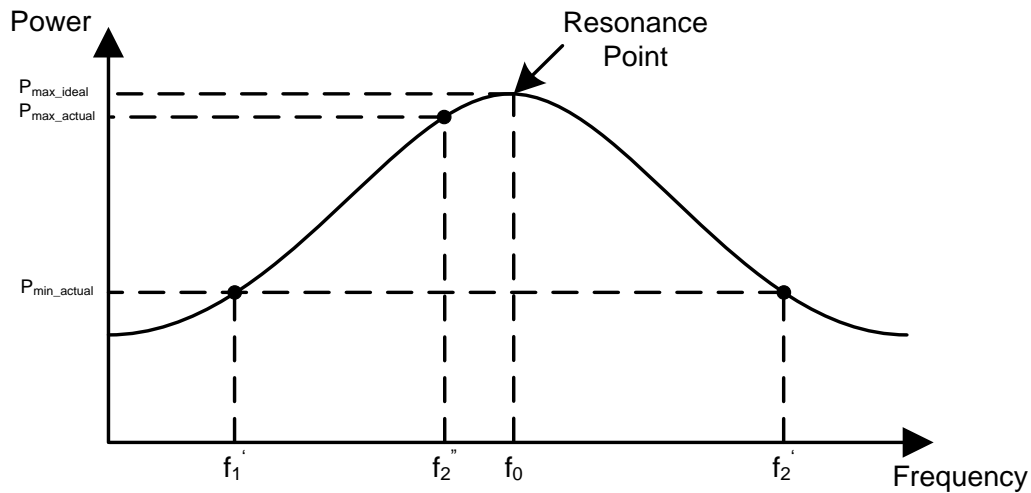


**Fig. 2-16: General structure of frequency control of primary track current**

It can be seen from Fig. 2-16 that the original track tuning capacitance is separated into two capacitances, which are  $C_{t-f}$  and  $C_{t-v}$  representing a fixed tuning capacitor and a variable tuning capacitor respectively. An error signal is generated based on the secondary output voltage feedback signal and then fed into a controller for varying the equivalent tuning capacitance so a variable operating frequency can be obtained. The variable operating frequency is given by [21, 66]:

$$\omega = \left[ \sqrt{\left(1 - \frac{1}{4Q_p^2}\right)} / \left[ L_t (C_{t-f} + C_{t-v}) \right] - \frac{\varphi}{T} \right] / \left( 1 + \frac{2\varphi}{\pi} \right) \quad (2-35)$$

where  $Q_p$ ,  $\varphi$ , and  $T$  are the quality factor, initial phase angle, and time constant of a push-pull resonant converter respectively. As can be seen from the above equation, the operating frequency is dependent on the capacitance of  $C_{t-v}$ .



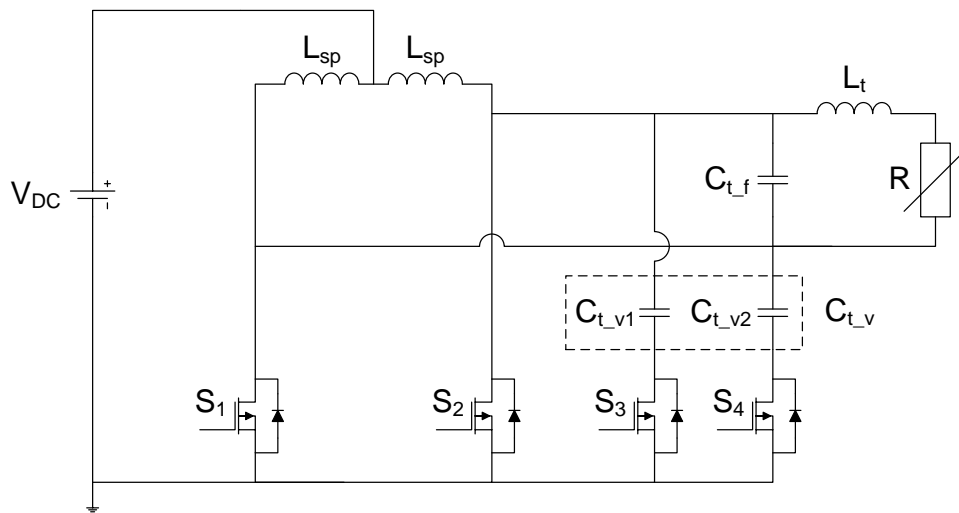
**Fig. 2-17: Relationship between power and frequency of primary power supply**

Figure 2-17 shows the relationship between the output power and frequency of primary track power supply. The maximum power is obtained when the primary resonant tank is tuned to the nominal operating frequency  $f_0$ , and lower power is achievable by having a resonant frequency other than the nominal operating value. The resonant frequencies  $f_1'$  and  $f_2'$  are determined by the equivalent tuning capacitances  $(C_{t,f} + C_{t,v})$  and  $C_{t,f}$  respectively, and the primary output power is controllable within the range of these two frequencies [66, 67].

A simple PI controller is often employed to generate control signals for changing the equivalent tuning capacitance. However, since the operating frequency has a parabolic relationship with the power, the adopted PI controller is unable to achieve full-range control and restrained to only operate in one of the two operating regions that are separated by the nominal frequency  $f_0$ . The frequency  $f_2''$  shown in Fig. 2-17 indicates the actual available maximum operating frequency instead of the ideal  $f_2'$ . Note that the frequency  $f_2''$  is different from the nominal frequency  $f_0$  by a safety margin, and this safety margin is used to prevent the PI tracking process from traversing between the two operating regions and results in control failure.

Practical implementation for frequency control of the track current can be shown in Fig. 2-18. Similar to ordinary push-pull converters,  $S_1$  and  $S_2$  are switched complementarily for injecting current into the resonant tank. A variable tuning capacitance is achieved by switching two fixed capacitors namely  $C_{t,v1}$  and  $C_{t,v2}$  using  $S_3$  and  $S_4$  with control signals

generated from the PI controller, and the two capacitors are identical for a balanced operation. The switching of  $S_3$  and  $S_4$  follows closely to the on/off period of  $S_1$  and  $S_2$ . When  $S_1$  is on and  $S_2$  is off,  $S_3$  is on and  $S_4$  is off correspondingly to switch  $C_{t_v1}$  into and have  $C_{t_v2}$  out of the resonant tank in the positive cycles of the ac resonant tank voltage. Vice versa, when  $S_2$  is on and  $S_1$  is off,  $S_4$  is on and  $S_3$  is off correspondingly to switch  $C_{t_v2}$  into and have  $C_{t_v1}$  out of the resonant tank in the negative cycles of the ac resonant tank voltage. The effective capacitance of  $C_{t_v1}$  and  $C_{t_v2}$  can be changed through varying the duty cycle of the switches. As such, the primary resonant tank is able to have a range of operating frequencies, and the power delivered to the power pickup can therefore be changed according to the actual load demands.



**Fig. 2-18: Basic topology of variable frequency push-pull resonant converter**

Despite the above two control methods can effectively control the power transfer between the primary and the secondary side within a predefined range of parameter variations, the IPT systems using primary track current control however, have a major disadvantage associated with the architecture of the control method. Since the track current controller needs to be specifically designed to compensate for parameter variations that occur in the power pickup of particular interest, it eliminates the possibilities of IPT systems to have multiple pickups operation, unless if all the pickups are absolutely identical which is unlikely to happen in practice. Optimization of the primary current control based on loading conditions of each power pickup could be a viable solution if the power requirements have little differences between each one of them. Nevertheless, when the power requirements are different, the controller may completely fail the power flow

regulation and result in shutting down of the whole system for the worst case. Therefore, in order to have a robust power flow control for the IPT systems, the primary track current control is normally employed in applications where the track power supply is only required to transfer power to a single power pickup at a time [66].

## 2.4 Existing Power Flow Control Methods of Secondary Power Pickup

Instead of applying control at the primary side of the IPT systems, having control in individual power pickups provides effective power flow management to the system. Several control strategies have been researched in the past and they are described in details in the following sections.

### 2.4.1 Voltage Regulator

Figure. 2-19 shows a series-tuned power pickup which is commonly used in IPT applications. A linear voltage regulator is used for its output voltage regulation [62, 67].

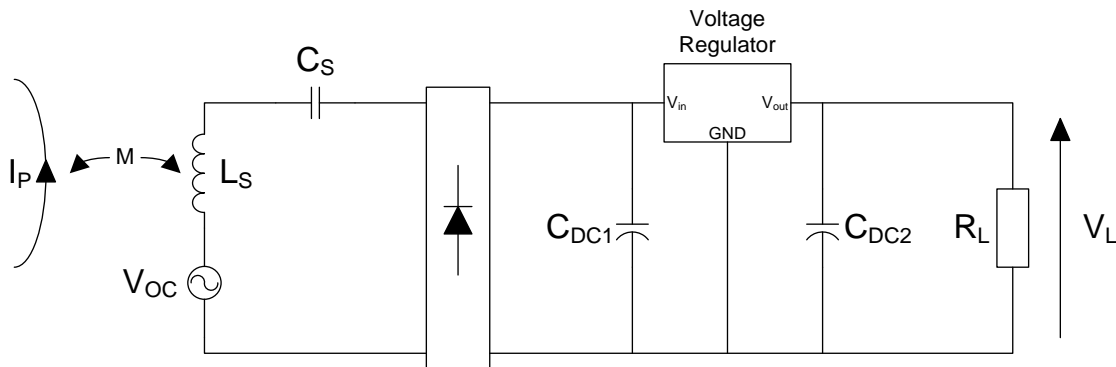


**Fig. 2-19: Series-tuned power pickup with linear voltage regulation**

A dc capacitor  $C_{DC1}$  is used to ensure the smoothness of the input voltage for the voltage regulator. The voltage regulator then regulates the rectified and filtered dc voltage to a desired level for the load. Another dc capacitor  $C_{DC2}$  is placed at the output of the voltage regulator and in parallel to the load for stabilizing the output voltage  $V_L$ . Tuning circuit of the pickup is generally required to be fine-tuned to the nominal operating frequency so the power transfer capability of the IPT system can be maximized. Since parameter variations in magnetic coupling, operating frequency, tuning capacitance, load, etc., may occur in the

power pickups at any instances during the power transfer, the maximum power transfer capacity of the pickup is generally oversized to accommodate these possible variations. The oversized maximum power may cause the power pickup to have low power efficiency when the load is having a low power demand. Advantages of using such a method for the output voltage regulation include its design simplicity and low cost. However it is an inefficient method as the excessive power cannot be effectively used and needs to be dissipated through heat sinks which consequently increase the size of the pickup. Applications with high power ratings worsen the inefficiency of this method and may require additional cooling mechanisms to assist the heat dissipation.

Placing a Zener diode in parallel to the load is a comparable approach with similar pros and cons to the voltage regulator [67]. But the available output voltage value is quite limited to the manufacturing range of Zener diode which is not as flexible as a variable voltage regulator. In addition, it has an output variation problem which can vary with component's tolerance.

### 2.4.2 Shorting-Control

Shorting-control is the most well-known control technique used in the IPT systems and has gained many applications as well as patents due to its design simplicity and effectiveness to the power flow control of IPT systems [70, 90-92]. Figure 2-20 shows a parallel-tuned power pickup with shorting-control for the output voltage regulation.

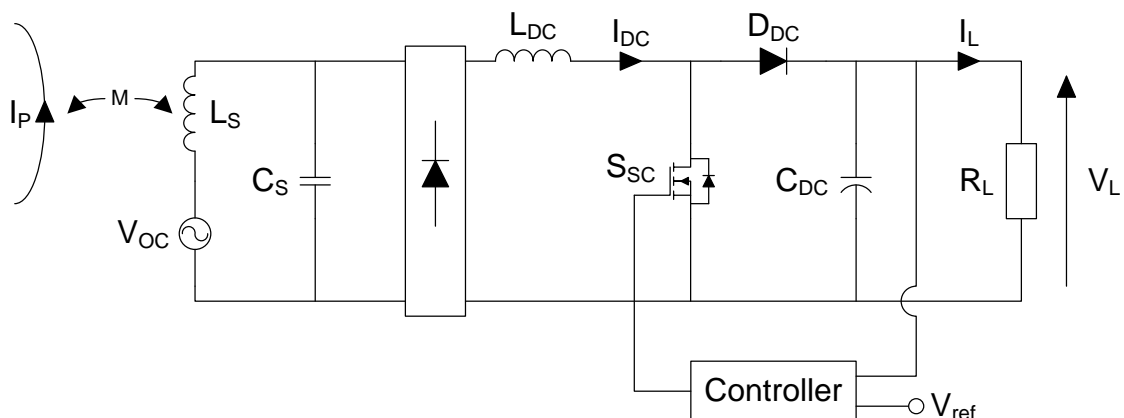


**Fig. 2-20: Parallel-tuned power pickup with shorting-control**

A dc inductor  $L_{DC}$  and a dc capacitor  $C_{DC}$  are used to filter out the high frequency components of the rectified voltage for providing a smooth dc output voltage to the load. A controller, a shorting switch  $S_{SC}$ , and a freewheeling diode  $D_{DC}$  are used for output voltage regulation of the pickup. The tuning condition of the pickup is designed based on the reasons that have been previously stated in the method using voltage regulator, so the secondary resonant tank is also tuned to the nominal operating frequency for obtaining the maximum power transfer capacity, in order to compensate for the parameter variations. There are two operating modes in the shorting-control corresponding to the on/off state of switch  $S_{SC}$ . When  $S_{SC}$  is switched on, the additional current flowing path provided by the shorting switch can redirect the output current to go around the load and stops the power being delivered to it. The output voltage of the pickup ( $V_L$ ) is temporarily sustained through the energy discharging of the dc capacitor  $C_{DC}$ , and the reversing current caused by the discharging of  $C_{DC}$  is blocked by the dc diode  $D_{DC}$ . Contrary when  $S_{SC}$  is switched off, the output current goes directly through the dc diode and charges up the dc capacitor while delivering power to the load.

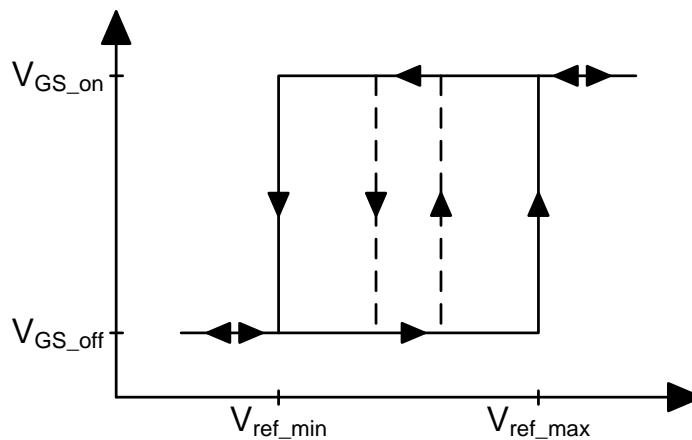


**Fig. 2-21: Hysteresis band for switching on/off  $S_{SC}$**

The switching of  $S_{SC}$  can be controlled by either hysteresis or PWM control. In the hysteresis control, the controller is normally a simple comparator which compares the output voltage of the pickup with a preset voltage reference  $V_{ref}$  having a maximum value at  $V_{ref\_max}$  and a minimum value at  $V_{ref\_min}$  as shown in Fig. 2-21. Results of the comparison are directly used as the switching signals for  $S_{SC}$ . The advantage of using the hysteresis control is that it is very easy to design, and its output voltage ripple can be



strictly controlled within a predefined hysteresis band as shown in Fig. 2-21. However, if a more precise output voltage is required, the hysteresis band has to be consequently narrowed down (Fig. 2-21, in dot-lines) and may result in the increase of switching frequency and power losses. Furthermore, since the actual output current is controlled according to the load demands under a constant output voltage, it changes the charging and discharging rate of the dc capacitor. This makes the switching frequency load dependent and causes the EMI (Electro-Magnetic Interference) to radiate over a wide range of spectrums which result in difficult EMI filtering design for IPT applications such as moving sensors [93].

To reduce the EMI problem that occurs in the hysteresis control, PWM signal was used to switch  $S_{SC}$  [93]. By using a simple PI controller with output voltage of the pickup as a feedback signal, a varying reference voltage can be produced and compared to a time-varying signal with constant frequency, for example, a triangular wave, for generating the PWM signal. A high fundamental frequency for the PWM signal helps to minimize the size of the EMI filters but increases the switching losses, thus a trade-off is inevitable when designing a practical circuit.

In a PWM controlled power pickup, the load current  $I_L$  (see Fig. 2-20) is expressed as:

$$I_L = D_S I_{DC} = \frac{D_S I_{SC}}{\sqrt{2}} \quad (2-36)$$

where  $D_S$  is the duty cycle of the PWM signal for the shorting switch  $S_{SC}$ . Considering  $V_L = I_L R_L$ , the output power of the parallel-tuned power pickup can be determined by:

$$P_L = V_L I_L = (D_S I_{DC})^2 R_L \quad (2-37)$$

From (2-37), it can be seen that the power can be kept constant by controlling the duty cycle  $D_S$  to compensate for the  $R_L$  variations. Assuming the system is having a fixed coupling and gives a constant  $I_{SC}$  as well as  $I_{DC}$ , then the maximum power is reached with  $R_L$  being at its maximum rated value and  $D_S$  equals to unity.

Despite the facts that the shorting-control is easy to implement and can effectively control the power flow of the pickups, it however suffers from inefficient operations when  $R_L$  is

lightly loaded or at no-load conditions, i.e., large load resistance or open-circuited [66-68]. In some IPT applications where loads may enter into sleep mode, the power demands of these loads are usually very low which requires the duty cycle  $D_S$  to be small for maintaining low output power. In this situation, the switch  $S_{SC}$  will need to take most of or the complete short-circuit current of the pickup according to  $(1 - D_S)$ . As such, the power pickups may require large heat sinks for dissipating significant conduction losses and result in larger size of the pickup.

Low immunity to parameter variations other than load changes is another disadvantage of using the shorting-control. As stated earlier, the design philosophy of shorting-control is to obtain the maximum power transfer capacity for each pickup to cover the full-range of their load variations, and it dissipates the power through a shorting switch if the power is considered excessive to the load. Parameter variations in operating frequency, magnetic coupling, and tuning capacitance are normally ignored or roughly estimated to be included in the covering range of shorting-control, limiting the pickups to work with applications having monotonic coupling geometry, stable ambient temperature, and high quality track current. A pickup with higher tolerance to the parameter variations is achievable by using a shorting switch with higher power ratings to have a wider control range. However this increases the size and cost of the power pickup substantially.

The conventional parallel-tuned power pickup also has a circuit sensitivity problem under high  $Q$  operation. Using high  $Q$  in the power pickups is very advantageous for the IPT systems since the output voltage of the pickup can be boosted to a sufficient level without increasing the track current magnitude or needing more number of turns in the pickup coil windings, which essentially reduces the size and cost of the overall system. In addition, the pickups will also be able to operate from a further distance with respect to the primary power supply, and thereby increase the portability of the secondary power pickups. However, the pickup circuit sensitivity increases with the  $Q$  factor and can cause significant power drop under high  $Q$  operation even if there is only a slight change in the circuit parameters. Figure 2-22 illustrates the power curve of a parallel-tuned pickup with different  $Q$  factors.

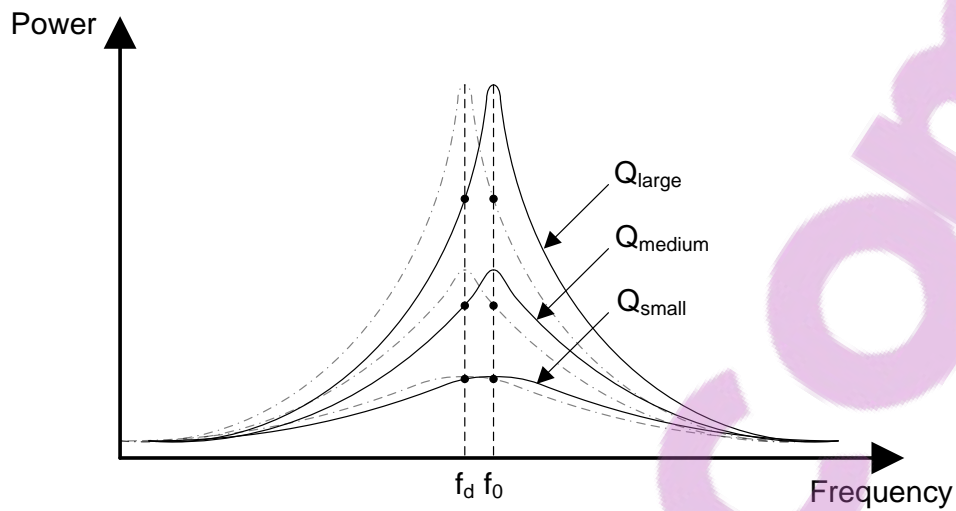


**Fig. 2-22: Power curve of parallel-tuned pickup with different  $Q$  factors**

The center frequency drift is used as an example to illustrate how the secondary output power gets affected by the parameter variations under different  $Q$  values. There are two major parameters that could cause the secondary power pickups to detune, and they are the secondary tuning capacitance and the primary operating frequency. Generally the tuning capacitance can be affected by the changes in ambient temperature during operations and causes the center frequency of the secondary resonant tank to drift from the nominal frequency  $f_0$  to  $f_d$  (or to similar position on the other side) [67]. The variations in primary operating frequency have similar detuning effect on the secondary power pickups. However, instead of having the same nominal frequency  $f_0$  and a drifted resonant tank frequency  $f_d$ , the actual nominal frequency  $f_0$  is shifted to  $f_d$  as shown in Fig. 2-22 with faded dashed-lines, and left the pickups being detuned from the position of the original nominal operating frequency. Depending on the value of  $Q$  factor, the power drop can be quite different. If the pickup is operating with low  $Q$ , the decrease in output power is almost negligible whereas the power drop becomes significant when the pickup is operating with high  $Q$ . In a practical IPT system design, the detuning of the pickup is unlikely to be avoided even the tuning circuit is fine-tuned to a constant primary operating frequency. Therefore, in order to prevent the system from having significant power drop, the  $Q$  factor is normally kept below 10 or sometimes even lower than that. Such a design allows the pickup to have better tolerance to some of the parameter variations but a lower voltage boosting capability is obtained as a trade-off.

### 2.4.3 Dynamic Tuning/Detuning Control

An alternate control method which has been investigated to improve the power flow control of IPT systems is the dynamic tuning/detuning control technique proposed in [68, 71, 94, 95]. Instead of fine-tuning the power pickups to obtain the maximum power and then controlling it to meet the load requirements, this control strategy regulates the pickup such that it only takes sufficient power required by the load. The fundamental concept here is similar to the frequency control of the primary track current that has been previously discussed. But the focus here is to dynamically change the tuning condition of the power pickups according to the actual load demands. Theoretically, if the maximum power is needed, the circuit will be capable of going to the tuned-point where the maximum power can be obtained, and lower output power is achieved by detuning the pickup circuit. The variable tuning conditions of the pickup is attained by deliberately putting a capacitor or an inductor in parallel with a fixed tuning capacitor. A basic dynamic tuning/detuning controlled pickup is shown in Fig. 2-23.

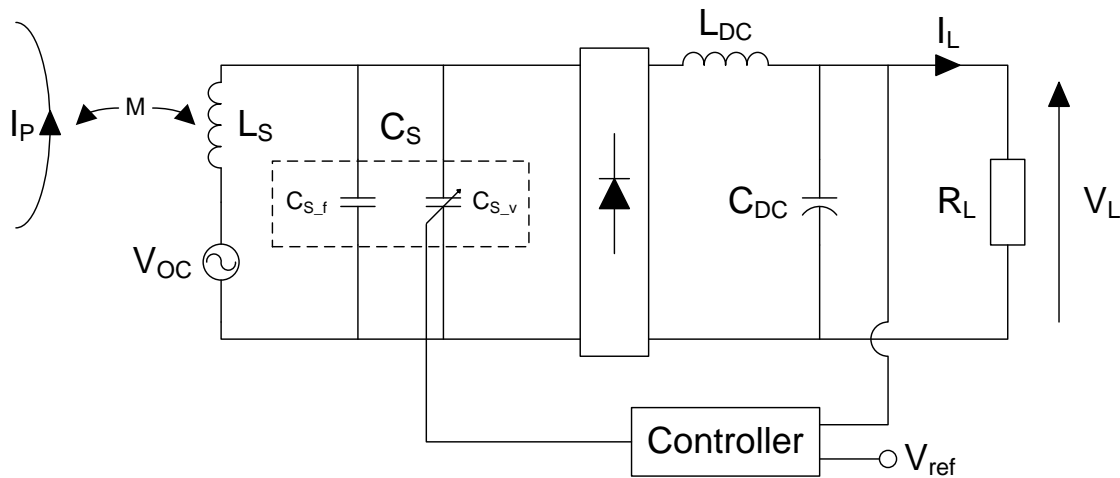


**Fig. 2-23: Power pickup with dynamic tuning/detuning control**

The figure above shows that the output voltage of the pickup is used as a feedback signal to the controller for comparing with a preset voltage reference  $V_{ref}$ . The comparison results are used for generating control signals to vary the capacitance of the variable capacitor. The tuning capacitance  $C_S$  in the resonant tank is the summation of the fixed tuning capacitor  $C_{S_f}$  and the variable tuning capacitor  $C_{S_v}$ . Hence by changing the value of the variable capacitor, the tuning condition of the pickup can be consequently changed

according to  $\omega_{s0} = 1/\sqrt{L_s(C_{s\_f} + C_{s\_v})}$ , where  $\omega_{s0}$  is the center frequency of the secondary resonant tank, and thereby tune/detune the power pickups to meet the actual load demands. A variable inductor can also be used to function as an equivalent variable tuning capacitance to achieve the same dynamic tuning/detuning control for the pickup. However the inductor introduces a positive reactance into the resonant tank and needs a controller design that is different from that of the actual variable tuning capacitance [68].

There are basically two ways to achieve a variable capacitor, one is by mechanically changing the electric coupling geometry of the moving and the stationary plates inside the capacitor to obtain different capacitances, and another is by using a semiconductor device to control the charging current of the capacitor that has a fixed value which has been commonly implemented in power systems for VAR controls [96, 97]. The former requires the capacitance to be changed off-line manually whereas the latter can vary the capacitance on-line through control signals. Therefore the capacitors controlled by semiconductor devices are preferable in the dynamic tuning/detuning control to function as a variable tuning capacitor.

By controlling the average charging current of a capacitor, a variable equivalent capacitance can be obtained. A PI controller is normally used for this type of control. Three different topologies are commonly employed for implementing the switching of the capacitors, and they are the hysteresis control, PWM control, and the linear control.

The hysteresis control and the PWM control are basically identical to the ones that have been previously discussed in the shorting-control. For these two control methods, the practical implementation can be achieved by either half-cycle topology or full-cycle topology. Figure 2-24 shows the configuration of these two topologies.

In the half-cycle topology, the charging current is controlled by switching on/off  $S_{DT1}$  and  $S_{DT2}$  simultaneously. When the switches are switched on, the current can continuously flow through and charges up the tuning capacitor. When the switches are turned off, the body-diodes of the switches block the current from flowing through the capacitor branch, and the voltage across the capacitors are maintained at a certain constant level given that the capacitors have already been partially charged. As soon as the resonant tank voltage decreases to a certain value, which is lower than the voltage across the capacitors, the

body diodes of the switches start being forward-biased and the energy of the capacitors gets discharged through this process. Since the half-cycle control only controls positive cycles of the resonant tank voltage for the variable tuning capacitor, the effective capacitance for a single variable capacitor is therefore halved and requires two branches as shown in the figure to achieve the full variable range that is originally provided by a single variable tuning capacitor.

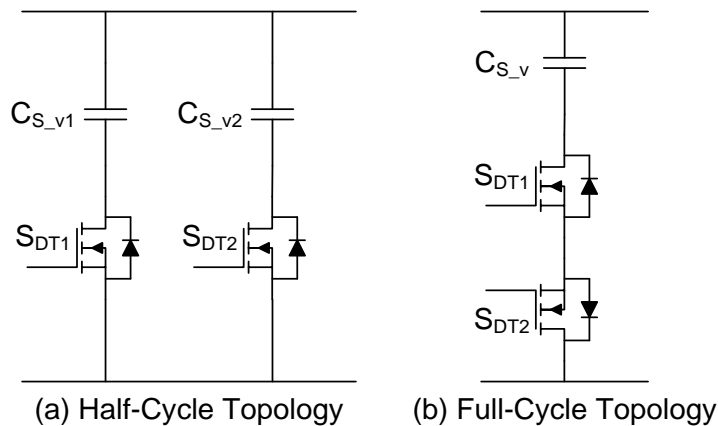


**Fig. 2-24: Configurations of switching capacitor**

Control concept of the full-cycle topology is similar to that of the half-cycle topology, except that the two switches  $S_{DT1}$  and  $S_{DT2}$  are used to have full control of the ac charging current for the tuning capacitor in both the positive and the negative cycles of the resonant tank voltage respectively. When  $S_{DT1}$  is on, the current is allowed to charge up the tuning capacitor without being blocked by switches or their body-diodes, and when  $S_{DT1}$  is off, the current stops flowing into the capacitor branch as the flowing path becomes an open-circuit. The working principle of  $S_{DT2}$  is identical to  $S_{DT1}$  with the only difference being the direction of charging current.

For the above two topologies, if the switching frequency is purely load dependent, i.e., using hysteresis control, without synchronizing to the natural oscillation frequency of the secondary resonant tank, it may cause high voltage and/or current stresses to the switches and results in high switching losses. The random switching noises caused by the hysteresis control also make the EMI filtering design difficult. However, these problems can all be improved by using the PWM control with the reasons that have been discussed. In the PWM control, soft-switching techniques for reducing the switching losses are also

achievable by using ZVD (Zero-Voltage Detection) across the switches or ZCD (Zero-Current Detection) across the body-diodes.

The third method of achieving switch-controlled variable capacitor, namely the linear control, is quite different from the previous two control methods. It also uses a semiconductor transistor to control the current flowing through the tuning capacitor, but instead of switching the capacitor in/out of the resonant tank, the semiconductor actually works in its linear region to function as a variable resistor. This way, the current flowing through the capacitor gets controlled according to the level of the switch's gate driving signal, and no switching harmonics will be generated during the control process.

A simplified model shown in Fig. 2-25 can be used to analyze the dynamically tuned/detuned power pickup without considering the ac-dc rectification.

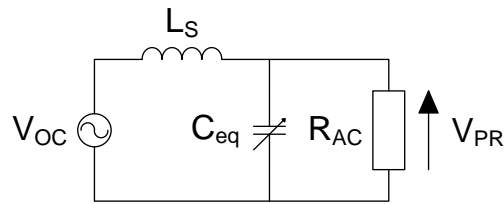


**Fig. 2-25: Simplified dynamic tuning/detuning power pickup model**

To maintain the output voltage constant, the equivalent tuning capacitance can be calculated according to [68]:

$$C_{eq} = C_{S0} \left( 1 - \frac{1}{Q_{S-p}} \sqrt{\left( \frac{Q_{S-p}}{k_{SV}} \right)^2 - 1} \right) \quad (2-38)$$

where  $C_{S0}$  is the original capacitance for full tuning and  $k_{SV}$  is the actual required boost factor from the open-circuit voltage  $V_{OC}$  to the output voltage  $V_{PR}$ . It can be seen that in order to have a valid solution,  $Q_{S-p}$  must be larger than  $k_{SV}$ , which is the maximum boost factor that a fully-tuned pickup can have. In the situation of the pickup being lightly loaded or no-load, the  $Q_{S-p}$  becomes infinity according to (2-15). The equivalent tuning capacitance reaches its minimum value and can be determined by [68]:

$$C_{eq} = \lim_{Q \rightarrow \infty} C_{S0} \left( 1 - \frac{1}{Q_{S-p}} \sqrt{\left( \frac{Q_{S-p}}{k_{SV}} \right)^2 - 1} \right) = C_{S0} \left( 1 - \frac{1}{k_{SV}} \right) \quad (2-39)$$

From (2-39), it can be seen that the minimum equivalent tuning capacitance varies in proportion to  $k_{SV}$ . The larger the voltage boosting factor  $k_{SV}$ , the smaller the capacitor tuning ratio which is needed. This is advantageous for pickups that are required to have high output voltage but with their pickup coil size being confined.

Since the fundamental concept of the dynamic tuning/detuning control is very similar to the frequency control of the track current in the primary power supply, therefore they have many common features. In a dynamic tuning/detuning controlled power pickup, the relationship between the tuning capacitance and the output power is also bell-shaped and results in two possible operating points with one being in the over-tuning region and the other in the under-tuning region. The over-tuning here means that the equivalent tuning capacitance of the pickup resonant circuit is controlled over the nominal value required by the fully-tuned condition, whereas the under-tuning means the equivalent tuning capacitance is controlled under the nominal value [66]. Figure 2-26 shows the relationship between the tuning capacitance and the pickup output power.

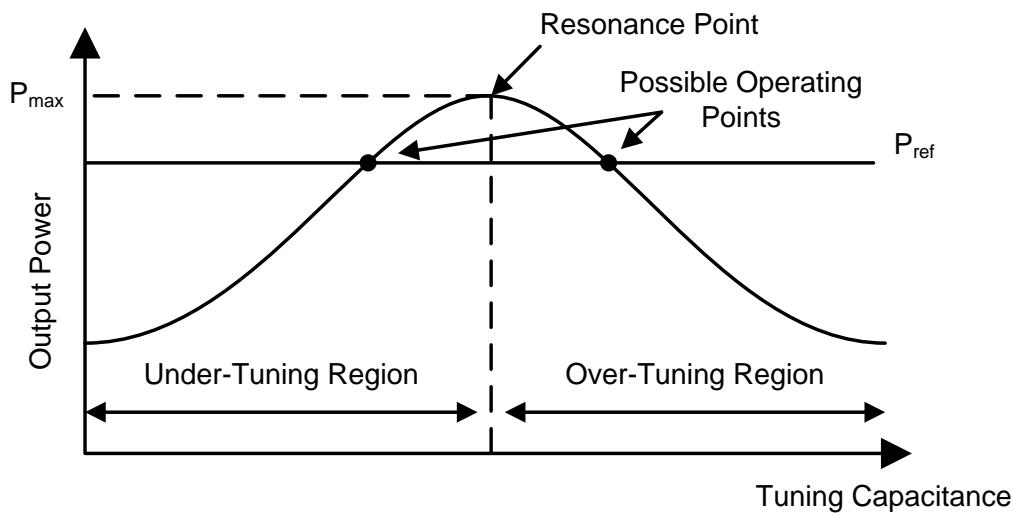


**Fig. 2-26: Relationship between tuning capacitance and output power of pickup**

After selecting one of the two operating points from the power curve and defining an operating range, a single-side tuning control method can be achieved. Due to the nature of



a PI controller is unable to perform tracking for a bell-shaped curve, it is difficult to use the dynamic tuning/detuning method to achieve maximum power transfer. An operating point close to the tuned-point is normally avoided to prevent the tracking process from traversing between the two tuning regions, and when the operating point shifts to the other region due to a vast or sudden circuit parameter change, the controller may track in the wrong direction and fail to regulate the pickup output power. As a result, the dynamic tuning/detuning method needs a controller that: 1) can adapt to the bell-shaped curve in order to overcome the reduced maximum power transfer capacity, and 2) be able to track the closest reference point along the power curve for achieving full-range tuning control.

## 2.5 Summary

A general overview of the complete IPT system and its existing power flow control methods have been undertaken in this chapter. All the major parts and associated control strategies have been discussed.

The primary track power supply is in its third generation up to date, with its G1 (First Generation) and G2 (Second Generation) power supplies developed based on the current-fed and the voltage-fed converters respectively. The G3 (Third Generation) power supplies are developed based on the properties enhanced version of the previous two generations, having  $\pi$  and T networks at the input of the resonant tank of the current-fed and voltage-fed converters respectively. The track power supply can be designed to have a fixed operating frequency but may cause high voltage and/or current stresses to the switches of the inverting network, or be variably controlled to follow the natural circuit resonance and enabling the soft-switching operation for higher power efficiency.

The secondary power pickups are magnetically coupled to the primary track and the coupling degree can be measured by a term called coupling factor. Two different types of tuning circuits are commonly used for the compensation of induced emf in the pickup coil, and they are the series tuning circuit and the parallel tuning circuit. In a series-tuned pickup, the load is voltage sourced and very advantageous to be used in IPT applications where a constant output voltage is required. However, the parallel-tuned pickup has gained its popularity owing to its voltage boosting capability which allows the pickup to operate

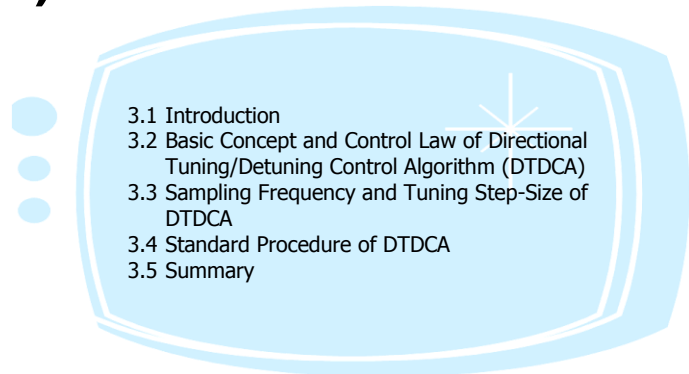
with the primary current track from a further distance, but it requires an effective power flow control to cope with the output voltage fluctuation that caused by the load variations.

The power flow control of the IPT systems can either be applied in the primary track power supply or the secondary power pickups. By applying the power flow control in the primary side of the IPT system, two strategies are commonly used which are the magnitude and the frequency control of the track current. Both the methods can be used to effectively control the pickup output power to meet the load demands. However they cannot be applied in multiple pickups systems since a primary track power supply can only be designed to compensate for parameter variations of a specific power pickup. In addition, the adopted PI controller is incapable of covering the full bell-shaped frequency control range; therefore the power flow control can only be achieved in a selected tuning region.

To simultaneously operate with multiple pickups using single track power supply, it is necessary to perform the power flow control to each pickup individually. Three different methods being voltage regulator, shorting-control, and the dynamic tuning/detuning control, are used for this purpose. The methods using voltage regulator and shorting-control are easy to design and implement, but they have low immunity to multiple circuit parameter variations. Both of them also suffer from low power efficiency particularly under light-load or no-load conditions, and may require large heat sinks for the excessive power dissipation which increases the size and cost of the IPT system. The dynamic tuning/detuning control is designed to tune or detune the power pickups so they only receive sufficient power from the primary track current for meeting the load demands. It is more power efficient in terms of the individual secondary pickup, but also suffers from the incapability of covering the full control range that happens in the frequency control of the primary track current, therefore results in only single-side control with reduced maximum power transfer capacity.

## Chapter 3

# Directional Tuning/Detuning Control Algorithm (DTDCA)



---

### 3.1 Introduction

In Chapter 2, two different tuning configurations and three popular control methods have been proposed in the past for controlling the power flow of the IPT systems [21, 62, 68, 91]. Each of them has clear advantages and drawbacks which need to be improved either structurally or algorithmically for providing better control results against possible circuit parameter variations. In this chapter, a novel control method, called as Directional Tuning/Detuning Control Algorithm (DTDCA) is proposed to solve the problems associated with the existing control schemes. The main objective of the proposed control algorithm is to provide constant output voltage and deliver the power required by the load. The concept of DTDCA is to perform smart tuning for the power pickup so that the power pickup circuit can change the tuning condition according to the load demands, as well as be able to cover both the under-tuning and over-tuning regions to achieve full-range tuning control.

### 3.2 Basic Concept and Control Law of Directional Tuning/Detuning Control Algorithm (DTDCA)

Because the output voltage behaviors of power pickups exhibit a bell-shaped relationship with the tuning components of the resonant circuit, a normal PI controller can only

provide a single-side tuning control with a monotonic trend, rather than achieving full-range control along a turning curve [66]. A novel control algorithm called DTDC (Directional Tuning/Detuning Control) is developed here to solve the problem, so a full-range control can be achieved against parameter variations to keep the output voltage of the pickup to be constant at a desired level.

In order to develop a controller having the capability of regulating the output voltage of the pickup under different operating conditions, all possible correct tracking processes on the tuning curve need to be thoroughly studied and compared.

The tuning curve has been divided into four different operating regions such as A, B, C, and D as shown in Fig. 3-1. Each operating region of the tuning curve is defined as follows:

- Region A -  $V(t_n) < V_{ref}$ , and the pickup is operating in the under-tuning region.
- Region B -  $V(t_n) > V_{ref}$ , and the pickup is operating in the under-tuning region.
- Region C -  $V(t_n) > V_{ref}$ , and the pickup is operating in the over-tuning region.
- Region D -  $V(t_n) < V_{ref}$ , and the pickup is operating in the over-tuning region.

Note that the operating points shown in Fig. 3-1 are corresponding to different values of tuning inductance/capacitance, and by changing the tuning inductance/capacitance the operating point can be shifted and this results in different output voltages. For example, by shifting operating point from  $P_1$  to  $P_2$ , the output voltage will change from  $V(t_1)$  to  $V(t_2)$ . The tracking process in these regions is divided into coarse tuning stage and fine tuning stage. The coarse tuning stage takes place immediately after the initialization of the controller (start-up of the pickup circuit) or when the output voltage is considerably deviated from the reference voltage. Once the output voltage reaches around the reference voltage, the circuit will be fine-tuned to approach it.

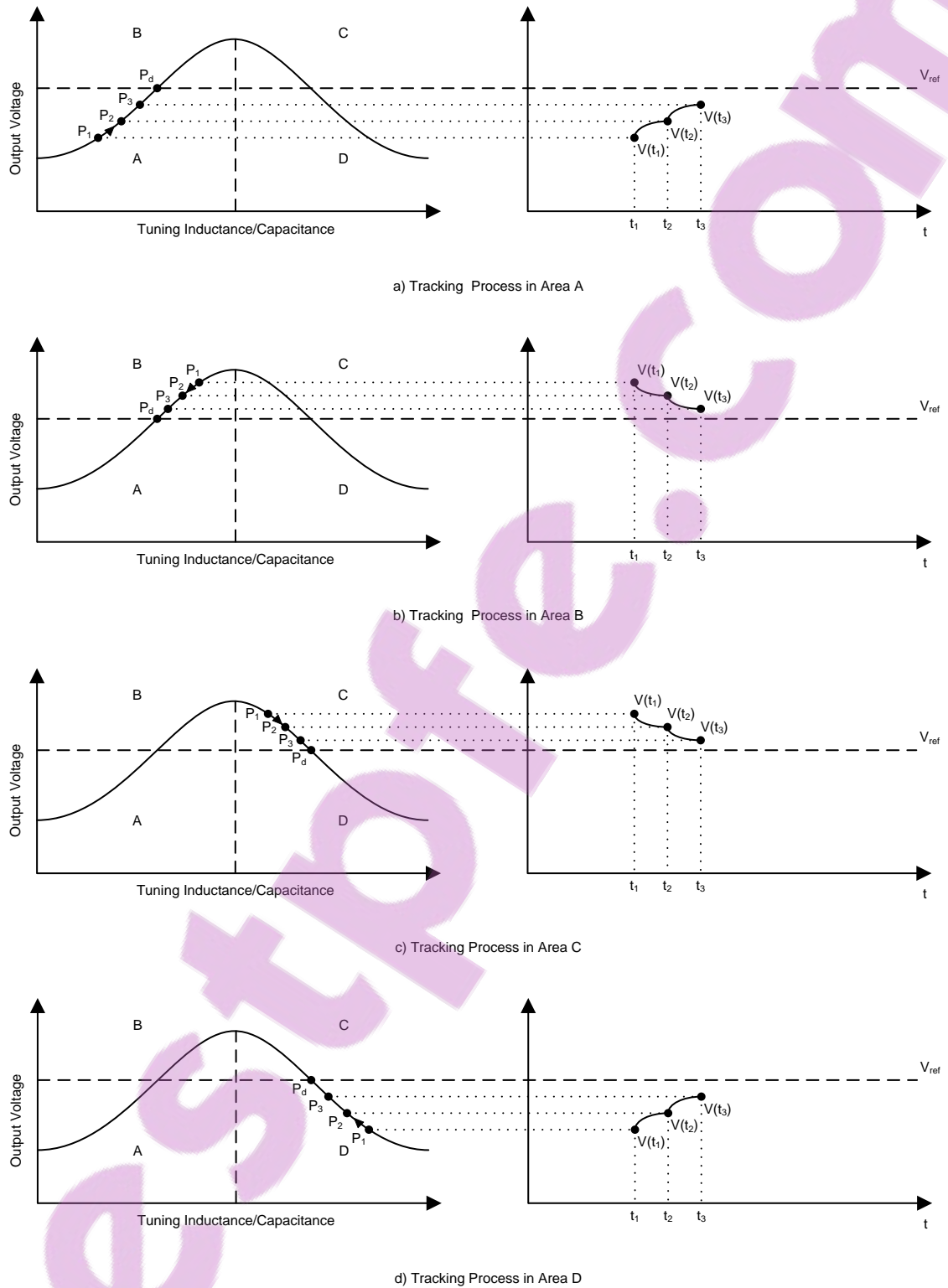


**Fig. 3-1: Tracking process of coarse tuning stage in different areas of output voltage tuning curve and corresponding time-domain results**

**Coarse tuning in region A**

The tracking process in the region A can be clearly observed from the time-domain illustration of Fig. 3-1 a). It can be seen that between any two successful sampling instances, if the voltage lies exclusively in one of the operating regions, the sign of the error remains unchanged. For example, if between two successful sampling instances  $t_1$  and  $t_2$  the voltage  $V(t_1)$  and  $V(t_2)$  are in the same operating region A, then the error remains positive. Therefore the error signal defined as:

$$e(t_n) = V_{ref} - V(t_n) \quad (3-1)$$

where  $t_n$  is the sampling instance, is always positive in the region A, and this error goes on decreasing as time progresses. In addition, the rate of error defined as:

$$\dot{e}(t_n) = e(t_n) - e(t_{n-1}) \quad (3-2)$$

is always negative in this region. To obtain a correct tracking in the region A to bring the operating point  $P_1$  to  $P_d$ , the tuning parameter, e.g., T.L/C (Tuning Inductance or Capacitance) should be increased from the initial starting point to the value which corresponds to the desired output voltage.

**Coarse tuning in region B**

In the region B, it can be seen from Fig. 3-1 b) that the error signal is always negative and decreases in terms of magnitude as time progresses. The rate of error in this case is always positive. To perform a correct tracking in the region B, the T.L/C needs to be decreased from point  $P_1$  to  $P_d$ .

**Coarse tuning in region C**

In the region C, the error signal which has been observed from Fig. 3-1 c) is always negative and decreases in terms of magnitude as time progresses. The rate of error in this case is always positive. It can be seen that the error and rate of error are identical in both region B and C, and the only difference between them is that to perform a correct tracking in the region C, the T.L/C needs to be increased from point  $P_1$  to  $P_d$ .

### **Coarse tuning in region D**

In the region D, the error signal which has been observed from Fig. 3-1 d) is always positive and decreases as time progresses. The rate of error in this case is always negative. It can be seen that the error and rate of error are identical in both region A and D, and the only difference between them is that to perform a correct tracking in the region D, the T.L/C needs to be decreased from point  $P_1$  to  $P_d$ .

Figure 3-2 shows where the fine tuning stage occurs in the output voltage tuning curve and how it appears in the time-domain. As it can be seen, the fine tuning process can occur between any two possible operating points shown in the figure. Note that the coarse tuning stage and fine tuning stage are represented by the shaded and un-shaded area (€) respectively. The area € is a variable which its position and size are dependent on the positions of  $P_1$  and  $P_2$ .

### **Fine tuning between region A and B**

The term ‘fine tuning stage’ here means the controller is at a phase where it has just ended the tracking process of coarse tuning stage (shaded area) and started to fine tune the circuit to reach the reference point within the area €. In the tracking process of fine tuning stage between the region A and B, there are two possible situations that needs to be considered, i.e., whether the operating point is approaching towards the reference from region A or from region B.

#### **A to B**

If the two consecutively sampled voltages are taken from region A across to region B, a negative error and a positive error are always obtained at the two successful sampling instances  $t_n$  and  $t_{n-1}$ , respectively. The rate of error under such a condition is always negative for both the illustrations shown in Fig. 3-2 a) and b) between  $t_1$  and  $t_2$ . The correct tuning action for this particular case is to decrease T.L/C.

#### **B to A**

On the other hand, if the two consecutively sampled voltages are taken from region B across to region A as shown in Fig. 3-2 a) and b) between  $t_1'$  and  $t_2'$ , a positive error and a negative error are always obtained at the two successful sampling instances  $t_n$  and  $t_{n-1}$ ,

respectively. The rate of error under such a condition is always positive. The correct tuning action for this particular case is to increase T.L/C.

### ***Fine tuning between region C and D***

In the tracking process of fine tuning stage between the region C and D, it can also be separated into two different situations depending on which direction the operating points are approaching the reference either from region C or D.

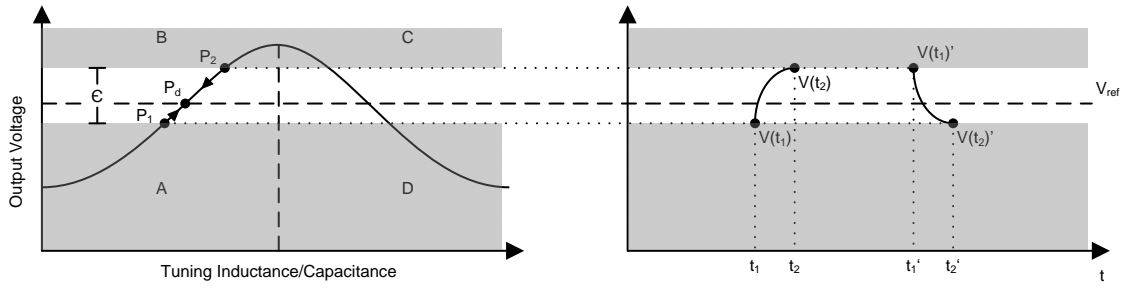
#### **D to C**

If the two consecutively sampled voltages are taken from region D across to region C, a negative error and a positive error are always obtained at the two successful sampling instances  $t_n$  and  $t_{n-1}$ , respectively. The rate of error under such a condition is always negative for both the illustrations shown in Fig. 3-2 c) and d) between  $t_1$  and  $t_2$ . The correct tuning action for this particular case is to increase T.L/C.

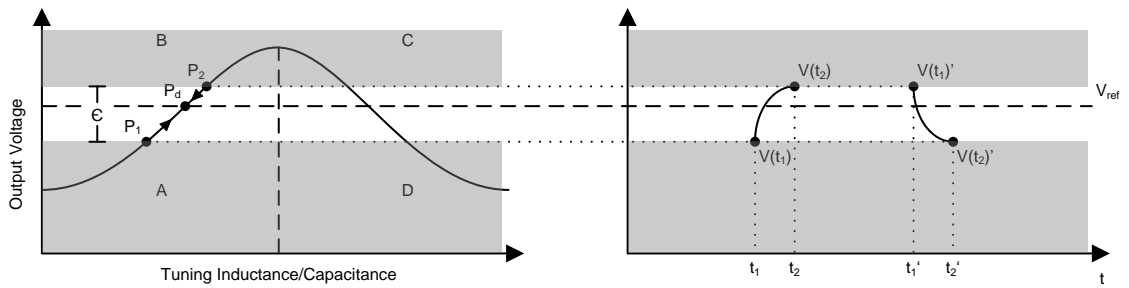
#### **C to D**

And if the two consecutively sampled voltages are taken from region C across to region D as shown in Fig. 3-2 c) and d) between  $t_1'$  and  $t_2'$ , a positive error and a negative error are always obtained at the two successful sampling instances  $t_n$  and  $t_{n-1}$ , respectively. The rate of error under such a condition is always positive. The correct tuning action for this particular case is to decrease T.L/C.

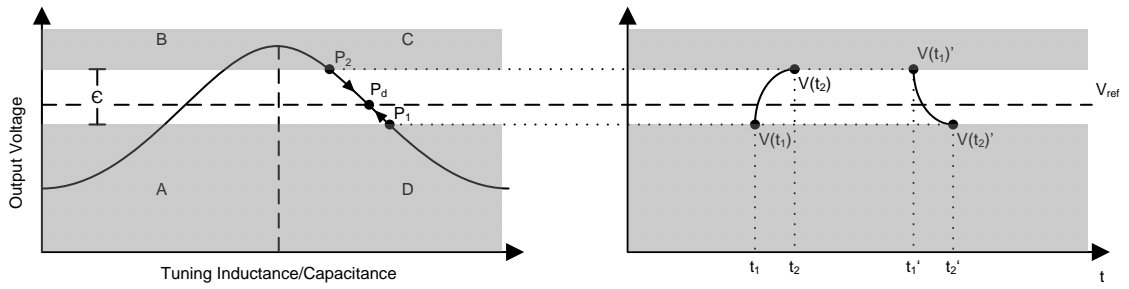




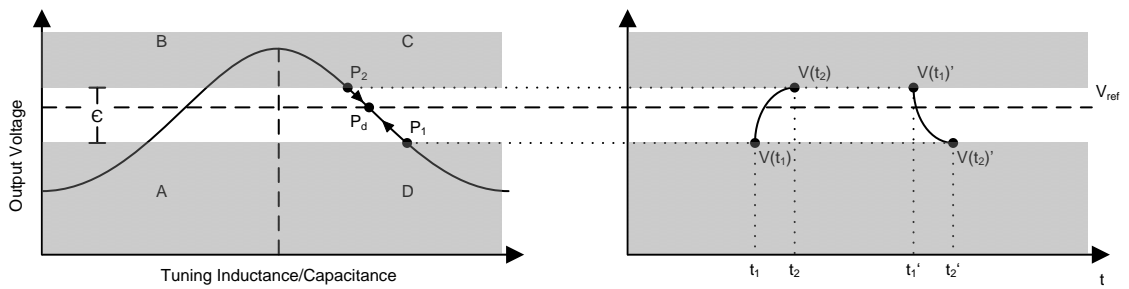
a) Tracking Process between Area A and B having  $|e(t_2)| > e(t_1)$  or  $e(t_2)' < |e(t_1)'|$



b) Tracking Process between Area A and B having  $|e(t_2)| < e(t_1)$  or  $e(t_2)' > |e(t_1)'|$



c) Tracking Process between Area C and D having  $|e(t_2)| > e(t_1)$  or  $e(t_2)' < |e(t_1)'|$



d) Tracking Process between Area C and D having  $|e(t_2)| < e(t_1)$  or  $e(t_2)' > |e(t_1)'|$

**Fig. 3-2: Tracking process of fine tuning stage in different areas of output voltage tuning curve and corresponding time-domain results**

**Table 3-1: Results in tracking process of coarse and fine tuning stages**

<b>Coarse Tuning</b>	$e(t_n) > e(t_{n-1})$	$\dot{e}(t_n)$	$V(t_n) > V(t_{n-1})$	$T.L/C(t_n) > T.L/C(t_{n-1})$
<i>Region A</i>	0	-ve	1	1
<i>Region B</i>	1	+ve	0	0
<i>Region C</i>	1	+ve	0	1
<i>Region D</i>	0	-ve	1	0
<b>Fine Tuning</b>				
<i>Region A-to-B Outcome1</i>	0	-ve	1	0
<i>Region B-to-A Outcome1</i>	1	+ve	0	1
<i>Region C-to-D Outcome1</i>	1	+ve	0	0
<i>Region D-to-C Outcome1</i>	0	-ve	1	1

Table 3-1 summarizes the results in the tracking process of coarse and fine tuning stages. Comparisons have been made between similar operations as follows: region of A and D, region of B and C, region of A-to-B and D-to-C, and region of B-to-A and C-to-D. It has been found that the error in the region A and D is always positive whereas it is negative in region B and C. In addition, the rate of error in the region A and D is always negative whereas it is positive in region B and C. It is therefore impossible to distinguish the difference between the pickup being operated in region A and D or region B and C by using the error signal alone. However, by using the immediate past tuning result, it is possible to distinguish the exact operating region of the pickup. The following conditions are given for determining the operating region of the pickup:

- Region A:  $V(t_n) < V_{ref}$  and  $T.L/C(t_n) > T.L/C(t_{n-1})$  and  $V(t_n) > V(t_{n-1})$ , or  $V(t_n) < V_{ref}$  and  $T.L/C(t_n) < T.L/C(t_{n-1})$  and  $V(t_n) < V(t_{n-1})$ .
- Region B:  $V(t_n) > V_{ref}$  and  $T.L/C(t_n) > T.L/C(t_{n-1})$  and  $V(t_n) > V(t_{n-1})$ , or  $V(t_n) > V_{ref}$  and  $T.L/C(t_n) < T.L/C(t_{n-1})$  and  $V(t_n) < V(t_{n-1})$ .
- Region C:  $V(t_n) > V_{ref}$  and  $T.L/C(t_n) > T.L/C(t_{n-1})$  and  $V(t_n) < V(t_{n-1})$ , or  $V(t_n) > V_{ref}$  and  $T.L/C(t_n) < T.L/C(t_{n-1})$  and  $V(t_n) > V(t_{n-1})$ .

- Region D:  $V(t_n) < V_{ref}$  and  $T.L/C(t_n) > T.L/C(t_{n-1})$  and  $V(t_n) < V(t_{n-1})$ , or  $V(t_n) < V_{ref}$  and  $T.L/C(t_n) < T.L/C(t_{n-1})$  and  $V(t_n) > V(t_{n-1})$ .

From the above conditions, it can be seen that the under-tuning and over-tuning regions are differentiated by the immediate past tuning result in terms of the tuning direction of the T.L/C and moving direction of the output voltage. In addition, the upper and lower regions of each tuning region are differentiated by their relative position to the reference voltage. To correctly track the desired output voltage from different operating regions of the tuning curve, the possible operating conditions are given as:

- Condition 1: If  $V(t_n) < V_{ref}$  and  $T.L/C(t_n) < T.L/C(t_{n-1})$  and  $V(t_n) < V(t_{n-1})$ , then  $T.L/C(t_{n+1})$  should be increased.
- Condition 2: If  $V(t_n) < V_{ref}$  and  $T.L/C(t_n) > T.L/C(t_{n-1})$  and  $V(t_n) < V(t_{n-1})$ , then  $T.L/C(t_{n+1})$  should be decreased.
- Condition 3: If  $V(t_n) < V_{ref}$  and  $T.L/C(t_n) < T.L/C(t_{n-1})$  and  $V(t_n) > V(t_{n-1})$ , then  $T.L/C(t_{n+1})$  should be decreased.
- Condition 4: If  $V(t_n) < V_{ref}$  and  $T.L/C(t_n) > T.L/C(t_{n-1})$  and  $V(t_n) > V(t_{n-1})$ , then  $T.L/C(t_{n+1})$  should be increased.
- Condition 5: If  $V(t_n) > V_{ref}$  and  $T.L/C(t_n) < T.L/C(t_{n-1})$  and  $V(t_n) < V(t_{n-1})$ , then  $T.L/C(t_{n+1})$  should be decreased.
- Condition 6: If  $V(t_n) > V_{ref}$  and  $T.L/C(t_n) > T.L/C(t_{n-1})$  and  $V(t_n) < V(t_{n-1})$ , then  $T.L/C(t_{n+1})$  should be increased.
- Condition 7: If  $V(t_n) > V_{ref}$  and  $T.L/C(t_n) < T.L/C(t_{n-1})$  and  $V(t_n) > V(t_{n-1})$ , then  $T.L/C(t_{n+1})$  should be increased.
- Condition 8: If  $V(t_n) > V_{ref}$  and  $T.L/C(t_n) > T.L/C(t_{n-1})$  and  $V(t_n) > V(t_{n-1})$ , then  $T.L/C(t_{n+1})$  should be decreased.

By summarizing the above possible operating conditions and categorizing the results once again into the coarse tuning stage and the fine tuning stage, a truth table for determining the tuning direction of T.L/C can be given as shown in Table 3-2.

**Table 3-2: Truth table for determining tuning direction signal  $S_4$**

<i>Coarse Tuning</i>	$V(t_n) > V_{ref}$ $S_1(t_n)$	$V(t_n) > V(t_{n-1})$ $S_2(t_n)$	$T.L/C(t_n) > T.L/C(t_{n-1})$ $S_3(t_n)$ or $S_4(t_{n-1})$	$T.L/C(t_{n+1}) > T.L/C(t_n)$ $S_4(t_n)$
<i>A (Cond. 4)</i>	0	1	1	1
<i>B (Cond. 5)</i>	1	0	0	0
<i>C (Cond. 6)</i>	1	0	1	1
<i>D (Cond. 3)</i>	0	1	0	0
<b><i>Fine Tuning</i></b>				
<i>A-to-B (Cond. 8)</i>	1	1	1	0
<i>B-to-A (Cond. 1)</i>	0	0	0	1
<i>C-to-D (Cond. 2)</i>	0	0	1	0
<i>D-to-C (Cond. 7)</i>	1	1	0	1

Instead of purely depending on the error signals to generate the control signals as the conventional PI controllers do, the proposed controller is developed based on the result of Table 3-2, which has also included the validity of the previous control action into considerations. To further simplify the results in Table 3-2, a Boolean expression can be derived as:

$$S_4 = S_3(S_1 \oplus S_2) + \overline{S_3}(S_1 \equiv S_2) \quad (3-3)$$

where  $S_4$  is the signal in the control algorithm for determining the tuning direction with logic 1 to increase or logic 0 to decrease the T.L/C. The actual output signal of the controller can therefore be expressed by:

$$U(t_n) = U(t_{n-1}) + (-1)^{S_4+1} \cdot \Delta H(t_n) \quad (3-4)$$

where  $U(t_n)$  is the present-state control signal,  $U(t_{n-1})$  is the previous-state control signal, and  $\Delta H(t_n)$  is the step-size of the adjustment in the present-state. The practical implementation of the proposed DTDCA for changing the T.L/C of the pickup will be discussed in Chapter 4 and Chapter 6.

### 3.3 Sampling Frequency and Tuning Step-Size of DTDCA

After each tuning action in the pickup tuning circuit, the circuit would require certain time period (time constant of pickup circuit) for the output voltage to stabilize. Since the complete effect of each control action on the output voltage is required to be fully observed for a proper validity check before the controller can take the next step, the controller therefore has to wait for the pickup circuit to reach its steady state. This makes the selection of sampling frequency for the controller to read the output voltage very important as it may significantly affect the controller performance. Because the time constant of different pickups with different configurations and parameters, may be different, the selection of sampling frequency will need to be determined individually. In this thesis, the sampling frequency of the proposed controller will be separately determined for the LCL and the parallel LC power pickups.

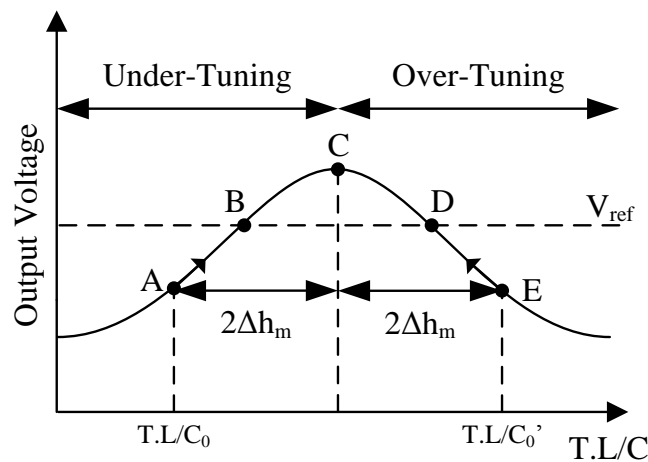


Fig. 3-3: Relationship between T.L/C and pickup output voltage

The performance of the proposed controller is not only dependent on the sampling frequency for the output voltage detection, but also on the tuning step-size of the controller when it takes tuning actions. The relationship between the T.L/C and the pickup output voltage is shown in Fig. 3-3. From Fig. 3-3, it can be seen that the output voltage can be controlled by operating the pickup in either in the under-tuning or over-tuning region from the initial operating point A or E, corresponding to the initial T.L/C of  $T.L/C_0$  or  $T.L/C_0'$ . For the DTDCA to perform an efficient control so the operating point can be stabilized to the desired voltage with the shortest tuning distance, the operating points of

the circuit should not jump across the two regions during any two consecutive samples. At the initial controller startup, this can be ensured if the value of each tuning adjustment does not exceed a maximum T.L/C variation range  $\Delta h_m$ . This can vary, depending on the circuit characteristics and dynamic performance required. But its theoretical maximum should be confined between the initial operating point ( $A$  or  $E$ ) and the maximum point ( $C$ ). However, since the tuning relationship between the T.L/C and the output voltage may still be varied by the circuit parameter variations, the value of  $\Delta h_m$  therefore will also need to be determined under extreme operating conditions for both the LCL and the LC power pickups in order to cover all possible operations.

Once the maximum tuning step-size is determined, the controller can use it as a coarse tuning adjustment but should also be able to perform fine tuning since the performance of the controller is critically dependent on the step change of T.L/C ( $\Delta h$ ). A large fixed value of  $\Delta h$  can make the system respond faster; but this may cause the output voltage to have large oscillations around the reference voltage. Conversely, a small fixed value of  $\Delta h$  makes the system sluggish but leads to a more stable output. A judicious compromise between these two is needed to avoid output chattering and still obtain a reasonably fast response. This can be obtained by adaptively changing  $\Delta h$  at each sampling instant  $t_n$  as follows:

If the output voltage does not oscillate around the reference point ( $|e(t_n)| > \epsilon$ , see Fig. 3-2), then  $\Delta h$  is kept constant at the predefined maximum step  $\Delta h_m$ . Contrary, when the output voltage oscillates around the reference ( $|e(t_n)| \leq \epsilon$ ),  $\Delta h$  is changed according to:

$$\begin{cases} \Delta h(t_n) = \Delta h_m = \alpha \cdot \Delta H_m & \text{Coarse tuning} \\ \Delta h(t_n) = \Delta h = \alpha \cdot [\Delta H(t_{n-1}) - \beta \cdot \Delta H_m] & \text{Fine tuning} \end{cases} \quad (3-5)$$

where  $\alpha$  is a scaling factor (depending on the physical controller design) between the step-size of control signal  $\Delta H$  and the physical tuning step-size  $\Delta h$ , and  $\beta$  is a scaling factor less than one.

The above introduced method is called Simple Step-Size Adjustment (SSSA) since it is based on a very simple and straight forward method on changing the tuning step-size of the controller. The determination for the value of  $\beta$  is however difficult since the pickup

circuit behavior may be constantly changing due to the circuit parameter variations. Therefore, it can only be designed through heuristic method.

The decision on whether the controller should be performing coarse tuning or fine tuning is purely dependent on  $S_1$  and  $S_2$  at any two consecutive sampling instances. If the controller is in the coarse tuning stage which requires the tuning step-size with coarse tuning value, then the logic signal  $S_1S_2$  (from Table 3-2) should be either 01 or 10 at any two consecutive sampling instances. Contrary if the controller is in the fine tuning stage which requires the tuning step-size with fine tuning value, then  $S_1S_2$  should be switching between 00 and 11 at any two consecutive sampling instances. Under such an assumption, the control result of applying SSSA can lead to two different outcomes which are the ideal control result and the indefinite control result. Figure 3-4 shows the two possible outcomes when the SSSA is applied. It can be seen from Fig. 3-4 a) that if an ideal control result is obtained, the controller would bring the output voltage gradually towards  $V_{ref}$  and eventually reaches  $V_{ref}$  by reducing the tuning step-size according to (3-5). The reduction in the tuning step-size occurs at each time that the output voltage traverses the voltage reference.

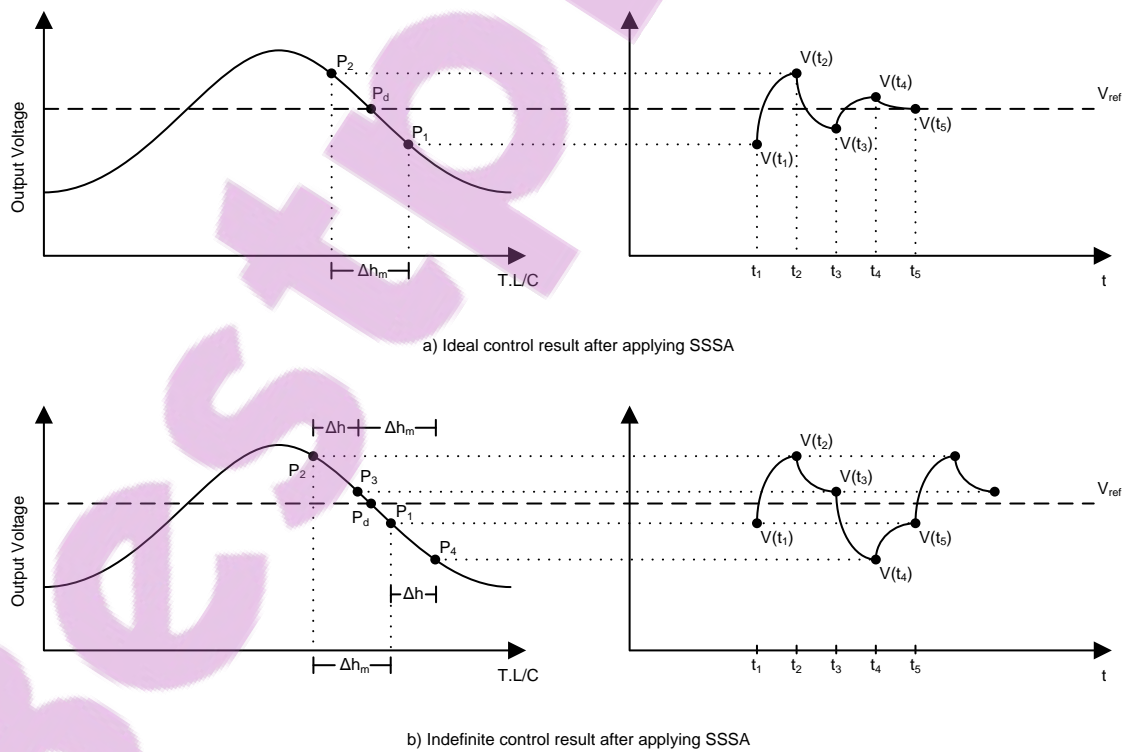


Fig. 3-4: Possible control results after applying SSSA

The second possible outcome is shown in Fig. 3-4 b). It can be observed from the figure that the controller reduces the tuning step-size ( $\Delta h_m$  to  $\Delta h$ ) at  $t_2$  since the output voltage has entered the fine tuning stage, which allows the output voltage at the next time instance move towards the voltage reference ( $P_2$  to  $P_3$ ). However, as the output voltage at  $t_3$  does not traverse the voltage reference but stays above it, the controller switches back to the coarse tuning mode and uses  $\Delta h_m$  as the tuning step-size. The mode switching then results in an infinite looping between the coarse tuning and fine tuning stage of the control algorithm and the output voltage can never reach to the desired value, which eventually leads to an indefinite control result. In order to solve this problem, a prior knowledge about whether the output voltage has entered the fine tuning stage or not is required so that the tuning step-size can be adjusted correctly.

**Table 3-3: Truth table for  $\Delta h$  adjustment determination ( $S_7$ )**

<i>Possible Cases</i>	$V(t_n) > V_{ref}$ $S_1(t_n)$	$V(t_n) > V(t_{n-1})$ $S_2(t_n)$	$V(t_{n-1}) > V_{ref}$ $S_5(t_n)$	$V(t_{n-2}) > V_{ref}$ $S_6(t_n)$	$S_7(t_n)$
Case 1	0	0	0	0	1
Case 2	0	0	0	1	1
Case 3	0	0	1	0	0
Case 4	0	0	1	1	0
Case 5	0	1	0	0	1
Case 6	0	1	0	1	0
Case 7	0	1	1	0	N/A
Case 8	0	1	1	1	N/A
Case 9	1	0	0	0	N/A
Case 10	1	0	0	1	N/A
Case 11	1	0	1	0	0
Case 12	1	0	1	1	1
Case 13	1	1	0	0	0
Case 14	1	1	0	1	0
Case 15	1	1	1	0	1
Case 16	1	1	1	1	1

Table 3-3 shows the determination of  $\Delta h$  adjustment. From Table 3-3, all possible cases are categorized into three different categories as below:



**Category I**

This includes case 1, 2, 15, and 16. Regardless of the result of  $S_6$ , the signal  $S_1$ ,  $S_2$ , and  $S_5$  have implied that the tuning direction from the previous control action is incorrect and therefore requires  $\Delta h$  to have the coarse tuning value (represented by logic 1) in the present state.

**Category II**

This includes case 3, 4, 13, and 14. Regardless of the result of  $S_6$ , the signal  $S_1$ ,  $S_2$ , and  $S_5$  have implied that the output voltage has entered the fine tuning stage and therefore requires  $\Delta h$  to have the fine tuning value (represented by logic 0) in the present state.

**Category III**

This includes case 5, 6, 11, and 12. The signal  $S_1$ ,  $S_2$ , and  $S_5$  in this category have shown that the tuning direction from the previous control action is correct, and whether the controller is in the coarse tuning or fine tuning stage is completely dependent on the location of  $V(t_{n-2})$ . As a result, both the case 5 and 12 belong to tracking stage and therefore requires  $\Delta h$  to have the coarse tuning value in the present state. Conversely, the case 6 and 11 belong to fine tuning stage and hence requires  $\Delta h$  to have the fine tuning value in the present state.

Note that the result of case 7, 8, 9, and 10 are marked with N/A; since these cases are impossible to happen. By summarizing the obtained result in Table 3-3, a Boolean expression for determining whether the pickup should be coarse-tuned or fine-tuned (logic 1 for coarse tuning and logic 0 for fine tuning) can be derived as:

$$S_7 = (S_1 \equiv S_2 \equiv S_5) + (S_1 \equiv S_5 \equiv S_6) \quad (3-6)$$

### 3.4 Standard Procedure of DTDCA

To effectively control the output voltage of the pickup using the proposed DTDCA, a standard procedure for executing the algorithm has been recommended as shown in Fig. 3-5. The proposed DTDCA can be implemented by using a standard embedded controller such as PSoc (Programmable System-on-Chip).

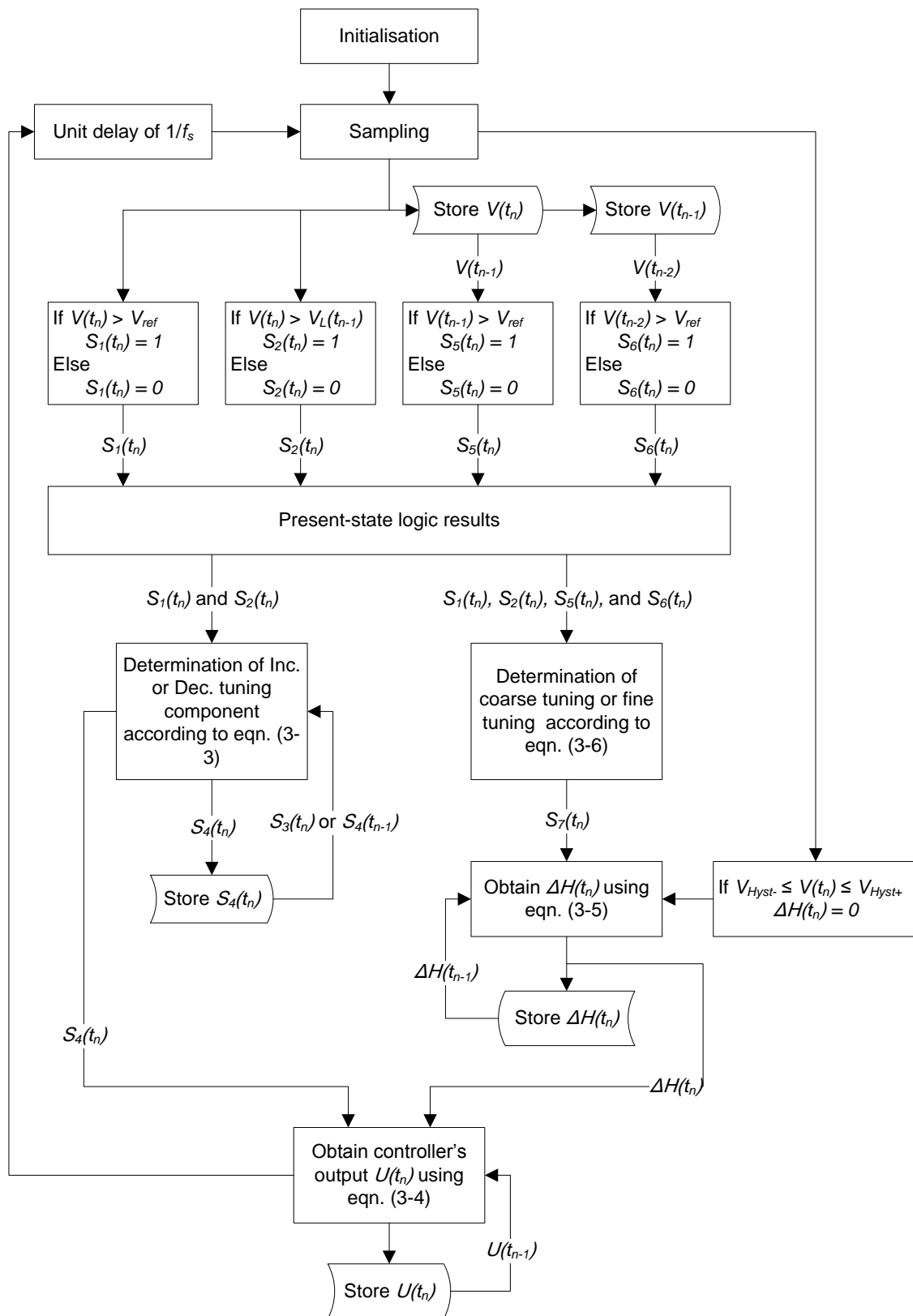


Fig. 3-5: Flowchart of standard procedure of DTDCA

The procedure starts with the initialization of the algorithm. In this process, the controller initializes the settings according to the user specifications and the system characteristic that the controller is applied to. These include sampling time of the controller, initial state of each processing block (shown in the square blocks), maximum increment (or decrement) level of the controller's output, and the hysteresis band around the voltage reference.

After the initialization, the first sampled output voltage  $V(t_n)$  will be stored in the memory blocks with an unit delay in each one of them before outputting to the next processing block, and this allows the controller to still have the memory of the present output voltage after two executions of the algorithm. For example,  $V(t_n)$  will become  $V(t_{n-1})$  in the first memory block after the first execution and then become  $V(t_{n-2})$  in the second memory block after the second execution. Note that in order to perform a proper tracking process at the initial stage, the controller should not provide tuning actions to the pickup anytime before the third execution of the algorithm since the knowledge of  $V(t_{n-1})$  and  $V(t_{n-2})$  are still lacking in the first and second execution. Assuming that the value of  $V(t_{n-1})$  and  $V(t_{n-2})$  are properly stored in the memory blocks after executions of the algorithm, the present sampled output voltage  $V(t_n)$  will be compared with  $V_{ref}$  and  $V(t_{n-1})$  to generate the logic signals of  $S_1(t_n)$  and  $S_2(t_n)$  respectively, and  $V(t_{n-1})$  and  $V(t_{n-2})$  will be compared with  $V_{ref}$  to generate the logic signals of  $S_5(t_n)$  and  $S_6(t_n)$  respectively.

The obtained logic signals of  $S_1(t_n)$ ,  $S_2(t_n)$ ,  $S_5(t_n)$ , and  $S_6(t_n)$  are used in two different branches of the algorithm in the next stage. The left branch is used for determining the tuning direction of the pickup, and it uses  $S_1(t_n)$ ,  $S_2(t_n)$ , and  $S_3(t_n)$  to determine the logic signal  $S_4(t_n)$  which has an output of 1 for increasing or 0 for decreasing the value of the controlled tuning component. Note that  $S_3(t_n)$  is based on the previous result of  $S_4(t_n)$  which has been stored in the memory block and delayed by one unit. The right branch is used for determining the value of  $\Delta H(t_n)$ , and it uses  $S_1(t_n)$ ,  $S_2(t_n)$ ,  $S_5(t_n)$ , and  $S_6(t_n)$  to determine the logic signal  $S_7(t_n)$  which has an output of 1 for coarse or 0 for fine tuning the pickup. The obtained  $S_7(t_n)$  will then be passed onto the next processing block for calculating the actual value of  $\Delta H(t_n)$  according to (3-5). Note that the value of  $\Delta H(t_n)$  may be based on  $\Delta H(t_{n-1})$  depending on the result of  $S_7(t_n)$ . Therefore  $\Delta H(t_n)$  also needs to be stored in the memory block and delayed by one unit for the next calculation.

A subroutine is introduced here to allow the controller take no further control actions after the output voltage reaches to a satisfactory value. This is achieved by establishing a hysteresis band around the voltage reference. If the sampled output voltage lies outside the hysteresis band then  $\Delta H(t_n)$  will still be calculated by the main algorithm. On the contrary if the output voltage lies inside the hysteresis band then the value of  $\Delta H(t_n)$  will be set to zero as the output voltage has reached the satisfactory value and requires no further tuning actions from the controller.

By combining the result of  $S_d(t_n)$  and  $\Delta H(t_n)$ , the output  $U(t_n)$  of the controller can finally be calculated using (3-4), and it would then be stored in the memory block with an unit delay for the next calculation. After executing the complete standard procedure of the proposed DTDCA, the controller will need to wait for a delay of  $1/f_s$  ( $f_s$  represents the sampling frequency of the controller) before going back to the start of the procedure, since the effective control result can only be verified after the output voltage of the pickup has reached to its steady state.

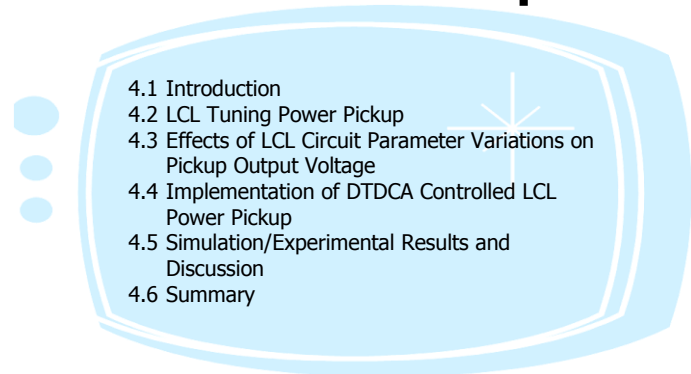
The proposed DTDCA can be applied to other secondary pickup systems with bell-shaped tuning characteristic irrespective of the power ratings and sizes of the pickup system.

### 3.5 Summary

In this chapter, a novel Directional Tuning/Detuning Control Algorithm (DTDCA) has been developed. By observing the output voltage behaviors of the pickup at different areas of the bell-shaped tuning curve, two tracking modes have been proposed for coarse tuning and fine tuning of the pickup circuit to reach the reference voltage quickly and accurately. After summarizing the considered logic signals from the above two operating modes, a control law for the DTDCA has been derived in the form of a Boolean expression. The performance of the proposed DTDCA is dependent on both the sampling frequency and the tuning step-size, and the determination of these two parameters has to be individually examined for different pickup circuits. A sub-algorithm to perform simple tuning step-size adjustment has been introduced for the controller to perform either coarse or fine tuning of the pickup circuit. A standard procedure for the proposed DTDCA has also been recommended for proper execution of the algorithm.

## Chapter 4

# DTDCA Control of LCL Power Pickup



---

### 4.1 Introduction

As it has been discussed in Chapter 2, the power pickup can generally have either a series-tuned or a parallel-tuned LC circuit as its tuning circuit [21]. Both configurations have distinguishing advantages and shortcomings. For the series-tuned power pickup, the output voltage is invariant to the load variations, but the circuit does not have the voltage boosting ability. And as for the parallel-tuned power pickup, its output voltage can be boosted up by the circuit quality factor, but has a current source feature which presents a load dependent output voltage. A power pickup based on the LCL (Inductor-Capacitor-Inductor) tuning configuration is therefore studied here as an alternative to the conventional tuning methods, which is able to boost up the output voltage, and also has a voltage source property under fully-tuned conditions.

### 4.2 LCL Tuning Power Pickup

#### 4.2.1 Basic Structure of LCL Tuning Pickup

Figure 4-1 shows the complete structure of the LCL power pickup. The LCL power pickup can be basically separated into two parts: the ac part and the dc part. The ac part is the part of the pickup before the rectifier bridge where the voltage and current waveforms are running at the primary operating frequency. It consists of a secondary pickup coil with a self-inductance of  $L_{S1}$ , a tuning capacitor  $C_{ST}$ , and a tuning inductor  $L_{S2}$  to form an LCL

T-network, or more commonly refer to as the composite tuning circuit since it is a composition of the series tuning circuit and the parallel tuning circuit. The dc part of the pickup consists of a dc capacitor  $C_{DC}$  and a dc load resistance  $R_L$ . Unlike the power pickups whose load is current sourced, i.e., parallel tuning power pickups, and require a large dc inductor right after the rectifier bridge for achieving continuous current conduction so as to obtain possible maximum power capacity, the composite power pickup only requires a dc capacitor for stabilizing the output voltage.

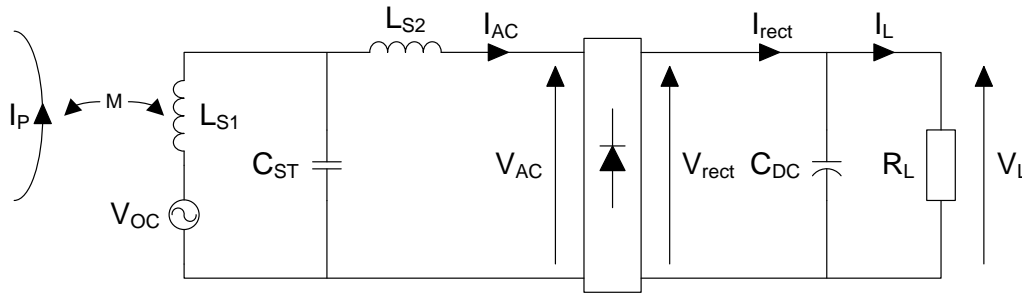


**Fig. 4-1: Basic structure of LCL power pickup**

Similar to the other conventional power pickups, through the magnetic coupling between the primary current track and the secondary pickup coil, an emf can be induced in the coil having an open-circuit voltage and a short-circuit current given as [21, 66]:

$$V_{OC} = j\omega_0 M I_P, \quad I_{SC} = \frac{V_{OC}}{j\omega_0 L_{S1}} \quad (4-1)$$

where  $I_P$  is the primary track current,  $M$  is the mutual inductance between the primary current track and the secondary pickup coil, and  $\omega_0$  is the nominal primary operating frequency. The LCL tuning circuit here functions as a compensator for the unregulated  $V_{OC}$  and generates an ac voltage  $V_{AC}$  with its magnitude and phase angle dependent on the characteristics of the LCL tuning circuit. After the ac-dc rectification, the dc capacitor  $C_{DC}$  filters out the high frequency components of the rectified current  $I_{rect}$  to provide a dc load current  $I_L$  and hence gives a dc output voltage  $V_L$ .

Assuming the value of the dc capacitor  $C_{DC}$  is selected such that it is large enough to completely remove ripples in the output voltage, the secondary resonant tank voltage  $V_{AC}$  will become square wave that has the magnitude equal to  $V_L$ . Figure 4-2 shows the steady

state voltage and current waveforms of the composite pickup. Note that  $\theta$  is the phase angle difference between the input and output of the composite tuning circuit.

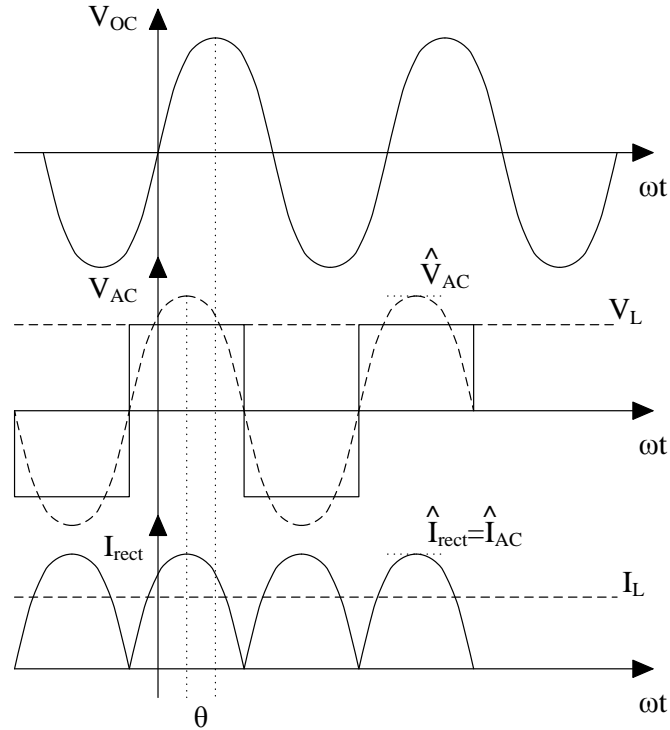


**Fig. 4-2: Voltage and current waveforms of LCL power pickup**

By neglecting the harmonics of the square wave, the relationship between the output voltage  $V_L$  and the resonant tank voltage  $V_{AC}$  can be presented by:

$$V_L = V_{rect} = \frac{\pi}{4} \hat{V}_{AC} \quad (4-2)$$

where  $\hat{V}_{AC}$  is the peak value of the sinusoidal waveform of  $V_{AC}$ . For ac-dc current conversion of the LCL pickup, the load current  $I_L$  can simply be calculated by taking the average of the rectified current  $I_{rect}$ . But since  $I_{rect}$  has the same magnitude as the resonant tank current  $I_{AC}$ , the load current  $I_L$  can be expressed as:

$$I_L = \frac{2}{\pi} \hat{I}_{rect} = \frac{2}{\pi} \hat{I}_{AC} \quad (4-3)$$

where  $\hat{I}_{rect}$  and  $\hat{I}_{AC}$  are the peak value of  $I_{rect}$  and  $I_{AC}$  respectively. Considering  $R=V/I$ , the relationship between the dc load resistor  $R_L$  and the equivalent ac load resistance  $R_{AC}$  can be expressed by:

$$R_L = \frac{\pi^2}{8} R_{AC} \quad (4-4)$$

### 4.2.2 Characteristics of LCL Tuning Circuit in Steady State

A simplified model of LCL power pickup is shown in Fig. 4-3 without considering the ac-dc rectification. As can be seen from the figure, the general structure of an LCL tuning circuit consists of a secondary pickup coil inductance  $L_{S1}$ , a tuning capacitor  $C_{ST}$ , and a tuning inductor  $L_{S2}$ . The resistance  $R_{AC}$  is the ac equivalent resistance of the dc load resistor  $R_L$  (see Fig. 4-1).

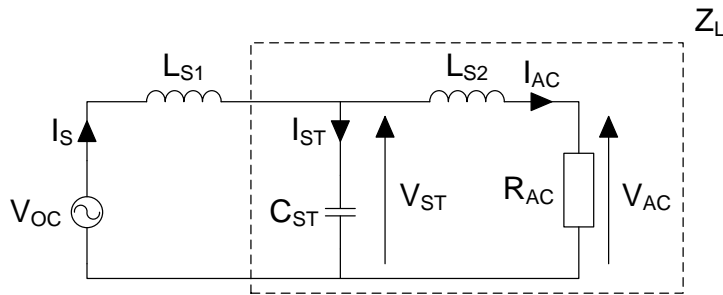


Fig. 4-3: Simplified model of LCL power pickup circuit

Considering  $C_{ST}$ ,  $L_{S2}$ , and  $R_{AC}$  as lumped circuit elements to form an impedance  $Z_L$ , the voltage across the tuning capacitor  $C_{ST}$  in Laplace domain is expressed as:

$$V_{CT}(s) = \frac{\frac{R_{AC}}{L_{S1}L_{S2}C_{ST}} + \frac{1}{L_{S1}C_{ST}}s}{s^3 + \frac{R_{AC}}{L_{S2}}s^2 + \frac{L_{S1} + L_{S2}}{L_{S1}L_{S2}C_{ST}}s + \frac{R_{AC}}{L_{S1}L_{S2}C_{ST}}} \cdot V_{OC}(s) \quad (4-5)$$

The voltage across the ac resistor  $R_{AC}$  can then be obtained by using the voltage division method to give the voltage transfer function  $H_V(s)$  of the LCL tuning circuit as:



$$H_V(s) = \frac{V_{AC}(s)}{V_{OC}(s)} = \frac{\frac{R_{AC}}{L_{S1}L_{S2}C_{ST}}}{s^3 + \frac{R_{AC}}{L_{S2}}s^2 + \frac{L_{S1} + L_{S2}}{L_{S1}L_{S2}C_{ST}}s + \frac{R_{AC}}{L_{S1}L_{S2}C_{ST}}} \quad (4-6)$$

Considering  $I_{AC}(s) = V_{AC}(s)/R_{AC}(s)$ ,  $V_{AC}(s) = H_V(s) \cdot V_{OC}(s)$  and  $V_{OC}(s) = sL_{S1} \cdot I_{SC}(s)$ , the current transfer function  $H_I(s)$  can be obtained from:

$$H_I(s) = \frac{I_{AC}(s)}{I_{SC}(s)} = \frac{s/L_{S2}C_{ST}}{s^3 + \frac{R_{AC}}{L_{S2}}s^2 + \frac{L_{S1} + L_{S2}}{L_{S1}L_{S2}C_{ST}}s + \frac{R_{AC}}{L_{S1}L_{S2}C_{ST}}} \quad (4-7)$$

Equation (4-6) and (4-7) can also be expressed in the frequency-domain using rectangular form:

$$H_V(j\omega) = \frac{R_{AC}^2(1 - \omega^2 L_{S1} C_{ST}) - j\omega R_{AC}(L_{S1} + L_{S2} - \omega^2 L_{S1} L_{S2} C_{ST})}{R_{AC}^2(1 - \omega^2 L_{S1} C_{ST})^2 + \omega^2(L_{S1} + L_{S2} - \omega^2 L_{S1} L_{S2} C_{ST})^2} \quad (4-8)$$

$$H_I(j\omega) = \frac{\omega^2 L_{S1}(L_{S1} + L_{S2} - \omega^2 L_{S1} L_{S2} C_{ST}) + j\omega R_{AC} L_{S1}(1 - \omega^2 L_{S1} C_{ST})}{R_{AC}^2(1 - \omega^2 L_{S1} C_{ST})^2 + \omega^2(L_{S1} + L_{S2} - \omega^2 L_{S1} L_{S2} C_{ST})^2} \quad (4-9)$$

where  $\omega$  is the primary operating frequency. The LCL power pickup can be fully-tuned by separating the tuning capacitor  $C_{ST}$  into  $C_{S1}$  and  $C_{S2}$  and tuning these capacitances to  $L_{S1}$  and  $L_{S2}$  respectively. The LCL pickup circuit under the fully-tuned condition becomes as shown in Fig. 4-4. The simplification of a fully-tuned LCL circuit is carried out by a two-stage circuit transformation.

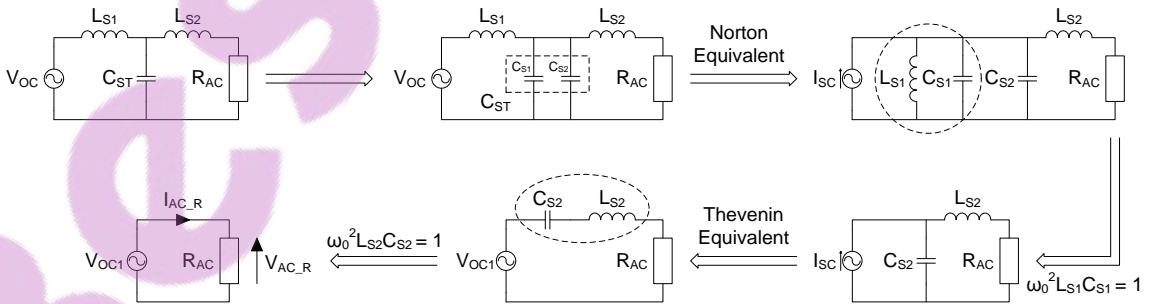


Fig. 4-4: Simplification of fully-tuned LCL pickup circuit

The first stage is having the original circuit transformed into a Norton equivalent circuit with the short-circuit current of the pickup coil as its input source. Under fully-tuned condition, the inductance  $L_{S1}$  and the capacitance  $C_{S1}$  would form an infinitely large resultant impedance and can be regarded as an open-circuit in the circuit analysis. In second stage of the transformation, the Norton equivalent circuit of the power pickup is transformed into a Thevenin equivalent circuit having an input voltage of  $V_{OC1}$ . The inductance  $L_{S2}$  and the capacitance  $C_{S2}$  here would cancel each other and the resultant impedance is treated as a short-circuit in the circuit analysis. After the two-stage simplification, it is obvious to see that the LCL power pickup acts like a voltage source with an output voltage equals to the value of  $V_{OC1}$ .

By substituting  $\omega = \omega_0 = 1/\sqrt{L_{S1}C_{S1}} = 1/\sqrt{L_{S2}C_{S2}}$  into (4-8) and rearranging (4-8), the output voltage of a fully-tuned LCL power pickup becomes:

$$V_{AC\_R} = V_{OC1} = \frac{L_{S2}}{L_{S1}} V_{OC} = \frac{C_{S1}}{C_{S2}} V_{OC} = k_{VR} V_{OC} \quad (4-10)$$

where  $k_{VR}$  is the voltage boosting factor of the LCL tuning circuit under fully-tuned condition. The load current under fully-tuned condition can also be calculated using similar method, and it can be expressed as:

$$I_{AC\_R} = \frac{\omega_0 L_{S1}}{R_{AC}} k_{VR} I_{SC} = Q_{S\_s} k_{VR} I_{SC} = k_{IR} I_{SC} \quad (4-11)$$

where  $Q_{S\_s}$  is the quality factor of a conventional series-tuned circuit, and  $k_{IR}$  is the current boosting factor of the LCL tuning circuit under fully-tuned condition.

### 4.2.3 Controllable Power Transfer Capacity

When the LCL power pickup is fully-tuned, the power available to the load can be determined from:

$$P_{AC\_R} = V_{AC\_R} \cdot I_{AC\_R} = Q_{S\_s} k_{VR}^2 V_{OC} I_{SC} \quad (4-12)$$

Similar to a simple series-tuned LC power pickup, the LCL tuning circuit can give a constant output voltage. Moreover, its power transfer capacity is boosted by a factor of  $k_{VR}^2$  under fully-tuned condition.

The output power of the LCL pickup can also be variably controlled by changing the tuning condition of the resonant tank to meet the actual load demands. To simplify the system analysis, the value of  $L_{S1}$  and  $C_{S1}$  are assumed to be fixed and they are tuned to the nominal resonant frequency. This leaves  $L_{S2}$  or  $C_{S2}$  in the tuning circuit to be variably controlled. In the case of variable  $L_{S2}$ , the value of  $C_{S2}$  is selected according to the voltage boosting factor  $k_{VR}$  of the LCL tuning circuit. The nominal tuning capacitance  $C_{ST}$  can therefore be expressed as:

$$C_{ST} = C_{S1} + C_{S2} = C_{S1} \left( 1 + \frac{1}{k_{VR}} \right) \quad (4-13)$$

By substituting (4-13) into (4-8) and (4-9) and rearranging the equations with respect to  $V_{AC}$  and  $I_{AC}$ , the magnitude of output voltage and load current of the LCL tuning circuit using variable  $L_{S2}$  can be presented by:

$$|V_{AC}(j\omega_0)| = k_{VR} B_{C\_L} \cdot |V_{OC}(j\omega_0)| \quad (4-14)$$

$$|I_{AC}(j\omega_0)| = k_{IR} B_{C\_L} \cdot |I_{SC}(j\omega_0)| \quad (4-15)$$

where  $B_{C\_L}$  is the controllable boosting coefficient. This is expressed as:

$$B_{C\_L} = \frac{R_{AC} \sqrt{R_{AC}^2 + [\omega_0 k_{VR} L_{S1} (1 - r_{adj})]^2}}{R_{AC}^2 + [\omega_0 k_{VR} L_{S1} (1 - r_{adj})]^2} \quad (4-16)$$

where the variable  $r_{adj}$  is given by:

$$r_{adj} = \frac{L_{S2\_v}}{L_{S2\_r\_o_0}} \quad (4-17)$$

where  $L_{S2\_v}$  is the variable or actual operating inductance of  $L_{S2}$  and  $L_{S2\_r\_ \omega_0}$  is the inductance of  $L_{S2}$  under fully-tuned condition with a resonant frequency equals to the nominal frequency  $\omega_0$ . The output power can therefore become:

$$P_{AC} = k_{VR} k_{IR} B_{C\_L}^2 \cdot V_{OC} I_{SC} \quad (4-18)$$

$$= \frac{R_{AC}^2}{R_{AC}^2 + [\omega_0 k_{VR} L_{S1} (1 - r_{adj})]^2} \cdot k_{VR} k_{IR} V_{OC} I_{SC}$$

Figure 4-5 shows the output power of the LCL power pickup with a variable  $L_{S2}$ . It can be seen that the power pickup has an initial output power of  $P_{AC\_ini}$  when  $L_{S2} = 0$  (e.g., without using  $L_{S2}$ ). Moreover, different values of  $k_{VR}$  would result in different  $P_{AC\_ini}$ .

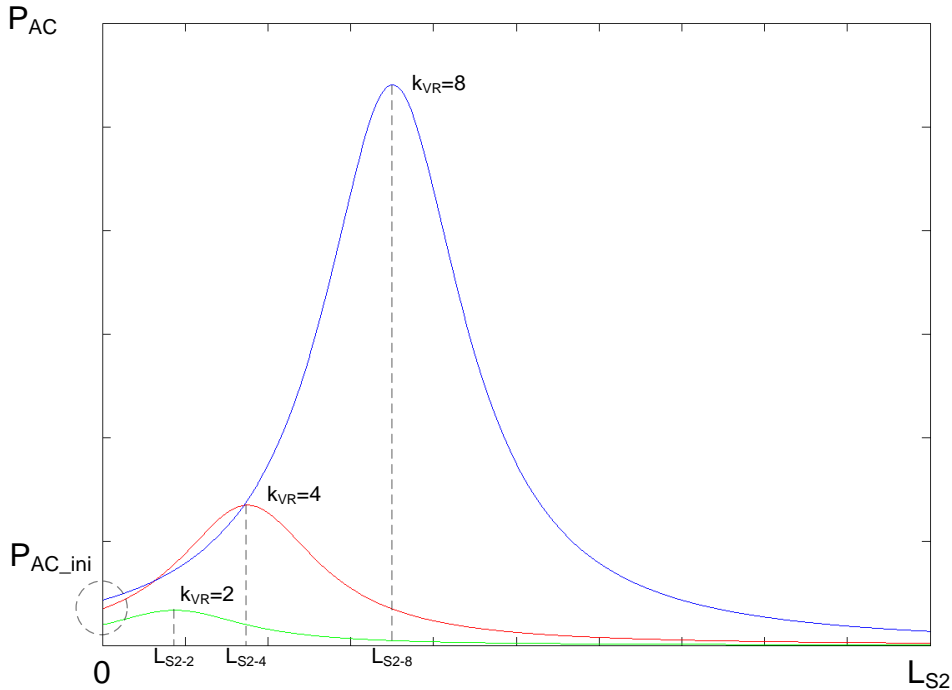


**Fig. 4-5: Output power of LCL power pickup using variable  $L_{S2}$  under different  $k_{VR}$**

The maximum  $P_{AC\_ini}$  can be approximated using the following equation when  $k_{VR}$  is approaching infinity.

$$P_{AC\_ini\_max} = \frac{V_{OC} I_{SC}}{Q_{S\_s}} \quad (4-19)$$

The pickup reaches its maximum output power when the circuit is fully-tuned, i.e.,  $L_{S2\_v} = L_{S2\_r\_w_0}$ , and as the value of  $L_{S2\_v}$  keeps increasing, the output power decreases and eventually reaches zero when  $L_{S2\_v}$  is infinitely large. Different maximum output power can be achieved by using different  $k_{VR}$ . However,  $L_{S2\_r\_w_0}$  would also have to have different values such as  $L_{S2-2}$ ,  $L_{S2-4}$ , and  $L_{S2-8}$  (as shown in Fig. 4-5), for the corresponding  $k_{VR}$  to reach the fully-tuned condition. This is due to the value of tuning capacitor  $C_{S2}$  being selected according to the value of  $k_{VR}$  and used to tune to  $L_{S2}$ , which means that if  $k_{VR}$  is changed the value of  $L_{S2}$  under fully-tuned condition would also have to change in accordance with the change of  $C_{S2}$ . By differentiating (4-18) with respect to  $r_{adj}$ , the gradient of the LCL pickup output power ( $g_{P\_L}$ ) can be shown by Fig. 4-6. It can be observed from the figure that the increase in  $k_{VR}$  would also increase the circuit sensitivity of the pickup.

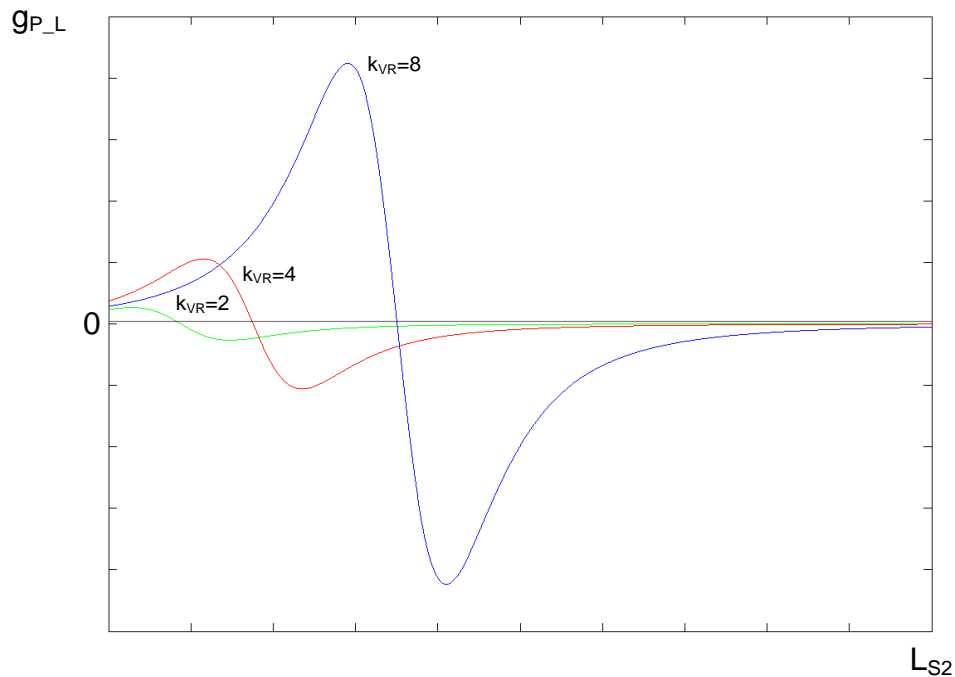


**Fig. 4-6: Gradient of output power using variable  $L_{S2}$  under different  $k_{VR}$**

Besides the variable  $L_{S2}$ , the output power can also be changed by using variable  $C_{S2}$ . Following similar procedures that have been used in the case of variable  $L_{S2}$ , expressions of the output voltage and load current for the LCL pickup using variable  $C_{S2}$  can be obtained as follows:

$$|V_{AC}(j\omega_0)| = k_{VR} B_{C-C} \cdot |V_{OC}(j\omega_0)| \quad (4-20)$$

$$|I_{AC}(j\omega_0)| = k_{IR} B_{C-C} \cdot |I_{SC}(j\omega_0)| \quad (4-21)$$

where  $B_{C-C}$  is the controllable boosting coefficient using variable  $C_{S2}$  and can be expressed as:

$$B_{C-C} = \frac{R_{AC} \sqrt{(R_{AC} r_{adj})^2 + [\omega_0 k_{VR} L_{S1} (1 - r_{adj})]^2}}{(R_{AC} r_{adj})^2 + [\omega_0 k_{VR} L_{S1} (1 - r_{adj})]^2} \quad (4-22)$$

The adjusting ratio  $r_{adj}$  here, has a similar definition to (4-17), however, it is equal to  $C_{S2\_v} / C_{S2\_r\_o_0}$ , where  $C_{S2\_v}$  is the variable or actual operating capacitance of  $C_{S2}$  and  $C_{S2\_r\_o_0}$  is the capacitance of  $C_{S2}$  under fully-tuned condition with a resonant frequency equals to the nominal frequency  $\omega_0$ . Considering  $P_{AC} = V_{AC} I_{AC}$ , the output power can be expressed as:

$$\begin{aligned} P_{AC} &= k_{VR} k_{IR} B_{C-C}^2 \cdot V_{OC} I_{SC} \\ &= \frac{R_{AC}^2}{(R_{AC} r_{adj})^2 + [\omega_0 k_{VR} L_{S1} (1 - r_{adj})]^2} \cdot k_{VR} k_{IR} V_{OC} I_{SC} \end{aligned} \quad (4-23)$$

By differentiating (4-23) with respect to  $r_{adj}$ , the gradient of the output power can be presented by:

$$g_{P-C} = \frac{2R_{AC}^2 [(\omega_0 k_{VR} L_{S1})^2 (1 - r_{adj}) - R_{AC}^2 r_{adj}]}{[(R_{AC} r_{adj})^2 + [\omega_0 k_{VR} L_{S1} (1 - r_{adj})]^2]^2} \cdot k_{VR} k_{IR} V_{OC} I_{SC} \quad (4-24)$$

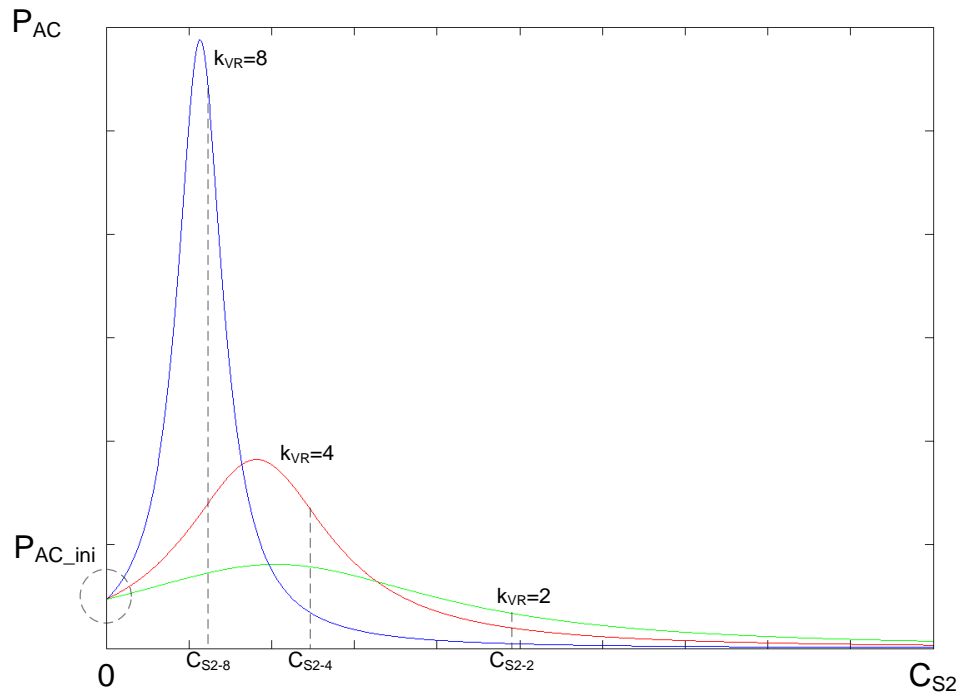


Fig. 4-7: Output power of LCL power pickup using variable  $C_{S2}$  under different  $k_{VR}$

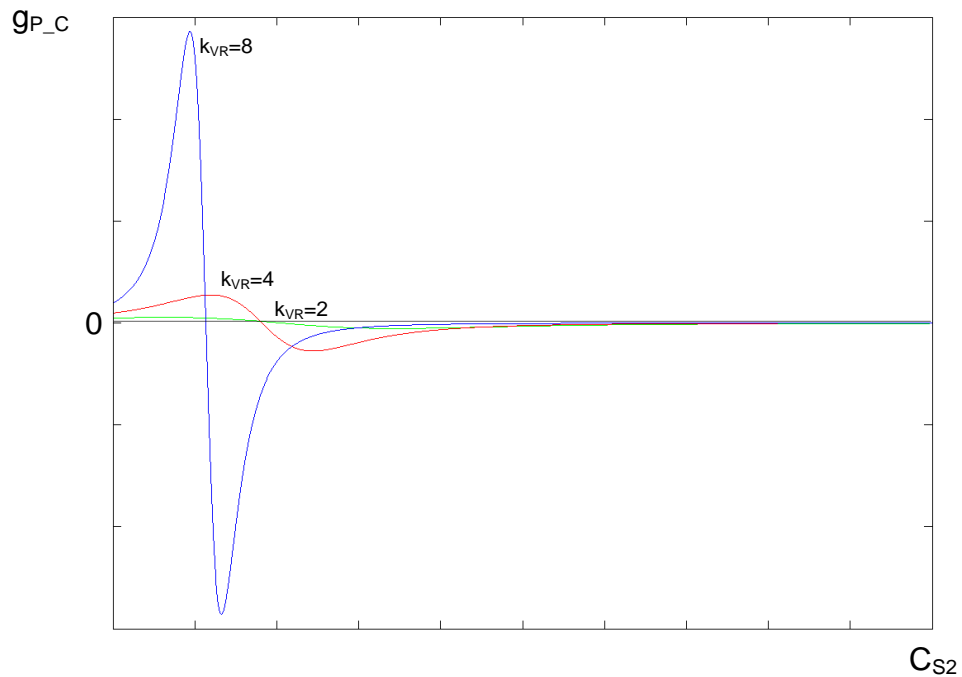


Fig. 4-8: Gradient of output power using variable  $C_{S2}$  under different  $k_{VR}$

Figure 4-7 and 4-8 show the output power and gradient of output power of the LCL power pickup using variable  $C_{S2}$  respectively. The initial power  $P_{AC\_ini}$  here is independent of  $k_{VR}$

variations and can be determined by (4-14). At the tuned-points where they have been indicated as  $C_{S2-2}$ ,  $C_{S2-4}$ , and  $C_{S2-8}$  in Fig. 4-7, the  $C_{S2}$  controlled pickup provides the same output power as the  $L_{S2}$  controlled pickup under fully-tuned condition. However, the maximum power of the pickup does not occur at these tuned-points. The ratio  $r_{adj}$  to achieve the maximum power can be calculated by having:

$$g_{P-C} = 0 \quad \text{or} \quad (\omega_0 k_{VR} L_{S1})^2 (1 - r_{adj}) - R_{AC}^2 r_{adj} = 0$$

Solving the above equation to obtain the value of  $r_{adj}$ , the required adjusting ratio is equal to:

$$\frac{Q_{S-s}^2 k_{VR}^2}{1 + Q_{S-s}^2 k_{VR}^2} \quad (4-25)$$

By substituting (4-25) into (4-23), the actual maximum power of the  $C_{S2}$  controlled pickup can be obtained. To compare the maximum power between the  $C_{S2}$  and the  $L_{S2}$  controlled pickup, a ratio  $r_{Pmax\_CL}$  is defined as:

$$r_{Pmax\_CL} = \frac{P_{ACmax\_C}}{P_{ACmax\_L}} = \frac{(1 + Q_{S-s}^2 k_{VR}^2)^2}{(Q_{S-s} k_{VR})^4} \quad (4-26)$$

where  $P_{ACmax\_C}$  and  $P_{ACmax\_L}$  are the maximum power of the pickup using a variable  $C_{S2}$  and variable  $L_{S2}$  respectively. The ratio  $r_{Pmax\_CL}$  clearly shows that a  $C_{S2}$  controlled pickup obtains a higher maximum output power than a  $L_{S2}$  controlled pickup under low  $k_{VR}$  operation, but the ratio approaches to unity when a high  $k_{VR}$  is applied.

To further compare the effect of variations of  $L_{S2}$  or  $C_{S2}$  on the output power of the LCL pickup, the gradient of the output power for both cases are shown together in Fig. 4-9. The adjusting ratio  $r_{adj}$  is selected to lie within a range of 0 ~ 2. It can be seen that when the pickup is operating with lower voltage boosting factor, the pickup circuit is more sensitive to the change of  $C_{S2}$ . However, the difference in circuit sensitivity with respect to the tuning components between the  $L_{S2}$  controlled and the  $C_{S2}$  controlled pickup decreases as the voltage boosting factor gets increased.



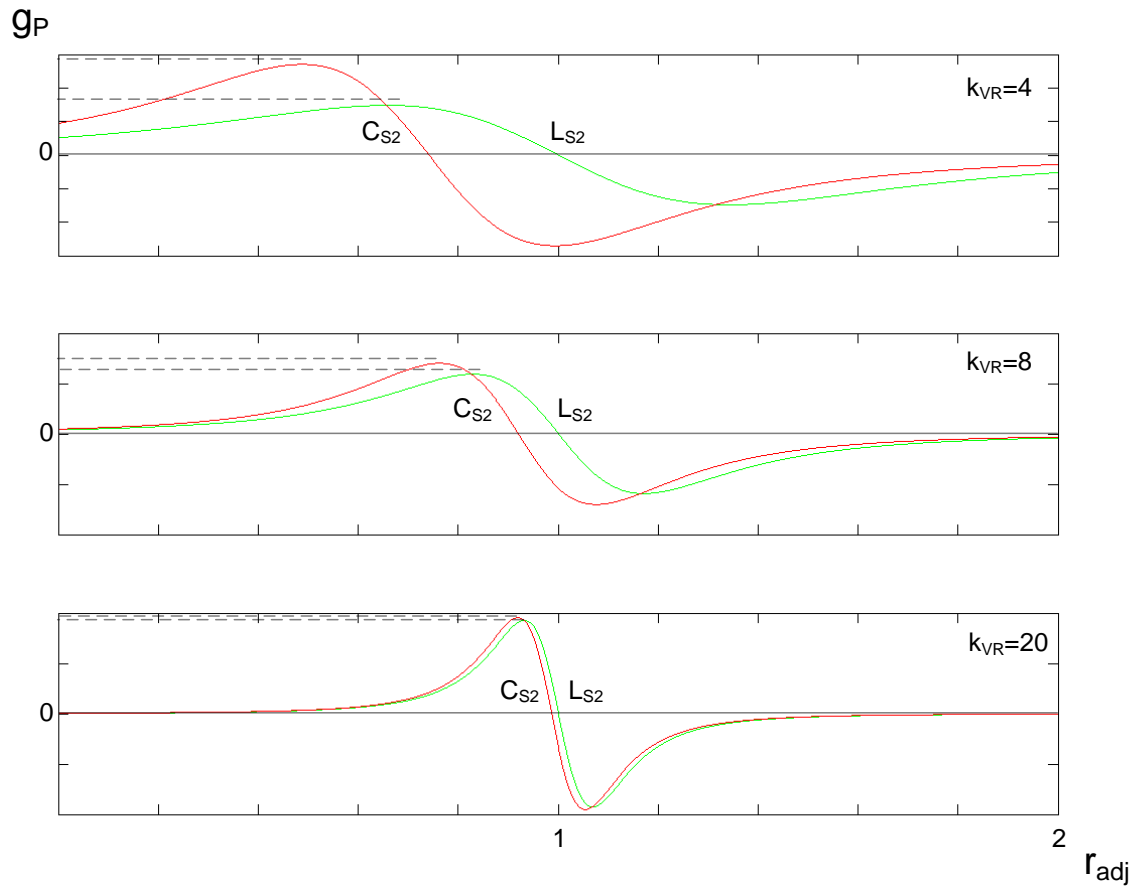


**Fig. 4-9: Gradient of output power using variable  $L_{S2}$  or  $C_{S2}$  under different  $k_{VR}$**

Although it is obvious that power flow control for the LCL power pickup can be done either by controlling the inductance of  $L_{S2}$  or the capacitance of  $C_{S2}$ , a preferable choice can still be selected based on the characteristics of these two methods. Advantages of using the variable  $C_{S2}$  include the initial startup power for the pickup is independent of  $k_{VR}$  and has a higher maximum output power under low  $k_{VR}$  operation. Nevertheless, to achieve higher value of  $k_{VR}$  ( $> 10$ ) than the conventional IPT systems with fixed tuning to improve the loose coupling properties of the power pickup, the features of the  $C_{S2}$  controlled power pickup become imperceptible because the initial and maximum power of the pickup using variable  $L_{S2}$  or variable  $C_{S2}$  are almost of the same according to (4-19) and (4-26). The major factor that differentiates these two methods is the circuit sensitivity of the pickup with respect to the change of these two variable components. As it is well-known in engineering practices, if a system's output is sensitive to the control signal, the employed controller would need to have high resolution in both its feedback and output signals, which often increase the size and cost of the system, and failure to do so, may

result in poor or undesirable control result. It can be seen from Fig. 4-9 that the LCL power pickup is more sensitive to the change of  $C_{S2}$  than the change of  $L_{S2}$  even though the difference between these two circuit sensitivities decreases as the value of  $k_{VR}$  increases. The power flow control of the LCL power pickup is therefore based on using the variable  $L_{S2}$  due to the reasons discussed.

### 4.3 Effects of LCL Circuit Parameter Variations on Pickup Output Voltage

In practical operations, the power pickups are often deviated from its designated operating point in terms of the circuit tuning condition due to the variation of circuit parameters [66, 67]. This causes the output voltage of the power pickup to fluctuate or chatter, which results in an undesirable output characteristic for most electrical applications. In order to regulate the output voltage of the LCL power pickup by using the variable  $L_{S2}$ , it is appropriate to know how the resonant tank voltage  $V_{AC}$  is affected by variations in different circuit parameters. These effects are analyzed here.

#### 4.3.1 Operating Frequency Variation

As it has been discussed in Chapter 2, the primary track power supply can have two different operating modes which are the fixed frequency operation and the variable frequency operation. The fixed frequency operation offers a constant operating frequency for the IPT system whereas the variable frequency operation allows the operating frequency to follow the primary natural circuit resonance [21]. Advantage of having the IPT system to operate with a fixed frequency is that a constant power transfer between the primary and the secondary side can be maintained, and the output power of the secondary pickup would not be affected by the variations of the operating frequency. However, since the reflected impedance from the secondary pickup often causes the primary resonant tank to detune from its nominal operating frequency, semiconductor devices in the primary inverting network that are forced to switch at a constant nominal frequency may be imposed with high voltage and/or current stresses and result in high switching losses. To reduce the potential high switching losses, the semiconductor devices in the inverting network can be switched using ZVS or ZCS techniques by following the natural circuit resonance with certain degree of variation in the nominal operating frequency. Such a

method provides a better power efficiency for the primary converter of the IPT system, but it may also cause significant power drop for an LCL power pickup under high  $k_{VR}$  operation (or for an LC power pickup under high  $Q$  operation). As the primary power supply may either use the fixed or the variable frequency converter topology in a practical IPT system design due to their distinguishing features, it is therefore of great importance to analyze the effects of the potential operating frequency variation on the output voltage of the LCL power pickup, so a desired inductance of  $L_{S2}$  can be obtained based on the analyses to compensate for this particular variation.

As it has been discussed in Section 4.2, the output voltage of the LCL pickup is controlled by a boosting coefficient according to (4-14) when the circuit is operating at the nominal frequency  $\omega_0$ . However, when the IPT system has an operating frequency variation, the boosting coefficient would be affected and needs to be re-examined. To do so, the magnitude of operational voltage boosting factor of the LCL tuning circuit is obtained by taking the absolute value of (4-8) as:

$$\begin{aligned} \frac{|V_{AC}(j\omega)|}{|V_{OC}(j\omega)|} &= \frac{R_{AC} \sqrt{R_{AC}^2 [1 - \omega^2 L_{S1} (C_{S1} + C_{S2})]^2 + \omega^2 [L_{S1} + L_{S2} - \omega^2 L_{S1} L_{S2} (C_{S1} + C_{S2})]}}{R_{AC}^2 [1 - \omega^2 L_{S1} (C_{S1} + C_{S2})]^2 + \omega^2 [L_{S1} + L_{S2} - \omega^2 L_{S1} L_{S2} (C_{S1} + C_{S2})]} \\ &= k_V \end{aligned} \quad (4-27)$$

By defining the actual operating frequency  $\omega$  as:

$$\omega = \alpha_f \omega_0 \quad (4-28)$$

where  $\alpha_f$  is the normalized frequency variation index, i.e.,  $\alpha_f$  equals to 1.1 if the nominal operating frequency  $\omega_0$  is +10% higher. Considering  $\omega_0 = 1/\sqrt{L_{S1}C_{S1}} = 1/\sqrt{L_{S2}C_{S2}}$ ,  $r_{adj} = L_{S2\_v}/L_{S2\_r\_o}$ , and  $k_{VR} = C_{S1}/C_{S2}$ , equation (4-27) can be rewritten as:

$$\begin{aligned} \frac{|V_{AC}(j\omega)|}{|V_{OC}(j\omega)|} &= \frac{k_{VR} R_{AC} \sqrt{R_{AC}^2 [k_{VR} (\alpha_f^2 - 1) + \alpha_f^2]^2 + (\alpha_f \omega_0 k_{VR} L_{S1})^2 [1 - r_{adj} [k_{VR} (\alpha_f^2 - 1) + \alpha_f^2]]^2}}{R_{AC}^2 [k_{VR} (\alpha_f^2 - 1) + \alpha_f^2]^2 + (\alpha_f \omega_0 k_{VR} L_{S1})^2 [1 - r_{adj} [k_{VR} (\alpha_f^2 - 1) + \alpha_f^2]]^2} \\ &= k_V \end{aligned} \quad (4-29)$$

It has been noticed that not only the operational voltage boosting factor gets affected by the operating frequency variation but the open-circuit voltage of the pickup coil would also be affected according to (4-1), and it is crucial to consider both of them in the analysis. The output voltage of the LCL pickup under variation of the operating frequency is therefore obtained by rearranging (4-29) and can be expressed as:

$$\begin{aligned} |V_{AC}(j\omega)| &= k_V \cdot |V_{OC}(j\omega)| = k_V \cdot |V_{OC}(j\alpha_f\omega_0)| \\ &= \alpha_f k_V \cdot |V_{OC\_o}(j\omega_0)| \end{aligned} \quad (4-30)$$

where  $V_{OC\_o}$  is the nominal open-circuit voltage of the pickup coil without being affected by any parameter variations and it is given in (4-1). Figure 4-10 shows the output voltage behavior under different operating frequency variations. It can be seen from the figure that due to the effect of frequency variation, the ratio  $r_{adj}$  for the pickup to achieve fully-tuned condition has been shifted and indicated as  $r_{adj\_fvr1}$ ,  $r_{adj\_fvr2}$ , and  $r_{adj\_fvr3}$  for the pickup having +1%, 0%, and -1% variation in the operating frequency respectively. In addition, the maximum output voltage of the pickup has also been changed. From (4-29), it can be seen that the maximum output voltage is reached when:

$$1 - r_{adj} [k_{VR}(\alpha_f^2 - 1) + \alpha_f^2] = 0$$

By solving the above equation to obtain the required ratio  $r_{adj}$  for the pickup to fully tune to the drifted operating frequency, the solution is given by:

$$r_{adj\_fvr} = \frac{1}{k_{VR}(\alpha_f^2 - 1) + \alpha_f^2} \quad (4-31)$$

Substituting (4-31) back to (4-29), the operational voltage boosting factor  $k_V$  can be simplified and the maximum output voltage corresponding to the drifted operating frequency can be expressed as:

$$|V_{AC\_fvr\_max}(j\omega)| = \frac{\alpha_f k_{VR}}{k_{VR}(\alpha_f^2 - 1) + \alpha_f^2} \cdot |V_{OC\_o}(j\omega_0)| \quad (4-32)$$

The maximum output voltage under different frequency variations has been indicated as  $V_{AC\_fvr\_max1}$ ,  $V_{AC\_fvr\_max2}$ , and  $V_{AC\_fvr\_max3}$  in Fig. 4-10.

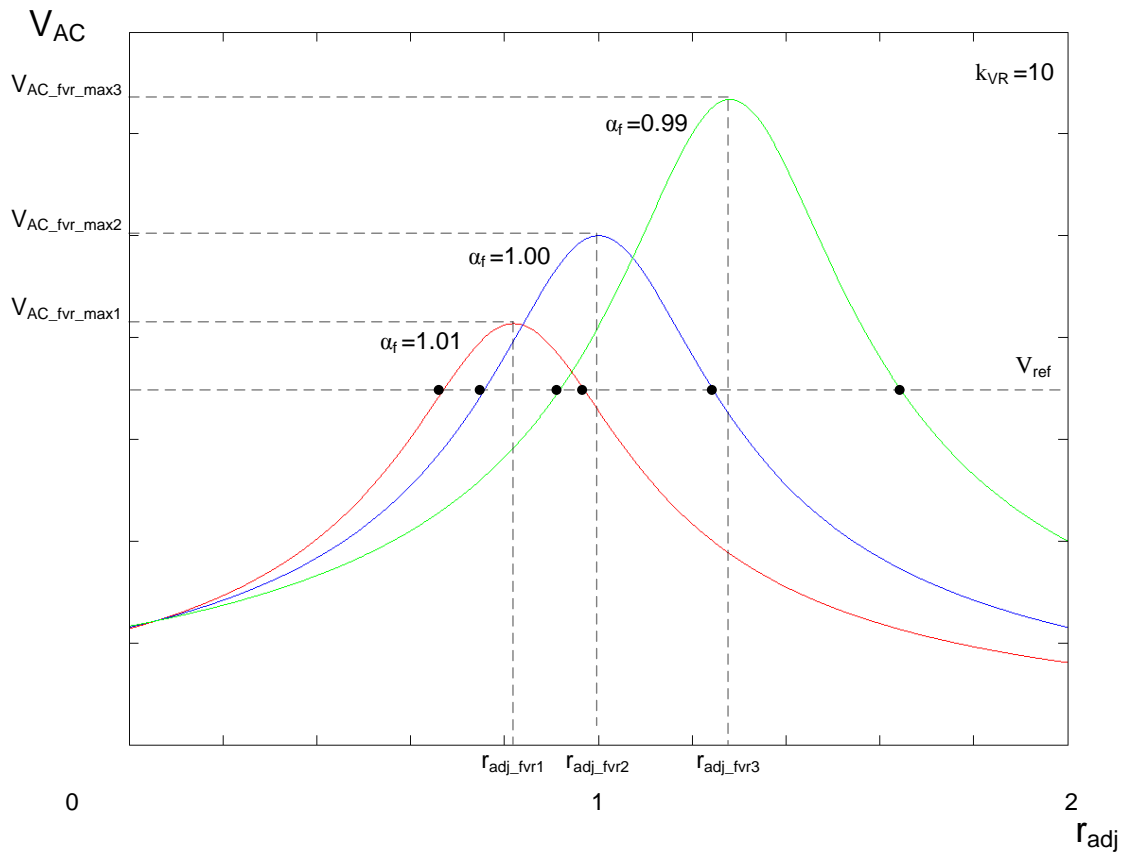


**Fig. 4-10: Output voltage behavior of LCL power pickup using variable  $L_{S2}$  under operating frequency variations**

The result obtained in Fig. 4-10 shows that even the LCL pickup possesses a voltage source property under fully-tuned condition, the output voltage would still be changed when the pickup experiences an operating frequency variation. In addition, even the circuit is retuned to the drifted frequency; the output voltage will no longer be the same as the maximum output voltage which is obtained at the nominal operating frequency. It can also be observed from Fig. 4-10 that if a constant output voltage  $V_{ref}$  is required, the LCL pickup has to be operated in the detuning region in order to compensate for the operating frequency variation through adjusting  $L_{S2}$ . This causes the LCL tuning circuit to lose its voltage source property. Furthermore, the MMOV (Minimum of the Maximum Output Voltages, it is  $V_{AC\_fvr\_max1}$  in this case) caused by the variation has to be larger than the required constant voltage so the control range provided by the variable  $L_{S2}$  can be fully used to compensate for the variation. Otherwise the pickup would be required to operate with a reduced tolerance to the variation. From (4-30), it is obvious to see that in order to keep the output voltage constant, the term  $\alpha_f k_V$  must be kept constant. By putting the

expression of  $\alpha_f k_V$  into a quadratic equation of  $r_{adj}$  and solving it to obtain the desired adjusting ratio for the corresponding frequency variation, the solutions can be presented as:

$$r_{adj\_fv} = \frac{1}{k_{VR}(\alpha_f^2 - 1) + \alpha_f^2} \cdot \left[ 1 \pm \frac{R_{AC} \sqrt{\frac{1}{r_k^2} - \left[ \frac{k_{VR}(\alpha_f^2 - 1) + \alpha_f^2}{\alpha_f} \right]^2}}{\omega_0 k_{VR} L_{S1}} \right] \quad (4-33)$$

where  $r_k$  ( $= k_{V\_ref} / k_{VR}$  or  $V_{ref} / V_{AC\_R}$ ) is the ratio between the desired voltage boosting factor  $k_{V\_ref}$  that needs to be kept constant and the voltage boosting factor  $k_{VR}$  under fully-tuned condition, or it can also be regarded as a ratio between the desired output voltage  $V_{ref}$  and the maximum output voltage of the pickup  $V_{AC\_R}$  under the nominal operating frequency. Note that in order to have a valid solution for the ratio  $r_{adj\_fv}$ , the following condition must be met.

$$r_k \leq \frac{\alpha_f}{k_{VR}(\alpha_f^2 - 1) + \alpha_f^2}$$

The ratio  $r_k$  therefore has to be selected within the range of  $0 \leq r_k < 1$  to cover both the positive and negative variations in the operating frequency. If the pickup is designed to have an output voltage that is equal to the output voltage at the nominal tuned-point, then only negative variations in the operating frequency will be allowed. Figure 4-11 shows the relationship between the operating frequency variations and the adjusting ratio for achieving the required  $r_k$ . The ratio to achieve fully-tuned condition is represented by  $r_{adj\_fv}$ . The solutions of the required ratio for achieving the desired  $r_k$  are separately shown in the figure according to their operating region and represented by  $r_{adj\_fv\_OT}$  and  $r_{adj\_fv\_UT}$  for the ratios in the over-tuning region and the under-tuning region respectively.

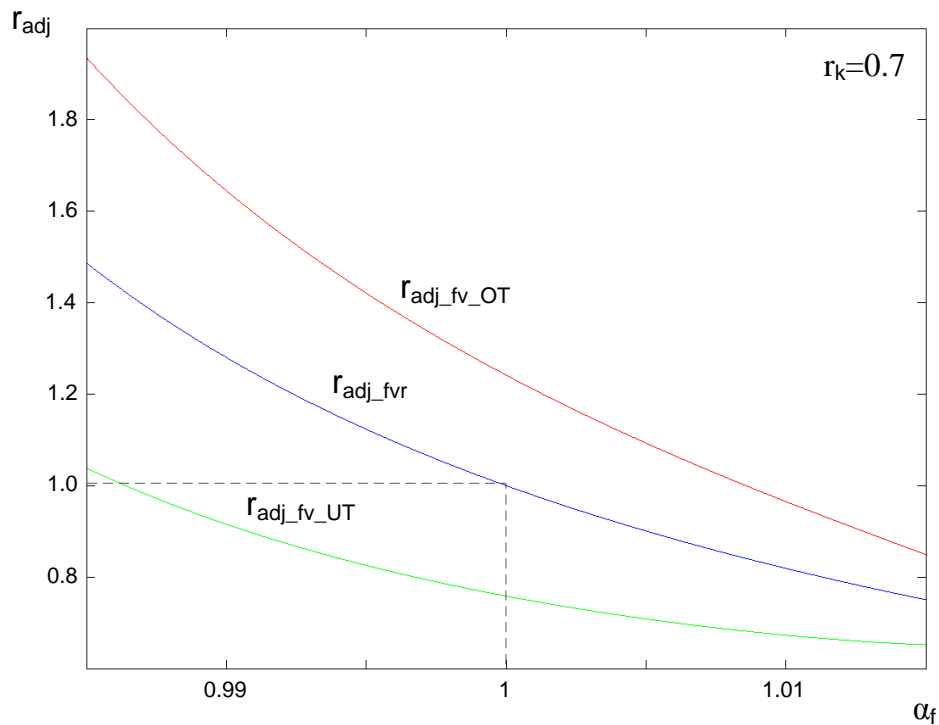


**Fig. 4-11: Adjusting ratio of  $L_{S2}$  for LCL power pickup to achieve desired  $r_k$  under operating frequency variations**

### 4.3.2 Magnetic Coupling Variation

Contactless power transfer through loose magnetic coupling is a major feature of the IPT system and has gained many different applications owing to its advantageous operating distance between the stationary primary current track and the movable secondary power pickups. Normally, the system is designed such that the secondary power pickups only have lateral movements with respect to the primary track, for example, monorail systems, for keeping the open-circuit voltage of the pickup coil more or less constant and therefore reduces or excludes the need of compensation for any potential variations that may be caused by unintended coupling situations [80]. However, as the applications of IPT systems extend to different fields, the restricted lateral movements are no longer sufficient to cope with the versatile operating environments such as applications involving 3-D movements, and require the pickup to be designed to receive power from different orientations within a power-zone created by the primary track current [23, 55, 57, 66]. Such a system involves constant variation in the magnetic coupling between the primary and the secondary side of the IPT system, causing the output voltage of the pickup to fluctuate and hence needs to be compensated. Major effect of the magnetic coupling

variation on the secondary power pickups is identified in the open-circuit voltage of the pickup coil since the mutual inductance  $M$  in (4-1) is proportional to the magnetic coupling. The open-circuit voltage under the magnetic coupling variation is expressed as:

$$V_{OC} = j\omega_0 \alpha_{oc} M I_p = \alpha_{oc} \cdot V_{OC_o} \quad (4-34)$$

where  $\alpha_{oc}$  is the normalized open-circuit voltage variation index and can also be regarded as the normalized mutual inductance variation index since these two are proportional to each other. Similar procedures that have previously been used in the analysis of effects of variations of the operating frequency on the output voltage of the pickup is followed here to study the effects of magnetic coupling variation on the voltage boosting factor  $k_V$ . The voltage boosting factor under magnetic coupling variations can be expressed as:

$$\begin{aligned} \frac{|V_{AC}(j\omega_0)|}{|V_{OC}(j\omega_0)|} &= \frac{k_{VR} R_{AC} \sqrt{R_{AC}^2 + (\omega_0 k_{VR} L_{S1})^2} (1 - r_{adj})^2}{R_{AC}^2 + (\omega_0 k_{VR} L_{S1})^2 (1 - r_{adj})^2} \\ &= k_V \end{aligned} \quad (4-35)$$

By rearranging (4-35) and taking the effect of magnetic coupling variation on the open-circuit voltage of the pickup coil into consideration, the output voltage of the pickup can be obtained by:

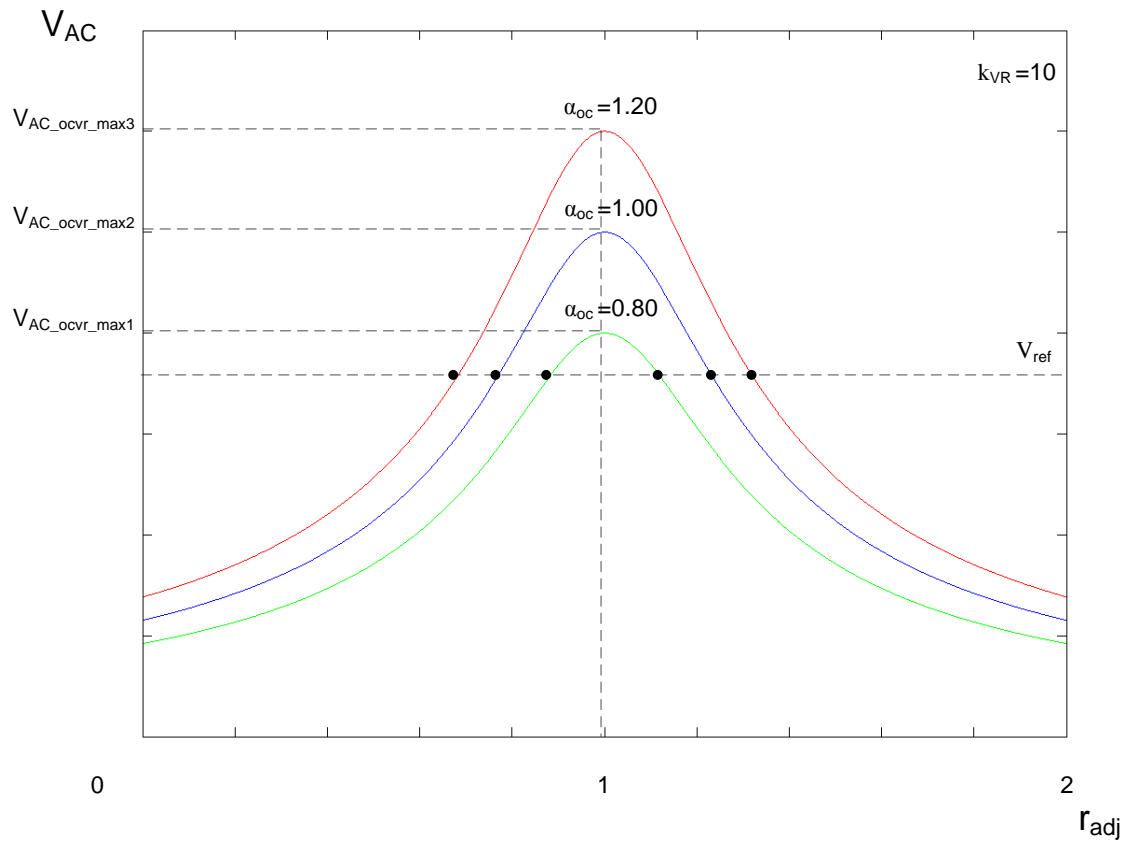
$$|V_{AC}(j\omega_0)| = k_V \cdot |V_{OC}(j\omega_0)| = \alpha_{oc} k_V \cdot |V_{OC_o}(j\omega_0)| \quad (4-36)$$

Figure 4-12 shows the output voltage behavior of the LCL pickup under different magnetic coupling variations. It can be seen that the tuned-point has remained unchanged, but the maximum output voltage of the pickup has been affected. The maximum output voltage is obtained when  $r_{adj} = 1$ , and can be determined from:

$$|V_{AC_{ocvr\_max}}(j\omega)| = \alpha_{oc} k_{VR} \cdot |V_{OC_o}(j\omega_0)| \quad (4-37)$$

And the affected maximum output voltage is indicated as  $V_{AC_{ocvr\_max1}}$ ,  $V_{AC_{ocvr\_max2}}$ , and  $V_{AC_{ocvr\_max3}}$  in the figure.





**Fig. 4-12: Output voltage behavior of LCL power pickup using variable  $L_{S2}$  under magnetic coupling variations**

In order to fully compensate for this particular variation and provide a constant voltage at the output, the pickup has to be operated in the detuning region with the term  $\alpha_{oc}k_V$  in (4-36) being kept constant. By rearranging the expression of  $\alpha_{oc}k_V$  into a quadratic equation of ratio  $r_{adj}$  and solving it to obtain the solutions, the required ratio for achieving the desired output voltage is determined from:

$$r_{adj\_ocv} = 1 \pm \frac{R_{AC} \sqrt{\left(\frac{\alpha_{oc}}{r_k}\right)^2 - 1}}{\omega_0 k_{VR} L_{S1}} \quad (4-38)$$

And the following condition has to be met for obtaining valid solutions in (4-38).

$$r_k \leq \alpha_{oc}$$

The equality shows that if the pickup has been designed to operate with a certain specific  $r_k$ , the tolerable normalized variation index  $\alpha_{oc}$  has to be larger than  $r_k$  in order to keep the magnetic coupling variations within the control range provided by the variable  $L_{S2}$ .

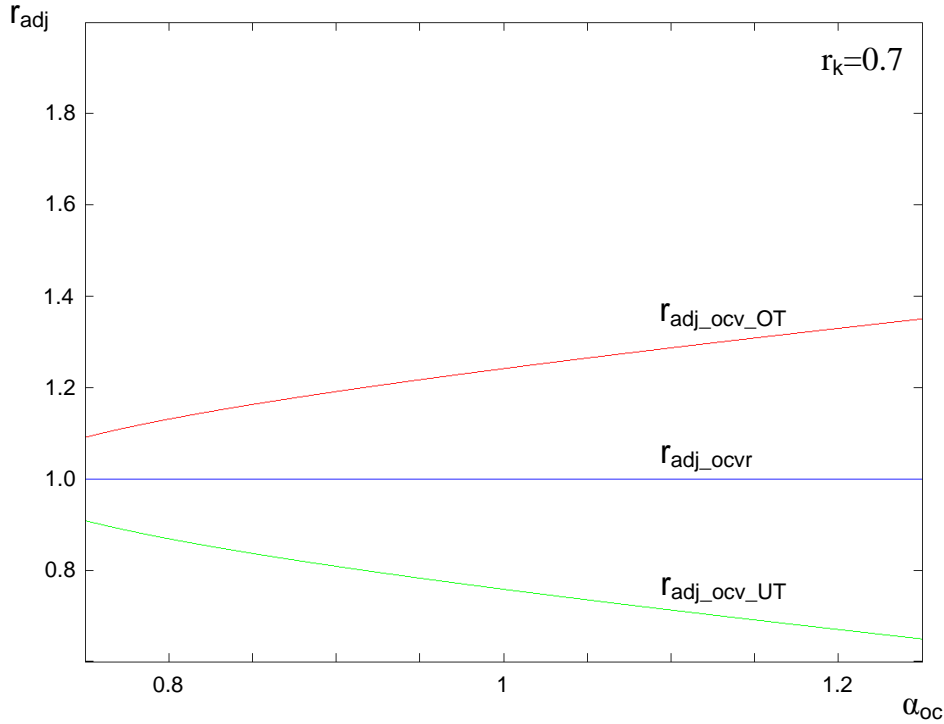


**Fig. 4-13: Adjusting ratio of  $L_{S2}$  for LCL power pickup to achieve desired  $r_k$  under magnetic coupling variations**

The relationship between the magnetic coupling variations and the adjusting ratio  $r_{adj}$  for achieving the desired  $r_k$  is shown in Fig. 4-13. The desired adjusting ratios are represented by  $r_{adj\_ocv\_OT}$  and  $r_{adj\_ocv\_UT}$  to separately show the results obtained in the over-tuning region and the under-tuning region respectively. Note that the ratio for achieving the maximum output voltage under different magnetic coupling variations is represented by  $r_{adj\_ocvr}$ , and it has a result of constant unity regardless of the variations in the considered parameter.

### 4.3.3 Tuning Capacitance Variation

By deliberately changing the tuning capacitor  $C_{S2}$  of the power pickup through a continuous control loop, the secondary pickup is able to deliver the output power according to the load demands. However, if unwanted variations of the tuning capacitor

occur which may be caused by ambient temperature changes, manufacturing tolerances, etc., the pickup output voltage would be affected due to the undesired change of the tuning condition. In the LCL power pickup, the capacitor  $C_{ST}$  (see Fig. 4-1) is subjected to this concerned variation. By introducing a variable  $\alpha_c$  which represents the normalized tuning capacitor variation index, the affected tuning capacitor  $C_{ST}$  can be given as:

$$C_{ST} = \alpha_c C_{ST\_O} = \alpha_c (C_{S1} + C_{S2}) = \alpha_c C_{S1} \left( 1 + \frac{1}{k_{VR}} \right) \quad (4-39)$$

where  $C_{ST\_O}$  is the nominal capacitance of  $C_{ST}$  having  $C_{S1}$  and  $C_{S2}$  selected according to the voltage boosting factor  $k_{VR}$ . Substituting (4-39) back to (4-27), the voltage boosting factor  $k_V$  can be obtained by:

$$\begin{aligned} \frac{|V_{AC}(j\omega)|}{|V_{OC}(j\omega)|} &= \frac{k_{VR} R_{AC} \sqrt{R_{AC}^2 [k_{VR}(\alpha_c - 1) + \alpha_c]^2 + (\omega_0 k_{VR} L_{S1})^2 [1 - r_{adj} [k_{VR}(\alpha_c - 1) + \alpha_c]]^2}}{R_{AC}^2 [k_{VR}(\alpha_c - 1) + \alpha_c]^2 + (\omega_0 k_{VR} L_{S1})^2 [1 - r_{adj} [k_{VR}(\alpha_c - 1) + \alpha_c]]^2} \\ &= k_V \end{aligned} \quad (4-40)$$

And the value of  $k_V$  reaches maximum when

$$1 - r_{adj} [k_{VR}(\alpha_c - 1) + \alpha_c] = 0.$$

Thus the required adjusting ratio for achieving the maximum output voltage can be given as:

$$r_{adj\_cvr} = \frac{1}{k_{VR}(\alpha_c - 1) + \alpha_c} \quad (4-41)$$

Substituting (4-41) into (4-40), the maximum output voltage under the tuning capacitor variations can be obtained from:

$$|V_{AC\_cvr\_max}(j\omega)| = \frac{k_{VR}}{k_{VR}(\alpha_c - 1) + \alpha_c} \cdot |V_{OC\_o}(j\omega_0)| \quad (4-42)$$

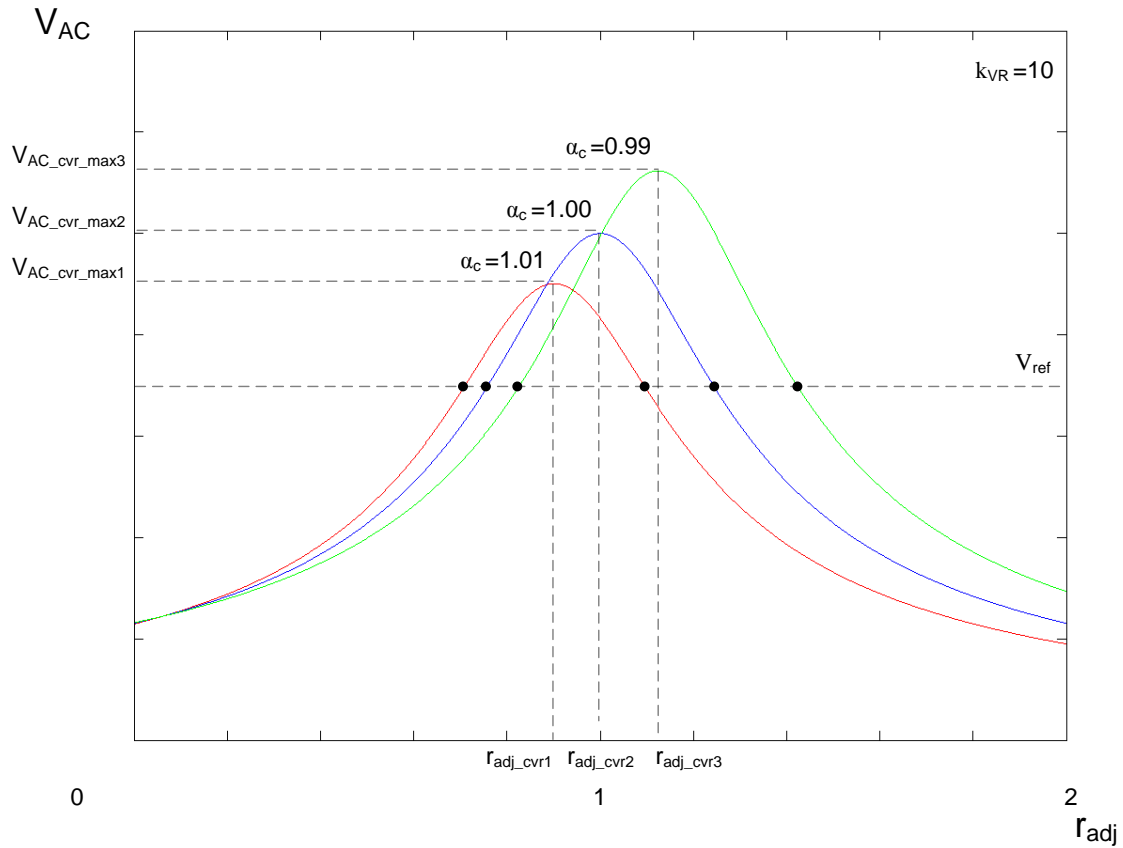


**Fig. 4-14: Output voltage behavior of LCL power pickup using variable  $L_{S2}$  under tuning capacitor  $C_{ST}$  variations**

Figure 4-14 shows the output voltage behavior of the pickup under different tuning capacitor variations. Similar to the case of operating frequency variation, the tuning capacitor variation also affects both the maximum output voltage and the ratio required for achieving the fully-tuned condition. The maximum output voltages of the pickup under different  $\alpha_c$  are indicated as  $V_{AC\_cvr\_max1}$ ,  $V_{AC\_cvr\_max2}$ , and  $V_{AC\_cvr\_max3}$  in the figure and corresponding to the tuned-points  $r_{adj\_cvr1}$ ,  $r_{adj\_cvr2}$ , and  $r_{adj\_cvr3}$  respectively. Solving the quadratic equation of  $r_{adj}$  after rearranging (4-40), the required adjusting ratio for the pickup to achieve the desired output voltage under tuning capacitor variations can be obtained from:

$$r_{adj\_cv} = \frac{1}{k_{VR}(\alpha_c - 1) + \alpha_c} \cdot \left[ 1 \pm \frac{R_{AC} \sqrt{\frac{1}{r_k^2} - [k_{VR}(\alpha_c - 1) + \alpha_c]^2}}{\omega_0 k_{VR} L_{S1}} \right] \quad (4-43)$$

The condition to achieve valid solutions in (4-43) is

$$r_k \leq \frac{1}{k_{VR}(\alpha_c - 1) + \alpha_c} \quad \text{or} \quad \frac{k_{VR} + \frac{1}{r_k}}{k_{VR} + 1} \geq \alpha_c.$$

From the above equality, it can be seen that the result obtained here is similar to that in the case of operating frequency variations, where the ratio  $r_k$  has a range from 0 ~ 1 with the pickup being operated in the detuning region when  $r_k$  is less than 1 and fully-tuned when  $r_k$  is equal to 1.

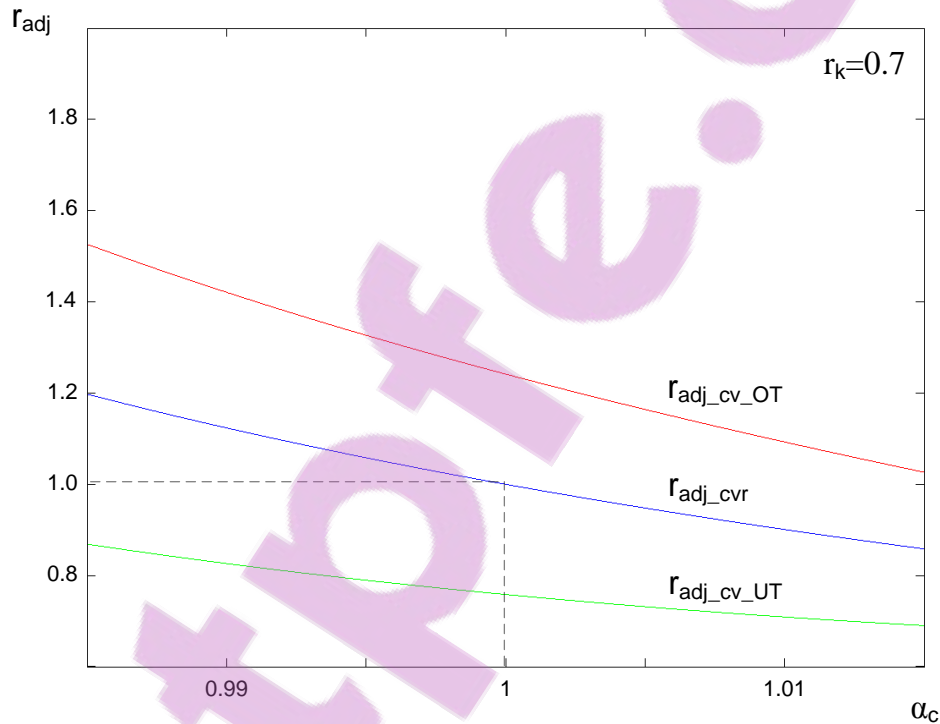


**Fig. 4-15: Adjusting ratio of  $L_{S2}$  for LCL power pickup to achieve desired  $r_k$  under tuning capacitor  $C_{ST}$  variations**

The tolerance of the pickup to the tuning capacitor variations is allowed to have both positive and negative variations in the nominal value of  $C_{ST}$  defined in (4-13) if  $r_k < 1$ . However, if  $r_k$  is selected to be 1 then only negative variations in the nominal  $C_{ST}$  will be allowed. Figure 4-15 shows the relationship between the tuning capacitor variations and the adjusting ratio for achieving the required  $r_k$ . The ratio to achieve fully-tuned condition is represented by  $r_{adj\_cvr}$ . The solutions of the ratio required for achieving the desired  $r_k$  are

represented by  $r_{adj\_cv\_OT}$  and  $r_{adj\_cv\_UT}$  to separately show the ratios in the over-tuning region and the under-tuning region respectively.

#### 4.3.4 Load Variation

Under fully-tuned condition, the LCL configuration provides a constant output voltage to the load regardless of the load variations. However, as it can be seen from the variation analyses of the parameters that have been discussed, the LCL pickup circuit has to be operated in the detuning region in order to fully compensate for the considered parameter variations. Therefore, an analysis for the load variation in the detuning operation of the LCL pickup is necessary to be carried out here.

The load resistance under variation is given by:

$$R_{AC} = \alpha_r R_{AC\_O} \quad (4-44)$$

where  $\alpha_r$  is the normalized load variation index and  $R_{AC\_O}$  is the nominal load resistance. By substituting (4-44) into (4-27), the voltage boosting factor  $k_V$  can be given as:

$$\begin{aligned} \frac{|V_{AC}(j\omega_0)|}{|V_{OC}(j\omega_0)|} &= \frac{k_{VR} \alpha_r R_{AC} \sqrt{(\alpha_r R_{AC})^2 + (\omega_0 k_{VR} L_{S1})^2} (1 - r_{adj})^2}{(\alpha_r R_{AC})^2 + (\omega_0 k_{VR} L_{S1})^2 (1 - r_{adj})^2} \\ &= k_V \end{aligned} \quad (4-45)$$

The maximum output voltage is reached when  $r_{adj} = 1$  and can be determined from:

$$|V_{AC\_rvr\_max}(j\omega)| = k_{VR} \cdot |V_{OC\_O}(j\omega_0)| \quad (4-46)$$

Equation (4-46) shows that when the LCL pickup is fully-tuned, the maximum output voltage is purely governed by the nominal voltage boosting factor and the LCL pickup would not be affected by any load variations. The relationship between the output voltage and the variable  $L_{S2}$  under different load variations is shown in Fig. 4-16. It can be seen that the maximum output voltage  $V_{AC\_rvr\_max}$  has remained unchanged at the tuned-point, but the voltage tuning curve gets widened when the load increases above the nominal value and narrowed when the load decreases below the nominal.

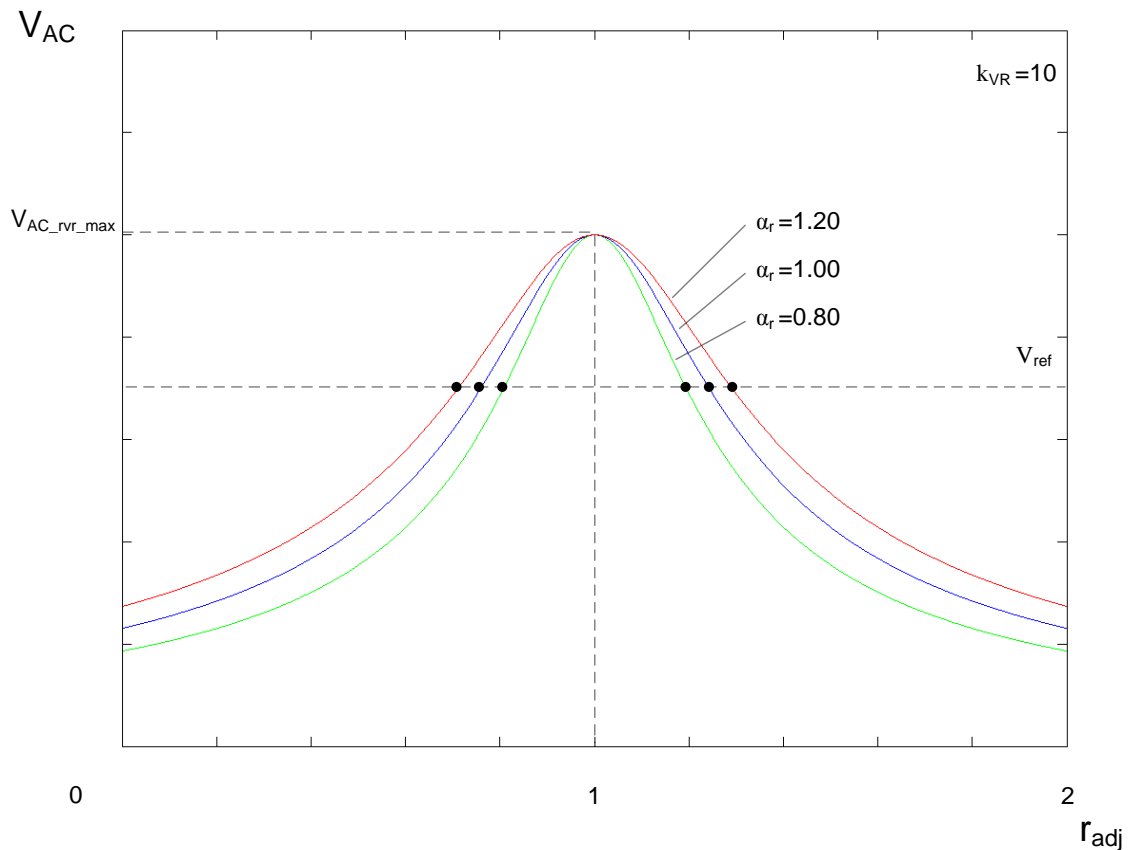


**Fig. 4-16: Output voltage behavior of LCL power pickup using variable  $L_{S2}$  under load variations**

The load variation in practical operations can be several times larger or smaller than the nominal value and causes the shape change in the output voltage tuning curve to be significant. In some extreme loading conditions such as open-circuit or short-circuit operations, the variable  $L_{S2}$  may fail to regulate the output voltage because of the tuning curve becoming too flat or too sharp to be controlled. The shape of the tuning curve directly reflects the output sensitivity of the LCL pickup to the adjusting ratio  $r_{adj}$ , which also determines whether a controller with high resolution output and/or input is required in the system or not.

Figure 4-17 shows the gradient of the output voltage ( $g_V$ ) under different load variations, and it can be observed from the figure that the circuit gets more sensitive to the variation of  $L_{S2}$  if the load decreases but less sensitive if the load increases. The shape change of the output voltage curve also happens in the case of operating frequency variation and tuning capacitor variation. However, since these two variations are generally tolerated by the

pickup in a very small percentage, i.e., 1 ~ 2% for the operating frequency variation and 1 ~ 5% for the tuning capacitor variation, the effect caused by these two variations on the shape of the tuning curve are very limited compared with that of the load variations and therefore have been omitted in the analyses.

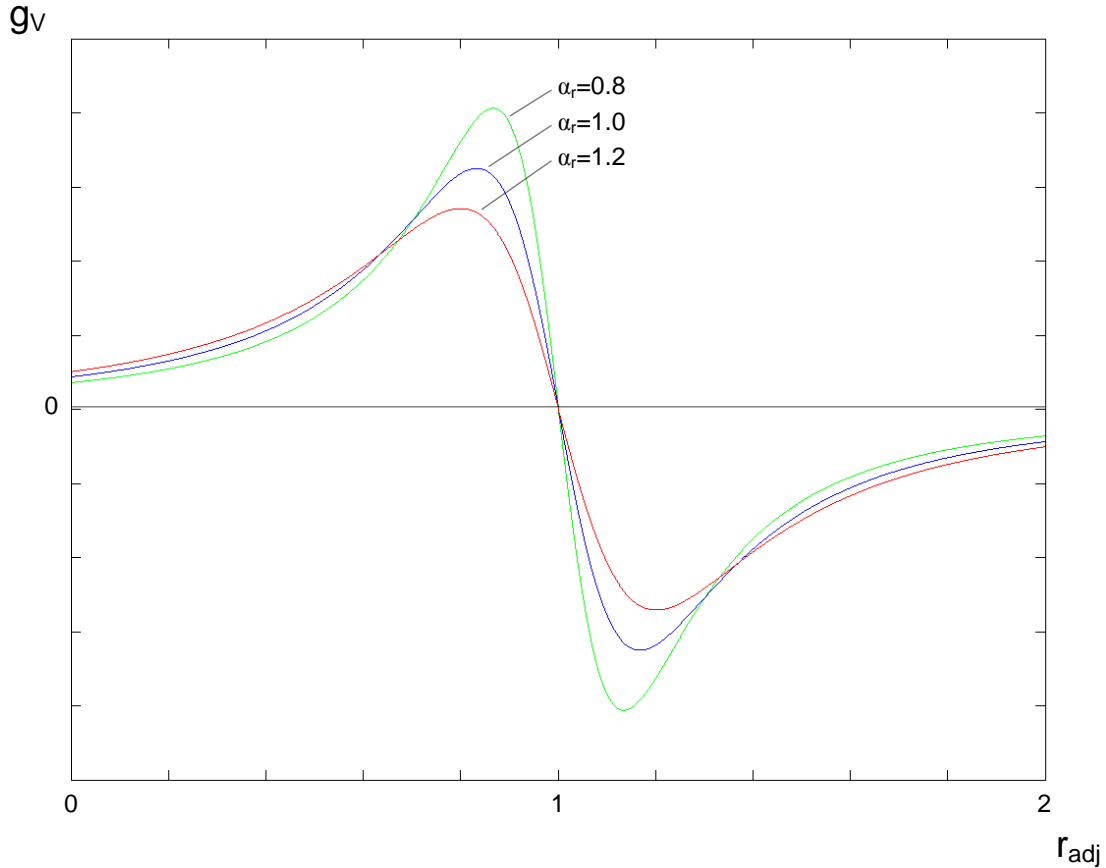


**Fig. 4-17: Gradient of output voltage under different load variations**

Given a desired output voltage  $V_{ref}$ , the required adjusting ratio can be determined from:

$$r_{adj\_rv} = 1 \pm \frac{\alpha_r R_{AC} \sqrt{\frac{1}{r_k^2} - 1}}{\omega_0 k_{VR} L_{S1}} \quad (4-47)$$

And in order to obtain valid solutions from the above equation,  $r_k$  has to be less than or equal to 1 to ensure that the control range provided by the variable  $L_{S2}$  will always be able to compensate for the load variations. The relationship between the load variation and the adjusting ratio is presented in Fig. 4-18, having the result of the ratio required for



achieving the desired  $r_k$  in the over-tuning region and the under-tuning region represented by  $r_{adj\_rv\_OT}$  and  $r_{adj\_rv\_UT}$  respectively. As for the ratio for achieving the maximum output voltage at fully-tuned condition, the result is represented by  $r_{adj\_rvr}$ .

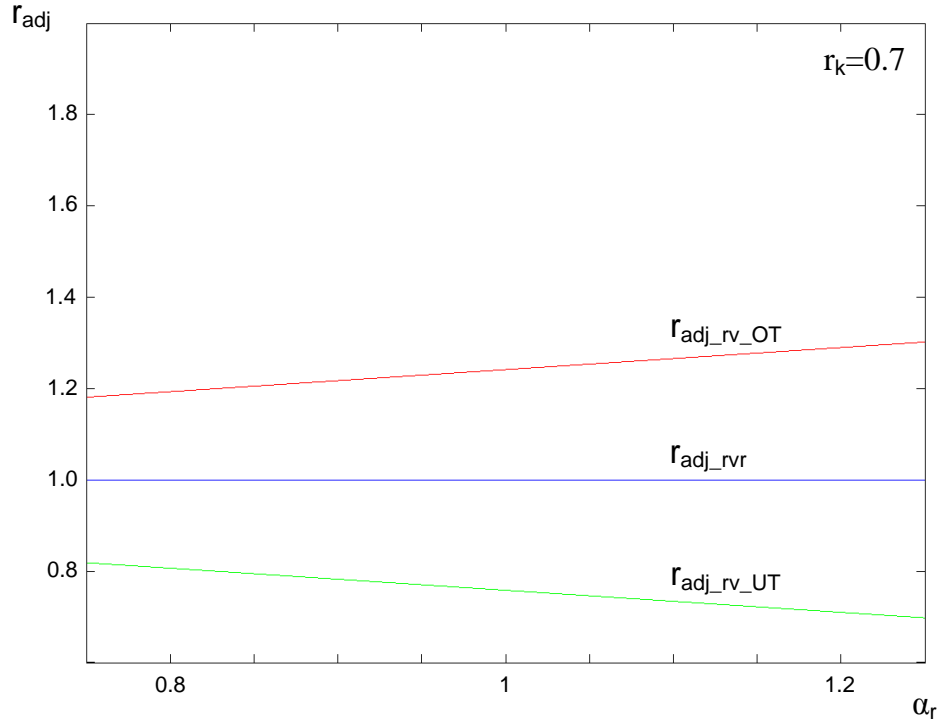


**Fig. 4-18: Adjusting ratio of  $L_{S2}$  for LCL power pickup to achieve desired  $r_k$  under load variations**

#### 4.3.5 Choice of $k_{VR}$ and $r_k$

From the analyses that have been carried out in the previous sections, it is known that in order to provide sufficient voltage at the output and also be able to compensate for all considered parameter variations by using the variable  $L_{S2}$ , the nominal voltage boosting factor  $k_{VR}$  and the ratio  $r_k$  have to be carefully selected. These two parameters under different values can cause different effects on the output voltage variation with respect to the circuit parameter variations and thus need to be further investigated for having a proper pickup tuning circuit design.

Note that the operating regions of the pickup can be separated into two regions which are the under-tuning region and the over-tuning region. However, since the relationships

between the output voltage variation,  $k_{VR}$ , and  $r_k$  are identical in these two regions, only the result of under-tuning region is analyzed in this section.

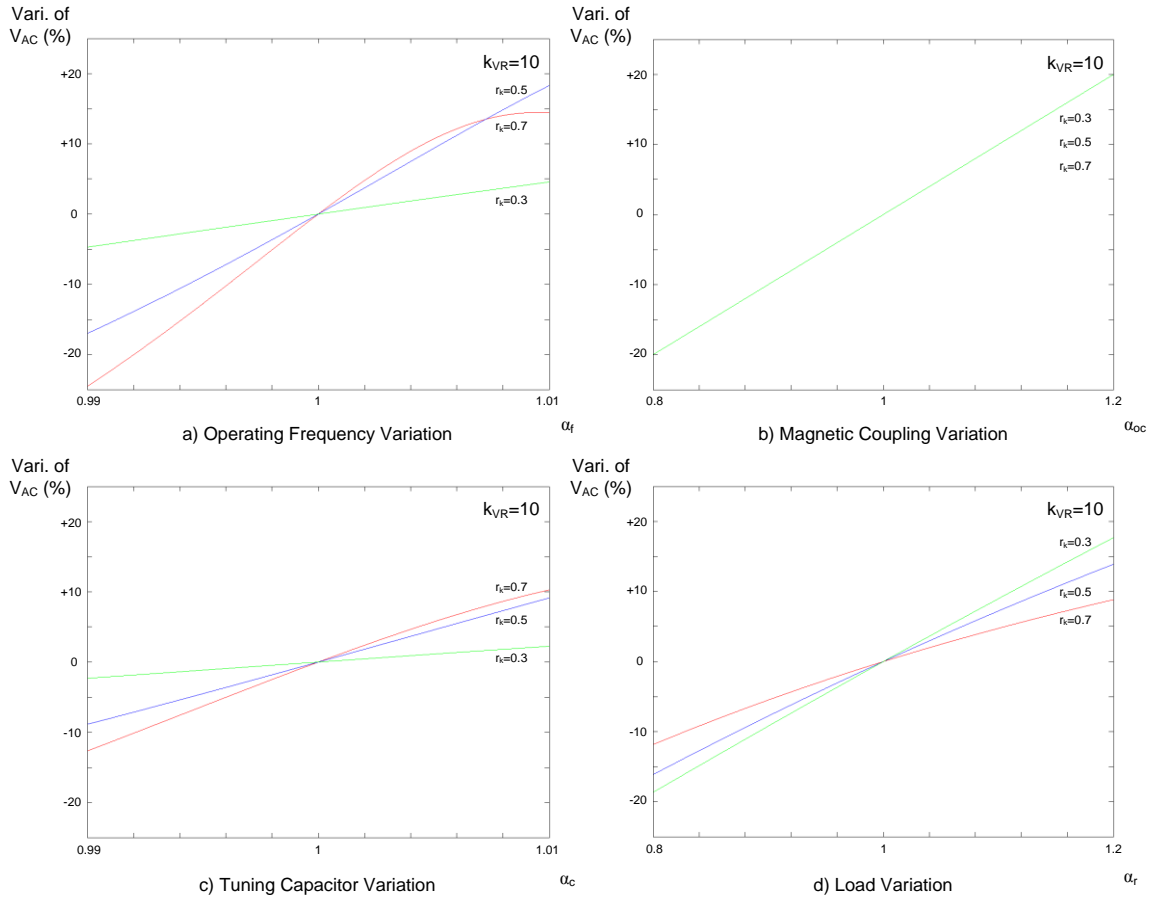


**Fig. 4-19: Relationship between output voltage variation and parameter variation under a constant  $k_{VR}$  and different  $r_k$**

Figure 4-19 shows the output voltage variations (in %) caused by: a) operating frequency variations, b) magnetic coupling variations, c) tuning capacitor variations, and d) load variations, under a constant  $k_{VR}$  with different  $r_k$ . Such a setup is used to see how changing the value of  $r_k$  affects the relationship between the output voltage variation and the parameter variations. It can be seen from the results of a) and c) that if a lower  $r_k$  is used, i.e., 0.3 and 0.5, not only the magnitude of the output voltage variations can be reduced but the linearity and symmetry between the output voltage variation and the parameters variation can also be improved. Contrary to the case of d), the magnitude, linearity, and symmetry of the result only get improved by operating with higher  $r_k$ . In the case of b), the result is not affected by any variations of  $r_k$ .

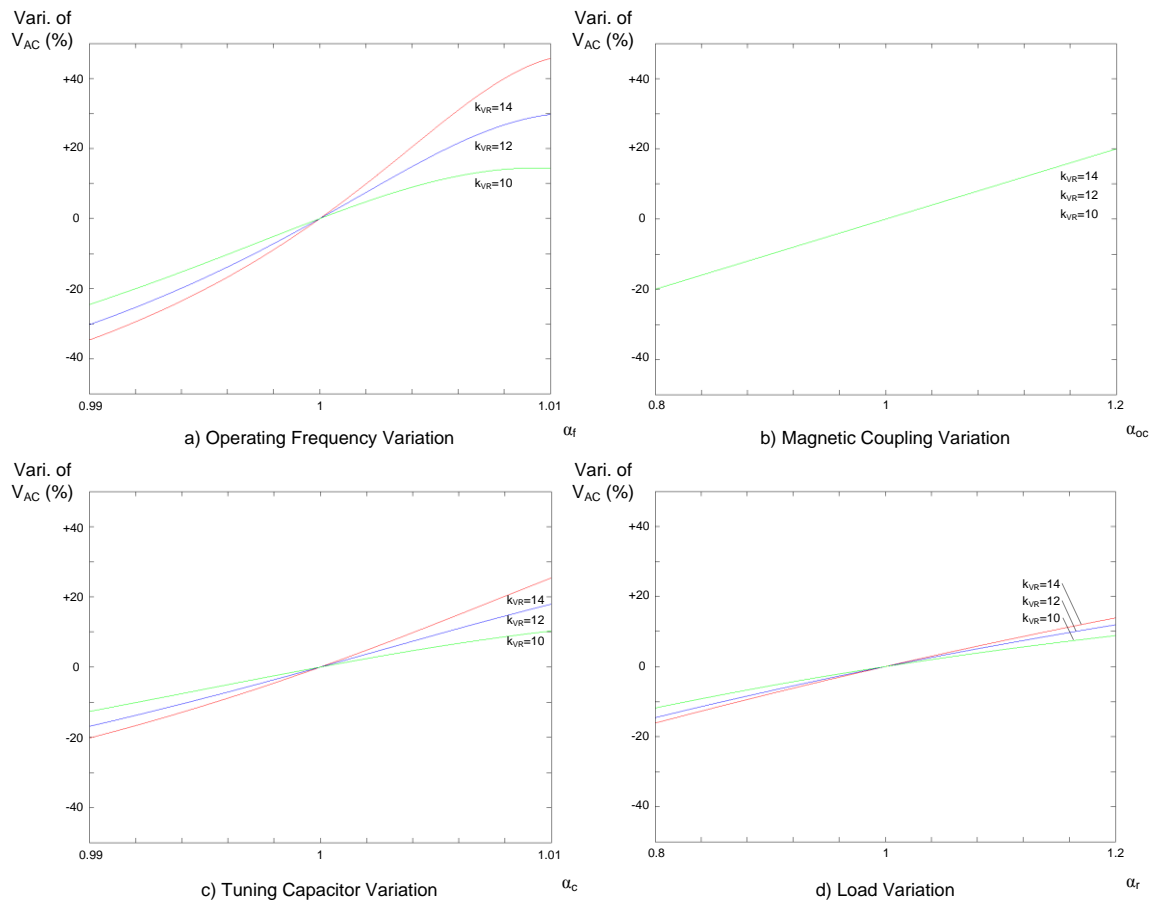


**Fig. 4-20: Relationship between output voltage variation and parameter variation under a constant  $V_{ref}$  and different  $k_{VR}$**

Figure 4-20 shows the output voltage variations (in %) caused by the considered parameters variation under a constant  $V_{ref}$  with different  $k_{VR}$ . The results obtained in a), c), and d) show that the magnitude of the output voltage variation can be reduced if a lower  $k_{VR}$  is used. In addition, the linearity and symmetry of the result can also be improved under low  $k_{VR}$  operation. Notice that the result of b) still remains unchanged, which shows that it is the only one of the four considered cases whose result is completely independent of the variations in both  $r_k$  and  $k_{VR}$ .

In terms of the circuit sensitivity, it can be seen from both Fig. 4-19 and Fig. 4-20 that the pickup is most sensitive to the operating frequency variation, followed by variation in the tuning capacitance, magnetic coupling, and the load. In the case of a) and c), the sensitivity of the output voltage increases to both  $r_k$  and  $k_{VR}$ . In the case of d), the output voltage sensitivity increases to  $k_{VR}$  but decreases to the increase of  $r_k$ . The case of b) is the

only parameter variation that has an unaffected linear relationship with the output voltage variation, and its positive and negative variations have symmetrical effect on the output voltage variation in terms of magnitude. Note that in the case of a), c), and d) have all been observed with nonlinearities in the result, and it would be very beneficial to keep the relationship between the output voltage variations and the considered parameter variations as linear and symmetrical as possible if a balanced control in both positive and negative parameter variations is to be obtained.

In a practical IPT system design, it is important to prevent any kind of instantaneous voltage increasing in the output to protect the load from overvoltage. If the output voltage is expected to have variations caused by the parameter variations, then the pickup should be designed to keep the output voltage variation as low as possible. From the results shown in Fig. 4-19 and Fig. 4-20, the sensitivity of the output voltage variation can generally be reduced by lowering  $k_{VR}$  and  $r_k$  despite the fact that operating the pickup with lower  $r_k$  would increase the output voltage sensitivity to the load variation. However, if a desired output voltage is predefined, lowering the value of  $k_{VR}$  will result in the increase of  $r_k$  and leads to a contradictory situation. Furthermore, the design of  $k_{VR}$  is directly depending on the ratio between open-circuit voltage of the pickup coil and output voltage of the pickup, and required to be adjusted inversely proportional to the open-circuit voltage for achieving the desired output voltage. Therefore with the reasons discussed, the output voltage sensitivity to the parameter variations can only be optimized to have lower output voltage variations on average.

#### 4.3.6 Operating Range of Variable $L_{S2}$

To determine the operating range of the variable  $L_{S2}$  which allows the pickup to fully compensate for all the parameter variations that have been discussed, the integrated effect of these parameter variations needs to be considered here. Under such a condition, the operational voltage boosting factor  $k_V$  can be expressed as:

$$k_V = \frac{\alpha_f \alpha_{oc} \alpha_r k_{VR} R_{AC} \sqrt{(\alpha_r R_{AC})^2 [k_{VR}(\alpha_T - 1) + \alpha_T]^2 + (\alpha_f \omega_0 k_{VR} L_{S1})^2 \{1 - r_{adj} [k_{VR}(\alpha_T - 1) + \alpha_T]\}^2}}{(\alpha_r R_{AC})^2 [k_{VR}(\alpha_T - 1) + \alpha_T]^2 + (\alpha_f \omega_0 k_{VR} L_{S1})^2 \{1 - r_{adj} [k_{VR}(\alpha_T - 1) + \alpha_T]\}^2} \quad (4-48)$$

where  $\alpha_T$  is equal to  $\alpha_f^2 \alpha_c$  which represents the integrated variation of the operating frequency and the tuning capacitor. Equation (4-48) can also be rearranged to obtain the required adjusting ratio  $r_{adj-pv}$  for achieving the desired output voltage under the integrated effect of the parameters variation, and the required ratio is determined from:

$$r_{adj-pv} = \frac{1}{k_{VR}(\alpha_T - 1) + \alpha_T} \cdot \left[ 1 \pm \frac{\alpha_r R_{AC} \sqrt{\frac{\alpha_{oc}^2}{r_k^2} - \left[ \frac{k_{VR}(\alpha_T - 1) + \alpha_T}{\alpha_f} \right]^2}}{\omega_0 k_{VR} L_{S1}} \right] \quad (4-49)$$

For equation (4-49) to have valid solutions, the following condition has to be met.

$$r_k \leq \frac{\alpha_f \alpha_{oc}}{k_{VR}(\alpha_T - 1) + \alpha_T}$$

In order to fully compensate for all the considered parameter variations, the worst-case scenario during practical operations has to be considered for obtaining the minimum and the maximum required adjusting ratio, so an operating range for the variable  $L_{S2}$  can be defined. Based on the results shown in Fig. 4-10, Fig. 4-12, Fig. 4-14, and Fig. 4-16, the minimum and the maximum required adjusting ratio can be calculated using (4-49) with the following conditions.

#### **Maximum required ratio**

- The LCL power pickup is operating in the over-tuning region of the output voltage tuning curves.
- The operating frequency and tuning capacitor variations are at *nominal value - maximum allowable tolerance*, and the magnetic coupling and load variations are at *nominal value + maximum allowable tolerance*.

#### **Minimum required ratio**

- The LCL power pickup is operating in the under-tuning region of the output voltage tuning curves.

- The considered parameter variations are all at *nominal value + maximum allowable tolerance*.

## 4.4 Implementation of DTDCA Controlled LCL Power Pickup

A variable inductor can be achieved by either using a switch-mode inductor or a saturable inductor [71, 98, 99]. Each of them has distinguishing advantages and shortcomings. For a switch-mode inductor, its equivalent inductance can be controlled by directly changing the duty cycles of the switching signal to perform precise tuning. But this technique generates switching noises and may require additional filter design to reduce the undesired harmonics. As for the saturable inductor, its equivalent inductance is dependent on the characteristics of the magnetic core material and can be directly controlled by a variable dc current, which is much easier to design, but may require more experiences and deep knowledge on the electromagnetic theories. A DTDCA controlled LCL power pickup based on a saturable inductor with variable equivalent inductance is proposed and implemented in this section as a means of power pickup control.

### 4.4.1 Linear-Mode Saturable Inductor

The fundamental concept of using a saturable inductor is to change the permeability of core material and thereby vary the inductance. This technique has commonly been used in the past for various control applications [100-105]. A linear-mode saturable inductor is adopted in the LCL power pickup to function as a variable tuning inductor. Note that the term ‘linear-mode’ here means the operating state of the semiconductor device that controls the dc current flowing through the core for changing the permeability of the core.

The inductance of  $L_{S2}$  using a saturable inductor is determined by:

$$L_{S2} = \frac{\mu_d N^2 S}{l} \quad (4-50)$$

where  $N$  is the total number of turns in the windings,  $S$  is the average cross-sectional area of the core, and  $l$  is the mean length of the magnetic flux path. The permeability  $\mu_d$  of the core material can be theoretically calculated by using  $dB/dH$ , where  $dB$  and  $dH$  are the

changing rate of the magnetic flux density and the magnetic field strength respectively, and these two parameters can often be obtained from the B-H curve that is given in the datasheet. However it is more appropriate to use a simple circuit shown in Fig. 4-21 to experimentally obtain the actual effective core permeability or inductance.

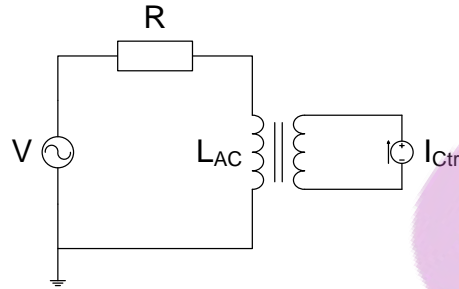


**Fig. 4-21: Testing circuit for obtaining effective core permeability**

By changing the dc control current  $I_{Ctrl}$  to vary the core permeability which consequently changes the inductance of  $L_{AC}$ , the voltage across  $L_{AC}$  would be varied and can be presented as:

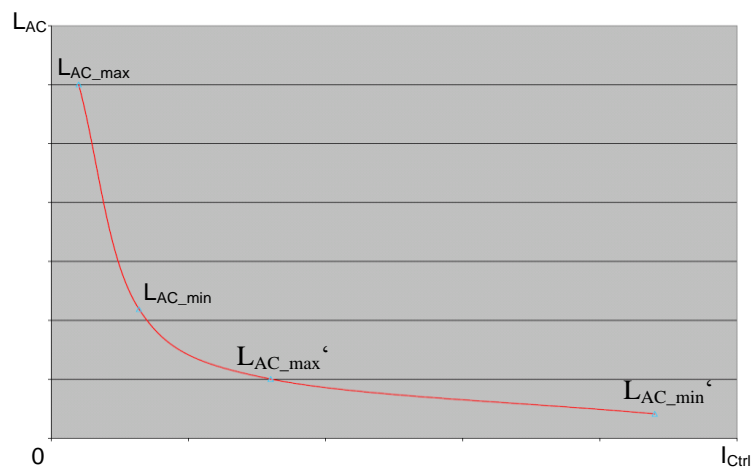
$$V_{L_{AC}} = \frac{\omega L_{AC}}{R + \omega L_{AC}} \cdot V \quad (4-51)$$

where  $\omega$  is the frequency of the input voltage and should be selected same as the nominal operating frequency of the IPT system that the saturable inductor being applied to. Given that the input voltage  $V$ , resistor  $R$ , and voltage across  $L_{AC}$  are either known parameter or can be directly measured, the inductance of  $L_{AC}$  can then be calculated from:

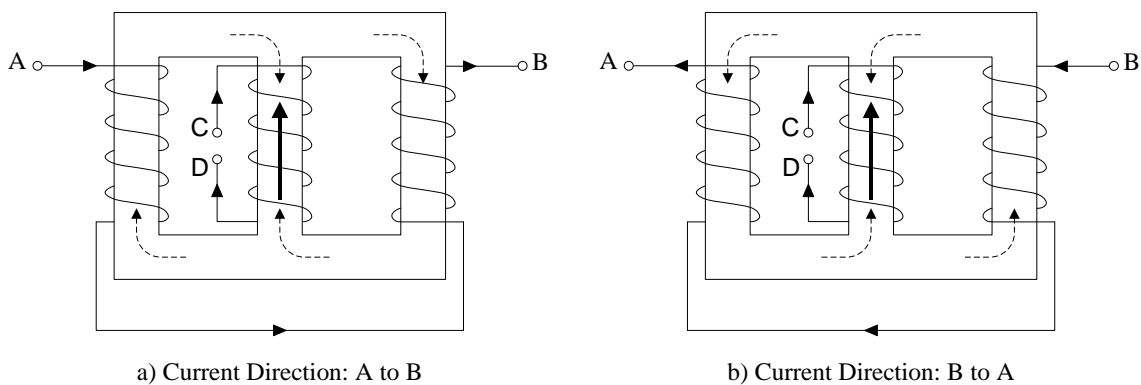
$$L_{AC} = \frac{V_{L_{AC}} R}{\omega(V - V_{L_{AC}})} \quad (4-52)$$

Figure 4-22 shows a typical relationship between the dc control current  $I_{Ctrl}$  and the effective inductance of a saturable inductor. As can be seen from the figure that the relationship is extremely nonlinear, and to prevent this nonlinearity being introduced between the controller and the actual  $L_{S2}$ , only the quasi-linear part of the relationship can be used. It can be seen that there are two quasi-linear parts as shown in the figure which are the region between  $L_{AC\_max}$  to  $L_{AC\_min}$  and  $L_{AC\_max}'$  to  $L_{AC\_min}'$ . However, the region between  $L_{AC\_max}'$  to  $L_{AC\_min}'$  requires more current and can only achieve very limited

variable inductance. Therefore the preferred operating range of the saturable inductor is selected to lie between  $L_{AC\_max}$  to  $L_{AC\_min}$ . Note that the range between  $L_{AC\_max}$  to  $L_{AC\_min}$  has to be sufficient to be equal to or larger than the operating range of  $L_{S2}$  that has been previously defined in the worst-case scenario. In fact, core materials with a linear relationship between the dc control current and the effective inductance should be used as it can extend the range of the variable inductance, which is particularly useful when the required operating range of  $L_{S2}$  is large.



**Fig. 4-22: Typical relationship between dc control current and effective inductance of saturable inductor**



**Fig. 4-23: Configuration of dc current controlled saturable inductor**

Figure 4-23 shows the adopted configuration of the saturable inductor. Point A and B of the outer ac windings are physically connected with the LCL tuning circuit, representing the variable tuning inductance  $L_{S2}$ . Point C and D of the inner dc windings are connected to a controllable dc current source for providing the required magnetizing force to achieve



the desired inductance. Using the configuration shown in Fig. 4-23, it can be seen that the flux produced by the ac current of the outer windings (thin-broken lines) is counteracted at the center core in both cases of a) and b), thereby leaving the dc control flux (thick-filled line) unaffected [99].

#### 4.4.2 General Structure of Linear-Mode Saturable Inductor Controlled LCL Power Pickup

The general structure of the proposed linear-mode saturable inductor controlled LCL power pickup is shown in Fig. 4-24. Besides the basic LCL power pickup, a directional tuning/detuning controller (DTDC), a MOSFET, and a saturable inductor are also collaborated with the pickup to form a complete secondary system. The saturable inductor shown in Fig. 4-23 can be directly used here having its point A, B, C, and D physically connected with the LCL power pickup as shown in Fig. 4-24. The inductance of  $L_{S2}$  is varied by changing the core permeability through the control of dc current  $I_{Ctrl}$ , and this dc control current is taking a very small portion (typically 1 ~ 3%) of the load current  $I_L$  so it does not affect the power efficiency of the secondary pickup too much.

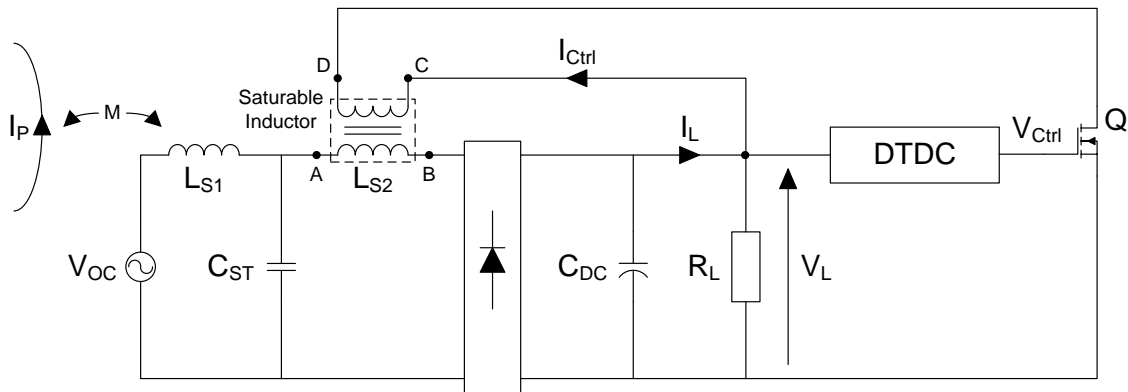


Fig. 4-24: General structure of saturable inductor controlled LCL power pickup

Strictly speaking the core permeability is varied by the magnetizing force produced from the dc control current, and the magnetizing force is given by:

$$H_{DC} = \frac{N_{DC} I_{Ctrl}}{l_{DC}} \quad (4-53)$$

where  $N_{DC}$  is the number of turns in the dc windings and  $l_{DC}$  is the mean length of the dc magnetic flux path. As can be seen from (4-53) that a trade-off between the size

(proportional to  $N_{DC}$ ) and the efficiency (inversely proportional to  $I_{Ctrl}$ ) of the pickup is inevitable.

The output voltage  $V_L$  of the pickup is used as a feedback signal to the DTDC for generating a voltage control signal  $V_{Ctrl}$ . The signal  $V_{Ctrl}$  is used to control the MOSFET  $Q$  which is designed to be operated in its linear region, so the MOSFET can function as a variable resistor and have the control of its conduction current which in this case is the dc control current  $I_{Ctrl}$ . Under such a controller structure, the proposed LCL power pickup would therefore be able to dynamically change the tuning condition of the pickup.

#### 4.4.3 Sampling Frequency for LCL Power Pickup

After each tuning adjustment in the inductance of  $L_{S2}$ , the pickup circuit would require certain time period to reach its steady state before the controller can take another valid sample from the output voltage. The CR (Capacitor-Resistor) circuit at the dc side of the LCL pickup has been identified as the major cause of this output delay. Figure 4-25 shows a simplified model for the dc side of the pickup.

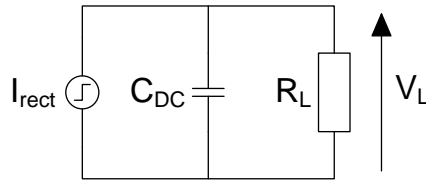


**Fig. 4-25: Model for dc output voltage analysis**

Since each control action would cause the output voltage to have a step change, the current  $I_{rect}$  is therefore modeled as a step current, and a differential equation can be derived as follows:

$$C_{DC} \frac{dV_L}{dt} + \frac{V_L}{R_L} = I_{rect} \quad (4-54)$$

By solving (4-54), the time-domain solution of the output voltage to this step change in the current can be approximated by:

$$V_L(t) = I_{rect} R_L \cdot \left(1 - e^{-t/R_L C_{DC}}\right) \quad (4-55)$$

Note that the solution obtained in (4-55) is not the actual solution for the output voltage. It is only being used for approximating the CR circuit response to the step change of output voltage. The settling time  $t_s$  which is the time required for the response to reach and stay within a specified tolerance band (usually 2 ~ 5%) of its final value, is given by (for 2% tolerance band)

$$e^{-t_s/R_L C_{DC}} = 0.02 \quad \text{or} \quad t_s \approx 4R_L C_{DC} \quad (4-56)$$

and the sampling frequency of the controller should be selected based on the time  $t_s$ . However, to have a controller with fast response, the time  $t_s$  needs to be reduced and this can only be achieved through a proper design of  $C_{DC}$ . This is because the value of  $R_L$  in (4-56) can only consider  $R_{L\_max}$  which is the maximum tolerable load resistance, since the time  $t_s$  selected based on this value will be able to give the maximum settling time covering the entire range of  $R_{L\_min}$  to  $R_{L\_max}$ . Generally the value of  $C_{DC}$  is selected to be large so that the output becomes a smooth dc voltage with maximum power available to the load. But using a large capacitance would cause the controller response to be sluggish with high ESR (Equivalent Series Resistance). In addition, this results in large inrush currents in the ac side of the pickup during startup which may cause overstress to the resonant components [106]. Conversely, a small dc capacitor will result in a discontinuous voltage after the rectifiers and lowers the amount of power that can be delivered. It is therefore important to determine the optimal dc capacitance for the pickup to get the possible maximum power while keeping the settling time of the circuit as small as possible.

Figure 4-26 shows the steady state waveforms of the current  $I_{AC}$ ,  $I_{rect}$ ,  $I_{DC}$ , and the voltage ripples  $V_{ripple}$  in the output voltage. Since the current flowing through the dc capacitance  $C_{DC}$  is equal to  $I_{rect} - I_L$ , the following differential equation can be obtained:

$$C_{DC} \frac{dV_{ripple}}{dt} = \hat{I}_{AC} |\sin(\omega t)| - I_L \quad (4-57)$$

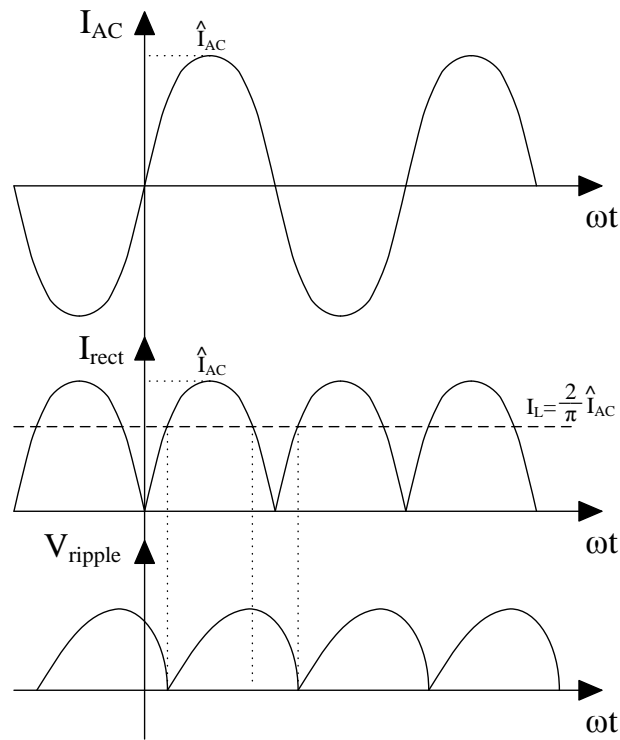


Fig. 4-26: Current and voltage waveforms under critical conduction condition

Considering the condition of  $V_{ripple} = 0$  when  $\omega t = \sin^{-1}(I_L / \hat{I}_{AC})$ , the complete solution of  $V_{ripple}$  can be presented by:

$$V_{ripple} = \frac{1}{\omega C_{DC}} \left[ I_L \sin^{-1}(I_L / \hat{I}_{AC}) + \sqrt{\hat{I}_{AC}^2 - I_L^2} - \hat{I}_{AC} \cos(\omega t) - I_L \omega t \right] \quad 0 \leq \omega t \leq \pi \quad (4-58)$$

Substituting  $I_L / \hat{I}_{AC} = 2/\pi$  into equation (4-58),  $V_{ripple}$  can further be simplified as:

$$V_{ripple} = \frac{I_L}{\omega C_{DC}} \left\{ 1.90147 - \left[ \frac{\pi}{2} \cos(\omega t) + \omega t \right] \right\} \quad 0 \leq \omega t \leq \pi \quad (4-59)$$

The maximum  $V_{ripple}$  can be obtained at  $\omega t = \pi - \sin^{-1}(2/\pi)$ . The relationship between  $V_{ripple\_max}$  and  $C_{DC}$  can therefore be expressed by:

$$V_{ripple\_max} \approx 0.66 \cdot \frac{I_L}{\omega C_{DC}} \quad \text{or} \quad C_{DC} \approx 0.66 \cdot \frac{I_L}{\omega V_{ripple\_max}} \quad (4-60)$$

By substituting (4-60) into (4-56), the sampling frequency can be obtained as:

$$f_s \approx 0.3788 \cdot \frac{\omega V_{ripple\_max}}{V_L} \quad (4-61)$$

Given that the value of  $\omega$  and  $V_L$  are constant, the value of  $V_{ripple\_max}$  has to be small to obtain a smooth dc output voltage, which consequently lowers the sampling frequency of the controller. Therefore, a trade-off between the response speed of the controller and the steadiness of the output voltage is needed. Note that (4-60) and (4-61) can be directly used in the practical design given that the dc output voltage is a constant value without any variations. Nevertheless, the output voltage may in fact be varied due to an instantaneous circuit parameter variation or a tuning control provided by the DTDCA during operations. Therefore in order to obtain optimal values for  $C_{DC}$  and  $f_s$ , the possible maximum  $I_L$  and  $V_L$  have to be considered in (4-60) and (4-61) respectively. The possible maximum value of  $I_L$  and  $V_L$  can be estimated using the analyses of output voltage response to the circuit parameter variations provided in Section 4.3.

#### 4.4.4 Tuning Step-Size for LCL Power Pickup

In order to successfully and efficiently perform the DTDCA, any two consecutive tuning adjustments should not cause the output voltage to jump across the two operating regions (under-tuning and over-tuning) of the tuning curve. To obtain the fixed maximum tuning steps-size  $\Delta h_m$  that is being used in the tracking process of coarse tuning stage at startup for the LCL pickup to avoid traversing between the operating regions under all possible tuning curves with different parameter variations, the extreme operating condition needs to be considered here. By observing the output voltage behavior from Fig. 4-10, Fig. 4-12, Fig. 4-14, and Fig. 4-16, the tuning curve with the shortest A-C range (see Fig. 3-3) can be identified and occurs under the operating condition of:

- The nominal operating frequency + maximum tolerable variation ( $\alpha_{f\_max}$ ).
- The nominal magnetic coupling - maximum tolerable variation ( $\alpha_{oc\_min}$ ).
- The nominal tuning capacitor + maximum tolerable variation ( $\alpha_{c\_max}$ ).
- The nominal load resistance - maximum tolerable variation ( $\alpha_{r\_min}$ ).

Under such a condition, the inductance of  $L_{S2}$  at position C can be obtained from:

$$L_{S2\_C} = \frac{L_{S2\_r-\omega_b}}{k_{VR}(\alpha_{f\_max}^2 \alpha_{c\_max} - 1) + \alpha_{f\_max}^2 \alpha_{c\_max}} \quad (4-62)$$

By presetting a startup voltage for the pickup and having a ratio between the startup voltage and the maximum output voltage under fully-tuned condition of  $r_{k\_startup}$ , the startup inductance of  $L_{S2}$  at position A and E can be obtained by:

$$L_{S2\_startup} = L_{S2\_C} \cdot \left[ 1 \pm \frac{\alpha_{r\_min} R_{AC} \sqrt{\frac{\alpha_{oc\_min}^2}{r_{k\_startup}^2} - \left[ \frac{k_{VR}(\alpha_{f\_max}^2 \alpha_{c\_max} - 1) + \alpha_{f\_max}^2 \alpha_{c\_max}}{\alpha_{f\_max}} \right]^2}}{\omega_0 k_{VR} L_{S1}} \right] \quad (4-63)$$

The maximum  $\Delta h_m$  for the LCL power pickup to perform coarse tuning can therefore be calculated by:

$$\begin{aligned} \Delta h_m &= \frac{L_{S2\_C} - L_{S2\_startup}}{2} \\ &= \frac{\alpha_{r\_min} R_{AC} \sqrt{\frac{\alpha_{oc\_min}^2}{r_{k\_startup}^2} - \left[ \frac{k_{VR}(\alpha_{f\_max}^2 \alpha_{c\_max} - 1) + \alpha_{f\_max}^2 \alpha_{c\_max}}{\alpha_{f\_max}} \right]^2}}{2\omega_0 k_{VR} L_{S1}} \cdot L_{S2\_C} \end{aligned} \quad (4-64)$$

## 4.5 Simulation/Experimental Results and Discussion

### 4.5.1 Simulation Study of DTDCA Controlled LCL Power Pickup

The simulation study was conducted in Matlab/Simulink environment using a toolbox called PLECS which emulates the circuit behavior of the LCL wireless power pickup. An LCL power pickup model shown in Fig. 4-27 was created under an ideal situation without taking into account the effects of ESR, forward voltage drop of diodes, and power consumed by the controller.

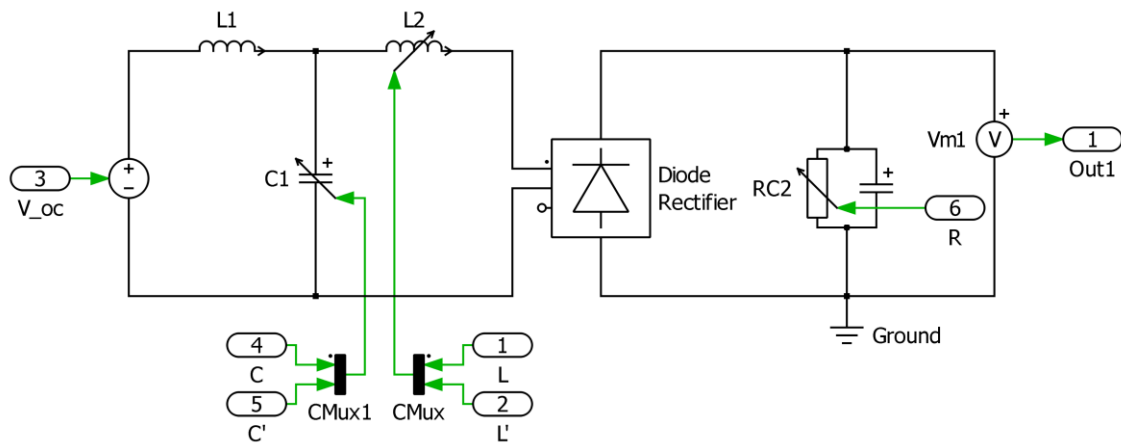


**Fig. 4-27: PLECS model of LCL power pickup**

The desired output voltage of the model is a constant 5 V with a  $\pm 2\%$  hysteresis band (4.9 ~ 5.1 V). The open-circuit voltage ( $V_{oc}$ ) of the pickup coil is a pure sinusoidal waveform having an amplitude of 2.8 V with a nominal operating frequency of 38.4 kHz, and the pickup coil  $L1$  has a self-inductance of 8.75  $\mu\text{H}$ . The tuning capacitance  $C1$  (equals to  $C_{S1}+C_{S2}$ ) has a nominal value of 2.395  $\mu\text{F}$  ( $C_{S1}=1.9632 \mu\text{F}$  and  $C_{S2}=0.4317 \mu\text{F}$ ) to provide a output voltage boosting factor  $k_{VR}$  of approximately 4.5473 for a maximum dc output voltage of 10 V under fully-tuned condition. The dc capacitance  $C2$  is selected to be 110  $\mu\text{F}$  so the maximum output voltage ripple can be kept below 0.05 V. The sampling frequency of the controller is approximately 455 Hz with the assumption that the maximum output voltage may go up to 10 V due to possible fully resonant operation or any instantaneous parameters change. The load resistance  $R$  has a nominal value of 5  $\Omega$ . Notice that  $V_{oc}$ ,  $C1$ , and  $R$  have all been connected to external variable sources to emulate the parameter variations that have been considered in section 4.3.

Figure 4-28 shows the complete Simulink model of a DTDCA controlled LCL power pickup. The simulation is initialized with a delay of 0.02 s in the DTDCA execution and has an initial  $L_{S2}$  of 20  $\mu\text{H}$  to provide an initial output voltage of approximately 6.5 V for easing the observation on the tracking process. Furthermore, a  $\Delta h_m$  of 7.01  $\mu\text{H}$  with a  $\beta$  of 0.1 have been used for the SSSA. To see the performance of DTDCA in compensating for each parameter variation, the model is simulated in extreme operating conditions where each considered parameter is varied instantaneously from its maximum to minimum tolerable value in their individual testing simulation.

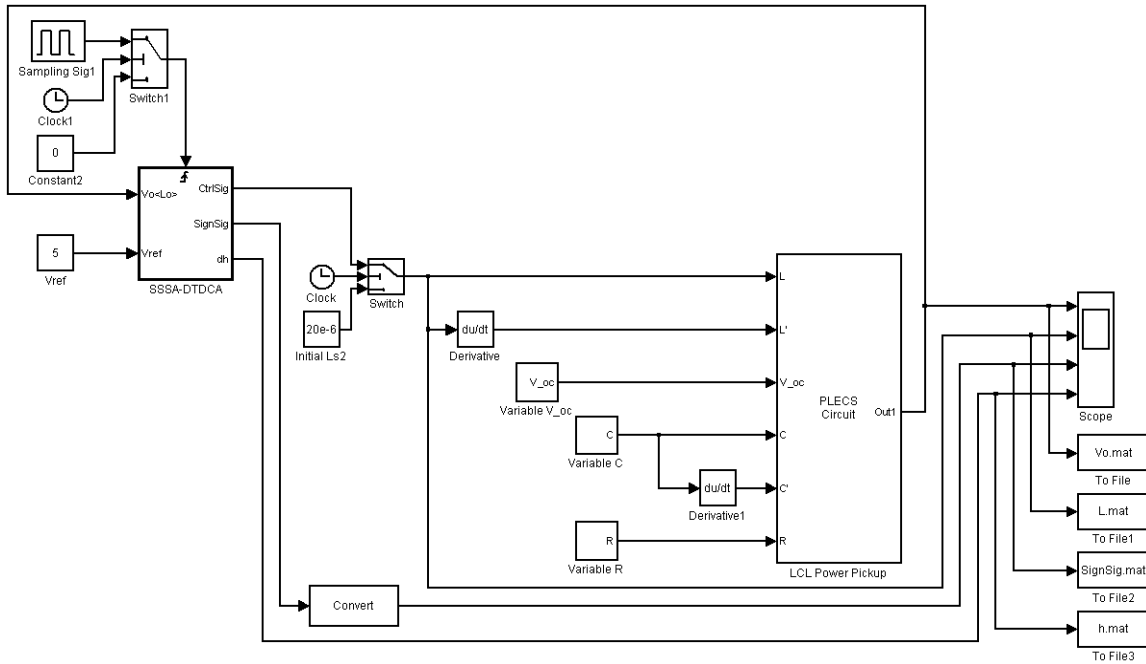


Fig. 4-28: Simulink model of DTDCA controlled LCL power pickup

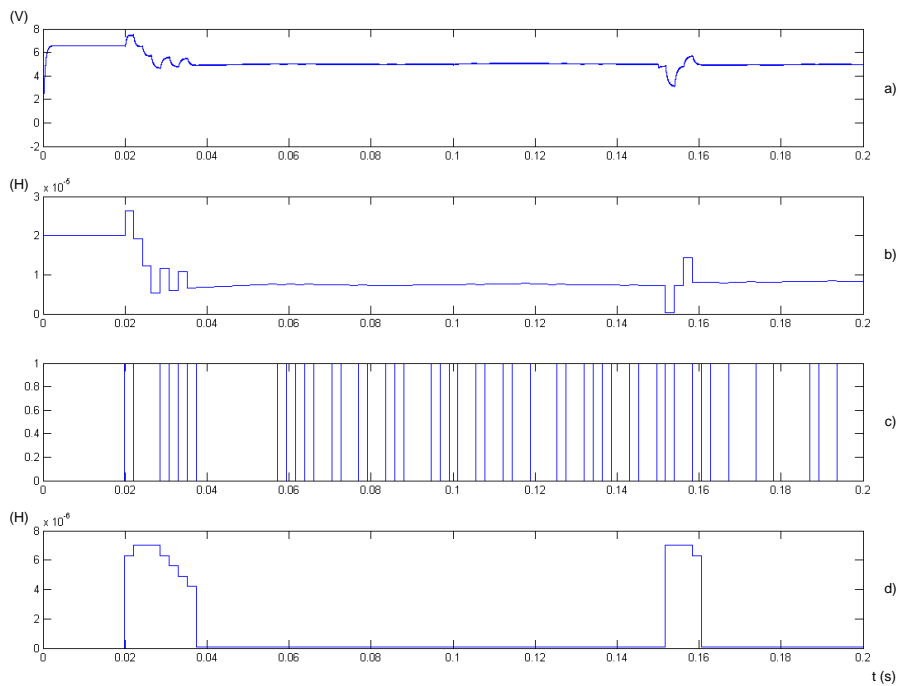
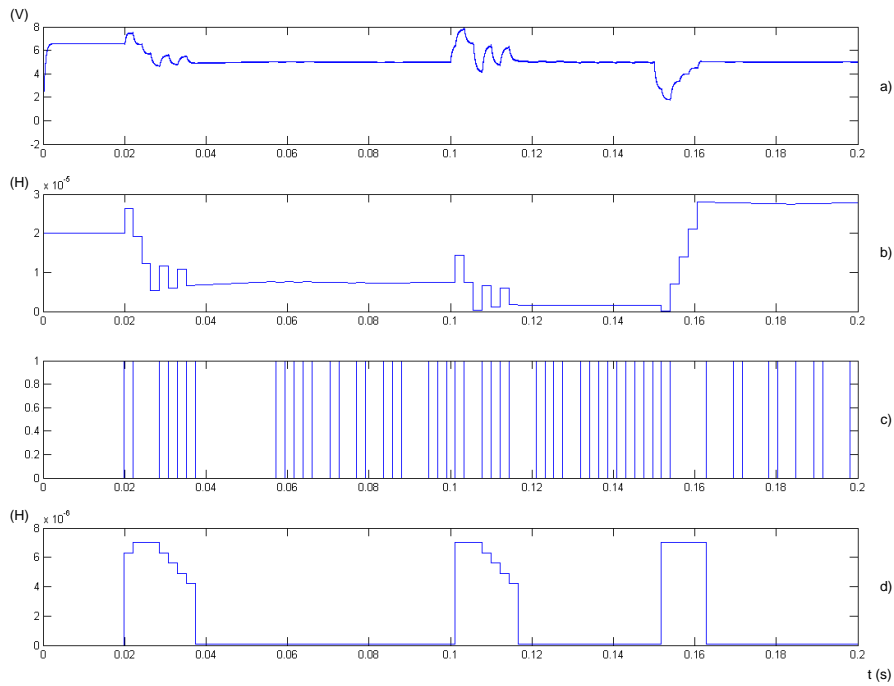


Fig. 4-29: Simulation result of: a) output voltage  $V_L$ , b) inductance of  $L_{S2}$ , c) tuning direction signal  $S_4$ , and d) tuning step-size  $\Delta h$ , of a DTDCA controlled LCL power pickup under operating frequency variations

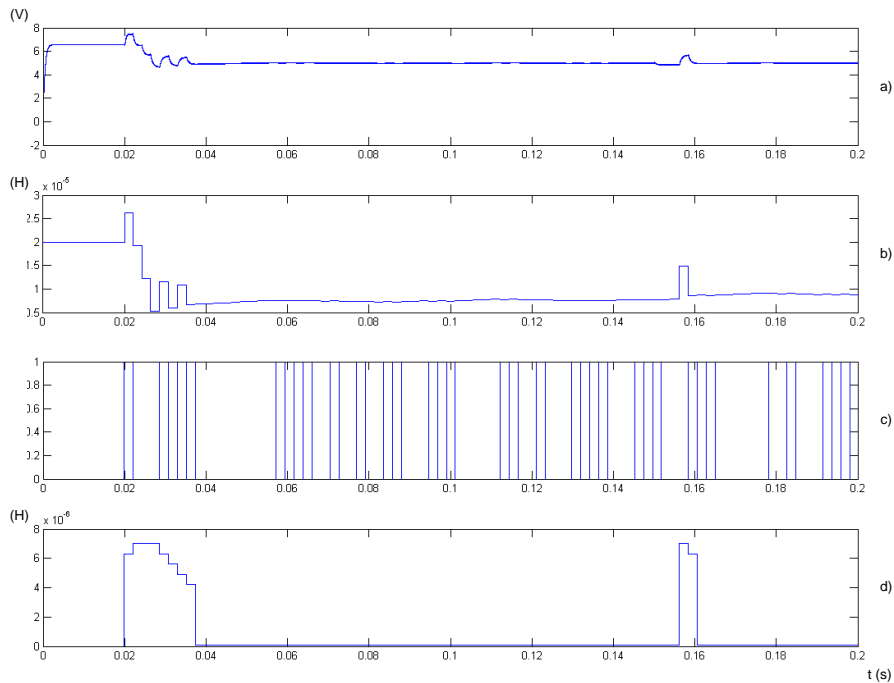


Figure 4-29 shows the simulation result of the output voltage regulation under the operating frequency variations. The nominal operating frequency of the simulation model is assumed to have  $\pm 2\%$  variation, which would cause the operating frequency to be varied from 37632 ~ 39168 Hz with an amplitude change in the open-circuit voltage from 2.744 ~ 2.856 V. The first extreme operating condition occurs at  $t = 0.1$  s having an operating frequency of 39168 Hz with an open-circuit voltage of 2.856 V. The second extreme operating condition occurs at  $t = 0.15$  s having an operating frequency of 37632 Hz with an open-circuit voltage of 2.744 V. It can be seen from the result that the first extreme operating condition do not cause noticeable difference in the output voltage and therefore requires no control action. The second extreme operating condition causes the output voltage to drop, but the controller successfully regulates the output voltage back into the hysteresis band after three cycles of the DTDCA execution. However, it was noticed that the controller performed incorrect tuning at  $t = 0.02$  s (beginning of the tracking) and  $t = 0.15$  s (time after the second extreme operating condition). The reason for the first mistaken tuning attempt is due to the lack of knowledge of the previous tuning direction signal ( $S_3$ ) since there has been no tuning action by the controller prior to  $t = 0.02$  s. This requires the controller to take a tuning attempt with the step-size that has been predefined in the initialization so the correct tuning direction in the next-state can be identified. The second mistaken tuning attempt occurred due to the output voltage being kept constant within the hysteresis band and the controller being unable to verify the correctness of the previous tuning action. This also requires the controller to take a tuning attempt depending on the result of  $S_4$  at the time, which in fact have a 50% chance to tune to the wrong direction and therefore needs to be improved.

Figure 4-30, 4-31, and 4-32 show the simulation result of the output voltage regulation under the variations in magnetic coupling, tuning capacitor and load resistance respectively. The model was assumed to have  $\pm 30\%$  variation ( $V_{oc}$  from 1.96 ~ 3.64 V) in the magnetic coupling between the primary and the secondary of the IPT system,  $\pm 5\%$  variation ( $C1$  from 2.2752 ~ 2.5147  $\mu\text{F}$ ) in the tuning capacitor, and  $\pm 30\%$  variation ( $R$  from 3.5 ~ 6.5  $\Omega$ ) in the load resistance. As can be seen, a similar result is obtained in each case of parameter variations which have been considered here. It was observed that the output voltage was eventually regulated and maintained within the hysteresis band around the voltage reference.



**Fig. 4-30: Simulation result of: a) output voltage  $V_L$ , b) inductance of  $L_{S2}$ , c) tuning direction signal  $S_4$ , and d) tuning step-size  $\Delta h$ , of a DTDCA controlled LCL power pickup under magnetic coupling variations**



**Fig. 4-31: Simulation result of: a) output voltage  $V_L$ , b) inductance of  $L_{S2}$ , c) tuning direction signal  $S_4$ , and d) tuning step-size  $\Delta h$ , of a DTDCA controlled LCL power pickup under tuning capacitor variations**

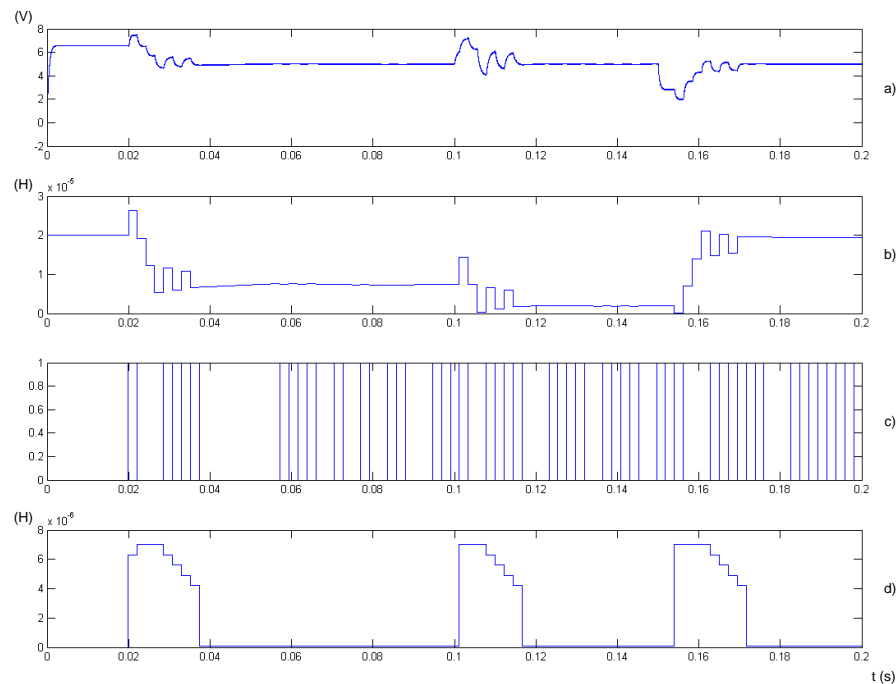


**Fig. 4-32: Simulation result of: a) output voltage  $V_L$ , b) inductance of  $L_{S2}$ , c) tuning direction signal  $S_d$ , and d) tuning step-size  $\Delta h$ , of a DTDCA controlled LCL power pickup under load variations**

### 4.5.2 Experimental Study of DTDCA Controlled LCL Power Pickup

To further show the effectiveness of the proposed controller, the DTDCA was applied onto an LCL power pickup in a practical IPT system. The primary track power supply of the prototype has a sinusoidal track current with an amplitude of 0.75 A and an operating frequency of 38.4 kHz with variations of less than  $\pm 1\%$ . The track was wound onto a cylindrical object with 34 turns to enhance the magnetic coupling between the primary and the secondary side of the system. The secondary pickup coil has a self-inductance of 8.75  $\mu\text{H}$  with 7 turns in the winding, and it has a nominal open-circuit voltage of 2.47 V when it was placed 6 mm away from the primary track. A capacitor with a capacitance of 2.2  $\mu\text{F}$  with a manufacturing tolerance of  $\pm 10\%$  was used as the tuning capacitor of the LCL tuning circuit. Considering the coupling factor  $k_f$  that has been introduced in Chapter 2 equals to  $N_s I_{SC} / N_p I_P = n_s I_{SC} / I_P$ , a nominal coupling factor of approximately 0.32 was obtained from this experiment setup. A controller development platform called dSPACE which allows rapid control algorithm development and testing was used for executing the DTDCA. The output voltage of the pickup was used as a feedback signal for the dSPACE

to produce a control signal ( $V_{GS}$ ) so as to control the conduction current of the linear-mode MOSFET BS107. Note that this controlled conduction current was also the dc control current of the saturable inductor which functions as the variable tuning inductor  $L_{S2}$ . The conduction current (dc control current) has a variable range of 0 ~ 0.1 A corresponding to the 2 ~ 3 V of the gate driving signal ( $V_{GS}$ ) range of the MOSFET, and the maximum signal level for each tuning step was set to 0.045 V to approximate the  $\Delta h_m$  of 7.01  $\mu\text{H}$ . Figure 4-33 shows a working prototype of the proposed LCL power pickup in the laboratory.

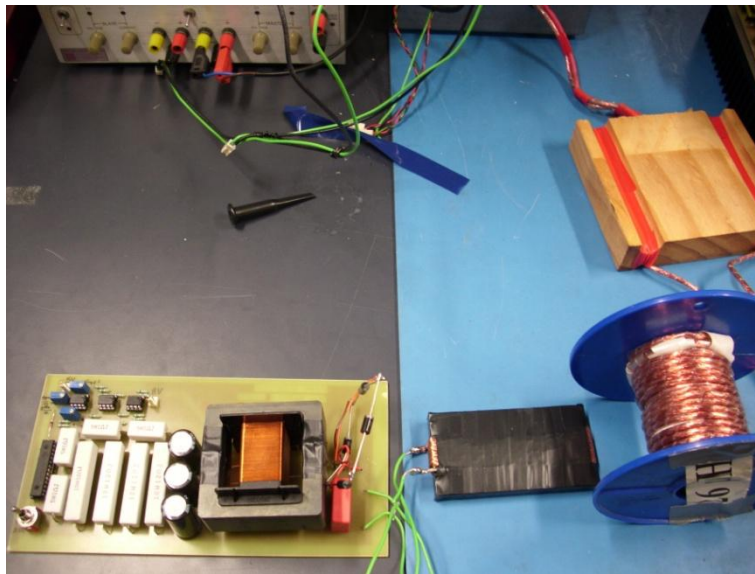
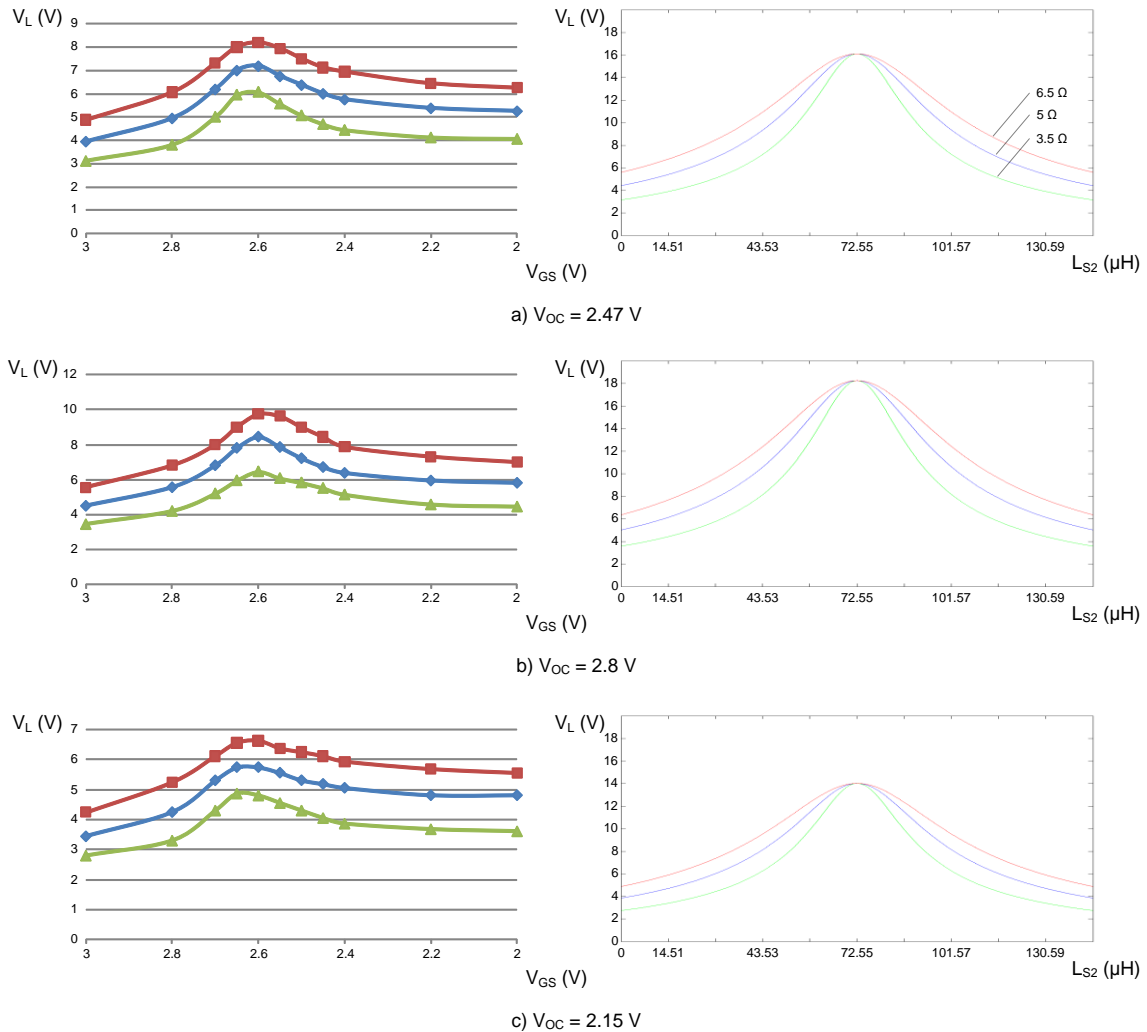


**Fig. 4-33: Working prototype of LCL power pickup**

Figure 4-34 shows the practical and ideal output voltage tuning curves under the open-circuit voltage and load variations, and the results were obtained under the condition of  $V_{OC}$  has a nominal value of 2.47 V with variations of  $\pm 13\%$  (2.15 ~ 2.8 V) and the load resistance has a nominal value of 5  $\Omega$  with variations of  $\pm 30\%$  (3.5 ~ 6.5  $\Omega$ ). Note that the x-axis ( $V_{GS}$ ) of the practical measurements are presented in the reverse direction due to the inductance of  $L_{S2}$  being inversely proportional to  $V_{GS}$ .

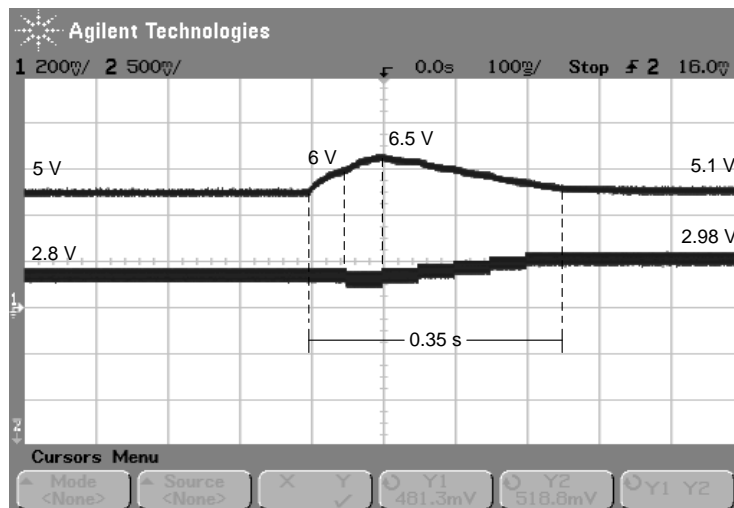
From Fig. 4-34, it can be seen that the practical measurements are considerably different from the ideal results. The reasons of the difference were identified after taking practical issues into consideration which include: 1) the ESR of the pickup coil, tuning capacitor, and variable tuning inductor, which were not being considered in the theoretical analyses of Section 4.2.2 for reducing the circuit model complexity, and 2) the voltage drop of the

full-bridge rectifier. Furthermore, it was found that since the saturable inductor was placed too close to the secondary pickup coil, the magnetic coupling between the primary and the secondary side of the system was affected and caused the LCL pickup to lose its voltage source property under fully-tuned condition.



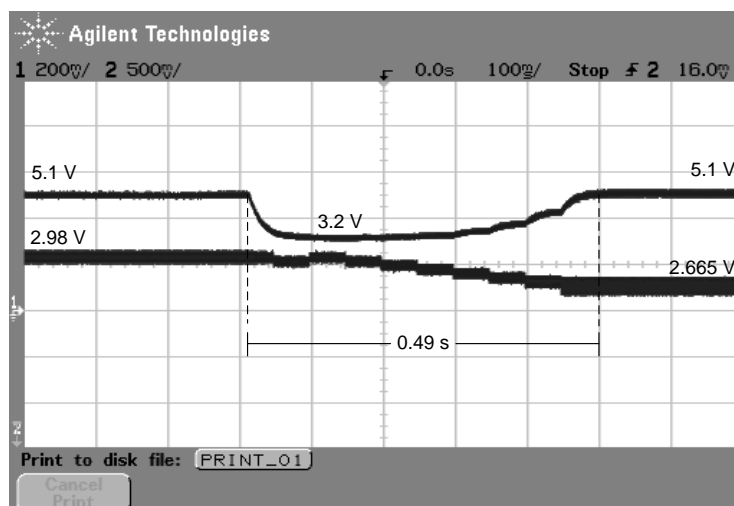
**Fig. 4-34: Practical and ideal output voltage tuning curves under load variations with a)  $V_{OC} = 2.47 \text{ V}$ , b)  $V_{OC} = 2.8 \text{ V}$ , and c)  $V_{OC} = 2.15 \text{ V}$**

In order to evaluate the performance of the DTDCA in the under-tuning region under load variations, the open-circuit voltage of the pickup coil was selected to be at the nominal value (2.47 V) and  $V_{GS}$  was initialized to 2.8 V. The load variations were proceeded in the sequence of 5  $\Omega$  (nominal and also the initial load resistance), 6.5  $\Omega$  (nominal +30% variation), 3.5  $\Omega$  (nominal -30% variation), and back to 6.5  $\Omega$ .



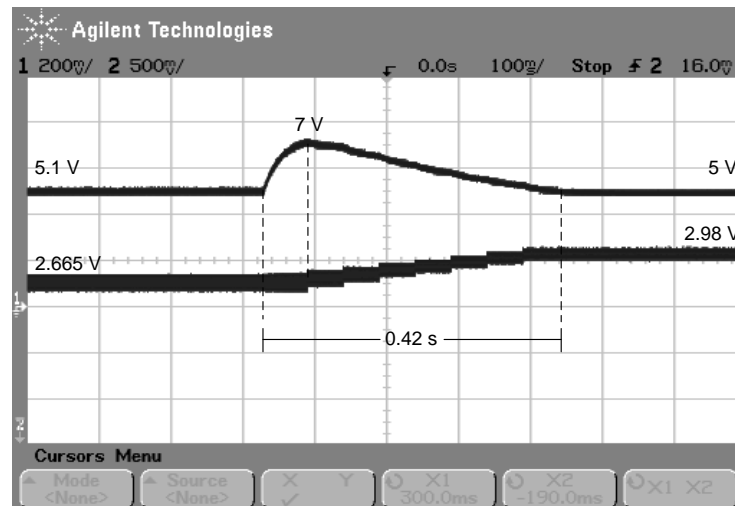
**Fig. 4-35: Output voltage waveform of DTDC controlled LCL power pickup under load variation (5 to 6.5  $\Omega$ ) in the under-tuning region**

Figure 4-35 shows the output voltage waveform when the load resistance was switched from 5 to 6.5  $\Omega$ . From Fig. 4-35, it can be observed that the output voltage was initially stabilized at 5 V with a  $V_{GS}$  of 2.8 V. After switching the load resistance to 6.5  $\Omega$ , the output voltage was increased to 6 V and followed by an incorrect tuning attempt in the next sampling instance which resulted in an extra error of 0.5 V to the output voltage. However, after checking the validity of the tuning attempt, the controller retuned the circuit in the opposite direction and stabilized the output voltage at 5.1 V.



**Fig. 4-36: Output voltage waveform of DTDC controlled LCL power pickup under load variation (6.5 to 3.5  $\Omega$ ) in the under-tuning region**

The load resistance was then switched to  $3.5 \Omega$  and the obtained result can be seen in Fig. 4-36. In this load change, the output voltage was dropped to 3.2 V. It can be seen from the result that the sampling frequency was faster than the settling time of the pickup circuit and caused the control signal  $V_{GS}$  to idle for the first two tuning attempts. But the controller then successfully identified the correct tuning direction in the third attempt and stabilized the output voltage at 5.1 V once again.



**Fig. 4-37: Output voltage waveform of DTDCA controlled LCL power pickup under load variation ( $3.5$  to  $6.5 \Omega$ ) in the under-tuning region**

Figure 4-37 shows the result of switching the load resistance from  $3.5$  back to  $6.5 \Omega$ . Similar to the results from the previous load variations, the output voltage of the pickup was regulated by the controller to the desired  $5$  V, the only difference being the control process did not involve any incorrect tuning attempt nor there is any idling of the control signal.

The second experiment was conducted for evaluating the performance of DTDCA under the magnetic coupling variations in the over-tuning region, and therefore had  $V_{GS}$  initialized to  $2.4$  V. Figure 4-38 shows the output voltage waveform under the magnetic coupling variations in the sequence of A, B, C, and D, with the following conditions:

- A)  $V_{OC} = 2.47$  to  $2.8$  V,  $k_f = 0.32$  to  $0.36$  (coupling distance  $6$  to  $2$  mm).
- B)  $V_{OC} = 2.8$  to  $2.47$  V,  $k_f = 0.36$  to  $0.32$  (coupling distance  $2$  to  $6$  mm).

- C)  $V_{OC} = 2.47$  to  $2.15$  V,  $k_f = 0.32$  to  $0.28$  (coupling distance 6 to 10 mm).
- D)  $V_{OC} = 2.15$  to  $2.47$  V,  $k_f = 0.28$  to  $0.32$  (coupling distance 10 to 6 mm).

The obtained result shows that the output voltage had a minimum of 4.31 V and a maximum of 5.68 V caused by the coupling variations, however it was still successfully regulated by the controller to the desired 5 V.

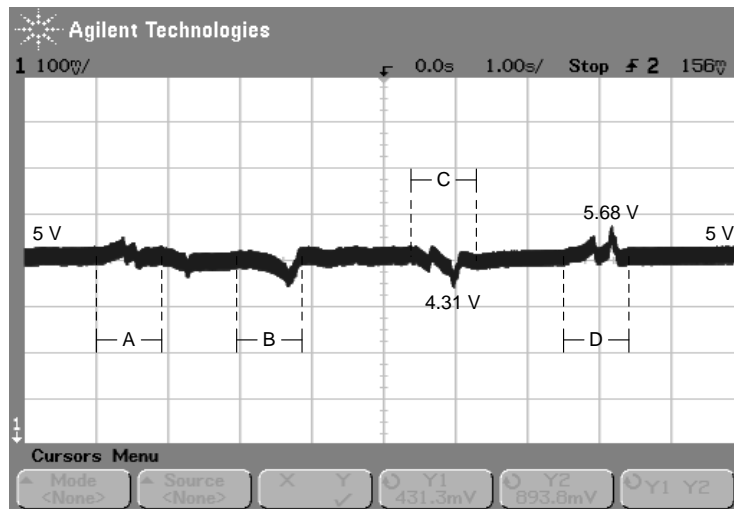


**Fig. 4-38: Output voltage waveform of DTDCA controlled LCL power pickup under magnetic coupling variations in the over-tuning region**

From the experimental results, it can be seen that the pickup can work in both under-tuning and over-tuning regions, which means that the proposed controller can control the pickup to have the desired voltage as long as the desired value is on the controlled tuning curve. This also allows the pickup to be fully-tuned on-line, if required, and therefore makes it possible to achieve high  $k_{VR}$  operation (or high  $Q$  operation for LC pickups).

### 4.5.3 Discussion

Despite the fact that the proposed DTDCA has been proven to be effective for the output voltage regulation of LCL power pickup in both the simulation and experimental results, several practical design issues have also been discovered while creating the simulation model and building the prototype. These issues are found to be valuable for understanding the limitations of DTDCA on the LCL power pickup and can also be taken into considerations for improving the proposed controller.



### Performance of LCL power pickup in full-range tuning control

Providing full-range tuning control for the output voltage regulation of the pickup is one of the major features of the DTDCA. However, when applying the DTDCA to the LCL power pickups, the performance of the controller may severely be affected by the characteristic of the LCL tuning configuration.

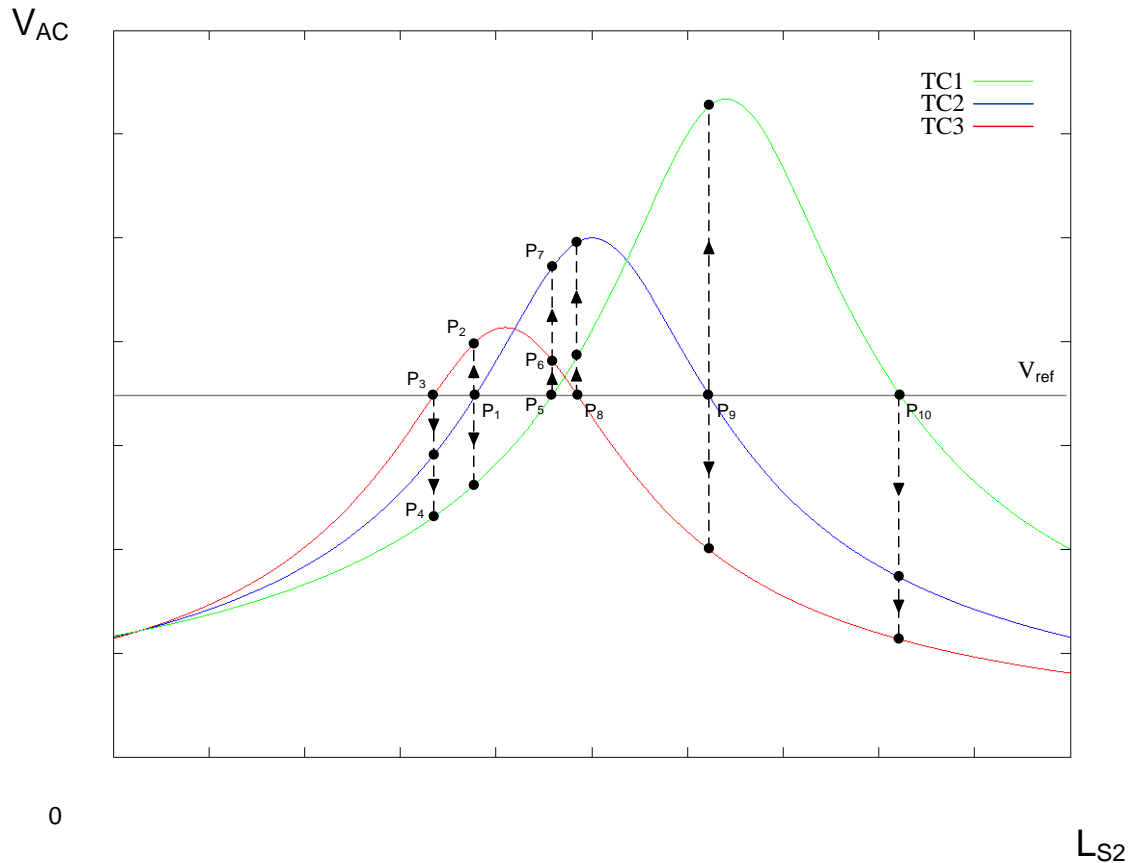


**Fig. 4-39: Output voltage behavior of LCL power pickup under operating frequency/tuning capacitance variations**

Figure 4-39 shows the output voltage behavior of the LCL power pickup under the operating frequency or the tuning capacitance variations, and all the possible output voltage increasing/decreasing directions are indicated by the arrows. By using TC2 as an example, it can be seen that the desired output voltage ( $V_{ref}$ ) can be achieved at either  $P_1$  in the under-tuning region or  $P_9$  in the over-tuning region of TC2. But the output voltage variations due to drastic change in the considered circuit parameters are much more significant in the over-tuning region and can be several times larger than in the under-tuning region. In addition, the time for the controller to bring the operating points to the

desired location may also be longer in the over-tuning region since the tuning distance ( $P_9$  to  $P_8$  or  $P_9$  to  $P_{10}$ ) is further compared with the distance ( $P_1$  to  $P_3$  or  $P_1$  to  $P_5$ ) in the under-tuning region.

In practice, the variations in capacitance of the tuning capacitor can be caused by ambient operating temperatures or degradation of the dielectric, however, these two factors would not cause an instantaneous change in the capacitance but only gradually vary the value. This essentially allows the controller to provide prompting voltage regulation to the output and prevents the load from overvoltage. However, the variations in the operating frequency are generally fast and random, which may cause severe negative effect on the transient performance of the LCL pickup. From these facts, it can be seen that in order to prevent the load from transient overvoltage, the LCL pickup has to either work with IPT systems whose operating frequency variation has a slow rate of change or with very low/none variations in the operating frequency.

### ***Tuning attempt***

As it has been shown in both the simulation and experiment results, since the proposed DTDCA requires information to validate control action from the previous state for generating the next control signal, the tuning attempts performed by the DTDCA as shown in Fig. 4-40, could occur at startup of the controller or after the output voltage has been stabilized for a certain period of time. It can be seen from Fig. 4-40 that after the output voltage has been stabilized, the logic signal  $S_4$  would start to idle between 1 and 0, because the tuning step-size has been adjusted to zero and the controller cannot verify the validity of each control action. This idle state of  $S_4$  would lead to two different results which are presented by  $S_4$  and  $S_4'$  in the figure. Assuming the pickup experiences certain parameter variation at  $t_1$  and causes the output voltage to increase to  $V(t_2)$  at  $t_2$ , the output voltage at  $t_3$  could have a value at the position of either  $V(t_3)$  or  $V(t_3)'$  depending on the logic result of  $S_4$  or  $S_4'$  respectively. This shows that the DTDCA has a 50% chance to tune to the incorrect direction and may result in adding more error to the output voltage. Since acquiring the validity of the previous state control action is necessary for the DTDCA to perform accurate tuning control in the next state, the controller will still need this possible mistaken tuning attempt for perturbation purpose, but the error caused by this tuning attempt should be reduced by algorithmically adjusting the tuning step-size so the

additional output voltage error is only sufficient for the controller to identify the correct tuning direction.

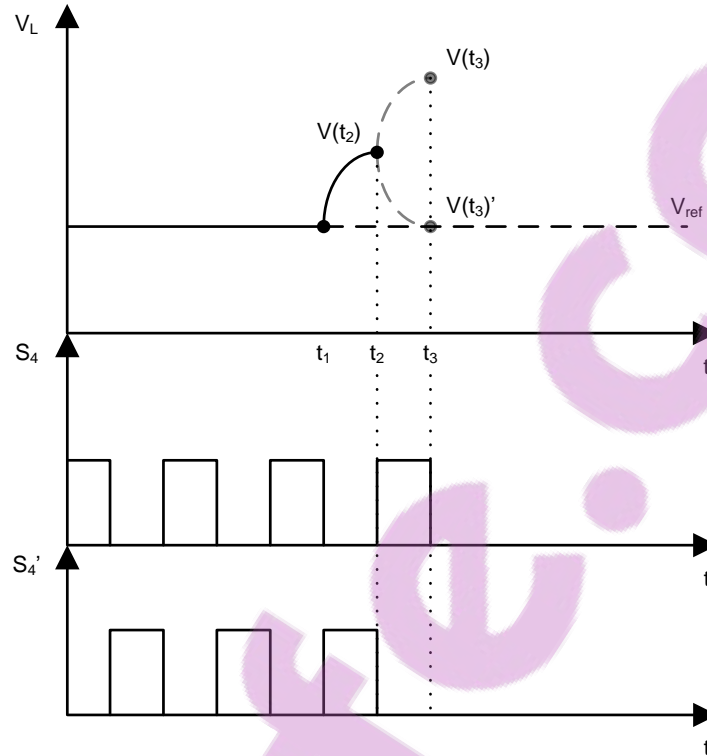
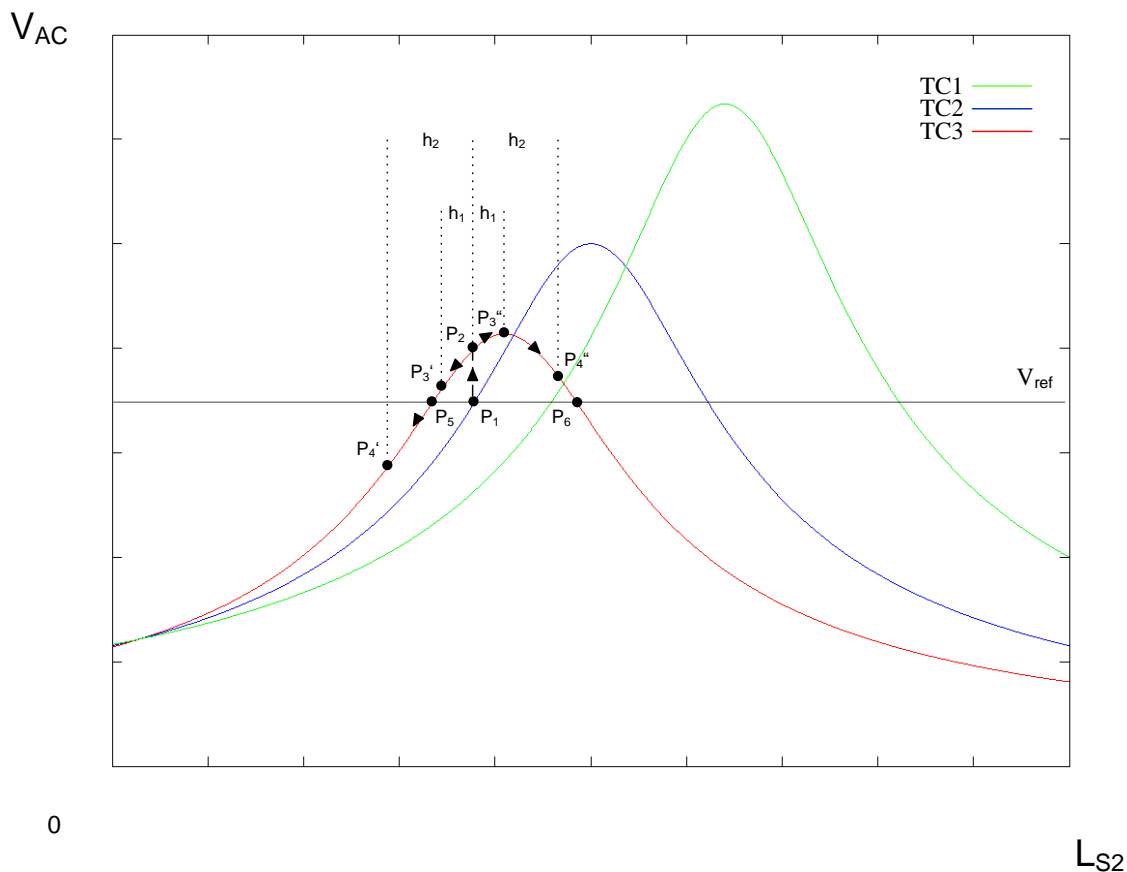


Fig. 4-40: Possible outcomes of tuning attempt

### Constant $\Delta h_m$

Based on the concept of SSSA, the tuning step-size is basically separated into a constant coarse tuning value ( $\Delta h_m$ ) and simple algorithmic fine tuning values. Such a method can be conveniently used when the controller is performing simple reference tracking and output voltage stabilization. However the simplicity of this method also lowers the performance of the controller. Since the SSSA sets the tuning step-size back to the constant coarse tuning value after the output voltage has been stabilized within the hysteresis band, the first tuning attempt, immediately after any parameter variation which causes the output voltage to go outside the hysteresis band would use the coarse tuning value without considering the actual level of the error. This could lead to the two possibilities that have been discussed before (see Fig. 4-40) with one of them may end up with large error in the output voltage. In addition, this may also cause the operating point at any two consecutive instances during the operation to switch between the under-tuning and the over-tuning region.



**Fig. 4-41: Possible locations of operating point using constant  $\Delta h_m$**

Figure 4-41 shows the possible tuning results after the pickup has experienced the operating frequency/tuning capacitance variation under different fixed tuning step-sizes. Assuming the output voltage of the pickup has been stabilized at  $P_1$  but suddenly experiences the operating frequency/tuning capacitance variation and causes the output voltage to jump to  $P_2$ , the output voltage after the first tuning attempt may result in either  $P_3'$  or  $P_3''$  if  $\Delta h_m$  is equal to  $h_1$ . In the case of  $P_3'$ , the controller would recognize the validity of the tuning action and gradually stabilizes the output voltage to  $P_5$  by using the DTDCA. As for the case of  $P_3''$ , the controller would need an extra turn to tune the pickup from  $P_3''$  back to  $P_2$  and then stabilizes the output voltage to  $P_5$  as well. However, if  $\Delta h_m$  has a larger value such as  $h_2$ , the operating point can result in either  $P_4'$  or  $P_4''$  and may require more time for stabilizing the output voltage to the desired location. In the situation of  $P_4'$ , the controller would also stabilize the output voltage to  $P_5$  which is very similar to the case of  $P_3'$  by stabilizing the output voltage to the desired value with the shortest tuning distance. But if the tuning attempt causes the output voltage to move from  $P_2$  to

$P_4$ “, the controller would still confirm the validity of this tuning action since  $P_4 < P_2$  and stabilizes the output voltage at  $P_6$  in the over-tuning region, which has a longer tuning distance compared with the distance between  $P_2$  and  $P_5$ .

Although, all four different operating cases that have been discussed are able to achieve the desired output voltage, it can be seen that the fixed coarse tuning step-size of the controller may either cause the output voltage to have considerable additional error or require longer time for stabilizing the output voltage due to a longer tuning distance. Therefore, the tuning step-size adjustment method of the controller can be improved and may require a non-model based solution since the system parameters can vary and cause the output voltage error which is difficult to predict.

## 4.6 Summary

In this chapter, the circuit parameter variations and their effect on the power flow of an LCL power pickup have been fully analyzed, and the DTDCA controller has been applied on the LCL power pickup for the output voltage regulation.

A power pickup based on LCL tuning configuration has been studied as an alternative to the conventional LC power pickup, due to its distinguishing voltage source property under fully-tuned condition. The effects of using a variable tuning inductance or capacitance on regulating the output power/voltage of the LCL power pickup have been compared, and found that the pickup is generally less sensitive to the variation of tuning inductance, which makes the pickup using a variable tuning inductance a preferable choice in performing precise control of the pickup tuning condition.

The effects on the pickup output voltage caused by variations in the operating frequency, magnetic coupling between the primary and secondary side of the IPT system, tuning capacitance, and the load resistance have been analyzed, and equations for calculating the required tuning inductance to achieve the desired output voltage under these parameter variations have been obtained. It has been found that in order to cover all the considered parameter variations, the LCL power pickup has to be operated in the detuning region which causes it to lose its voltage source property.

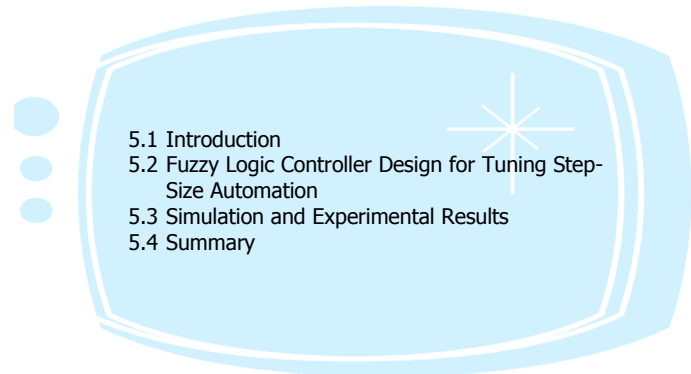
The effects of using different voltage boosting factor  $k_{VR}$  or different  $r_k$  (ratio between the desired output voltage and the nominal maximum output voltage) on the relationship between the output voltage variation and the considered parameter variations have also been investigated, and the obtained result shows that the linearity, symmetry and the magnitude of the relationship can be improved by using lower  $k_{VR}$  or  $r_k$ . Nevertheless, with a predefined constant output voltage, decreasing one of the two factors means increasing the other and therefore requires optimization.

The tuning step-size for the coarse tuning has been determined for the LCL power pickup under extreme operating conditions to avoid switching between the operating regions at any two consecutive sampling instances for an efficient tuning control at the controller startup. The sampling frequency of the controller has also been determined for the LCL power pickup, and it has a relationship proportional to both the operating frequency and the output voltage ripples but inversely proportional to the level of the output voltage.

Both the simulation and experimental results have demonstrated the effectiveness of the DTDCA in performing full-range control and output voltage regulation for the LCL power pickup. This enables the pickup to be fully-tuned on-line, if required, and makes the high  $k_{VR}$  operation possible. However, it has been found that in order to obtain a better transient performance for the DTDCA, the algorithm for adjusting the tuning step-size of the controller should be improved and may require a non-model based solution to deal with changing circuit parameters. In addition, the LCL power pickup being operated in the over-tuning region should avoid operating under fast and random operating frequency variations to prevent the load from drastic overvoltage.

## Chapter 5

# Fuzzy Logic DTDCA Control of LCL Power Pickup



---

### 5.1 Introduction

In Chapter 3, a novel control concept named the Directional Tuning/Detuning Control Algorithm (DTDCA) has been developed to achieve full-range tuning control in the output voltage regulation of the secondary pickup. The control process of the DTDCA has been divided into two stages which are the coarse tuning stage and the fine tuning stage. However, the output voltage response can have significant chattering or it may exhibit sluggish response if a fixed tuning step-size is employed while controlling the voltage. To overcome the disadvantages associated with fixed tuning step-size, an algorithm, called Simple Step-Size Adjustment (SSSA) has been developed to perform coarse and fine tuning for the coarse tuning and fine tuning stage respectively. The proposed DTDCA along with the SSSA have been applied to an LCL power pickup and proven to be effective on the output voltage regulation both via the simulation and experimental results. Nevertheless, it has been found that the performance of the proposed secondary power pickup may be degraded by several factors during the operation.

First, although the DTDCA can achieve full-range tuning in the LCL power pickup and regulates the output voltage to a desired level, the load may experience large overvoltage if the pickup is being operated in the over-tuning region under fast and random operating frequency variations. Second, since the DTDCA requires validity check for every previous

control action, the tuning attempt at the startup of the pickup or after the parameter variations occurred is needed. This may result in the pickup having additional error in the output voltage. And third, it is known that in order to have an efficient tuning control, the operating region should not be switched at any two consecutive instances during the control process so the operating point can be stabilized to the nearest desired location. However, it has been realized that although the switching of the operating regions at the startup of the pickup can be avoided by using a fixed  $\Delta h_m$ , which is predetermined under extreme operating conditions, it cannot be avoided during normal operations since the operating point is being constantly relocated on the tuning curves by the parameter variations.

For the first factor, possible overvoltages may be reduced by either setting additional constraints on the operating frequency variations, for example, only constant or slow variations in the primary operating frequency are allowed in the system, or having a controller with sampling rate faster than the rate of change in the variations of operating frequency. This can provide faster regulation of the output voltage before the overvoltage occurs. However, both of these two solutions are dependent on the characteristics of circuit/system which may or may not be applicable in some applications. As for the second and the third factors, the performance of the DTDC can be improved by dynamically changing the tuning step-size of each control action. This can be achieved by employing a better algorithm for determining the tuning step-size according to the actual operating condition.

A fuzzy logic controller for dynamic adjustment of the tuning step-size is therefore proposed in this chapter for a better output voltage regulation of the pickup. The fuzzy logic based controller has been found to be an effective alternative to conventional control techniques for controlling processes whose detailed and accurate mathematical descriptions are not available [107]. Since the output voltage of the pickup is extremely difficult to model, fuzzy logic based controller has been adopted to improve the performance of the DTDC. The linguistic feature of the fuzzy based controller allows incorporating non-numeric statements of human experts to form a rule base which can be used to obtain a coherent control strategy.



## 5.2 Fuzzy Logic Controller Design for Tuning Step-Size Automation

The design of fuzzy logic controller (FLC) has three major parts which are: 1) fuzzification of considered inputs, 2) formulation of control rule base, and 3) defuzzification of fuzzy sets. The design of these three parts for the tuning step-size automation of the DTDC is described in this section.

### 5.2.1 Fuzzification of Output Voltage Error and Rate of Error

The tuning step-size of the DTDC needs to be determined according to the condition of the pickup output voltage. Therefore, the output voltage error and the rate of error, which directly reflect the distance and speed of the output voltage with respect to the voltage reference, have been considered as the input variables for the fuzzy controller. These are defined as:

$$e(t_n) = V_{ref}(t_n) - V_L(t_n) \quad (5-1)$$

$$r(t_n) = e(t_n) - e(t_{n-1}) \quad (5-2)$$

where  $t_n$  is the sampling instance,  $V_{ref}(t_n)$  is the reference voltage, and  $V_L(t_n)$  is the sampled pickup output voltage. The output voltage error and the rate of error are denoted by  $e(t_n)$  and  $r(t_n)$  respectively. By introducing scaling factors to (5-1) and (5-2), the actual inputs of the FLC can be given as:

$$e_{IN}(t_n) = GE \cdot e(t_n) \quad (5-3)$$

$$r_{IN}(t_n) = GR \cdot r(t_n) \quad (5-4)$$

where  $GE$  and  $GR$  are the scaling factors for the error and rate of error respectively.

The input variable  $e_{IN}(t_n)$  can be fuzzified by four input fuzzy sets, and they are: Positive Error (PE), Positive Zero (PZ), Negative Zero (NZ), and Negative Error (NE). The membership functions of these four input fuzzy sets are shown in Fig. 5-1, and these are defined mathematically as:

$$\mu_{PE}(e_{IN}) = \begin{cases} 1, & e_{IN} > L \\ \frac{e_{IN}}{L}, & 0 \leq e_{IN} \leq L \\ 0, & e_{IN} < 0 \end{cases} \quad (5-5)$$

$$\mu_{PZ}(e_{IN}) = \begin{cases} 0, & e_{IN} > L \\ \frac{L - e_{IN}}{L}, & 0 \leq e_{IN} \leq L \end{cases} \quad (5-6)$$

$$\mu_{NZ}(e_{IN}) = \begin{cases} \frac{L + e_{IN}}{L}, & -L \leq e_{IN} \leq 0 \\ 0, & e_{IN} < -L \end{cases} \quad (5-7)$$

$$\mu_{NE}(e_{IN}) = \begin{cases} 0, & e_{IN} > 0 \\ -\frac{e_{IN}}{L}, & -L \leq e_{IN} \leq 0 \\ 1, & e_{IN} < -L \end{cases} \quad (5-8)$$

where interval  $L$  is a design parameter. The value of  $L$  affects the performance of the controller and should be carefully chosen. The guidelines for selection of  $L$  will be discussed later along with the guidelines for selecting the scaling factors.

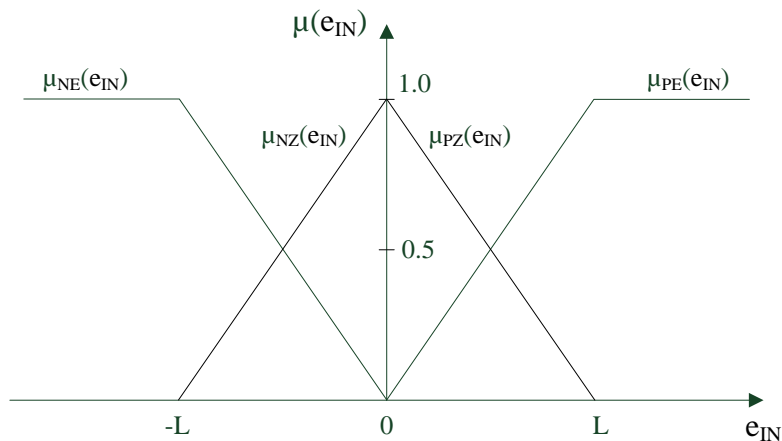


**Fig. 5-1: Input membership functions for  $e_{IN}$  of FLC**

Similarly, the input variable  $r_{IN}(t_n)$  can be fuzzified by four input fuzzy sets, and they are: Positive Rate (PR), Positive Rate Zero (PRZ), Negative Rate Zero (NRZ), and Negative Rate (NR). The membership functions of these four input fuzzy sets are shown in Fig. 5-2.

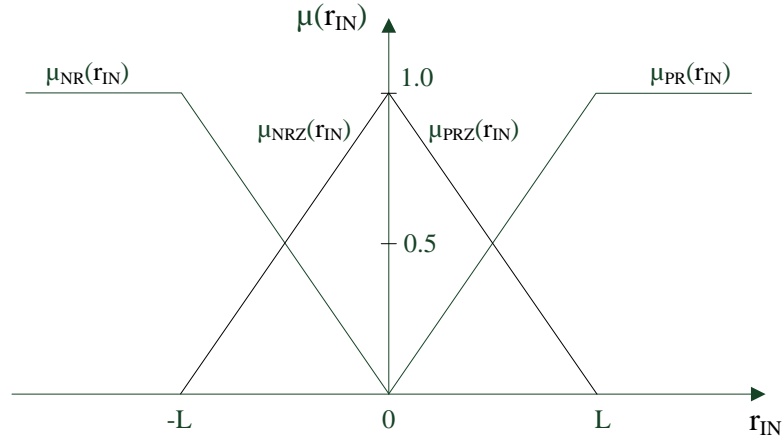


**Fig. 5-2: Input membership functions for  $r_{IN}$  of FLC**

These membership functions are defined mathematically as:

$$\mu_{PR}(r_{IN}) = \begin{cases} 1, & r_{IN} > L \\ \frac{r_{IN}}{L}, & 0 \leq r_{IN} \leq L \\ 0, & r_{IN} < 0 \end{cases} \quad (5-9)$$

$$\mu_{PRZ}(r_{IN}) = \begin{cases} 0, & r_{IN} > L \\ \frac{L - r_{IN}}{L}, & 0 \leq r_{IN} \leq L \end{cases} \quad (5-10)$$

$$\mu_{NRZ}(r_{IN}) = \begin{cases} \frac{L + r_{IN}}{L}, & -L \leq r_{IN} \leq 0 \\ 0, & r_{IN} < -L \end{cases} \quad (5-11)$$

$$\mu_{NR}(r_{IN}) = \begin{cases} 0, & r_{IN} > 0 \\ -\frac{r_{IN}}{L}, & -L \leq r_{IN} \leq 0 \\ 1, & r_{IN} < -L \end{cases} \quad (5-12)$$

### 5.2.2 Control Rule Base

The proposed FLC uses the following 9 control rules to dynamically change the tuning step-size of the DTDC. Note that this rule base has been carefully created such that the output voltage of the pickup should accurately track the reference voltage.

$R_1$ : IF  $e_{IN}(t_n)$  is Positive Error AND  $r_{IN}(t_n)$  is Positive Rate  
THEN  $\Delta u(t_n)$  is  $o_Z$ .

$R_2$ : IF  $e_{IN}(t_n)$  is Positive Error AND  $r_{IN}(t_n)$  is Positive Rate Zero  
THEN  $\Delta u(t_n)$  is  $o_L$ .

$R_3$ : IF  $e_{IN}(t_n)$  is Positive Error AND  $r_{IN}(t_n)$  is Negative Rate Zero  
THEN  $\Delta u(t_n)$  is  $o_L$ .

$R_4$ : IF  $e_{IN}(t_n)$  is Positive Error AND  $r_{IN}(t_n)$  is Negative Rate  
THEN  $\Delta u(t_n)$  is  $o_M$ .

$R_5$ : IF  $e_{IN}(t_n)$  is Negative Error AND  $r_{IN}(t_n)$  is Positive Rate  
THEN  $\Delta u(t_n)$  is  $o_M$ .

$R_6$ : IF  $e_{IN}(t_n)$  is Negative Error AND  $r_{IN}(t_n)$  is Positive Rate Zero  
THEN  $\Delta u(t_n)$  is  $o_L$ .

$R_7$ : IF  $e_{IN}(t_n)$  is Negative Error AND  $r_{IN}(t_n)$  is Negative Rate Zero  
THEN  $\Delta u(t_n)$  is  $o_L$ .

$R_8$ : IF  $e_{IN}(t_n)$  is Negative Error AND  $r_{IN}(t_n)$  is Negative Rate  
THEN  $\Delta u(t_n)$  is  $o_Z$ .

$R_9$ : IF  $e_{IN}(t_n)$  is Positive Zero OR Negative Zero  
THEN  $\Delta u(t_n)$  is  $o_Z$ .

In the rules,  $o_L$ ,  $o_M$ , and  $o_Z$  represent the output of the controller in the level of large, medium, and zero respectively, and  $\Delta u(t_n)$  stands for the crisp output of the controller.

The AND and OR fuzzy logics used in the above rules are those of Zadeh and of Lukasiewicz [108]. For example, if  $\mu_A$  and  $\mu_B$  represent the grades of membership of an object in fuzzy sets A and B, respectively, then these logics are defined as [109]:

*Zadeh logic*

$$\text{AND}(\mu_A, \mu_B) = \min(\mu_A, \mu_B)$$

$$\text{OR}(\mu_A, \mu_B) = \max(\mu_A, \mu_B)$$

*Lukasiewicz logic*

$$\text{AND}(\mu_A, \mu_B) = \max(0, \mu_A + \mu_B - 1)$$

$$\text{OR}(\mu_A, \mu_B) = \min(1, \mu_A + \mu_B)$$

When evaluating the control rules, the Zadeh AND is used to evaluate the individual control rules and the Lukasiewicz OR is used to evaluate the implied OR between the control rules. Table 5-1 summarizes the rules  $R_1$  to  $R_9$ .

**Table 5-1: Summarized result of control rule base**

		$e_{IN}(t_n)$			
		PE	PZ	NZ	NE
$r_{IN}(t_n)$	PR	$R_1(OZ)$	$R_9(OZ)$		$R_5(OM)$
	PRZ	$R_2(OL)$			$R_6(OL)$
	NRZ	$R_3(OL)$			$R_7(OL)$
	NR	$R_4(OM)$			$R_8(OZ)$

From Table 5-1, it can easily be seen that the rules can also be categorized according to their output level. For the rules  $R_2$ ,  $R_3$ ,  $R_6$ , and  $R_7$ , a large tuning step-size is assigned. Because the assumption of insufficient output voltage variation that caused by the previous tuning attempt has been made. This requires a large tuning step-size in the next state control to obtain a faster reference tracking speed. A zero tuning step-size is assigned

to the rules  $R_7$  and  $R_8$  because the output voltage variation in the previous state may be either the result of an incorrect tuning attempt or parameter variations. Under either of the conditions the controller requires a small perturbation signal to help the algorithm to identify the correct tuning direction in the next state control. The rule  $R_9$  is also assigned with zero tuning step-size. Because the output voltage is close enough to the reference and only requires being fine-tuned. As for the rules  $R_4$  and  $R_5$ , whose previous state control are performed in the correct tuning direction, a medium tuning step-size is assigned to them for providing moderate reference tracking speed to avoid overshoot in the output voltage.

### 5.2.3 Defuzzification of Output Fuzzy Sets

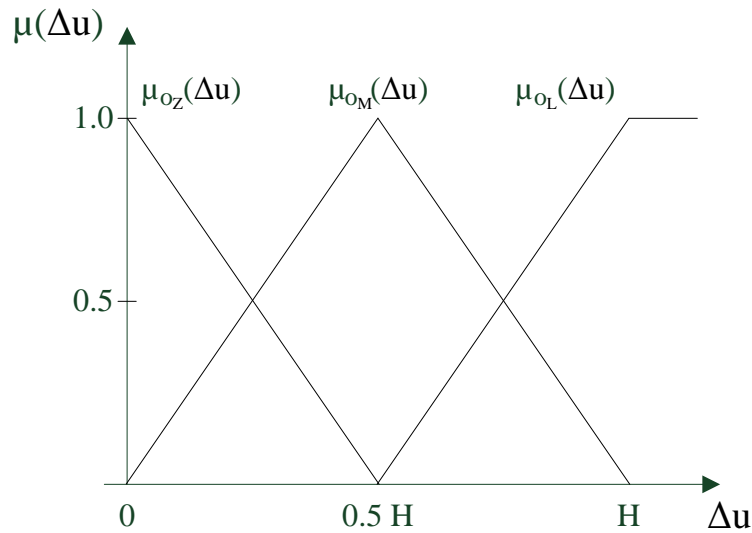


**Fig. 5-3: Output membership functions for  $\Delta u$  of FLC**

Figure 5-3 shows the output fuzzy sets of the controller with only positive values since the physical tuning step-size cannot be negative. The Mamdani reference is used here as the inference method for calculating the area of output fuzzy sets [110-112], and it is given by:

$$S(\mu) = \mu(2 - \mu)H \quad (5-13)$$

A centroid defuzzifier is used to produce the output of the FLC [107, 108, 113], and the crisp output can be expressed by:

$$\Delta u = \frac{H \cdot S(\mu_{R_2 R_3 R_6 R_7}) + 0.5H \cdot S(\mu_{R_4 R_5}) + 0 \cdot S(\mu_{R_1 R_8 R_9})}{S(\mu_{R_2 R_3 R_6 R_7}) + S(\mu_{R_4 R_5}) + S(\mu_{R_1 R_8 R_9})} \quad (5-14)$$

where  $H$  is a design parameter. The selection of  $H$  will be discussed later along with the selection of interval  $L$  and scaling factors of the FLC. The combined membership of output fuzzy sets for control rules  $R_2 R_3 R_6 R_7$ ,  $R_4 R_5$ , and  $R_1 R_8 R_9$  are obtained by using the extended Lukasiewicz fuzzy logic OR. Since the conditions being ORed are maximally negatively correlated, the values for these combined memberships are given by:

$$\mu_{R_2 R_3 R_6 R_7} = \min(1, \mu_{R_2} + \mu_{R_3} + \mu_{R_6} + \mu_{R_7})$$

$$\mu_{R_4 R_5} = \min(1, \mu_{R_4} + \mu_{R_5})$$

$$\mu_{R_1 R_8 R_9} = \min(1, \mu_{R_1} + \mu_{R_8} + \mu_{R_9})$$

The memberships  $\mu_{R_i}$ ,  $i = 1, \dots, 9$ , are obtained by the Zadeh logic AND and Lukasiewicz logic OR, and the values for these memberships are given by:

$$\mu_{R_1} = \min(\mu_{PE}, \mu_{PR}) \quad \mu_{R_2} = \min(\mu_{PE}, \mu_{PRZ}) \quad \mu_{R_3} = \min(\mu_{PE}, \mu_{NRZ})$$

$$\mu_{R_4} = \min(\mu_{PE}, \mu_{NR}) \quad \mu_{R_5} = \min(\mu_{NE}, \mu_{PR}) \quad \mu_{R_6} = \min(\mu_{NE}, \mu_{PRZ})$$

$$\mu_{R_7} = \min(\mu_{NE}, \mu_{NRZ}) \quad \mu_{R_8} = \min(\mu_{NE}, \mu_{NR}) \quad \mu_{R_9} = \min(1, \mu_{PZ} + \mu_{NZ})$$

The FLC output for producing the tuning step-size of the variable inductor can therefore be determined from:

$$\Delta H = GU \cdot \Delta u \quad (5-15)$$

where  $GU$  is the output scaling factor.

#### 5.2.4 Analytical Structure of Fuzzy Logic Controller

In order to obtain analytical expressions of the FLC with respect to  $e_{IN}(t_n)$  and  $r_{IN}(t_n)$ , the  $e_{IN}$ - $r_{IN}$  input space has been divided into 28 different input combinations (ICs) as shown in Fig. 5-4. This is obtained by putting the membership functions of error of Fig. 5-1 over the

horizontal axis ( $e_{IN}$ ) of Fig. 5-4 and putting the membership functions of rate of error of Fig. 5-2 over the vertical axis ( $r_{IN}$ ) of Fig. 5-4 [108].

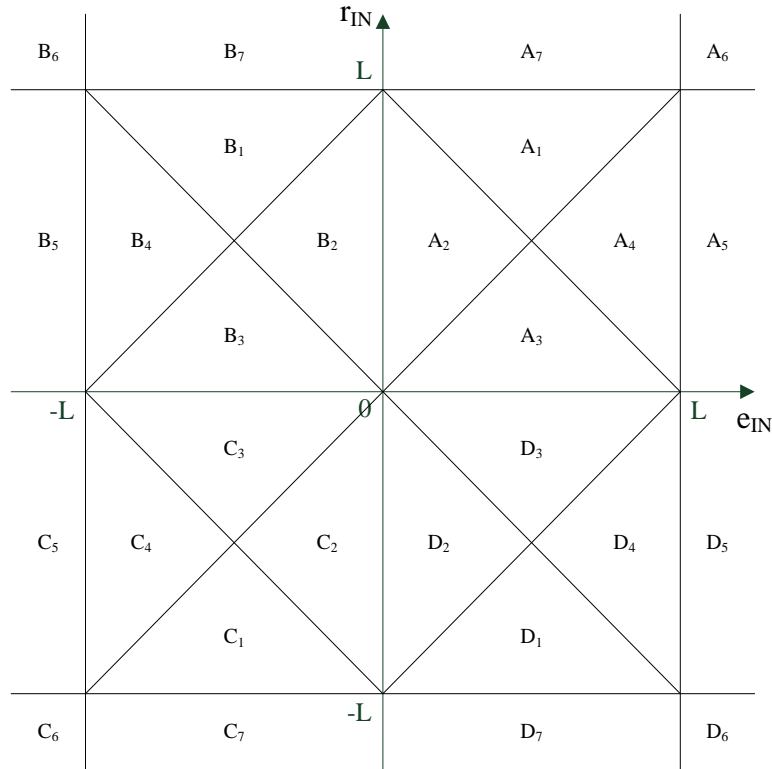


**Fig. 5-4: Possible input combinations of  $e_{IN}$  and  $r_{IN}$**

To further evaluate the ICs, they are separated into classes of  $e_{IN}-r_{IN}$  are within  $[-L, L]$  and  $e_{IN}-r_{IN}$  are not within  $[-L, L]$ . The results of evaluating the fuzzy control rules whose  $e_{IN}-r_{IN}$  are within  $[-L, L]$  and are not within  $[-L, L]$ , are separately given in Table 5-2 and Table 5-3 respectively.



**Table 5-2: Results of evaluating fuzzy control rules  $R_1$  to  $R_9$  for all ICs whose  $e_{IN}$  and  $r_{IN}$  are within  $[-L, L]$**

	$R_1$	$R_2$	$R_3$	$R_4$	$R_5$	$R_6$	$R_7$	$R_8$	$R_9$
$A_1$	PE	PRZ	0	0	0	0	0	0	PZ
$A_2$	PE	PE	0	0	0	0	0	0	PZ
$A_3$	PR	PE	0	0	0	0	0	0	PZ
$A_4$	PR	PRZ	0	0	0	0	0	0	PZ
$B_1$	0	0	0	0	NE	PRZ	0	0	NZ
$B_2$	0	0	0	0	NE	NE	0	0	NZ
$B_3$	0	0	0	0	PR	NE	0	0	NZ
$B_4$	0	0	0	0	PR	PRZ	0	0	NZ
$C_1$	0	0	0	0	0	0	NRZ	NE	NZ
$C_2$	0	0	0	0	0	0	NE	NE	NZ
$C_3$	0	0	0	0	0	0	NE	NR	NZ
$C_4$	0	0	0	0	0	0	NRZ	NR	NZ
$D_1$	0	0	NRZ	PE	0	0	0	0	PZ
$D_2$	0	0	PE	PE	0	0	0	0	PZ
$D_3$	0	0	PE	NR	0	0	0	0	PZ
$D_4$	0	0	NRZ	NR	0	0	0	0	PZ

**Table 5-3: Results of evaluating fuzzy control rules  $R_1$  to  $R_9$  for all ICs whose  $e_{IN}$  and  $r_{IN}$  are not within  $[-L, L]$**

	$R_1$	$R_2$	$R_3$	$R_4$	$R_5$	$R_6$	$R_7$	$R_8$	$R_9$
$A_5$	PR	PRZ	0	0	0	0	0	0	0
$A_6$	1	0	0	0	0	0	0	0	0
$A_7$	PE	0	0	0	0	0	0	0	PZ
$B_5$	0	0	0	0	PR	PRZ	0	0	0
$B_6$	0	0	0	0	1	0	0	0	0
$B_7$	0	0	0	0	NE	0	0	0	NZ
$C_5$	0	0	0	0	0	0	NRZ	NR	0
$C_6$	0	0	0	0	0	0	0	1	0
$C_7$	0	0	0	0	0	0	0	NE	NZ
$D_5$	0	0	NRZ	NR	0	0	0	0	0
$D_6$	0	0	0	1	0	0	0	0	0
$D_7$	0	0	0	PE	0	0	0	0	PZ

By using the results from Table 5-2 and Table 5-3, the analytical expressions for the crisp output of the FLC for each IC can then be obtained. These analytical expressions are listed in Table 5-4.

**Table 5-4: Analytical expressions for crisp output of FLC for ICs A<sub>1</sub> to A<sub>7</sub> (C<sub>1</sub> to C<sub>7</sub>) and B<sub>1</sub> to B<sub>7</sub> (D<sub>1</sub> to D<sub>7</sub>)**

Area	Analytical expression
A <sub>1</sub> and C <sub>1</sub>	$H \cdot \frac{L^2 - r_{IN}^2}{2L^2 - r_{IN}^2}$
A <sub>2</sub> and C <sub>2</sub>	$H \cdot \frac{ e_{IN}  \cdot (2L -  e_{IN} )}{ e_{IN}  \cdot (2L -  e_{IN} ) + L^2}$
A <sub>3</sub> and C <sub>3</sub>	$H \cdot \frac{ e_{IN}  \cdot (2L -  e_{IN} )}{ e_{IN}  \cdot (2L -  e_{IN} ) - ( e_{IN}  -  r_{IN} )^2 + L^2}$
A <sub>4</sub> and C <sub>4</sub>	$H \cdot \frac{L^2 - r_{IN}^2}{(2L^2 - r_{IN}^2) - ( e_{IN}  -  r_{IN} )^2}$
A <sub>5</sub> and C <sub>5</sub>	$H \cdot \frac{L^2 - r_{IN}^2}{(L^2 - r_{IN}^2) +  r_{IN}  \cdot (2L -  r_{IN} )}$
A <sub>6</sub> and C <sub>6</sub>	0
A <sub>7</sub> and C <sub>7</sub>	0
B <sub>1</sub> and D <sub>1</sub>	$H \cdot \frac{0.5 \cdot  e_{IN}  \cdot (2L -  e_{IN} ) + (L^2 - r_{IN}^2)}{ e_{IN}  \cdot (2L -  e_{IN} ) + (2L^2 - e_{IN}^2 - r_{IN}^2)}$
B <sub>2</sub> and D <sub>2</sub>	$H \cdot \frac{1.5 \cdot  e_{IN}  \cdot (2L -  e_{IN} )}{2 \cdot  e_{IN}  \cdot (2L -  e_{IN} ) + (L^2 - e_{IN}^2)}$
B <sub>3</sub> and D <sub>3</sub>	$H \cdot \frac{ e_{IN}  \cdot (2L -  e_{IN} ) + 0.5 \cdot  r_{IN}  \cdot (2L -  r_{IN} )}{ e_{IN}  \cdot (2L -  e_{IN} ) +  r_{IN}  \cdot (2L -  r_{IN} ) + (L^2 - e_{IN}^2)}$
B <sub>4</sub> and D <sub>4</sub>	$H \cdot \frac{0.5 \cdot  r_{IN}  \cdot (2L -  r_{IN} ) + (L^2 - r_{IN}^2)}{ r_{IN}  \cdot (2L -  r_{IN} ) + (2L^2 - e_{IN}^2 - r_{IN}^2)}$
B <sub>5</sub> and D <sub>5</sub>	$H \cdot \frac{0.5 \cdot  r_{IN}  \cdot (2L -  r_{IN} ) + (L^2 - r_{IN}^2)}{ r_{IN}  \cdot (2L -  r_{IN} ) + (L^2 - r_{IN}^2)}$
B <sub>6</sub> and D <sub>6</sub>	0.5H
B <sub>7</sub> and D <sub>7</sub>	$H \cdot \frac{0.5 \cdot  e_{IN}  \cdot (2L -  e_{IN} )}{ e_{IN}  \cdot (2L -  e_{IN} ) + (L^2 - e_{IN}^2)}$

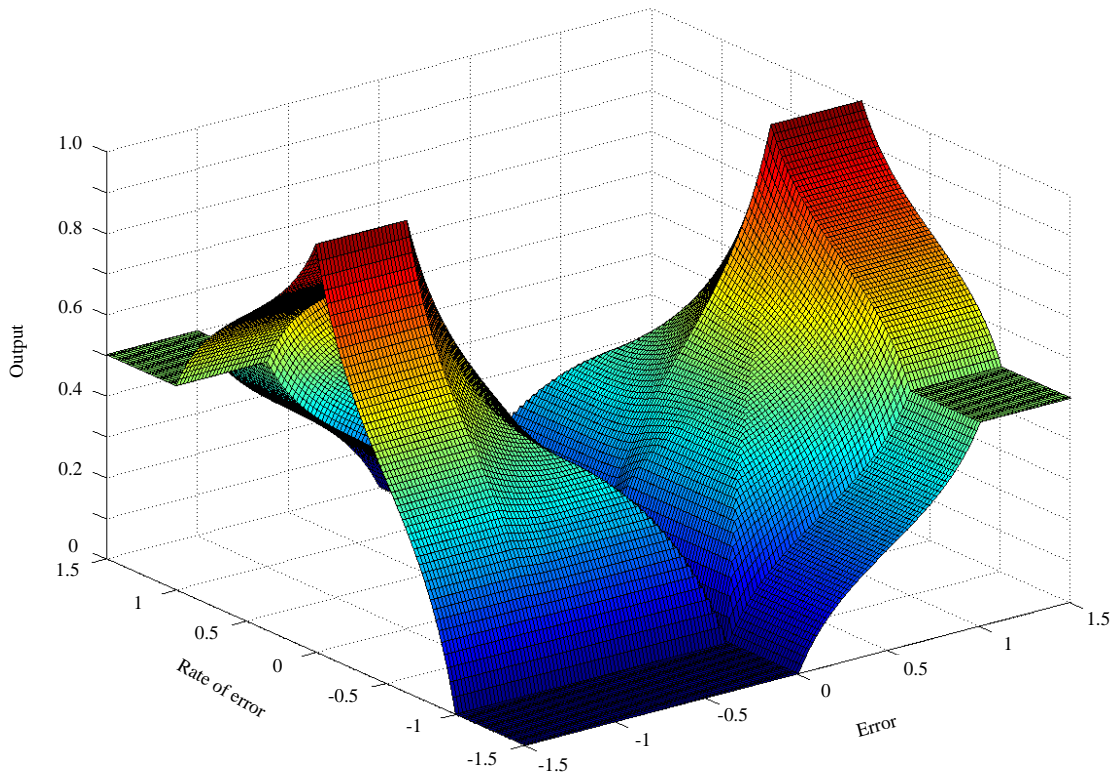


**Fig. 5-5: Interpolation of  $e_{IN}$ ,  $r_{IN}$ , and FLC output**

Figure 5-5 shows the interpolation of FLC inputs  $e_{IN}$  and  $r_{IN}$ , and FLC output, with  $L$  and  $H$  being unity. As it can be observed from the interpolation, the output of FLC is calculated by using different analytical expressions according to the corresponding input conditions.

Considering that the output of a linear discrete-time PD controller in position form [114, 115]:

$$\Delta u_{PD}(t_n) = K_P \cdot e_{IN}(t_n) + K_D \cdot r_{IN}(t_n) \quad (5-16)$$

where  $K_P$  and  $K_D$  are constant gains named proportional-gain and derivative-gain, respectively, the proposed FLC can be fitted into the form of classical linear P (proportional), D (derivative), or PD controller [115]. Table 5-5 shows the obtained analytical expressions (in Table 5-4) for all the possible ICs in the form of (5-16).

**Table 5-5: Analytical expressions for crisp output of FLC for ICs A<sub>1</sub> to A<sub>7</sub> (C<sub>1</sub> to C<sub>7</sub>) and B<sub>1</sub> to B<sub>7</sub> (D<sub>1</sub> to D<sub>7</sub>) in classical forms**

Area	PD expression	K <sub>P</sub>	K <sub>D</sub>
A <sub>1</sub> , C <sub>1</sub>	$K_D \cdot  r_{IN}  - K_D \cdot \frac{L^2}{ r_{IN} }$	0	$\frac{-H \cdot  r_{IN} }{2L^2 - r_{IN}^2}$
A <sub>2</sub> , C <sub>2</sub>	$K_P \cdot  e_{IN} $	$\frac{H \cdot (2L -  e_{IN} )}{ e_{IN}  \cdot (2L -  e_{IN} ) + L^2}$	0
A <sub>3</sub> , C <sub>3</sub>	$K_P \cdot  e_{IN} $	$\frac{H \cdot (2L -  e_{IN} )}{ e_{IN}  \cdot (2L -  e_{IN} ) - ( e_{IN}  -  r_{IN} )^2 + L^2}$	0
A <sub>4</sub> , C <sub>4</sub>	$K_D \cdot  r_{IN}  - K_D \cdot \frac{L^2}{ r_{IN} }$	0	$\frac{-H \cdot  r_{IN} }{2L^2 - r_{IN}^2 - ( e_{IN}  -  r_{IN} )^2}$
A <sub>5</sub> , C <sub>5</sub>	$K_D \cdot  r_{IN}  - K_D \cdot \frac{L^2}{ r_{IN} }$	0	$\frac{-H \cdot  r_{IN} }{L^2 - r_{IN}^2 +  r_{IN}  \cdot (2L -  r_{IN} )}$
A <sub>6</sub> , C <sub>6</sub>	0	0	0
A <sub>7</sub> , C <sub>7</sub>	0	0	0
B <sub>1</sub> , D <sub>1</sub>	$K_P \cdot  e_{IN}  + K_D \cdot  r_{IN}  - K_D \cdot \frac{L^2}{ r_{IN} }$	$\frac{0.5 \cdot H \cdot (2L -  e_{IN} )}{ e_{IN}  \cdot (2L -  e_{IN} ) + (2L^2 - e_{IN}^2 - r_{IN}^2)}$	$\frac{-H \cdot  r_{IN} }{ e_{IN}  \cdot (2L -  e_{IN} ) + (2L^2 - e_{IN}^2 - r_{IN}^2)}$
B <sub>2</sub> , D <sub>2</sub>	$K_P \cdot  e_{IN} $	$\frac{1.5 \cdot H \cdot (2L -  e_{IN} )}{2 \cdot  e_{IN}  \cdot (2L -  e_{IN} ) + (L^2 - e_{IN}^2)}$	0
B <sub>3</sub> , D <sub>3</sub>	$K_P \cdot  e_{IN}  + K_D \cdot  r_{IN} $	$\frac{H \cdot (2L -  e_{IN} )}{ e_{IN}  \cdot (2L -  e_{IN} ) +  r_{IN}  \cdot (2L -  r_{IN} ) + (L^2 - e_{IN}^2)}$	$\frac{0.5 \cdot H \cdot (2L -  r_{IN} )}{ e_{IN}  \cdot (2L -  e_{IN} ) +  r_{IN}  \cdot (2L -  r_{IN} ) + (L^2 - e_{IN}^2)}$
B <sub>4</sub> , D <sub>4</sub>	$K_D \cdot  r_{IN}  - K_D \cdot \frac{L(L +  r_{IN} )}{1.5 \cdot  r_{IN} }$	0	$\frac{-1.5 \cdot H \cdot  r_{IN} }{ r_{IN}  \cdot (2L -  r_{IN} ) + (2L^2 - e_{IN}^2 - r_{IN}^2)}$
B <sub>5</sub> , D <sub>5</sub>	$K_D \cdot  r_{IN}  - K_D \cdot \frac{L(L +  r_{IN} )}{1.5 \cdot  r_{IN} }$	0	$\frac{-1.5 \cdot H \cdot  r_{IN} }{ r_{IN}  \cdot (2L -  r_{IN} ) + (L^2 - r_{IN}^2)}$
B <sub>6</sub> , D <sub>6</sub>	0.5H	0	0
B <sub>7</sub> , D <sub>7</sub>	$K_P \cdot  e_{IN} $	$\frac{0.5 \cdot H \cdot (2L -  e_{IN} )}{ e_{IN}  \cdot (2L -  e_{IN} ) + (L^2 - e_{IN}^2)}$	0

From Table 5-5, it can be seen that the output expressions of the ICs fit into the linear classical P, D, or PD forms very well, except that the proportional gains and the derivative gains are nonlinear variables instead of constant values in the classical forms. Thus, the proposed FLC can also be treated as ‘local’ nonlinear P-like, D-like, or PD-like controller

with variable gains, where the ‘local’ here means that the control expression is only valid to the corresponding IC. The output of P-like controller is produced in the ICs of A<sub>2</sub>, A<sub>3</sub>, B<sub>2</sub>, B<sub>7</sub>, C<sub>2</sub>, C<sub>3</sub>, D<sub>2</sub>, and D<sub>7</sub>. The output of D-like controller is produced in the ICs of A<sub>1</sub>, A<sub>4</sub>, A<sub>5</sub>, B<sub>4</sub>, B<sub>5</sub>, C<sub>1</sub>, C<sub>4</sub>, C<sub>5</sub>, D<sub>4</sub>, and D<sub>5</sub>. And the output of PD-like controller is produced in the ICs of B<sub>1</sub>, B<sub>3</sub>, D<sub>1</sub>, and D<sub>3</sub>. However, by comparing the P-like, D-like, and PD-like output expressions of the ICs with the classical form, it is noticed that the D-like expressions and the PD-like expressions in B<sub>1</sub> and D<sub>1</sub> have an additional term. This additional term is dependent on the rate of error and can be regarded as a variable bias function for the D-like controller to produce positive tuning step change [112].

### 5.2.5 Choice of Scaling Factors

The choice of scaling factors  $GE$ ,  $GR$ , and  $GU$  can considerably affect the performance of the DTDCA and hence needs to be carefully selected. However, there exists no universal method to determine their values. Generally, the objective is to map the actual error and the rate of error into the interval  $[-L, L]$ , which can be expressed by the following equations:

$$GE = \frac{L}{|e|_{\max}} \quad (5-17)$$

$$GR = \frac{L}{|r|_{\max}} \quad (5-18)$$

where  $|e|_{\max}$  and  $|r|_{\max}$  is the maximum value of the absolute value of error and rate of error respectively. However, this requires prior knowledge of the range of error and rate of error of the pickup output voltage. In order to obtain the data for the error and rate of error of the output voltage, the pickup needs to be either simulated or experimented under possible parameter variations. The obtained data can simultaneously be processed to find out the actual  $|e|_{\max}$  and  $|r|_{\max}$  by using the following recursive method:

$$e_{\max}(t_n) = \max [ |e(t_n)|, e_{\max}(t_{n-1}) ] \quad (5-19)$$

$$r_{\max}(t_n) = \max [ |r(t_n)|, r_{\max}(t_{n-1}) ] \quad (5-20)$$

The idea of this recursive method is to obtain the true maximum value of the absolute value of error and rate of error at the end of the process, by continuously comparing the present sampled error and rate of error with the corresponding maximum value that has been previously stored. If the new value is higher than the present maximum, then the maximum value will be updated and be used to compute the scaling factors  $GE$  and  $GR$ .

The performance of the DTDCA can also be affected by the value of  $L$ . A small  $L$  makes the output of the pickup to stay outside the ICs whose  $e_{IN}$  and  $r_{IN}$  are within the interval  $[-L, L]$  more often, whereas a larger value does the opposite [114]. This effect can be clearly observed from Fig. 5-6. When the interval  $L$  has a smaller value, for example,  $L = 0.5$ ,  $e_{IN}$  and  $r_{IN}$  with a range of  $-1.5 \sim 1.5$  would have  $2/3$  of the values lying outside the interval  $[-L, L]$  and making the output of the FLC more sensitive to the change of  $e_{IN}$  and  $r_{IN}$ , whereas a larger value causes the output to be less sensitive to the change of  $e_{IN}$  and  $r_{IN}$ .

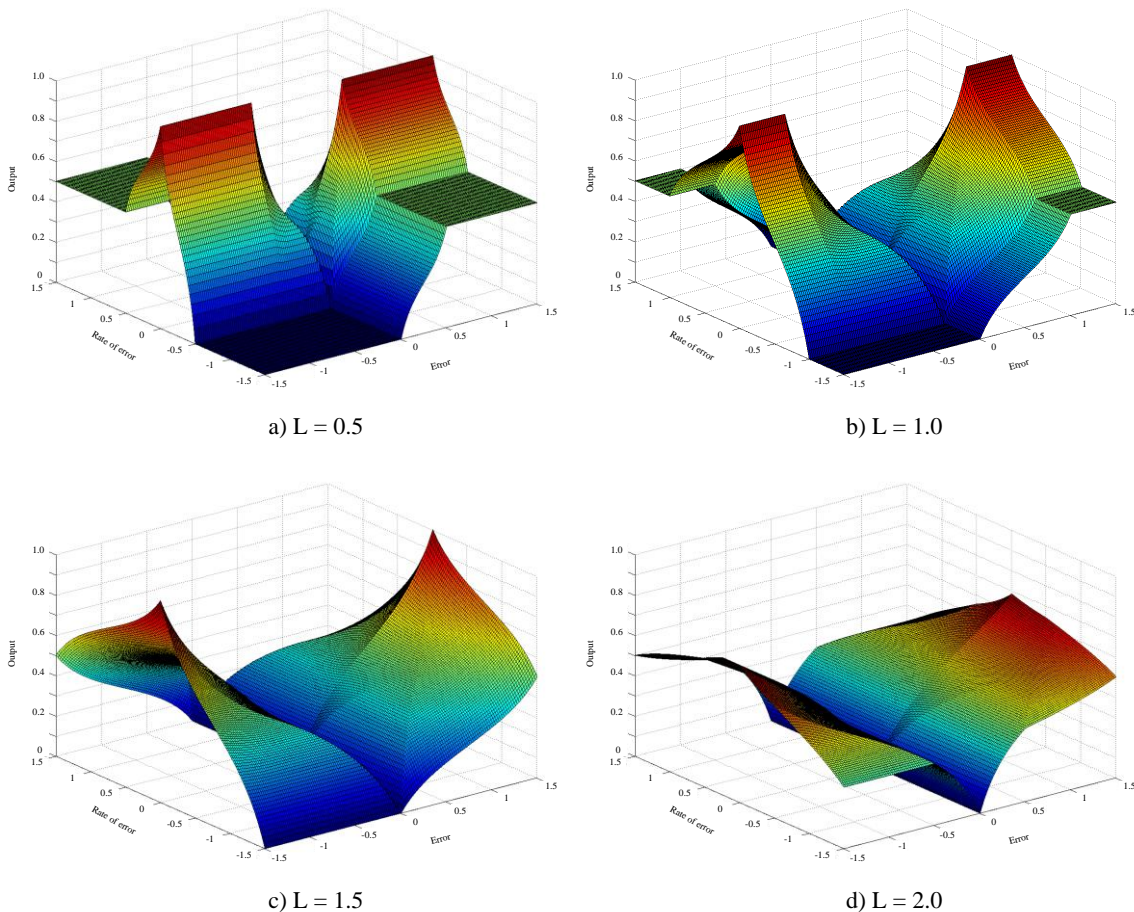


**Fig. 5-6: Interpolation of  $e_{IN}$ ,  $r_{IN}$ , and FLC output with: a)  $L = 0.5$ , b)  $L = 1.0$ , c)  $L = 1.5$ , and d)  $L = 2.0$**

Normally, the value of  $L$  is selected to be unity or some constant values to help defining the scaling factors  $GE$  and  $GR$ . However, it can also be adjusted afterwards based on the performance of the controller. For instance, in the proposed DTDC it requires a tuning attempt to identify the correct tuning direction after the output voltage has been varied from a stabilized position. The tuning step-size, as has been discussed before, is determined by the FLC based on the level of error and rate of error. Considering the situation of output voltage having a large error with a large rate of error in the wrong tuning direction, the output of the FLC would become zero according to the control rule base. This causes the output voltage to have a zero rate of error (insufficient perturbation) in the next state and requires the controller to take another tuning attempt which can lead to two different control outcomes; one having a correct tuning direction with a large tuning step-size and the other having an incorrect tuning direction with a large tuning step-size. To overcome the insufficient perturbation problem that has been discussed, the value of  $L$  needs be adjusted to a larger value so that the maximum rate of error would never reach  $L$ , and consequently the output of the FLC would never go to zero.

The selection of output scaling factor  $GU$  follows similar guidelines as has been used in mapping the error and rate of error into the interval  $[-L, L]$ . The maximum step-size of control signal is obtained as follows:

$$\Delta u_{\max} = H \quad (5-21)$$

$$\Delta H_{\max} = GU \cdot H \quad \text{or} \quad GU = \frac{\Delta H_{\max}}{H} \quad (5-22)$$

where  $\Delta u_{\max}$  and  $\Delta H_{\max}$  are the output signal of FLC before and after scaling, respectively, for producing the maximum tuning step-size. The selection of  $H$  is similar to  $L$  which is generally chosen to be unity or some constant values. But it can also be adjusted after defining  $GU$  if it is required to further improve the performance of controller. The effect of changing the value of  $H$  is shown in Fig. 5-7. It can be seen that this can be used to proportionally change the output level of FLC.

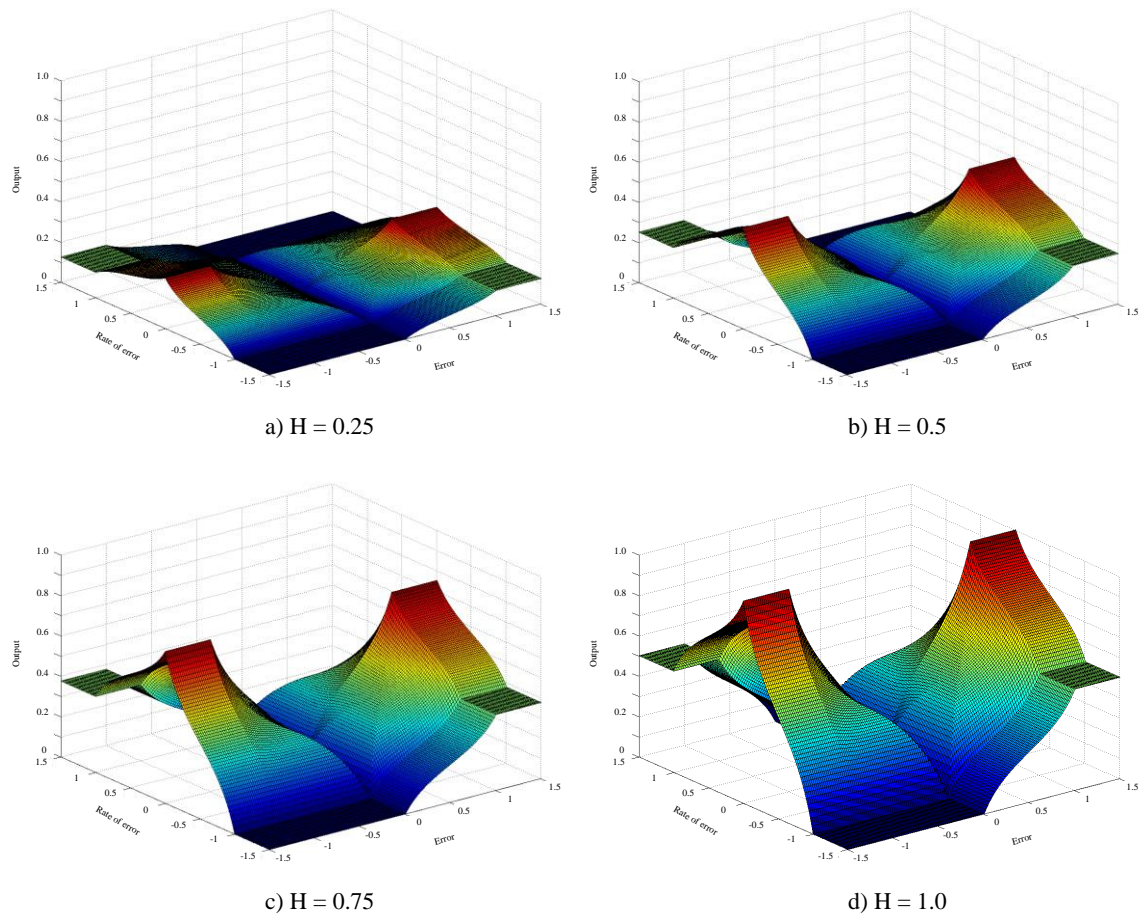


**Fig. 5-7:** Interpolation of  $e_{IN}$ ,  $r_{IN}$ , and FLC output with: a)  $H = 0.25$ , b)  $H = 0.5$ , c)  $H = 0.75$ , and d)  $H = 1.0$

### 5.2.6 Standard Procedure of Fuzzy Logic Based (FLB) DTDC

Since the fuzzy logic controller is designed with the objective to provide dynamic tuning step-size for the DTDC to achieve better performance, the standard procedure for executing the FLB-DTDC is similar to the original design for executing the SSSA-DTDC.

The standard procedure for the DTDC, after integrating it with the fuzzy logic controller, is shown in Fig. 5-8. Similar to the original procedure, the procedure of the FLB-DTDC can also be divided into two branches, with one for determining the tuning direction which has been described in Chapter 3, and the other for calculating the appropriate dynamic tuning step-size by using the FLCA (Fuzzy Logic Control Algorithm). These two branches are processed simultaneously.



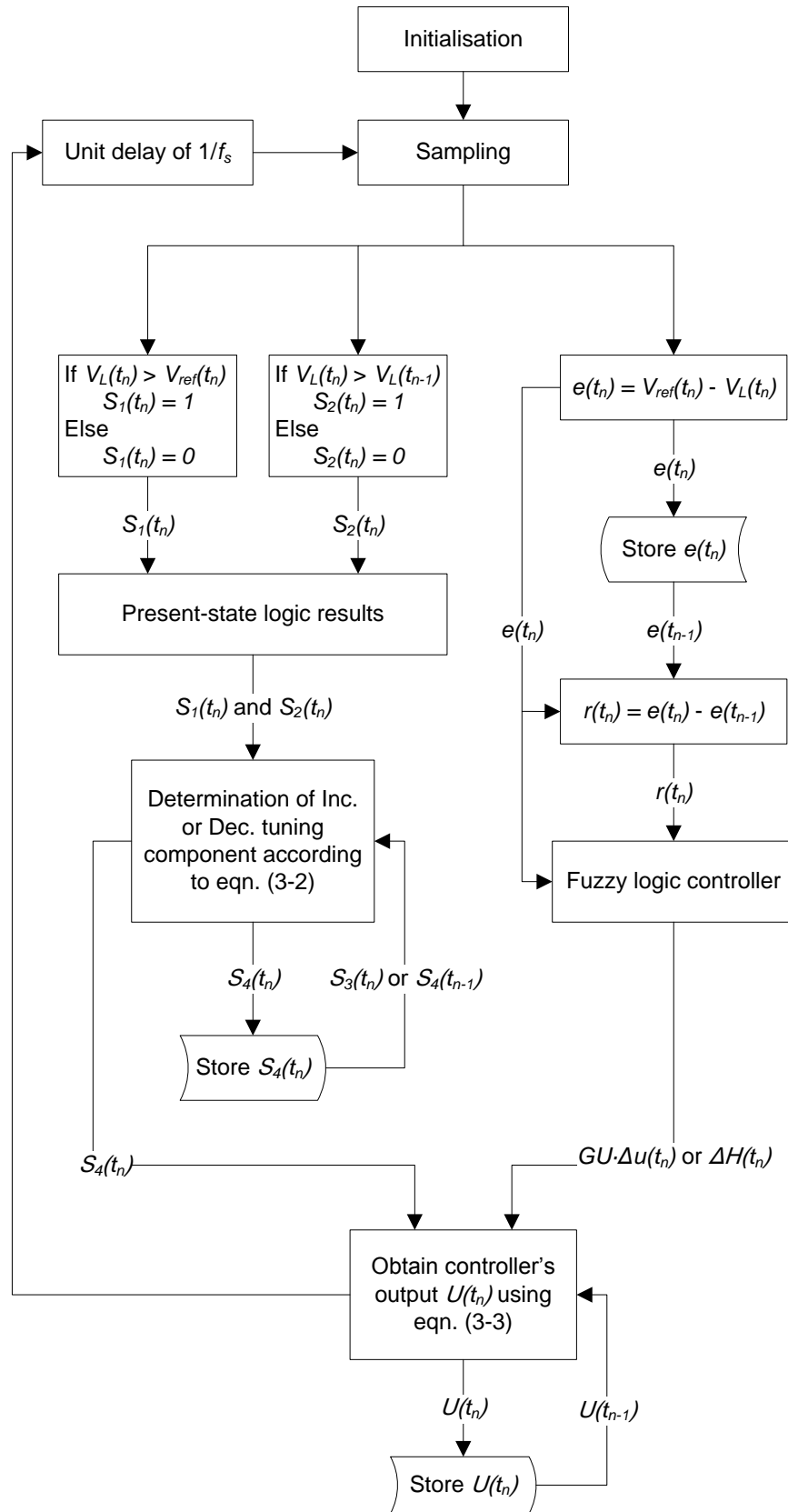


Fig. 5-8: Flowchart of standard procedure of FLB-DTDCA

In the left hand branch, the DTDC uses the comparison results  $S_1(t_n)$  and  $S_2(t_n)$  along with the previous direction signal  $S_3(t_n)$  to determine the next direction signal  $S_4(t_n)$ . In the right hand branch, the FLCA performs simple subtraction for the first two processing blocks to obtain the value of error  $e(t_n)$  and rate of error  $r(t_n)$ , and the output of the later fuzzy logic block produces a control signal  $GU \cdot \Delta u(t_n)$  (or  $\Delta H$ ) based on the obtained  $e(t_n)$  and  $r(t_n)$ . Finally, the signal of  $S_4(t_n)$  and  $GU \cdot \Delta u(t_n)$  would be collected and used in the last processing block for producing the control signal to vary the tuning component.

### 5.3 Simulation and Experimental Results

The effectiveness of the FLB-DTDC has been illustrated using both simulations and experiments. The LCL power pickups used for verification are based on the model and prototype which have been previously created, whose features have been discussed in Chapter 4. The results of FLB-DTDC are compared with the results obtained from SSSA-DTDC (DTDC using SSSA).

#### 5.3.1 Simulation Study of FLB-DTDC Controlled LCL Power Pickup

The simulation environment and conditions are exactly the same as the ones that have been conducted in Chapter 4. The FLB-DTDC controlled pickup is set to have an output voltage of 5 V, and it is initialized with a 0.02 s delay in the controller for easy observation and comparison. The scaling factors  $GE$ ,  $GR$ , and  $GU$  of the FLC are selected to be 0.6, 0.37, and  $4 \times 10^{-6}$ , respectively, based on the expected maximum error, maximum rate of error, and the ratio between the fuzzy logic output and its corresponding tuning step-size. The pickup model is simulated considering several parameter variations including variations in its operating frequency, magnetic coupling, tuning capacitance, and load resistance. The values and variations of these circuit parameters have been given in Chapter 4.

In the simulation, the pickup encounters the maximum tolerable value of each parameter at 0.1 s and minimum tolerable value at 0.15 s. Each parameter variation of the pickup is individually simulated, and the results are shown in Fig. 5-9, Fig. 5-10, Fig. 5-11, and Fig. 5-12.

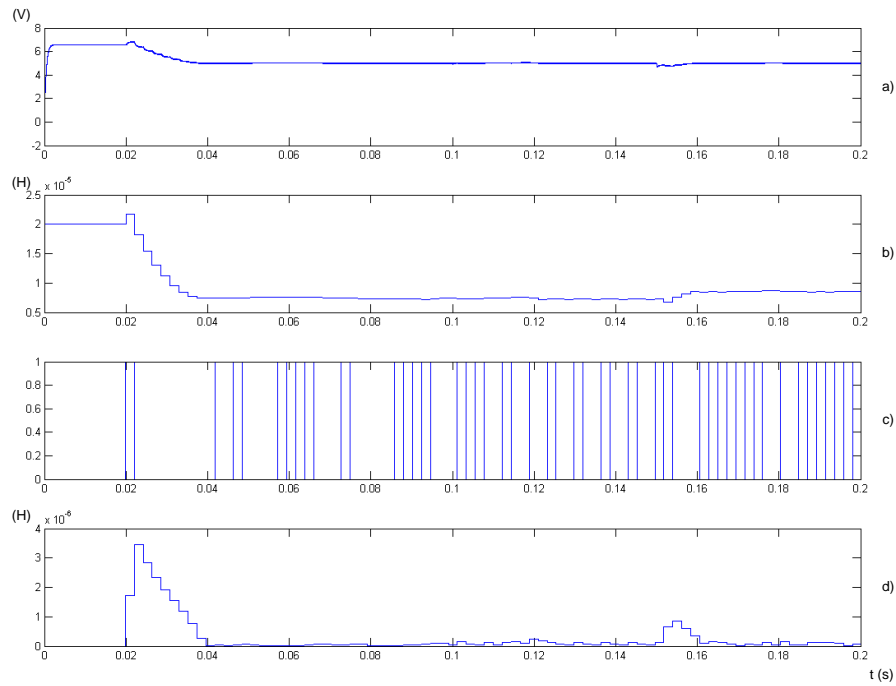


**Fig. 5-9: Simulation result of: a) output voltage  $V_L$ , b) inductance of  $L_{S2}$ , c) tuning direction signal  $S_4$ , and d) tuning step-size  $\Delta h$ , of a FLB-DTDC controlled LCL power pickup under operating frequency variations**

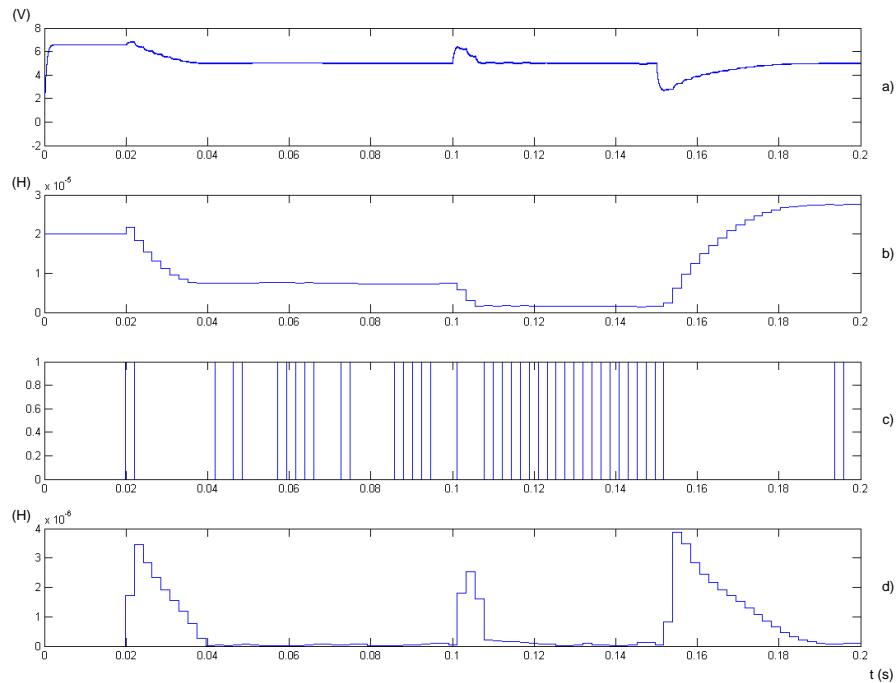


**Fig. 5-10: Simulation result of: a) output voltage  $V_L$ , b) inductance of  $L_{S2}$ , c) tuning direction signal  $S_4$ , and d) tuning step-size  $\Delta h$ , of a FLB-DTDC controlled LCL power pickup under magnetic coupling variations**

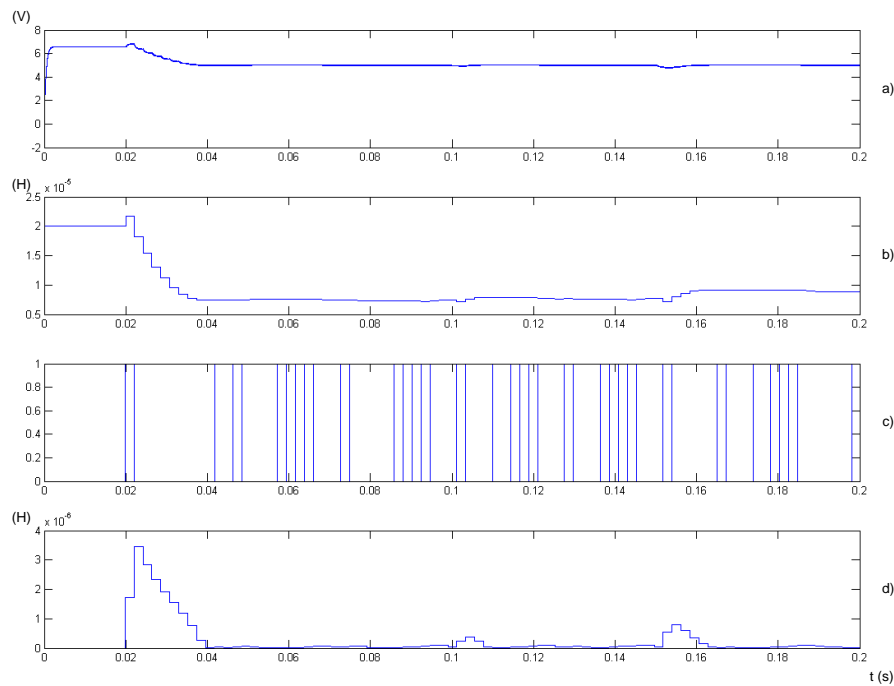


**Fig. 5-11: Simulation result of: a) output voltage  $V_L$ , b) inductance of  $L_{S2}$ , c) tuning direction signal  $S_4$ , and d) tuning step-size  $\Delta h$ , of a FLB-DTDC controlled LCL power pickup under tuning capacitor variations**

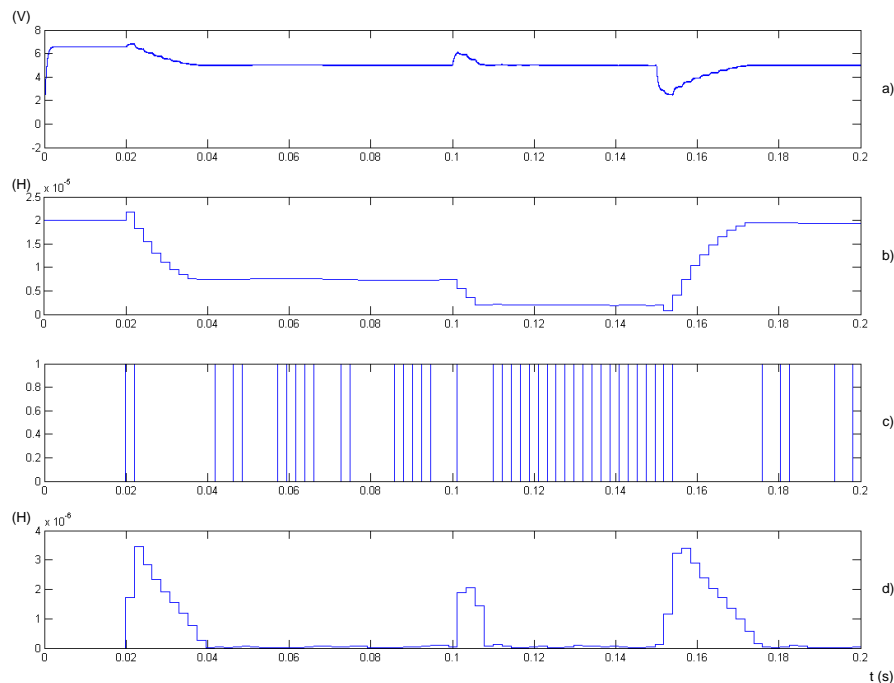


**Fig. 5-12: Simulation result of: a) output voltage  $V_L$ , b) inductance of  $L_{S2}$ , c) tuning direction signal  $S_4$ , and d) tuning step-size  $\Delta h$ , of a FLB-DTDC controlled LCL power pickup under load variations**

As can be seen from the results, the tuning step-size has changed dynamically according to the level of error and rate of error. The controlled output voltage is a constant 5 V with no steady state error. During the control process, the FLC gradually reduces the tuning step-size as the output voltage approaches to the desired value, which is a typical PD control action. This prevents the output voltage from overshooting. For comparison purpose, the simulation results of the controlled output voltage for the FLB-DTDC and the SSSA-DTDC are shown together in Fig. 5-13 and Fig. 5-14. The simulation conditions for both cases are identical, except that the maximum tuning step-size is 4  $\mu\text{H}$  for the FLB-DTDC and 7  $\mu\text{H}$  for the SSSA-DTDC. These two values are selected to give the controllers their best performance in terms of tracking speed and precision. Note that the control result in different parameter variations has been observed with similarities, therefore only the results of the operating frequency variation and the magnetic coupling variation are shown here.

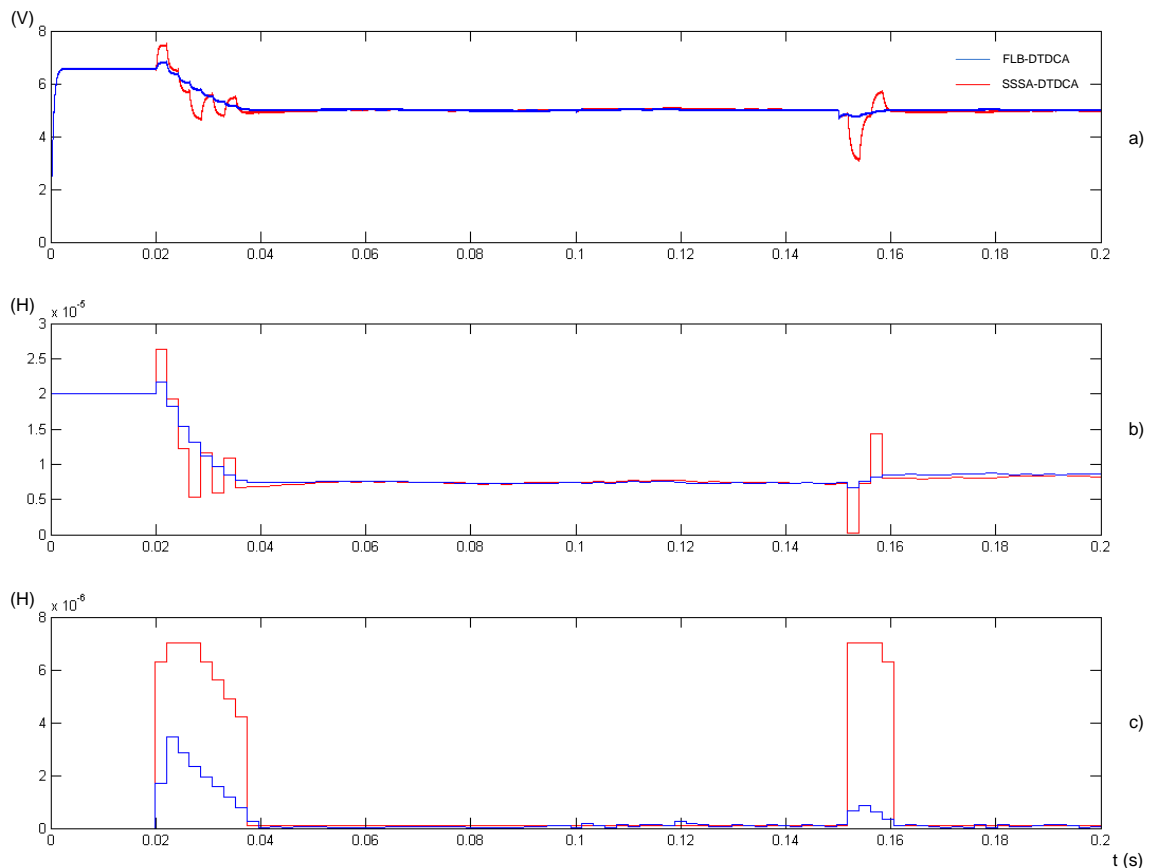


**Fig. 5-13: FLB-DTDC and SSSA-DTDC simulation results of: a) output voltage  $V_L$ , b) inductance of  $L_{S2}$ , and c) tuning step-size  $\Delta h$ , of a controlled LCL power pickup under operating frequency variations**

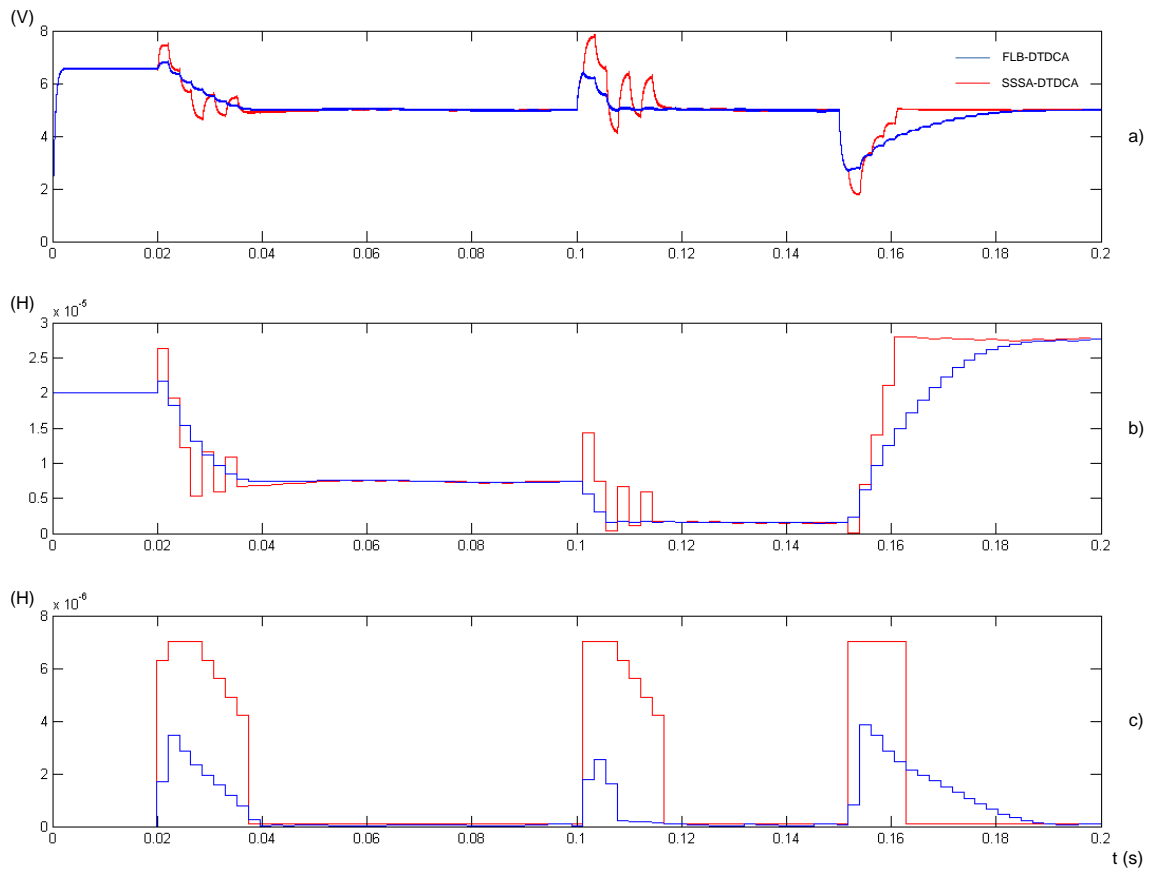


**Fig. 5-14: FLB-DTDC and SSSA-DTDC simulation results of: a) output voltage  $V_L$ , b) inductance of  $L_{S2}$ , and c) tuning step-size  $\Delta h$ , of a controlled LCL power pickup under magnetic coupling variations**

It can be seen that several improvements have been achieved in the output voltage regulation by using the FLB-DTDC. First of all, the pickup using FLB-DTDC dynamically adjusts the tuning step-size based on the value of error and rate of error. This not only allows the controller to perform smooth reference tracking, but also reduces the error when the controller is performing tuning attempts. On the contrary, the pickup using the SSSA-DTDC has a fixed tuning step-size, which may introduce more errors to the output voltage if a large tuning step-size is used or sluggish in the overall control speed if a small tuning step-size is used. Secondly, it can be observed from Fig. 5-13 and Fig. 5-14 that the SSSA-DTDC may cause significant chattering in the output voltage around the reference value before the output voltage enters the hysteresis band (HB), whereas the pickup using the FLB-DTDC does not have such a problem. And thirdly, steady state error may exist in the output voltage of the pickup using SSSA-DTDC since it uses a HB to avoid unnecessary tuning action after the output voltage reaches to a value close to the

reference voltage, whereas the pickup using the FLB-DTDCA does not have such an error since the tuning step-size here would only become zero when the reference value is exactly reached. It may be argued that the precision of the SSSA-DTDCA can be improved by reducing the width of the HB; however this can cause the controller to take more tuning adjustments for fine tuning the output voltage and consequently slows down the overall control speed. In addition, the noise problem may also arise, which may result in unnecessary tuning attempts and significant chattering in the output voltage. The stabilization speed of the SSSA-DTDCA is also heavily dependent on the position of the reference voltage relative to the output voltage in the fine tuning stage.

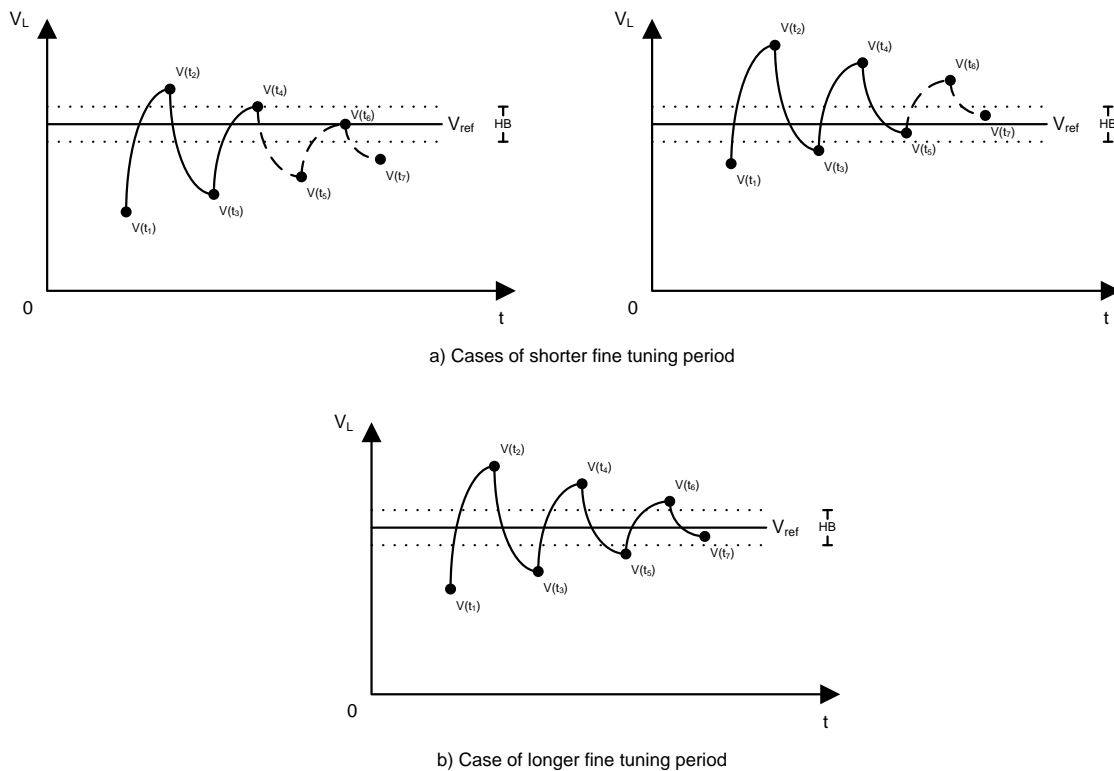


**Fig. 5-15: Possible output voltage conditions for SSSA-DTDCA to have: a) shorter fine tuning period and b) longer fine tuning period**

Figure 5-15 shows the output voltage conditions which can cause the SSSA-DTDCA to have either a short or long fine tuning period. As it can be seen from the figure, if the output voltage enters the fine tuning stage having its upper bound values of  $V(t_2)$ ,  $V(t_4)$ , and  $V(t_6)$ , or lower bound values of  $V(t_3)$ ,  $V(t_5)$ , and  $V(t_7)$ , close to the reference voltage  $V_{ref}$ , the SSSA-DTDCA uses less number of tuning adjustments to reach the values within

the HB. On the contrary, if the output voltage in the fine tuning stage has the reference voltage being in the middle of its upper and lower bound values, the SSSA-DTDC would require more tuning adjustments to reach the values within the HB. And since the above two output voltage conditions cannot be predicted during the operations, the SSSA-DTDC can randomly present short or long fining tuning periods.

### 5.3.2 Experimental Study of FLB-DTDC Controlled LCL Power Pickup

In order to compare the control result of the FLB-DTDC and the SSSA-DTDC, the experiments for both the controllers were conducted under the same testing conditions, including the maximum tuning step-size used. The specifications of the LCL power pickup have all been given in Chapter 4. Two different experiments were conducted to separately evaluate the controller performance under the load variations and the magnetic coupling variations for both the FLB-DTDC and the SSSA-DTDC. The controller performance under the load variations was evaluated by changing the load resistance in the sequence of  $5 \Omega$ ,  $6.5 \Omega$ ,  $3.5 \Omega$ ,  $6.5 \Omega$  and back to  $5 \Omega$ , and the results obtained are shown in Fig. 5-16, Fig. 5-17, Fig. 5-18, and Fig. 5-19. Note that the significant output voltage variations observed in the experiments were due to the high rate of change in the load resistance which was faster than the sampling frequency of the proposed controller. This undesirable situation can be improved if a faster sampling frequency was selected.

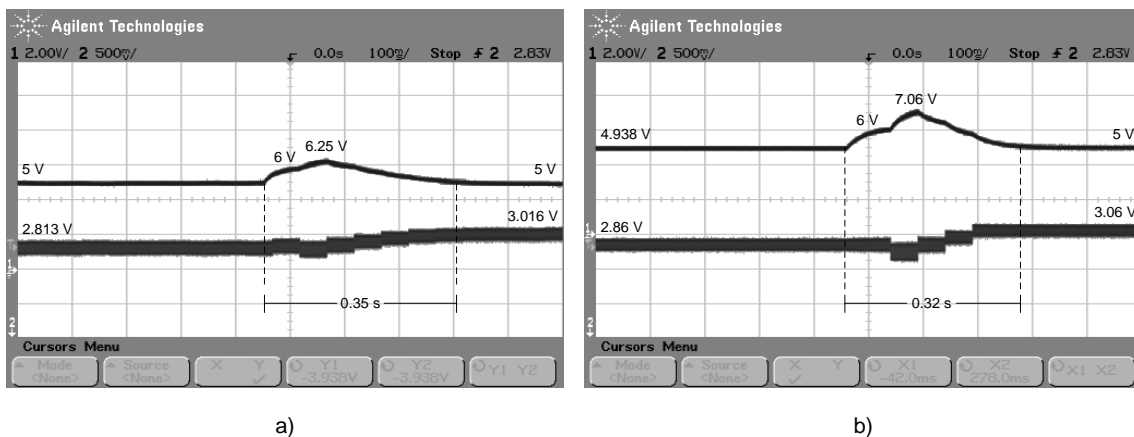
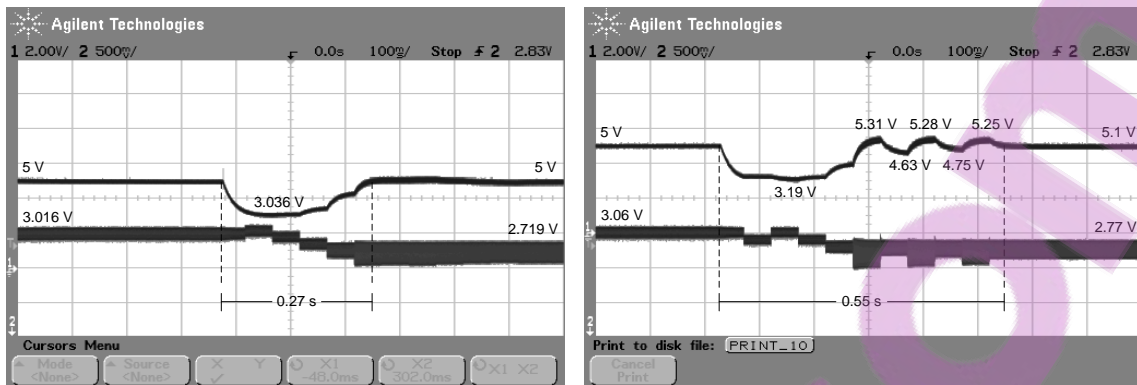


Fig. 5-16: Output voltage waveform of controlled LCL power pickup under load variation (5 to  $6.5 \Omega$ ) using: a) FLB-DTDC and b) SSSA-DTDC

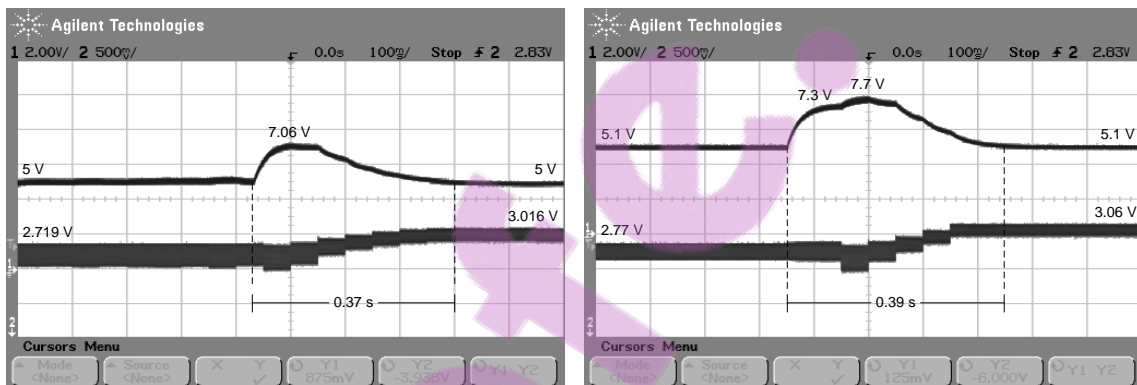




a)

b)

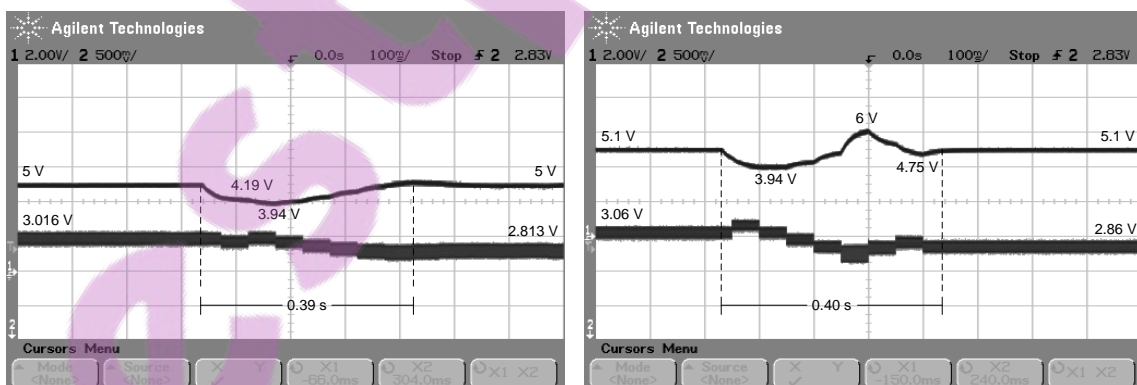
**Fig. 5-17: Output voltage waveform of controlled LCL power pickup under load variation (6.5 to 3.5 Ω) using: a) FLB-DTDCA and b) SSSA-DTDCA**



a)

b)

**Fig. 5-18: Output voltage waveform of controlled LCL power pickup under load variation (3.5 to 6.5 Ω) using: a) FLB-DTDCA and b) SSSA-DTDCA**



a)

b)

**Fig. 5-19: Output voltage waveform of controlled LCL power pickup under load variation (6.5 to 5 Ω) using: a) FLB-DTDCA and b) SSSA-DTDCA**

Experiments for evaluating the controller performance under the magnetic coupling variations were performed by changing the relative position between the pickup coil and the primary track in the sequence of A, B, C, and D, under the following conditions, and the results are shown in Fig. 5-20.

- A)  $V_{OC} = 2.47 \rightarrow 2.8$  V,  $k_f = 0.32 \rightarrow 0.36$  (coupling distance 6  $\rightarrow$  2 mm).
- B)  $V_{OC} = 2.8 \rightarrow 2.47$  V,  $k_f = 0.36 \rightarrow 0.32$  (coupling distance 2  $\rightarrow$  6 mm).
- C)  $V_{OC} = 2.47 \rightarrow 2.15$  V,  $k_f = 0.32 \rightarrow 0.28$  (coupling distance 6  $\rightarrow$  10 mm).
- D)  $V_{OC} = 2.15 \rightarrow 2.47$  V,  $k_f = 0.28 \rightarrow 0.32$  (coupling distance 10  $\rightarrow$  6 mm).

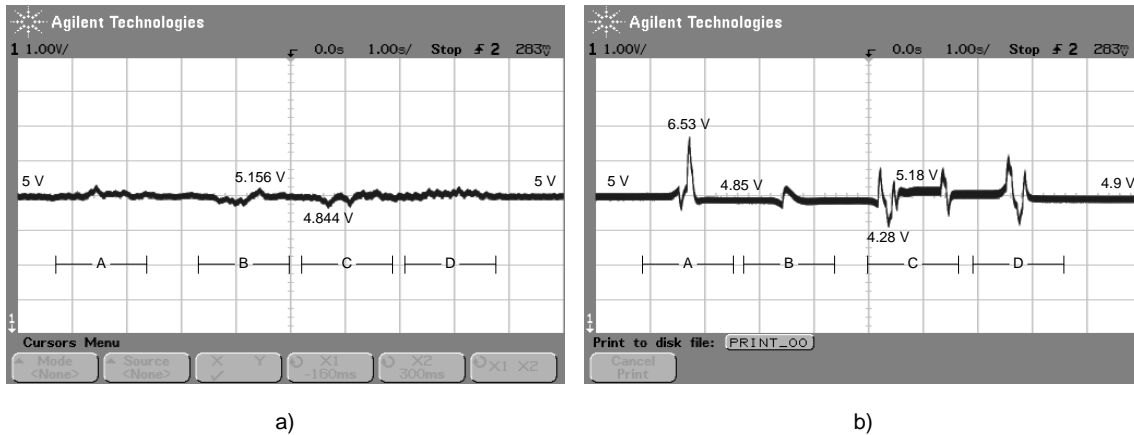


**Fig. 5-20: Output voltage waveform of controlled LCL power pickup under magnetic coupling variations using: a) FLB-DTDCA and b) SSSA-DTDCA**

The experimental results obtained in this section are in good agreement with the simulation results obtained in Section 5.3.1. In both cases it has been shown that the pickup using either the FLB-DTDCA or the SSSA-DTDCA can regulate the output voltage to be constant in the steady state. However, the FLB-DTDCA shows better overall dynamic performance than the SSSA-DTDCA in terms of:

1. Control precision – FLB-DTDCA has no steady state error.
2. Transient response – FLB-DTDCA has no large tuning attempts to cause significant output voltage spikes or chattering.

3. Control speed – FLB-DTDC has faster transient response than the SSSA-DTDC on average.

Note that the ripples observed in the controlled output voltage of LCL power pickup using FLB-DTDC were caused by the dSPACE platform due to its low resolution ADC output ports are incapable of handling high precision tuning step change. However, the ripples can be removed if high resolution ADC output ports are adopted.

## 5.4 Summary

This chapter has proposed and developed an improved DTDC by integrating the fuzzy logic controller into the classical DTDC to dynamically change the tuning step-size of the variable inductor in the LCL power pickup.

The design of the fuzzy logic controller consists of fuzzification, formulation of control rule base, and defuzzification. In the fuzzification stage, the fuzzy logic controller takes the error and rate of error of the output voltage as its inputs. The error is classified by using the membership functions of positive-error, positive-zero, negative-zero, and negative-error. And similarly the rate of error is classified by using the membership functions of positive-rate, positive-rate-zero, negative-rate-zero, and negative-rate. The control rule base is formulated to improve the transient performance of the DTDC, and there are 13 different analytical expressions that have been obtained for 28 different input combinations. These analytical expressions can be fitted into the forms of classical control theory, and the result shows that the proposed fuzzy logic controller can be regarded as a “local” nonlinear P-like, D-like, or PD-like controller with variable proportional gains and derivative gains. The defuzzification process is undertaken by the common centroid method with the Mamdani reference as the inference method.

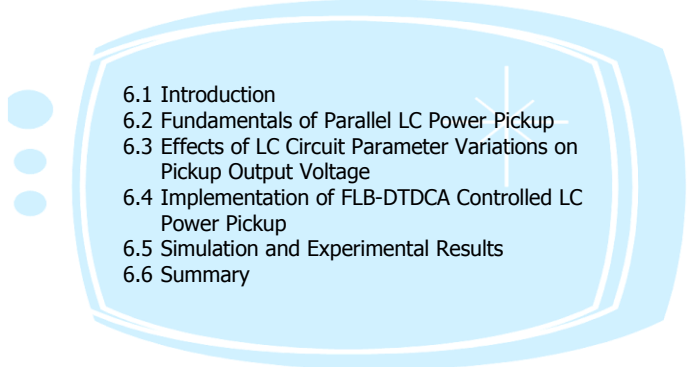
The guideline for selecting the value of input interval  $L$ , output membership value  $H$ , and scaling factors  $GE$ ,  $GR$ , and  $GU$  of the fuzzy logic controller has also been provided. It has been found that after the values for  $GE$ ,  $GR$ , and  $GU$  are determined, the values of  $L$  and  $H$  may be adjusted to improve the performance of controller if required.

Both the simulation and experimental results have demonstrated that the FLB-DTDC (DTDC using fuzzy logic controller) achieves better overall performance in the output

voltage regulation compared with the results of SSSA-DTDC (DTDC using simple step-size adjustment). The observed improvements in the control performance include: 1) the additional error that has been introduced by the control tuning attempts is reduced, 2) there is no steady state error, and 3) the chattering effect in the output voltage is eliminated and a smooth reference tracking is achieved.

## Chapter 6

# Fuzzy Logic DTDC Control of Parallel LC Power Pickup

- 
- 6.1 Introduction
  - 6.2 Fundamentals of Parallel LC Power Pickup
  - 6.3 Effects of LC Circuit Parameter Variations on Pickup Output Voltage
  - 6.4 Implementation of FLB-DTDC Controlled LC Power Pickup
  - 6.5 Simulation and Experimental Results
  - 6.6 Summary

---

### 6.1 Introduction

A secondary power pickup based on the LCL tuning configuration has been studied in Chapter 4 as an alternative to the conventional LC tuning circuit to achieve constant output voltage. LCL configuration has a theoretical advantage in keeping the output voltage constant under fully-tuned conditions. Nevertheless, the LCL power pickup loses its voltage source property under parameter variations such as variations in the operating frequency, magnetic coupling, and the tuning capacitance. It has been found that although the proposed DTDC can achieve full-range tuning in the LCL power pickup, large output voltage spikes may exist, particularly in the over-tuning region due to the complexity involved in high order circuit dynamics.

This chapter focuses on applying FLB-DTDC control to the conventional parallel LC power pickup for the output voltage regulation. Structurally, the LC power pickup has less energy storage elements and lower system orders, so the system dynamics are less complicated compared to the LCL power pickup.

## 6.2 Fundamentals of Parallel LC Power Pickup

### 6.2.1 Steady State Characteristics of LC Tuning Circuit

The parallel LC power pickup is most commonly seen in the IPT systems. The simplified circuit of the parallel LC power pickup without considering the ac-dc rectification is shown in Fig. 6-1. As can be seen from the figure, the LC power pickup consists of a secondary pickup coil with self-inductance  $L_S$ , a tuning capacitance  $C_S$ , and a load resistance  $R_{AC}$  to form a simple second order system. The resistance  $R_{AC}$  is the ac equivalent resistance of the dc load resistor  $R_L$  (see Fig. 2-20), and the ratio between these two resistances is  $R_{AC}/R_L = \pi^2/8$  [21, 77].

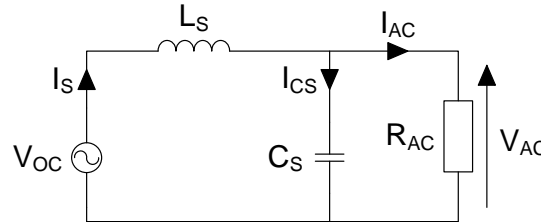


Fig. 6-1: Simplified model of LC power pickup circuit

The voltage transfer function of the power pickup can be determined from:

$$H_V(s) = \frac{V_{AC}(s)}{V_{OC}(s)} = \frac{1}{s^2 + \frac{1}{R_{AC}C_S}s + \frac{1}{L_S C_S}} \quad (6-1)$$

Considering  $I_{AC}(s) = V_{AC}(s)/R_{AC}$  and  $I_{SC}(s) = V_{OC}(s)/sL_S$ , the current transfer function of the parallel LC power pickup is obtained from:

$$H_I(s) = \frac{I_{AC}(s)}{I_{SC}(s)} = \frac{\frac{1}{R_{AC}C_S}s}{s^2 + \frac{1}{R_{AC}C_S}s + \frac{1}{L_S C_S}} \quad (6-2)$$

Equation (6-1) and (6-2) can also be expressed in the frequency-domain using rectangular form as:

$$H_V(j\omega) = \frac{R_{AC}^2(1 - \omega^2 L_S C_S) - j\omega R_{AC} L_S}{R_{AC}^2(1 - \omega^2 L_S C_S)^2 + \omega^2 L_S^2} \quad (6-3)$$

$$H_I(j\omega) = \frac{\omega^2 L_S^2 + j\omega R_{AC} L_S(1 - \omega^2 L_S C_S)}{R_{AC}^2(1 - \omega^2 L_S C_S)^2 + \omega^2 L_S^2} \quad (6-4)$$

Under fully-tuned condition where  $\omega_0^2 L_S C_S = 1$ , equation (6-3) and (6-4) can further be reduced to:

$$H_V(j\omega_0) = \frac{-jR_{AC}}{\omega_0 L_S} \quad (6-5)$$

$$H_I(j\omega_0) = 1 \quad (6-6)$$

The absolute value of (6-5) is also known as the quality factor  $Q_{S_p}$  of the parallel LC power pickup. From (6-6), it can be seen that the output current is equal to the short-circuit current of the pickup coil under fully-tuned condition.

### 6.2.2 Controllable Power Transfer Capacity of Parallel LC Power Pickup

The maximum power of the parallel LC power pickup has been given in Chapter 2, and it is governed by the quality factor  $Q_{S_p}$  of the circuit. However, the LC power pickup can also be controlled to perform detuning operation for meeting the actual load demands. The tuning condition of the LC power pickup can be changed by simply having a variable tuning capacitance in the resonant tank. Considering the normalized adjusting ratio of the tuning capacitance is presented by:

$$r_{adj} = \frac{C_{S_v}}{C_{S_r-\omega_0}} \quad (6-7)$$

where  $C_{S_v}$  is the variable or actual tuning capacitance and  $C_{S_r-\omega_0}$  is the tuning capacitance under fully-tuned condition which is equal to  $1/\omega_0^2 L_S$ , the magnitude of the output voltage and current can be obtained as:

$$V_{AC} = \frac{R_{AC} \sqrt{R_{AC}^2 (1-r_{adj})^2 + \omega_0^2 L_S^2}}{R_{AC}^2 (1-r_{adj})^2 + \omega_0^2 L_S^2} \cdot V_{OC} \quad (6-8)$$

$$I_{AC} = \frac{\omega_0 L_S \sqrt{R_{AC}^2 (1-r_{adj})^2 + \omega_0^2 L_S^2}}{R_{AC}^2 (1-r_{adj})^2 + \omega_0^2 L_S^2} \cdot I_{SC} \quad (6-9)$$

By substituting  $Q_{S-p} = R_{AC}/\omega_0 L_S$  into (6-8) and (6-9), the equations can be further simplified as:

$$V_{AC} = K_V \cdot V_{OC} = B_C \cdot Q_{S-p} V_{OC} \quad (6-10)$$

$$I_{AC} = B_C I_{SC} \quad (6-11)$$

where  $K_V$  is the operational voltage boosting factor of the tuning circuit and equals to  $B_C \cdot Q_{S-p}$ .  $B_C$  is a newly introduced variable which represents the controllable boosting coefficient and can be determined from:

$$B_C = \frac{\sqrt{Q_{S-p}^2 (1-r_{adj})^2 + 1}}{Q_{S-p}^2 (1-r_{adj})^2 + 1} \quad (6-12)$$

From (6-12), it can be seen that the controllable boosting coefficient has a maximum of unity when  $r_{adj}$  equals to 1 and a minimum of 0 when  $r_{adj}$  approaches infinity. Figure 6-2 and 6-3 show the system response of the parallel LC power pickup with respect to the variation of normalized tuning capacitance under different  $Q_{S-p}$ . From the figures it can be seen that the quality factor of the LC tuning circuit directly controls the magnitude of the maximum output voltage. But this has no effect on the maximum output current. The sensitivity of the LC circuit to the variation of tuning capacitor increases with the value of  $Q_{S-p}$  for both its output voltage and output current. Under high  $Q_{S-p}$  operation, the phase difference between the input and output voltage is approximately zero when  $r_{adj}$  equals to zero (fully-detuned in under-tuning region),  $-\pi/2$  when  $r_{adj}$  equals to unity (fully-tuned), and  $-\pi$  when  $r_{adj}$  approaches infinity (fully-detuned in over-tuning region). The phase difference between the input and output current is approximately  $\pi/2$ , 0, and  $-\pi/2$ , for  $r_{adj}$  equals to zero, unity, and approaches infinity respectively.



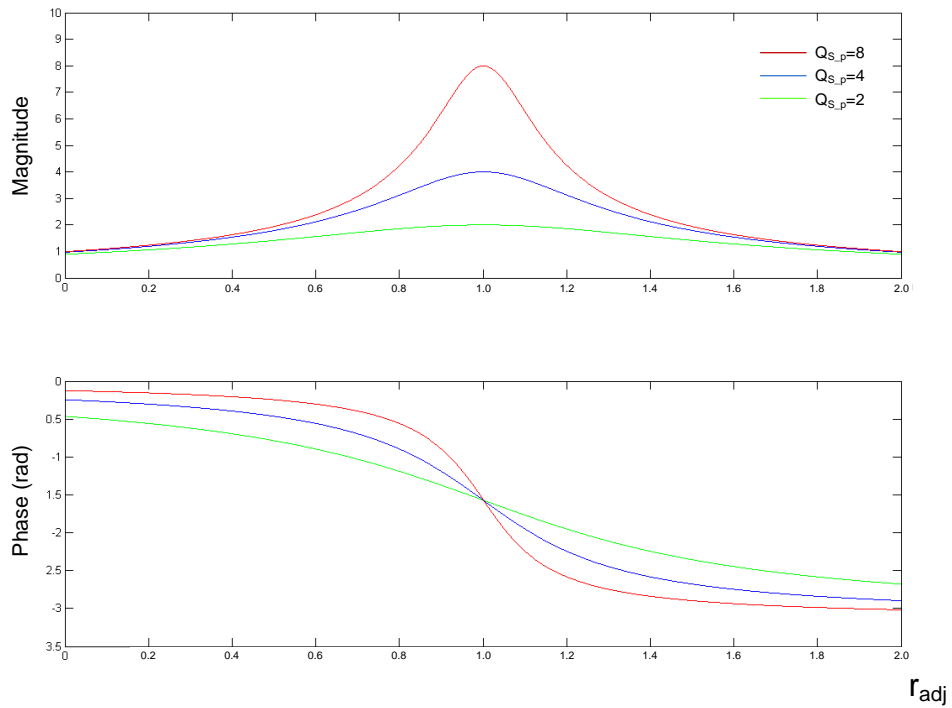


**Fig. 6-2: Output voltage response of parallel LC power pickup with respect to the variation of tuning capacitance under different  $Q_{s,p}$**

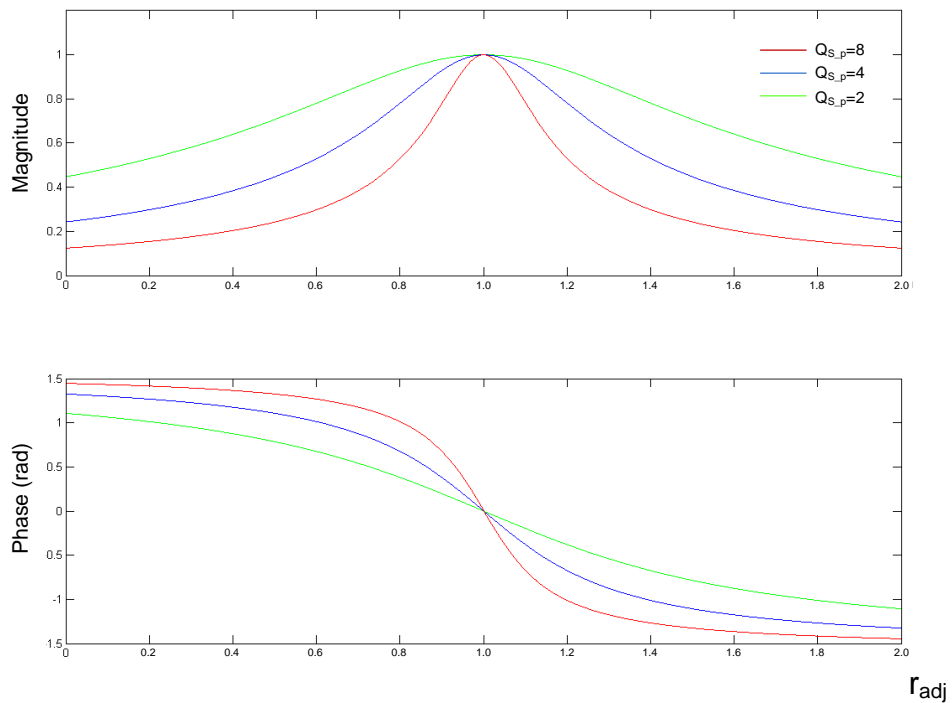


**Fig. 6-3: Output current response of parallel LC power pickup with respect to the variation of tuning capacitance under different  $Q_{s,p}$**

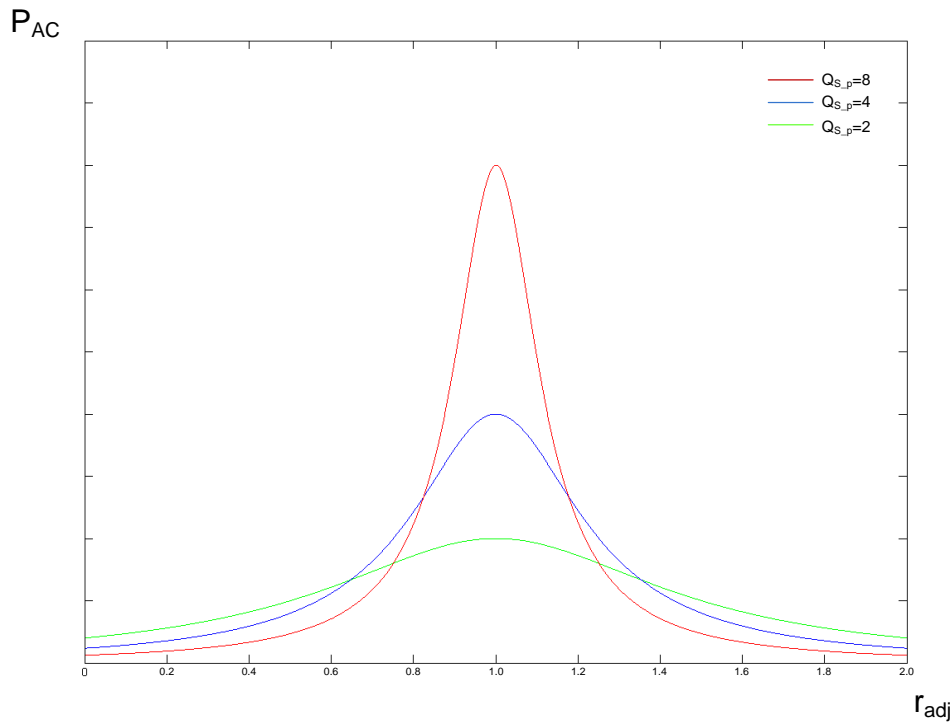


**Fig. 6-4: Power transfer capacity of parallel LC power pickup using variable tuning capacitor under different  $Q_{S-p}$**

Considering the output power of the pickup is  $P_{AC} = V_{AC} I_{AC}$ , the variable power transfer capacity of the parallel LC power pickup can therefore be determined from:

$$P_{AC} = \frac{Q_{S-p}}{Q_{S-p}^2 (1 - r_{adj})^2 + 1} \cdot V_{OC} I_{SC} \quad (6-13)$$

Figure 6-4 shows the power transfer capacity of the parallel LC power pickup using variable tuning capacitor.

### 6.3 Effects of LC Circuit Parameter Variations on Pickup Output Voltage

Similar to the LCL power pickups, the conventional LC power pickups also have parameter variations which can cause the output voltage of the pickup to fluctuate. The most common parameter variations that can be seen in the LC power pickup include but not limited to the variations in the operating frequency, magnetic coupling, and the load.

In order to compensate for these variations by using the variable tuning capacitor  $C_S$ , this section of the chapter is focused on the analyses of the relationships between the variable tuning capacitance and the output voltage of the parallel LC pickup under these parameter variations.

### 6.3.1 Operating Frequency Variation

As it has been discussed before, the variations in operating frequency can cause the secondary pickup to detune from its resonant frequency, as well as changes the magnitude of the open-circuit voltage of the pickup coil. Considering these two factors, the output voltage of the LC pickup under the operating frequency variations can be determined from:

$$V_{AC} = \frac{\sqrt{Q_{S-p}^2 \left( \frac{1}{\alpha_f} - \alpha_f r_{adj} \right)^2 + 1}}{Q_{S-p}^2 \left( \frac{1}{\alpha_f} - \alpha_f r_{adj} \right)^2 + 1} \cdot Q_{S-p} V_{OC} \quad (6-14)$$

where  $\alpha_f$  is the normalized frequency variation index that has been used in Chapter 4. From (6-14), it can be seen that the maximum output voltage of the pickup has remained unchanged. But the adjusting ratio  $r_{adj}$  for achieving the fully-tuned condition has been shifted to:

$$r_{adj\_fvr} = \frac{1}{\alpha_f^2}$$

Figure 6-5 shows the output voltage behavior of the LC power pickup under operating frequency variations. It can be seen that the entire tuning curve would be shifted to the left if it is a positive variation and to the right if it is a negative variation, and they show identical behavior in both the under-tuning and over-tuning regions.

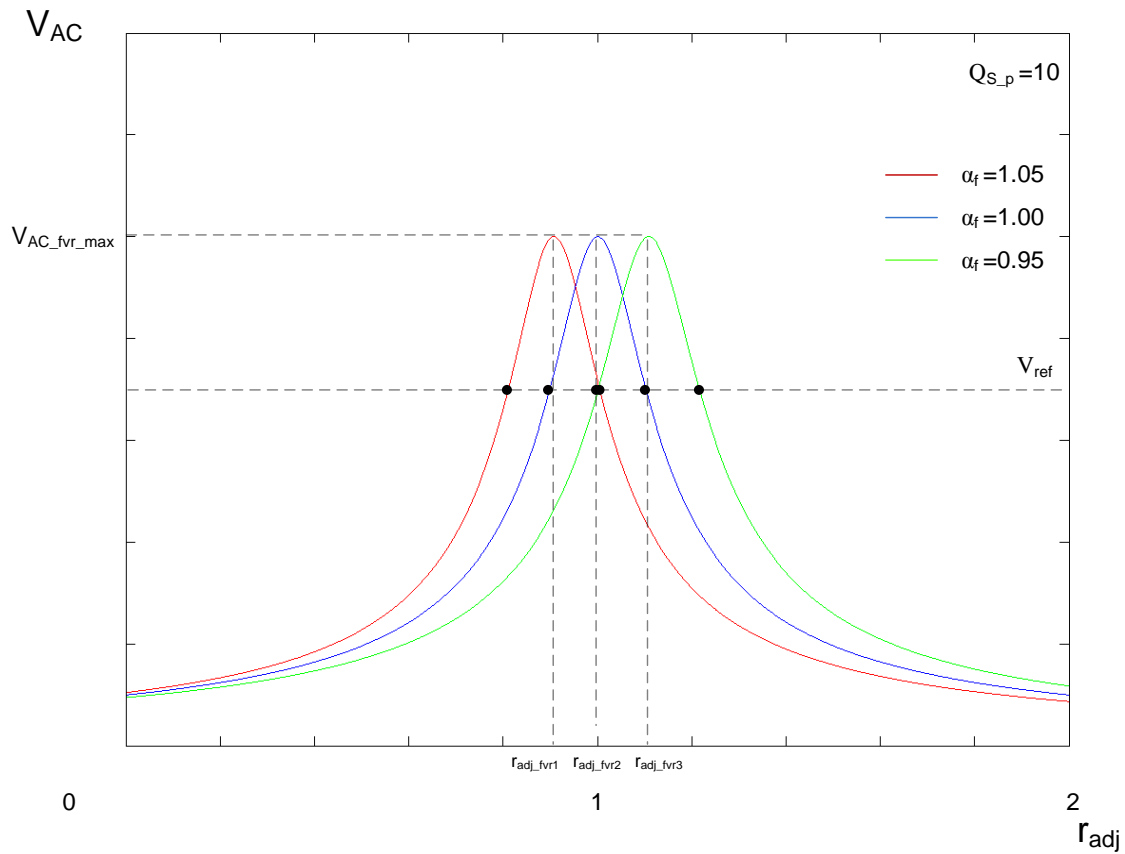


**Fig. 6-5: Output voltage behavior of parallel LC power pickup using variable  $C_s$  under operating frequency variations**

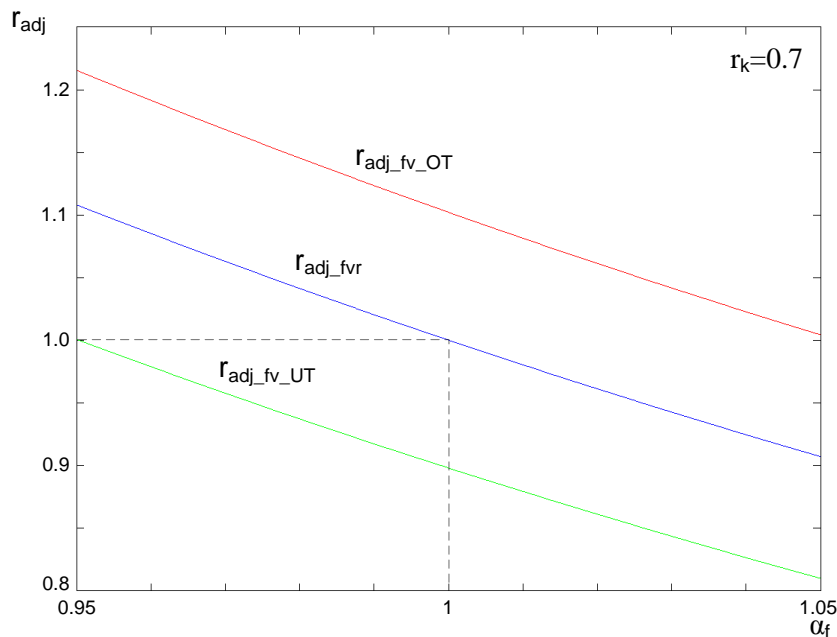
In order to maintain the output voltage to a constant desired value  $V_{ref}$ , the adjusting ratio of the tuning capacitance has to be varied accordingly. By rearranging (6-14) into a quadratic equation with respect to the ratio  $r_{adj}$  and solving it to find the desired ratio gives:

$$r_{adj\_fv} = \frac{1}{\alpha_f^2} \cdot \left[ 1 \pm \frac{\alpha_f \sqrt{\frac{1}{r_k^2} - 1}}{Q_{S\_p}} \right] \quad (6-15)$$

where  $r_k$  is the ratio between the desired voltage  $V_{ref}$  that needs to be kept constant and the maximum output voltage of the parallel LC power pickup ( $V_{AC\_R}$ ) under fully-tuned condition. And it can be expressed as:

$$r_k = \frac{V_{ref}}{V_{AC\_R}} = \frac{V_{ref}}{Q_{S\_p} V_{OC}} \quad (6-16)$$

From (6-15) it can be seen that the tuned-point of the output voltage is shifted by  $1/\alpha_f^2$ , and the span of the two solutions increases with increase of  $\alpha_f$  but decreases with increase of either  $r_k$  or  $Q_{S\_p}$ . To have valid solutions in (6-15), the ratio  $r_k$  has to be smaller than 1.



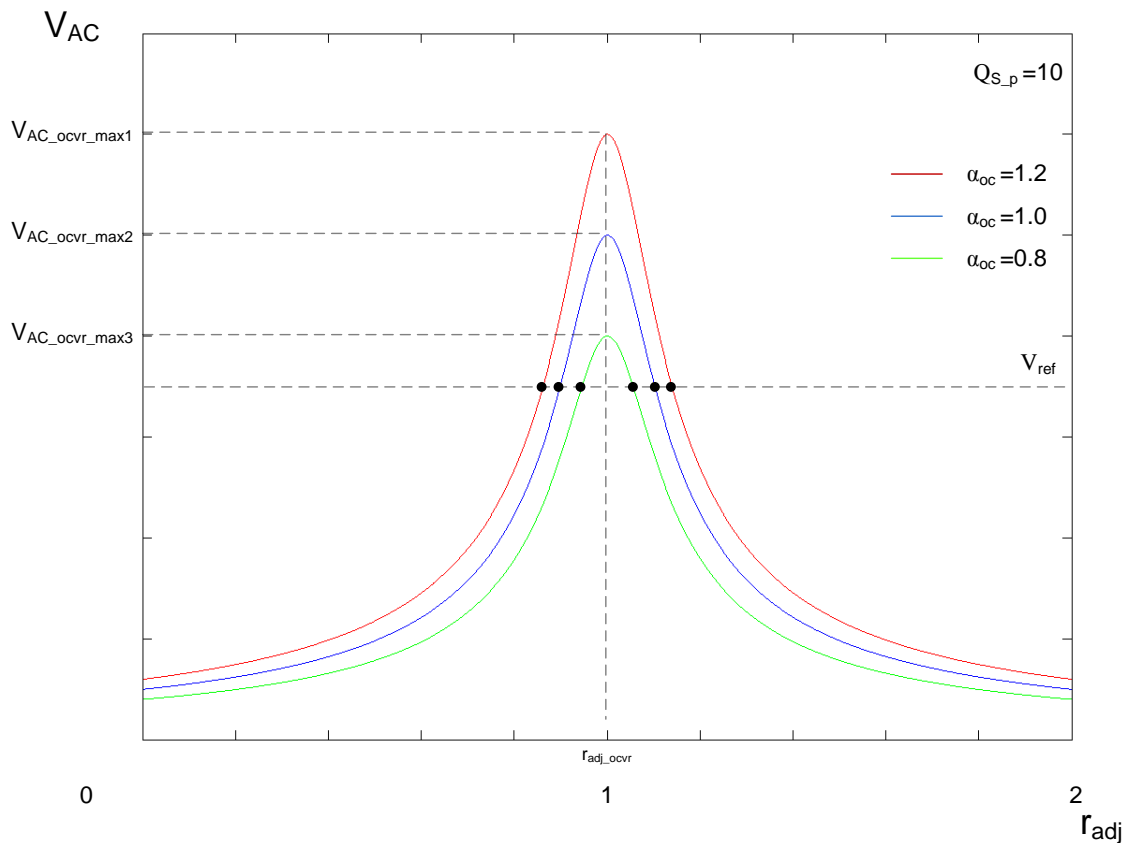
**Fig. 6-6: Adjusting ratio for parallel LC power pickup to achieve desired  $r_k$  under operating frequency variations**

Figure 6-6 shows the relationship between the operating frequency variation and the adjusting ratio for achieving the required  $r_k$  in the LC power pickup. The ratio to achieve fully-tuned condition is represented by  $r_{adj\_fvr}$ . The solutions of the required ratio are separately shown in the figure according to their operating region and represented by  $r_{adj\_fv\_OT}$  and  $r_{adj\_fv\_UT}$  for the ratios in the over-tuning region and the under-tuning region respectively. A quasi-linear relationship has been observed between the operating frequency variation and the adjusting ratio, and in addition, the amount of adjusting ratio that it takes for the tuning capacitor to compensate for the operating frequency variations in the under-tuning and over-tuning regions are almost identical to each other.

### 6.3.2 Magnetic Coupling Variation

The variations in the magnetic coupling between the primary current track and the secondary power pickup directly affect the open-circuit voltage of the pickup coil. Considering that the normalized magnetic coupling variation index is  $\alpha_{oc}$  and the affected open-circuit voltage is equal to  $\alpha_{oc} V_{OC}$ , the output voltage of the pickup under magnetic coupling variations can be expressed by:

$$V_{AC} = \frac{\alpha_{oc} \sqrt{Q_{S-p}^2 (1-r_{adj})^2 + 1}}{Q_{S-p}^2 (1-r_{adj})^2 + 1} \cdot Q_{S-p} V_{OC} \quad (6-17)$$



**Fig. 6-7: Output voltage behavior of parallel LC power pickup using variable  $C_s$  under magnetic coupling variations**

Figure 6-7 shows the output voltage behavior of the LC power pickup using variable tuning capacitor under magnetic coupling variations. From the figure it can be seen that the shape of the tuning curve remains unchanged, but the level of the tuning curve is lifted

or lowered by a factor of  $\alpha_{oc}$ , and therefore the maximum output voltage  $V_{AC\_ocvr\_max}$  under the magnetic coupling variations is changed according to  $\alpha_{oc} Q_{S\_p} V_{OC}$ .

To keep the output voltage constant at a desired level, the required adjusting ratio for the variable tuning capacitor can be obtained from:

$$r_{adj\_ocv} = 1 \pm \frac{\alpha_{oc} \sqrt{\frac{1}{r_k^2} - \frac{1}{\alpha_{oc}^2}}}{Q_{S\_p}} \quad (6-18)$$

It can be seen that the magnetic coupling variations do not affect the position of the tuned-point but the distance between the two solutions increases with the value of  $\alpha_{oc}$ , which shows that the tuning curve gets expanded with a larger  $\alpha_{oc}$ . Note that the valid solutions in (6-18) can only be obtained when  $r_k \leq \alpha_{oc}$ . This means that to allow the controller to successfully maintain the output voltage to be constant, the desired output voltage has to be less than or equal to the MMOV ( $V_{AC\_ocvr\_max3}$  shown in Fig. 6-7) at the tuned-point.

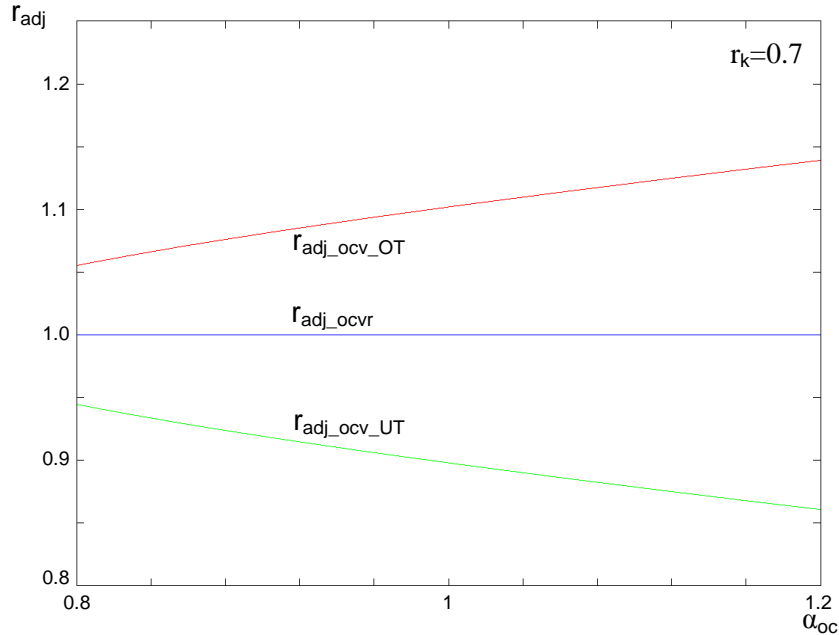


**Fig. 6-8: Adjusting ratio for parallel LC power pickup to achieve desired  $r_k$  under magnetic coupling variations**

Figure 6-8 shows the relationship between the ratio  $r_{adj}$  and the variation index  $\alpha_{oc}$  for achieving a predetermined  $r_k$ . The desired adjusting ratios are represented by  $r_{adj\_ocv\_OT}$  and

$r_{adj\_ocv\_UT}$  to separately show the results obtained in the over-tuning region and the under-tuning region respectively. The ratio for achieving the maximum output voltage has been found to be unity and represented by  $r_{adj\_ocvr}$ .

### 6.3.3 Load Variation

To observe the effects of the load variations on the output voltage of the pickup, the normalized load variation index  $\alpha_r$  is used here. The output voltage under the load variations can therefore be obtained from:

$$V_{AC} = \frac{\sqrt{Q_{S-p}^2(1-r_{adj})^2 + \frac{1}{\alpha_r^2}}}{Q_{S-p}^2(1-r_{adj})^2 + \frac{1}{\alpha_r^2}} \cdot Q_{S-p} V_{OC} \quad (6-19)$$

and the required adjusting ratio for maintaining the desired output voltage constant under the load variations can be determined from:

$$r_{adj\_rv} = 1 \pm \frac{\sqrt{\frac{1}{r_k^2} - \frac{1}{\alpha_r^2}}}{Q_{S-p}} \quad (6-20)$$

Notice that the valid solutions in (6-18) can only be obtained when the condition of  $r_k \leq \alpha_r$  is met, which also requires that the desired output voltage to be less than the MMOV ( $V_{AC\_rvr\_max3}$  shown in Fig. 6-9) that caused by the load variations at the tuned-point. Figure 6-9 and 6-10 show the output voltage behavior of the LC pickup under load variations and the required adjusting ratio for maintaining the output voltage to be constant with a given  $r_k$ , respectively. From Fig 6-9 it can be seen that the output voltage behavior in this case, is similar to the result of magnetic coupling variations, which the concerned parameter variations only cause the maximum output voltage of the pickup to vary but does not shift the tuned-point of the pickup. It can also be observed that by operating the LC pickup in the detuning region, the output voltage variation with respect to the load variation is much less than when the pickup is fully-tuned and can therefore prevent the load from significant overvoltage during sudden load changes.



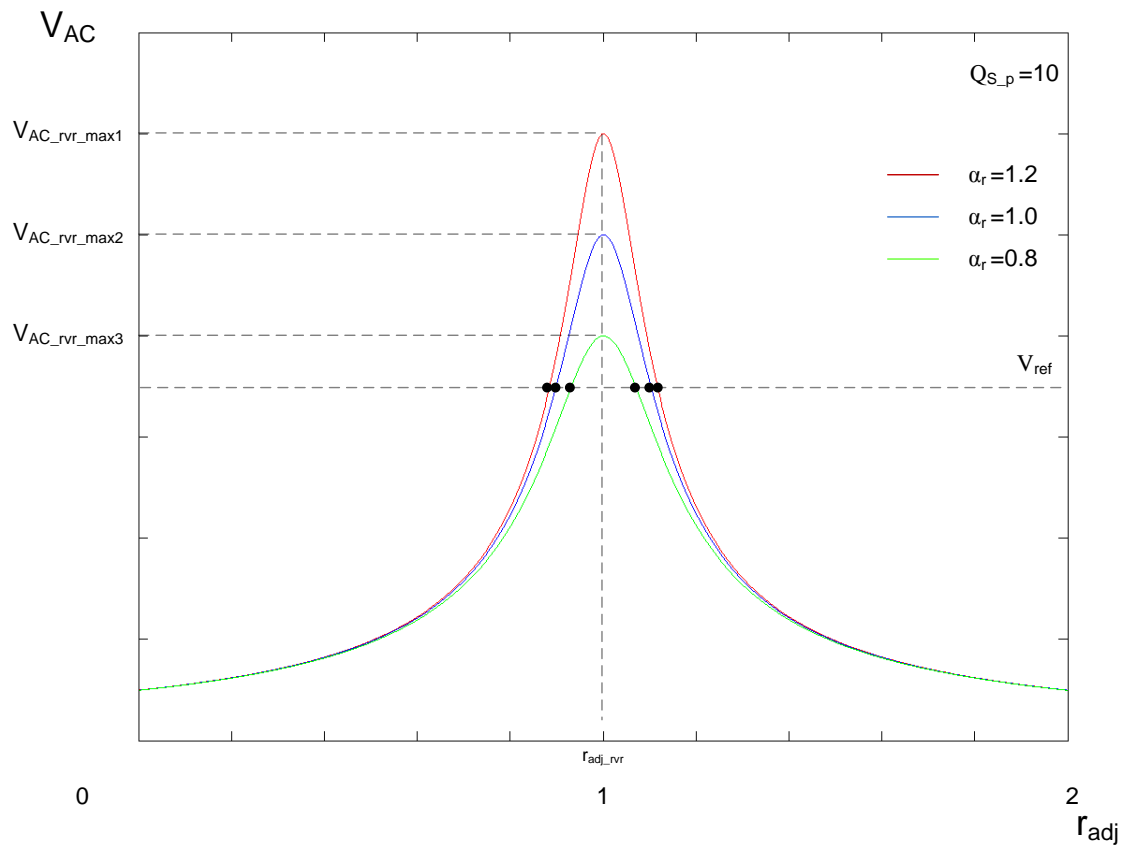


Fig. 6-9: Output voltage behavior of parallel LC power pickup using variable  $C_S$  under load variations

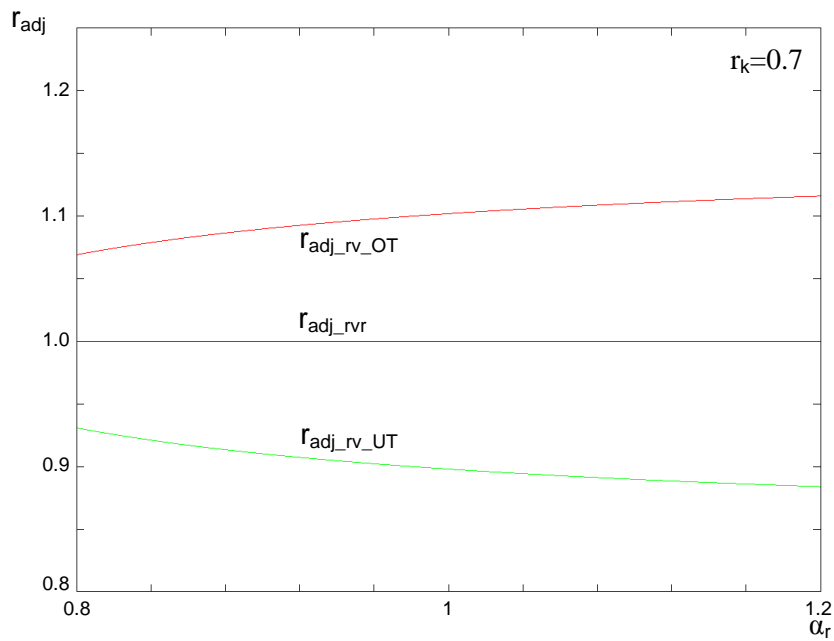
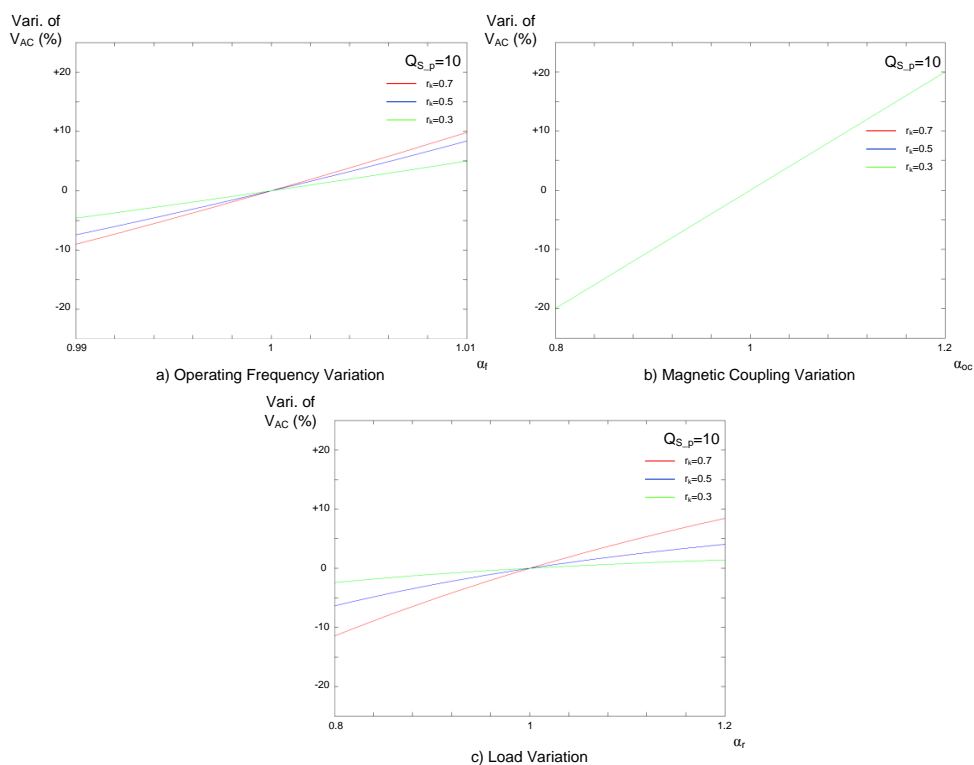


Fig. 6-10: Adjusting ratio for parallel LC power pickup to achieve desired  $r_k$  under load variations

### 6.3.4 Choice of $Q_{S_p}$ and $r_k$

It is known that the quality factor  $Q_{S_p}$  of the LC pickup can change the shape and magnitude of the tuning curve, and the choice of  $r_k$  can lead to different output voltage variations with respect to the concerned parameter variations. The effect of these two factors on the relationship between the output voltage variation and the parameter variation is therefore needed to be investigated. Since the output voltage behavior of the parallel LC pickup is almost identical in the under-tuning and over-tuning region, only the results in the under-tuning region are presented here.



**Fig. 6-11: Relationship between output voltage variation and parameter variation under a constant  $Q_{S_p}$  and different  $r_k$**

Figure 6-11 shows the output voltage variations (in %) caused by: a) operating frequency variations, b) magnetic coupling variations, and c) load variations, under a constant  $Q_{S_p}$  with different  $r_k$ . The output voltage variation increases with  $r_k$  in the case a) and c), but it has not been affected by  $r_k$  in the case of b). In addition, it may not be obvious to observe the nonlinearities that appear in the results of case a) and c), but the nonlinearities do exist and can be improved by using lower  $r_k$ . Figure 6-12 shows the output voltage variations (in %) caused by the considered parameter variations under a constant  $V_{ref}$  with different

$Q_{S_p}$ . From the figure, it can be seen that the output voltage variation increases with  $Q_{S_p}$  in the case a), but decreases to the increase of  $Q_{S_p}$  in the case c). Notice that the relationship between the output voltage variation and the magnetic coupling variation still remains unchanged, which makes it the only case that is not affected by either  $r_k$  or  $Q_{S_p}$  amongst the three cases that has been discussed.

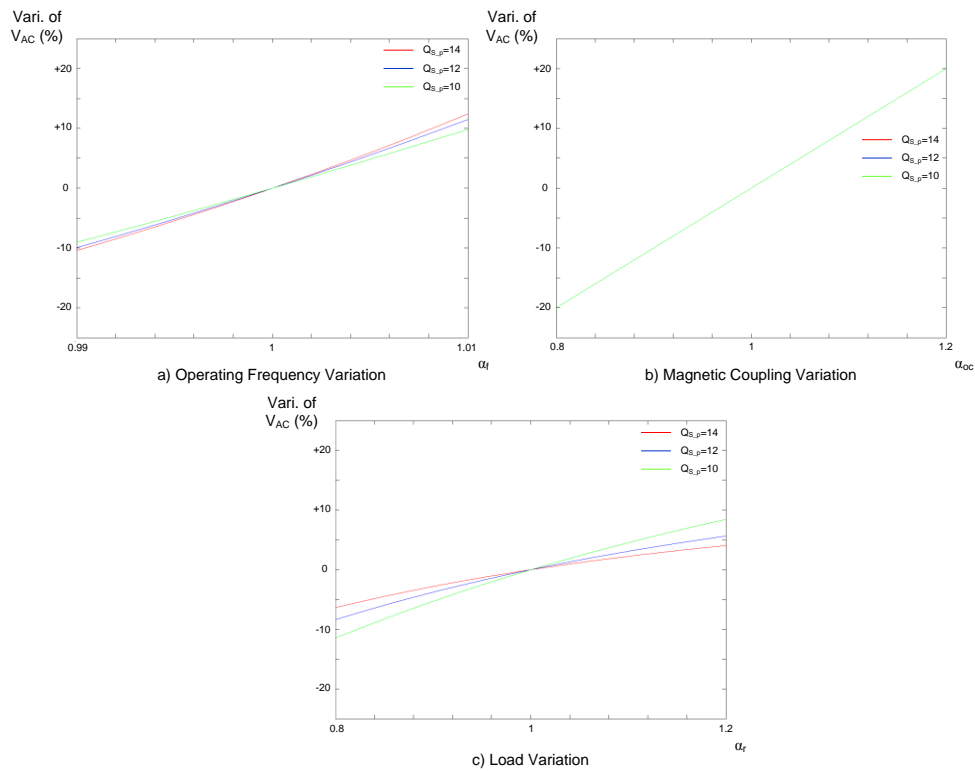


**Fig. 6-12: Relationship between output voltage variation and parameter variation under a constant  $V_{ref}$  and different  $Q_{S_p}$**

The results obtained from both Fig. 6-11 and Fig. 6-12 has shown that the LC pickup is most sensitive to a), followed by b), and c). Based on the obtained results, it can be seen that the sensitivity of output voltage in the case a) and c) can be reduced by using lower  $r_k$ . Varying  $Q_{S_p}$  can also achieve different circuit sensitivity, but it leads to two conflicting situations. The first conflict is that the sensitivity of the output voltage increases with  $Q_{S_p}$  in the case a), but decreases in the case c), which means that a tradeoff between the output sensitivity of case a) and c) is needed if  $Q_{S_p}$  is to be varied. The second conflict happens due to the direct relationship between  $Q_{S_p}$  and  $r_k$ . For example, under a given voltage reference, increase/decrease in  $Q_{S_p}$  would mean decrease/increase in  $r_k$ . Therefore,  $Q_{S_p}$  and  $r_k$  can only be selected by considering all three investigated cases together.

### 6.3.5 Operating Range of Variable $C_S$

To fully compensate for the parameter variations that have been previously analyzed, the integrated effect of these parameter variations on the output voltage needs to be investigated. The output voltage of the LC pickup under such a consideration can be expressed by:

$$V_{AC} = \frac{\alpha_{oc} \sqrt{Q_{S-p}^2 \left( \frac{1}{\alpha_f} - \alpha_f r_{adj} \right)^2 + \frac{1}{\alpha_r^2}}}{Q_{S-p}^2 \left( \frac{1}{\alpha_f} - \alpha_f r_{adj} \right)^2 + \frac{1}{\alpha_r^2}} \cdot Q_{S-p} V_{OC} \quad (6-21)$$

Equation (6-21) can also be rearranged to obtain the required adjusting ratio  $r_{adj\_pv}$  for achieving the desired output voltage under the integrated effect of the parameters variation, and the required ratio can be determined from:

$$r_{adj\_pv} = \frac{1}{\alpha_f} \cdot \left[ 1 \pm \frac{\alpha_f \alpha_{oc} \sqrt{\frac{1}{r_k^2} - (\alpha_{oc} \alpha_r)^2}}{Q_{S-p}} \right] \quad (6-22)$$

To have valid solutions in (6-22), the following condition has to be met:

$$r_k \leq \alpha_{oc} \alpha_r$$

To fully compensate for all the considered parameter variations, the worst-case scenario of the practical operations has to be considered for obtaining the minimum and the maximum of the adjusting ratio  $r_{adj\_pv}$ . The distance between the Min and Max of  $r_{adj\_pv}$  is defined as the operating range of the variable  $C_S$ . Based on the results shown in Fig. 6-5, Fig. 6-7, and Fig. 6-9, it can be seen that the Min and Max of  $r_{adj\_pv}$  can be calculated using (6-22) with the following conditions.

#### **Maximum required ratio ( $r_{adj\_pv\_max}$ )**

- The parallel LC power pickup is operating in the over-tuning region of the tuning curves.

- The operating frequency is at *nominal value - maximum allowable tolerance*, and the magnetic coupling and load variations are at *nominal value + maximum allowable tolerance*.

**Minimum required ratio ( $r_{adj\_pv\_min}$ )**

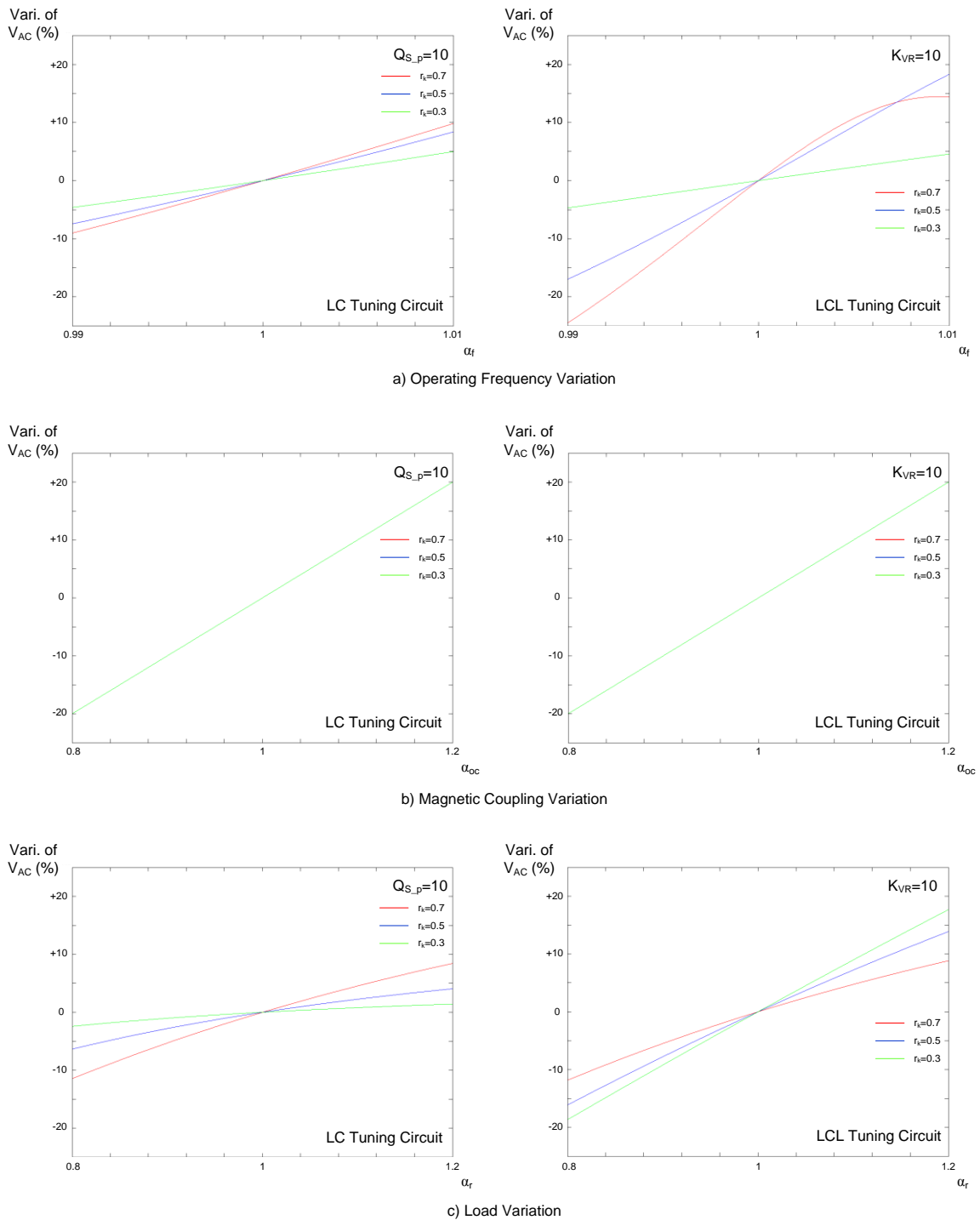
- The parallel LC power pickup is operating in the under-tuning region of the tuning curves.
- The considered parameter variations are all at *nominal value + maximum allowable tolerance*.

### 6.3.6 Comparison of Output Voltage Variation to Parameters Variation between LC and LCL Tuning Circuits

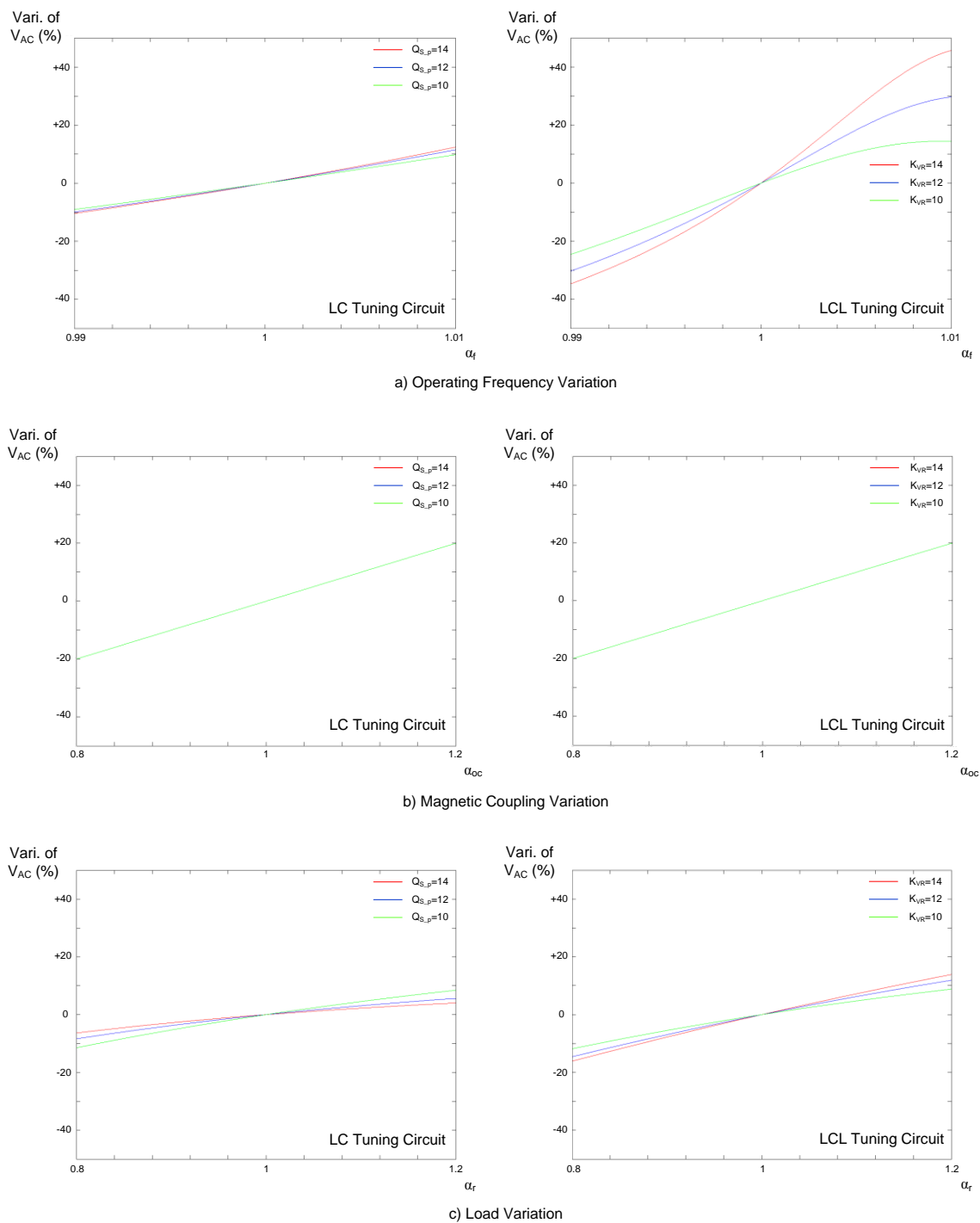
In this section, the output voltage variation to the parameters variation between the LC and the LCL power pickups is compared, so that the differences between these two tuning configurations can be understood.

Figure 6-13 and 6-14 show the comparison results with respect to: a) operating frequency variation, b) magnetic coupling variation, and c) load variation between the LC and the LCL pickup, under the condition of a constant  $k_{VR}$  or  $Q_{S\_p}$  with different  $r_k$  and a constant voltage reference with different  $k_{VR}$  or  $Q_{S\_p}$ , respectively. It can be seen from the results that the output voltage of the LCL pickup is more sensitive to the parameters variation especially under the condition of a), and as the voltage boosting factor increases, its output voltage variation increases further and can be 4 ~ 5 times larger than the LC pickup. In the case of c), the results show that the LC pickup would have lower voltage variation than the LCL pickup when it encounters sudden load changes. However, it should be noted that if  $r_k$  is set to unity, the LCL pickup would have zero voltage variation to the load variation due to its voltage source property.

Based on the results shown in Fig. 6-13 and Fig. 6-14, it can be seen that the LC pickup would have better transient performance than the LCL pickup due to its lower output sensitivity to the parameters variation. However, if the IPT system uses a primary power supply with a fixed switching frequency, then the LCL circuit may still be a good alternative to the tuning configurations of the power pickup due to its voltage source property.



**Fig. 6-13: Comparison of output voltage variation to parameters variation between LC and LCL tuning circuit under a constant  $k_{VR}$  or  $Q_{S\_p}$  with different  $r_k$**



**Fig. 6-14: Comparison of output voltage variation to parameters variation between LC and LCL tuning circuit under a constant  $V_{ref}$  with different  $k_{VR}$  or  $Q_{S_p}$**

## 6.4 Implementation of FLB-DTDC Controlled LC Power Pickup

### 6.4.1 Structure of Switch-Mode Variable Capacitor Controlled LC Power Pickup

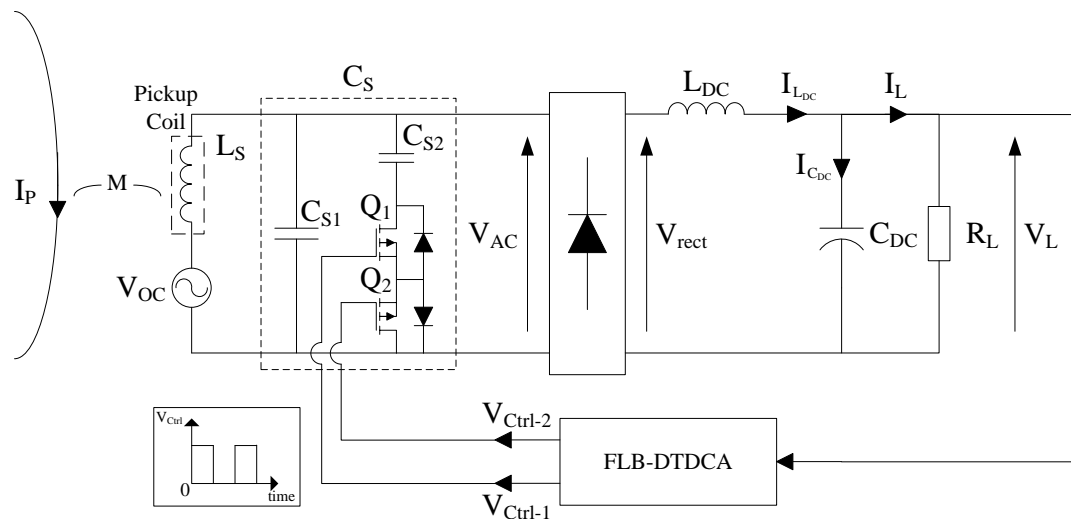


**Fig. 6-15: Structure of variable capacitor controlled parallel LC power pickup**

The basic structure of the proposed parallel LC power pickup is shown in Fig. 6-15. It consists of the main circuit of a parallel LC power pickup and a control circuitry to form a complete secondary system. The LC tuning configuration provides a constant output current to the load under fully-tuned conditions. The tuning capacitance  $C_S$  is divided into two parts; the first part is a fixed value capacitor  $C_{S1}$  which is used for starting up the pickup circuit, and the second part consists of a capacitor  $C_{S2}$  and two switches ( $Q_1$  and  $Q_2$ ), which functions as a switched-mode variable capacitor for changing the tuning condition of the power pickup. The output voltage  $V_L$  is used as a feedback signal to the FLB-DTDC for producing signals  $V_{Ctrl-1}$  and  $V_{Ctrl-2}$  with controlled duty cycles so that the ac switch  $Q_1$  and  $Q_2$  can be turned on/off accordingly to obtain the desired equivalent capacitance. This eventually allows the pickup to deliver the power as required by the load.



### 6.4.2 Selection of $C_{S1}$ and $C_{S2}$

In order to have sufficient output power to startup the controller at the initial stage, the capacitance of  $C_{S1}$  is required to be selected according to the location shown in Fig. 6-16.

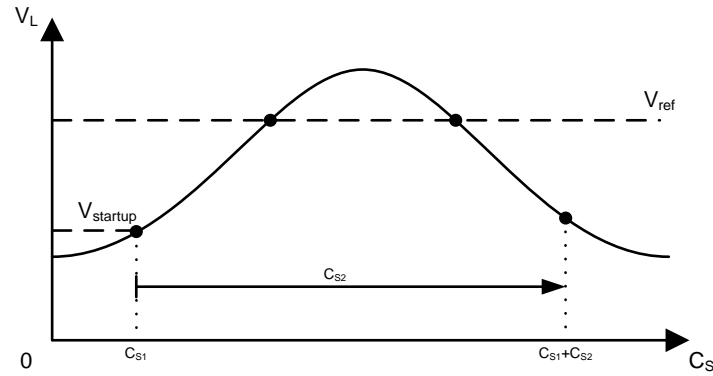


**Fig. 6-16: Proper location of  $C_{S1}$  on tuning curve of output voltage**

The voltage  $V_{startup}$  is the voltage required to startup the controller. The value of  $C_{S1}$  can be determined by using (6-22), with the operating frequency, magnetic coupling, and load variations being considered at *nominal value - maximum allowable tolerance*. Such a consideration would allow the pickup to startup the controller under all possible parameters variation that has been considered.

The operating range of  $C_S$  to fully compensate for all possible parameters variation has been determined previously, however since the capacitance obtained from the minimum required ratio  $r_{adj\_pv\_min}$  may not be equal to the value of  $C_{S1}$  determined here, the previous calculated operating range can only be regarded as the minimum operating range. Hence, the actual operating range of  $C_{S2}$  can be expressed as:

$$C_{S2} = C_{pv\_max} - C_{S1} \quad (6-23)$$

where  $C_{pv\_max}$  is the capacitance obtained from the maximum required ratio  $r_{adj\_pv\_max}$ .

### 6.4.3 Equivalent Capacitance of $C_{S2}$

For the resonant circuit using an ac switched capacitor, the waveform of the voltage in the ac tank and across the capacitor can be represented by  $V_{AC}$  and  $V_C$  respectively, in Fig. 6-17.

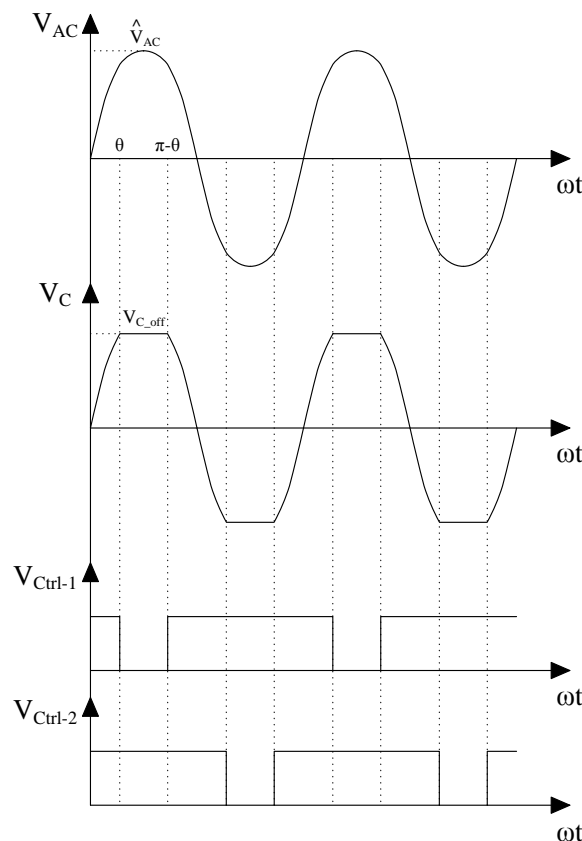


**Fig. 6-17: Voltages and control signals of ac switched capacitor**

From the above illustration, it can be seen that the signal  $V_{Ctrl-1}$  and  $V_{Ctrl-2}$  control the on/off period of the capacitor in the positive and the negative cycles respectively. When the capacitor is switched off (at  $\theta$ ), the voltage across the capacitor would be capped at  $V_{C\_off}$  since there is no more current flowing through the capacitor to charge it. The capacitor only gets discharged when  $V_{AC}$  is lower than  $V_C$  (at  $\pi-\theta$ ). Such a technique can control the amount of electric charges accumulated inside the capacitor and hence achieves a variable equivalent capacitance for changing the tuning condition of the pickup [66, 67].

The relationship between the switching angle and the voltages can be expressed as:

$$\theta = \sin^{-1} \left( \frac{V_{C\_off}}{\hat{V}_{AC}} \right) \quad (6-24)$$

The switching angle can also be directly related to the duty cycles of the control signal and has a linear proportional relationship of:

$$\theta = \frac{\pi}{100} (D - 50) \quad (6-25)$$

where  $D$  is the duty cycle of the control signal  $V_{Ctrl-1}$  and  $V_{Ctrl-2}$  in percentage. Considering that the electric charges stored inside an ac switched capacitor are equal to that of using an equivalent capacitance  $C_{eq}$ , an equation can be obtained as follows:

$$\int_0^{\pi} C_{S2} V_C d(\omega t) = \int_0^{\pi} C_{eq} \hat{V}_{AC} \sin(\omega t) d(\omega t) \quad (6-26)$$

By expanding (6-26) into segments according to  $V_C$  as shown in Fig. 6-17, the following equation can be obtained:

$$C_{eq} = \frac{1}{2\hat{V}_{AC}} \left[ \int_0^{\theta} C_{S2} \hat{V}_{AC} \sin(\omega t) d(\omega t) + \int_{\theta}^{\pi-\theta} C_{S2} V_{C\_off} d(\omega t) + \int_{\pi-\theta}^{\pi} C_{S2} \hat{V}_{AC} \sin(\omega t) d(\omega t) \right] \quad (6-27)$$

Solving (6-27), the variable equivalent capacitance which is obtained by changing the duty cycle of the control signals is determined from:

$$C_{eq} = C_{S2} \left[ 1 - \cos \left( \frac{\pi(D-50)}{100} \right) + \pi \left( 1 - \frac{D}{100} \right) \sin \left( \frac{\pi(D-50)}{100} \right) \right] \quad (6-28)$$

where  $D$  has a variable range of 50 ~ 100% since the control signals  $V_{Ctrl-1}$  and  $V_{Ctrl-2}$  are responsible for each 50% of the complete cycle. Figure 6-18 shows the relationship between the equivalent capacitance and the duty cycle. As it can be seen from the figure, the variable equivalent capacitance has a capacitance equals to  $C_{S2}$  when both switches are fully turned on and zero when both switches are at 50% duty cycle.

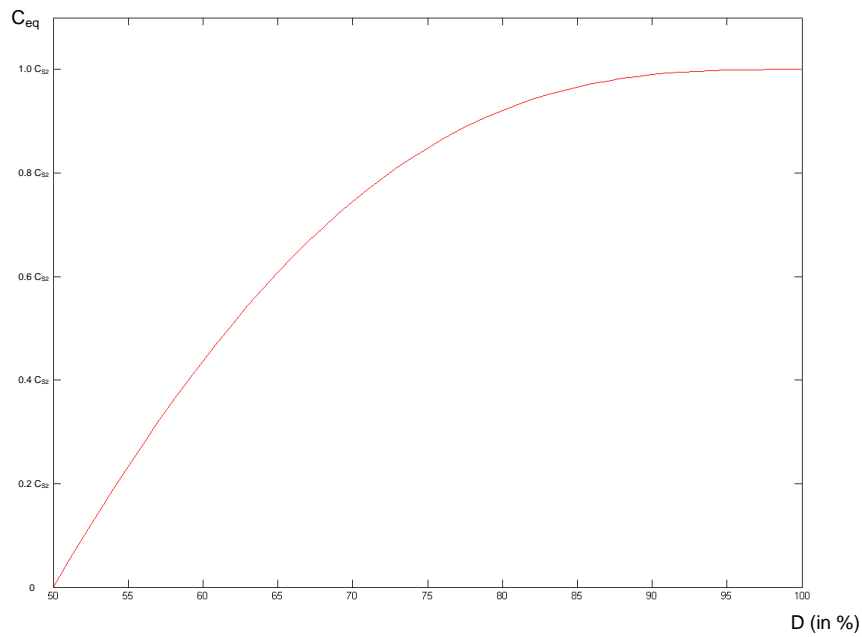


Fig. 6-18: Relationship between  $C_{eq}$  and  $D$  of ac switched  $C_{S2}$

#### 6.4.4 Switching Signals for $Q_1$ and $Q_2$

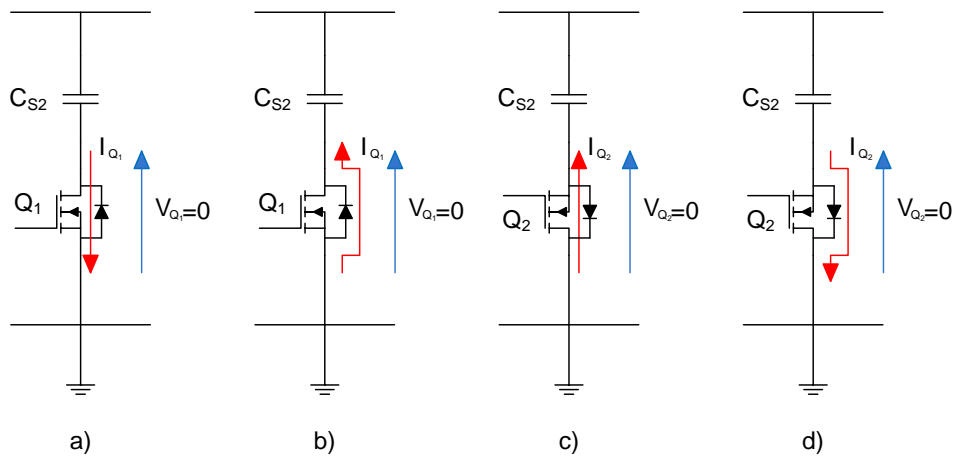
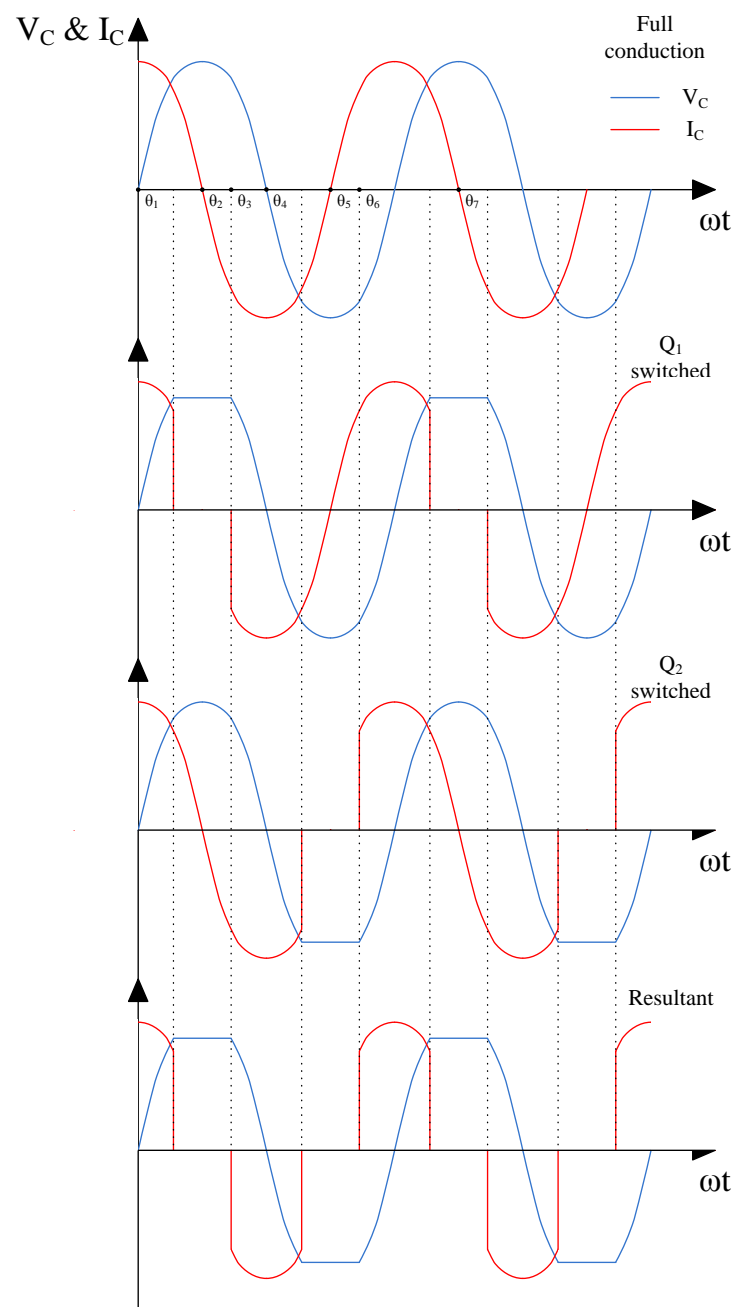


Fig. 6-19: Conditions of achieving ZVS in  $Q_1$  and  $Q_2$

To reduce the switching losses in  $Q_1$  and  $Q_2$ , soft-switching technique such as ZVS (Zero Voltage Switching) has to be employed. Figure 6-19 shows the conditions when the ZVS can be achieved in  $Q_1$  and  $Q_2$ . Assuming that both  $Q_1$  and  $Q_2$  are ideal switches and have no voltage drop in full conduction states, the conditions of a) and c) show that  $Q_1$  and  $Q_2$  can be turned off anywhere in between  $\theta_1$  to  $\theta_2$  and  $\theta_4$  to  $\theta_5$  as shown in Fig. 6-20, respectively, to achieve ZVS, as long as these switches are in forward conduction.



**Fig. 6-20: Voltage and current waveforms of  $C_{s2}$  under full conduction and being switched**

To achieve ZVS in the conditions of b) and d) where the current starts to flow through the body diode of the switches and the voltage across the switches equals to zero if the forward voltage drop of the diode is neglected,  $Q_1$  and  $Q_2$  have to be switched on in between  $\theta_3$  to  $\theta_5$  and  $\theta_6$  to  $\theta_7$ , respectively.

In order to achieve the ZVS while still giving the correct control signals to  $Q_1$  and  $Q_2$  and obtain the desired equivalent tuning capacitance, a CSC (Control Signal Conversion)

method is proposed here. Figure 6-21 shows the signal waveforms that are required for generating the control signals for  $Q_1$  and  $Q_2$  to achieve such a task.

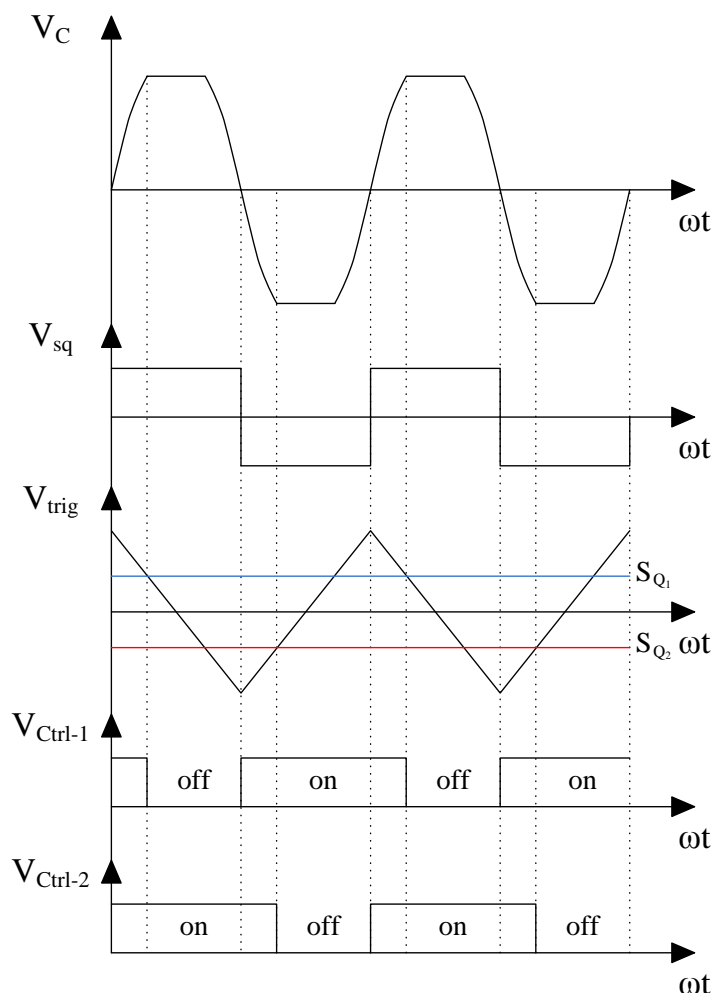


**Fig. 6-21: Waveform of signals used for generating  $V_{Ctrl-1}$  and  $V_{Ctrl-2}$**

The voltage signal  $V_{sq}$  is obtained by comparing  $V_{AC}$  with ground reference through a comparator as shown in Fig. 6-22 a), and it is used as an indicator for the positive ( $V_{sq} > 0$ ) and the negative ( $V_{sq} < 0$ ) cycles of  $V_{AC}$ . The voltage signal  $V_{trig}$  is obtained by integrating  $V_{sq}$  through a passive integrator as shown in Fig. 6-22 b), and it is used as a reference signal with which the control signals  $S_{Q_1}$  and  $S_{Q_2}$  are compared. The signals  $S_{Q_1}$  and  $S_{Q_2}$  have a relationship:

$$S_{Q_1} = -S_{Q_2} \quad (6-29)$$

where  $S_{Q_1}$  is equal to the output signal  $U(t)$  of the FLB-DTDC.

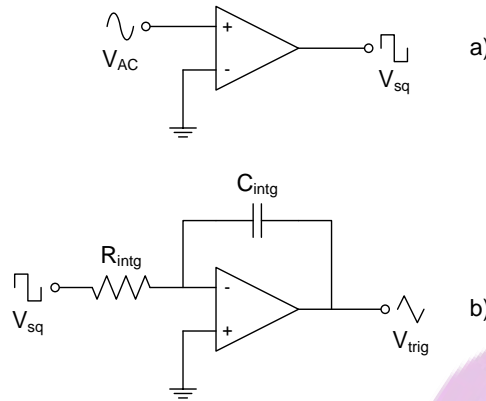


Fig. 6-22: Signal generation of: a)  $V_{sq}$  and b)  $V_{trig}$

The waveform of the signals shown in Fig. 6-21 has been summarized in Table 6-1.

Table 6-1: Truth table for  $V_{Ctrl-1}$  and  $V_{Ctrl-2}$  generation

Possible Cases	$V_{sq} > 0$ ( $x_1$ )	$S_{Q_1} > V_{trig}$ ( $x_2$ )	$S_{Q_2} > V_{trig}$ ( $x_3$ )	$V_{Ctrl-1}$	$V_{Ctrl-2}$
Case 1	0	0	0	1	0
Case 2	0	0	1	N/A	N/A
Case 3	0	1	0	1	0
Case 4	0	1	1	1	1
Case 5	1	0	0	1	1
Case 6	1	0	1	N/A	N/A
Case 7	1	1	0	0	1
Case 8	1	1	1	0	1

The result of Table 6-1 can further be simplified using Boolean expressions. Hence the control signals  $V_{Ctrl-1}$  and  $V_{Ctrl-2}$  can be obtained as:

$$V_{Ctrl-1} = \bar{x}_1 + \bar{x}_2 \quad (6-30)$$

$$V_{Ctrl-2} = x_1 + x_3 \quad (6-31)$$

#### 6.4.5 Guideline for Selecting Sampling Frequency of LC Power Pickup

Similar to the LCL power pickup, the LC pickup also requires certain time period for the circuit to reach its steady state after taking control action, and the controller has to wait for

that period of time to pass by before it can take another valid sample from the output voltage. The LCR (Inductor-Capacitor-Resistor) circuit at the dc side of the LC pickup has been identified as the major cause of this output delay. Figure 6-23 shows the dc side of the LC pickup, and the output voltage can be approximated by using the model shown in the figure.

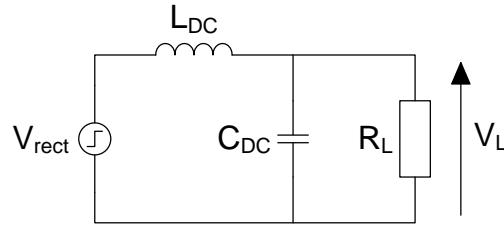


**Fig. 6-23: Model for dc output voltage analysis of parallel LC power pickup**

As each control action would cause the output voltage to have a step change, the rectified voltage  $V_{rect}$  is therefore modeled as a step voltage, and a differential equation can be derived as:

$$L_{DC}C_{DC} \frac{d^2V_L}{dt^2} + \frac{L_{DC}}{R_L} \frac{dV_L}{dt} + V_L = V_{rect} \quad (6-32)$$

The time-domain solution of the output voltage to this step change in the input voltage can be obtained from:

$$V_L(t) = V_{rect} \left\{ 1 + \frac{1}{2} e^{\frac{-t}{\tau}} \left[ A \left( e^{\frac{-t}{\alpha}} - e^{\frac{t}{\alpha}} \right) - \left( e^{\frac{-t}{\alpha}} + e^{\frac{t}{\alpha}} \right) \right] \right\} \quad (6-33)$$

where  $A = \frac{1}{\sqrt{B}}$ ,  $B = 1 - \frac{4R_L^2 C_{DC}}{L_{DC}}$ ,  $\tau = 2R_L C_{DC}$ , and  $\alpha = \tau A$ .

Equation (6-33) can be further simplified as:

$$V_L(t) = V_{rect} \left\{ 1 + e^{\frac{-t}{\tau}} \left[ -A \cdot \sinh\left(\frac{t}{\alpha}\right) - \cosh\left(\frac{t}{\alpha}\right) \right] \right\} \quad (6-34)$$



$$V_L(t) = V_{rect} \left\{ 1 + e^{\frac{-t}{\tau}} \left[ -jA \cdot \sin\left(\frac{t}{\alpha}\right) - \cos\left(\frac{t}{\alpha}\right) \right] \right\} \quad (6-35)$$

where  $\alpha$  is a real number in (6-34) and an imaginary number in (6-35). The nature of  $\alpha$  is determined by the term  $B$ , and  $\alpha$  has real numbers when  $L_{DC} \geq 4R_L^2 C_{DC}$  or imaginary numbers when  $L_{DC} < 4R_L^2 C_{DC}$ . Depending on the value of  $\alpha$ , the output voltage response can be under-damped, critically-damped, or over-damped. Figure 6-24 shows the three different types of the output voltage response.

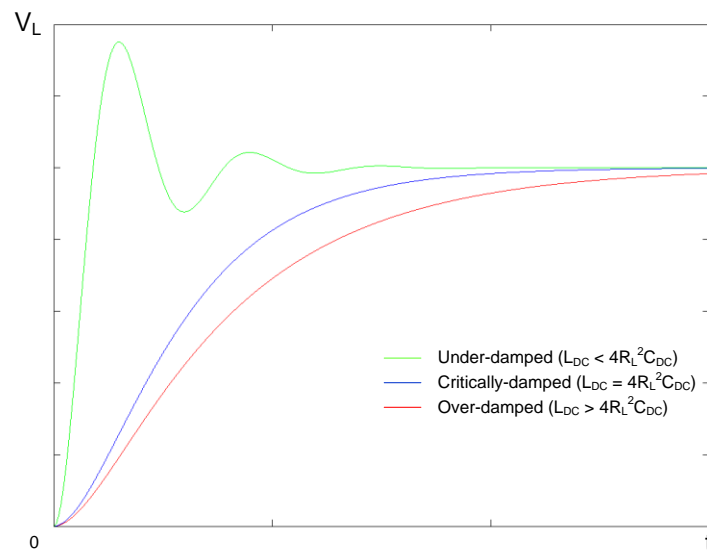


**Fig. 6-24: Output response of LCR circuit to a step voltage under different  $L_{DC}$**

The ideal output voltage response here is to have a fairly short settling time while still having low overshoot (under-damped but close to the boundary of critically-damped). This can be achieved by properly selecting the values for  $L_{DC}$  and  $C_{DC}$ . In [116], it has been found that in order to obtain a power transfer capacity that is close to the maximum ( $\geq 90\%$ ), the minimum inductance of  $L_{DC}$  has to be selected according to:

$$L_{DC\_min} = 0.992 \frac{R_{L\_min}}{\omega} \approx \frac{R_{L\_min}}{\omega} \quad (6-36)$$

where  $R_{L\_min}$  is the minimum load resistance. Note that the dc inductance obtained in (6-36) is only valid when the output of the pickup is a constant dc voltage. By substituting (6-

36) back to the term  $B$ , the critical capacitance of  $C_{DC}$  to give an ideal output voltage response under all possible load resistances can be obtained by meeting the condition of:

$$C_{DC\_c} \geq \frac{1}{4\omega R_{L\_min}} \quad (6-37)$$

However, it does not guarantee the constancy of the output voltage. To select a proper capacitance for  $C_{DC}$  so that it forms a low-pass filter together with the dc inductance  $L_{DC}$ , the reactance of  $C_{DC}$  has to be much smaller than that of  $L_{DC}$  ( $X_C \ll X_L$ ). This would allow the LC low-pass filter to function as a voltage divider with a large dividing ratio for the ac component of the actual rectified voltage  $V_{rect}$ , and hence can result in a constant voltage at the output. The ripple magnitude of the output voltage can be obtained from [117]:

$$V_{ripple} = \frac{1}{3\omega^2 L_{DC} C_{DC}} \cdot V_L \quad (6-38)$$

The capacitance of  $C_{DC}$  under a given ripple magnitude can be determined from:

$$C_{DC} = \frac{1}{3\omega^2 L_{DC}} \cdot \frac{V_L}{V_{ripple}} = \frac{1}{3\omega R_{L\_min}} \cdot \frac{V_L}{V_{ripple}} \quad (6-39)$$

Note that (6-39) is obtained by substituting the inductance of  $L_{DC}$  from (6-36).

Considering the settling time  $t_s$  is the time required for the output of LCR circuit to reach and stay within a specified tolerance band, for example, 2% of its final value, then the settling time is given by:

$$e^{-t_s/2R_L C_{DC}} = 0.02 \quad \text{or} \quad t_s \approx 8R_L C_{DC}, \quad (6-40)$$

and the sampling frequency of the controller needs to be designed base on the maximum settling time  $t_{s\_max} \approx 8R_{L\_max} C_{DC\_max}$ , where  $R_{L\_max}$  is the maximum load resistance and  $C_{DC\_max}$  is the maximum dc capacitance. The value of  $C_{DC\_max}$  can be obtained by substituting  $V_L = V_{L\_max}$  into (6-39). Therefore, the sampling frequency of the controller is determined from:

$$f_s = 0.375 \frac{\omega R_{L\_min}}{R_{L\_max}} \cdot \frac{V_{ripple}}{V_{L\_max}} \quad (6-41)$$

Equation (6-41) can be used as a general guideline for selecting the sampling frequency of the FLB-DTDC. A faster sampling frequency can be achieved by using a dc inductance larger than the minimum required dc inductance obtained in (6-36) despite the fact that the ESR of the inductor may be increased, which would reduce the required dc capacitance in (6-39) and hence increase the sampling frequency.

## 6.5 Simulation and Experimental Results

### 6.5.1 Simulation Study of FLB-DTDC Controlled LC Power Pickup

The FLB-DTDC controlled LC power pickup is simulated in Matlab/Simulink with PLECS. Figure 6-25 and 6-26 show the LC power pickup circuit emulated by PLECS and the complete simulation model respectively.

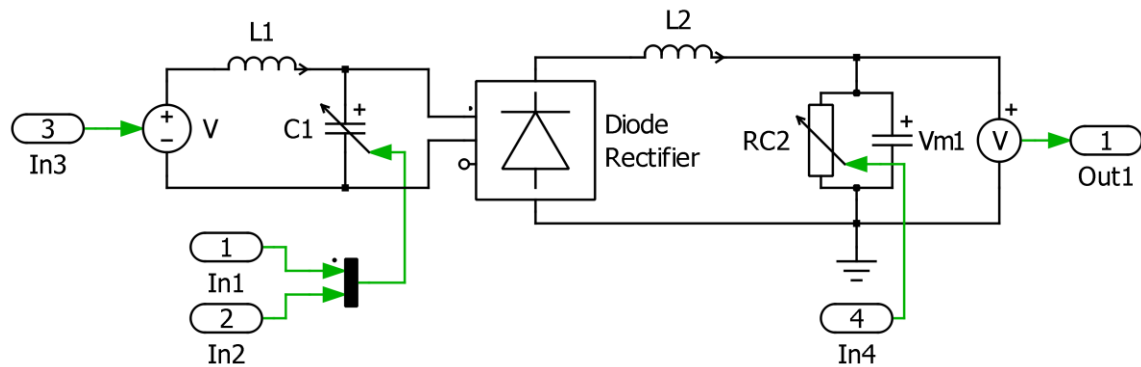
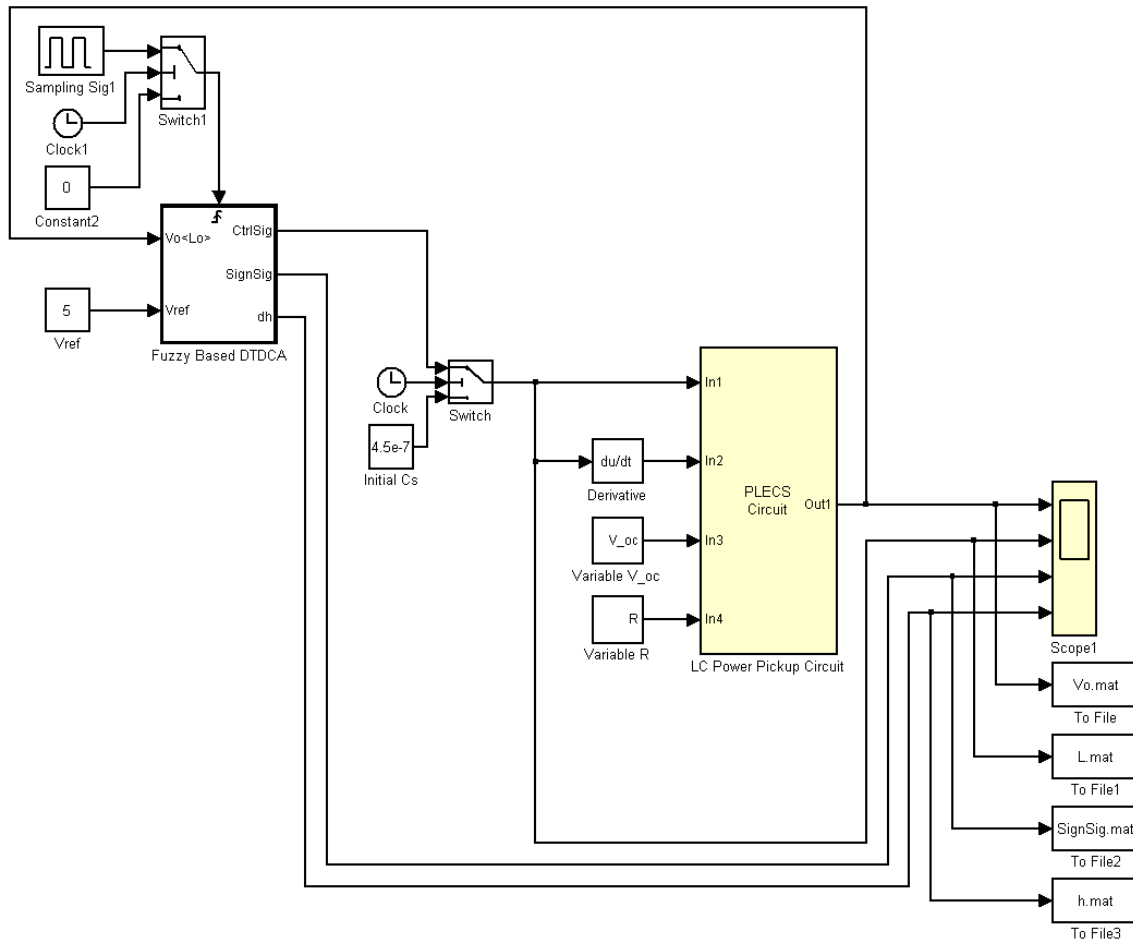


Fig. 6-25: PLECS model of parallel LC power pickup

The pickup coil has a self-inductance of  $17.8 \mu\text{H}$  ( $L_1$ ) with an open-circuit voltage of  $2.8 \text{ V}$  under the operating frequency of  $38.4 \text{ kHz}$ . The nominal dc load has a resistance of  $20 \Omega$ . This gives the quality factor  $Q_{S_p}$  of the tuning circuit to be approximately equal to  $5.75$  under fully-tuned condition. The maximum dc output voltage of the pickup can reach up to  $10 \text{ V}$ ; however the desired dc output voltage is predetermined to be  $5 \text{ V}$  in order to fully compensate for all possible parameters variation. The dc inductance  $L_2$  and capacitance  $C_2$  of the LC filter are selected to be  $49.736 \mu\text{H}$  and  $18.42 \mu\text{F}$ , respectively, with the assumptions that  $V_{L\_max}$  equals to  $8 \text{ V}$  and  $V_{ripple} \leq 0.05 \text{ V}$ . The calculated sampling

frequency based on the selected L2 and C2 is around 242 Hz. However a preliminary simulation has shown that by using a sampling frequency that is several times faster than the calculated sampling frequency can still give valid output voltage samples to the controller. The initial capacitance of the variable tuning capacitor C1 is predetermined at 0.45  $\mu\text{F}$  (in the under-tuning region; tuning circuit is fully-tuned when  $C1 = 0.965 \mu\text{F}$ ) to provide a minimum startup voltage ( $\approx 3 \text{ V}$ ) for the pickup.



**Fig. 6-26: Simulink model of FLB-DTDCA controlled parallel LC power pickup**

The parallel LC power pickup model is simulated under variations in the operating frequency, magnetic coupling and load resistance. These are represented by the function blocks of Variable V<sub>oc</sub> and Variable R in Fig. 6-26 and act as the inputs to the LC power pickup circuit. The operating frequency is varied within a range of  $\pm 2\%$ , which would cause the operating frequency to vary from 37632 ~ 39168 Hz. Under such a variation, the amplitude of the open-circuit voltage is varied from 2.744 ~ 2.856 V. Figure 6-27 shows

the controlled output voltage of the LC power pickup under the operating frequency variations.

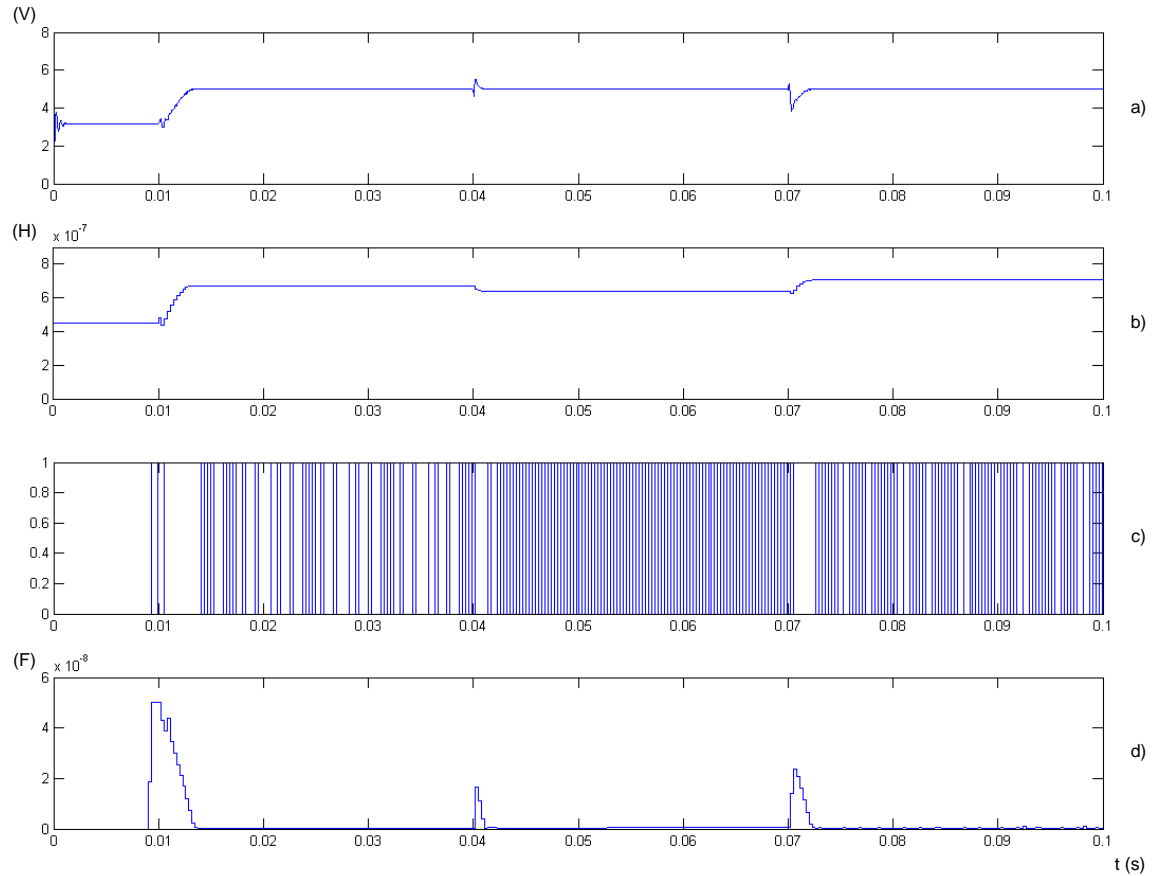


**Fig. 6-27: Simulation result of: a) output voltage  $V_L$ , b) capacitance of  $C_s$ , c) tuning direction signal  $S_4$ , and d) tuning step-size  $\Delta h$ , of a FLB-DTDC controlled LC power pickup under operating frequency variations**

As can be seen from the simulation result, the FLB-DTDC has been delayed for 0.01 s to allow the LC pickup to obtain an initial startup voltage at around 3 V. Then the controller proceeds with its algorithm to track the reference voltage and stabilizes at 5 V after 0.003 s. The pickup experiences the maximum tolerable operating frequency at 0.04 s and has a 0.48 V of voltage deviation from the reference. At time 0.07 s the pickup experiences the minimum tolerable operating frequency and the output voltage deviates from the reference by 1.14 V. It takes 0.0006 s and 0.0016 s for the FLB-DTDC to successfully regulate the output voltage back into the desired value for the maximum and the minimum tolerable operating frequency, respectively.

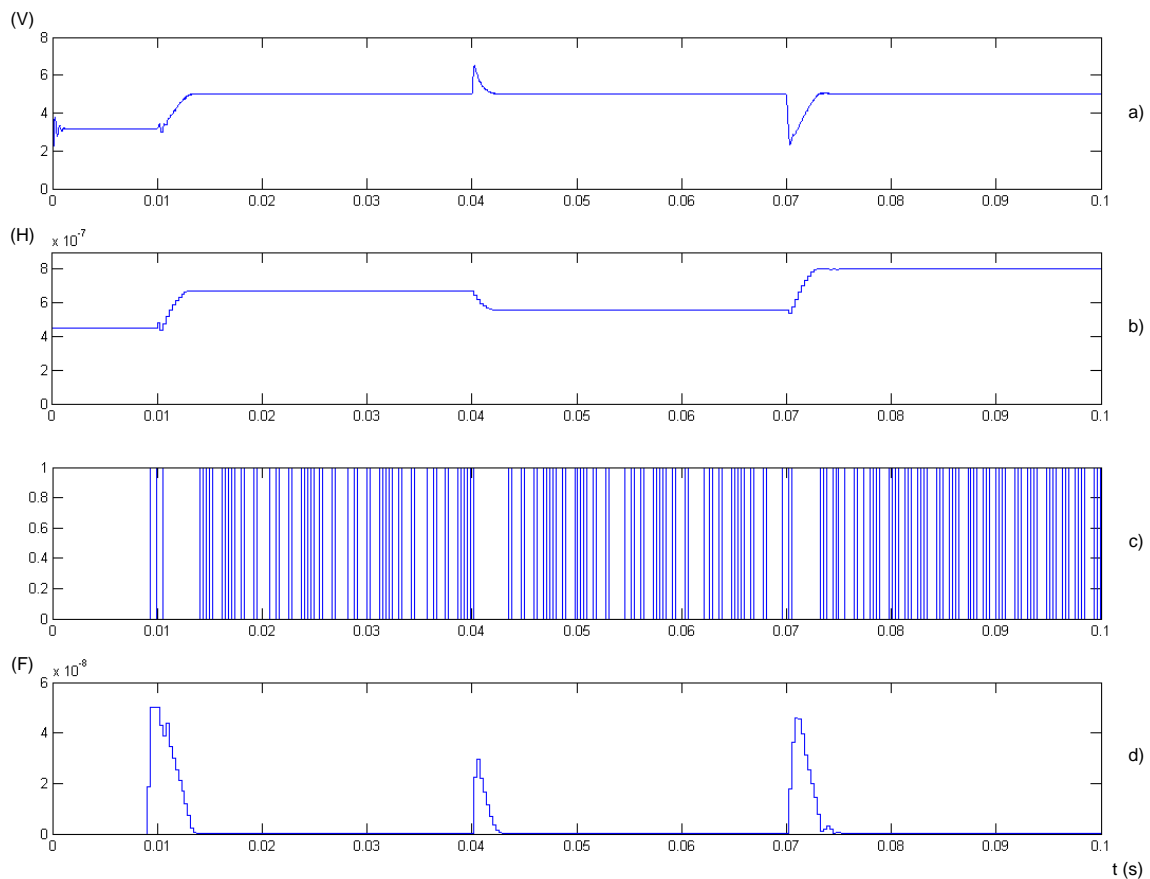


**Fig. 6-28: Simulation result of: a) output voltage  $V_L$ , b) capacitance of  $C_s$ , c) tuning direction signal  $S_d$ , and d) tuning step-size  $\Delta h$ , of a FLC-DTDC controlled LC power pickup under magnetic coupling variations**

Figure 6-28 shows the simulation result of the LC pickup under the magnetic coupling variations. The coupling variation is emulated by having a 30% rise in the open-circuit voltage (3.64 V) at 0.04 s and a 30% decrease in the open-circuit voltage (1.96 V) at 0.07 s. The rise in  $V_{OC}$  causes the output voltage to increase to 6.5 V and takes 0.0018 s for the controller to bring it back to the reference. The decrease in  $V_{OC}$  results the output voltage to have a 2.7 V drop and takes 0.003 s for recovery.

Figure 6-29 shows the simulation result of the LC pickup under the load variations. In this simulation, the pickup encounters a drastic +40% load change at 0.04 s which varies the nominal load resistance from 20  $\Omega$  to 28  $\Omega$  and causes small variation in the output voltage. Then the pickup encounters a -40% change in the load resistance at 0.07 s and changes the load resistance from 28  $\Omega$  to 12  $\Omega$ . This causes the output voltage to have a voltage drop of 0.93 V but is regulated by the controller after 0.0024 s.

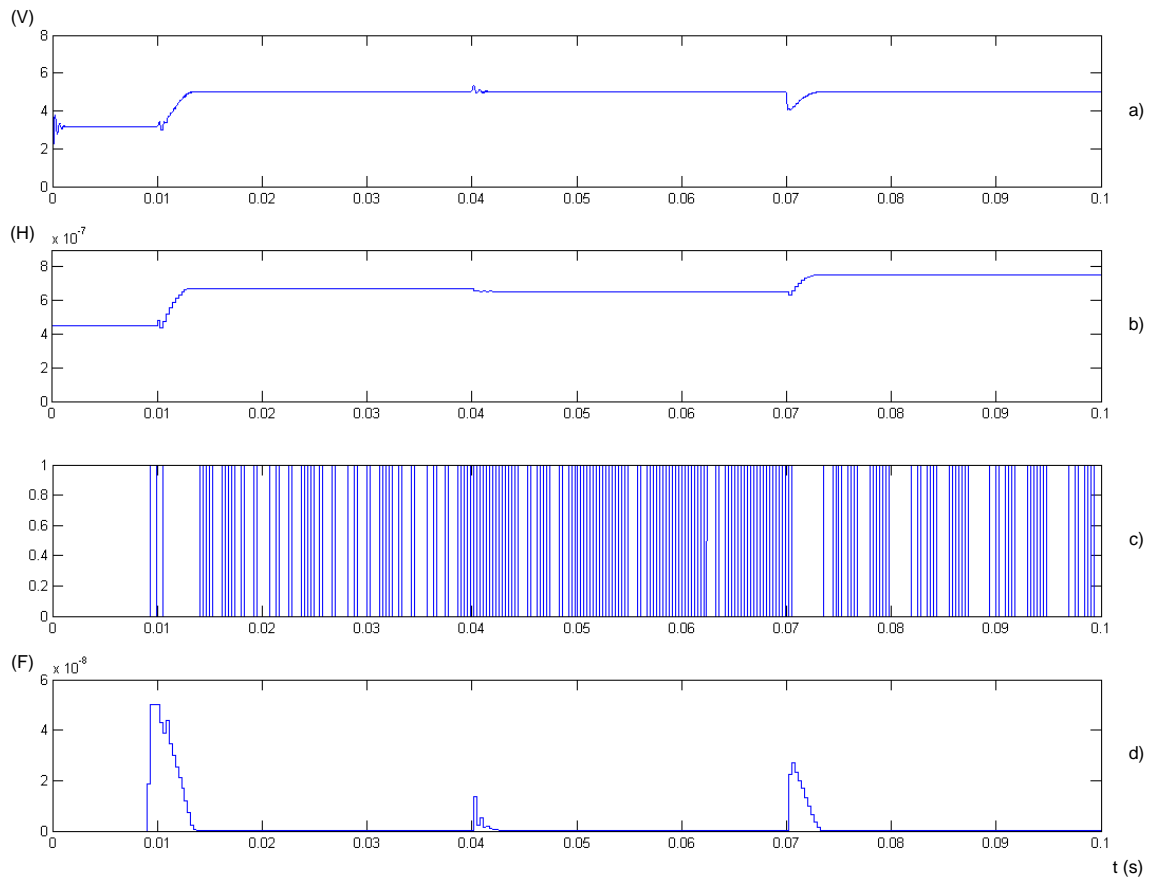


**Fig. 6-29: Simulation result of: a) output voltage  $V_L$ , b) capacitance of  $C_S$ , c) tuning direction signal  $S_4$ , and d) tuning step-size  $\Delta h$ , of a FLB-DTDC controlled LC power pickup under load variations**

### 6.5.2 Experimental Study of FLB-DTDC Controlled LC Power Pickup

A prototype has been built to verify the FLB-DTDC controlled LC power pickup. The secondary pickup coil has a self-inductance of  $17.8 \mu\text{H}$  ( $L_S$  in Fig. 6-15) with 11 turns of winding, and it has a nominal open-circuit voltage of 2 V when it is placed 20 mm away from the primary track. A nominal coupling factor of approximately 0.2 is obtained from this experiment setup. The fixed tuning capacitor  $C_{S1}$  has a capacitance of  $0.6 \mu\text{F}$  and is used to provide a startup voltage of approximately 3 V for the connected load having a nominal resistance of  $100 \Omega$ . The variable tuning capacitor  $C_{S2}$  has a capacitance of  $0.57 \mu\text{F}$ , which together with  $C_{S1}$  the tuning capacitor bank gives a variable range of 0.6 to  $1.17 \mu\text{F}$  for covering both the under-tuning and over-tuning regions of the LC power pickup. The equivalent capacitance of  $C_{S2}$  is controlled by switching the semiconductor devices  $Q_I$

and  $Q_2$  according to the control signals  $V_{Ctrl-1}$  and  $V_{Ctrl-2}$  respectively. Figure 6-30 shows a working prototype of the parallel LC power pickup in the laboratory.

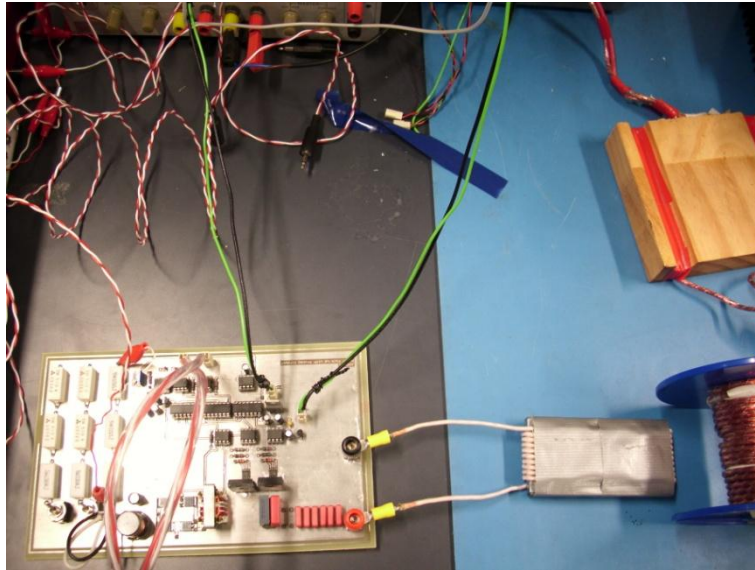


**Fig. 6-30: Working prototype of parallel LC power pickup**

Similar to the considerations that have been previously taken in the simulation studies, the control results to the variations in the operating frequency, magnetic coupling and load resistance are included here.

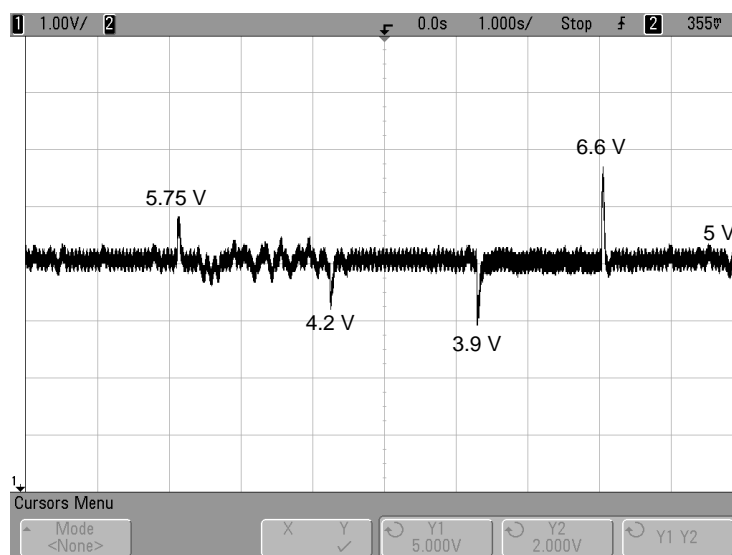


**Fig. 6-31: Output voltage waveform of FLB-DTDC controlled LC power pickup under load variations**



Figure 6-31 shows the controlled output voltage waveform of the pickup under the load variations. The resistance of the load was switched in the sequence of  $100 \rightarrow 140 \Omega$ ,  $140 \rightarrow 100 \Omega$ ,  $100 \rightarrow 60 \Omega$ , and  $60 \rightarrow 100 \Omega$ . Note that the primary power supply has a  $\pm 1\%$  variation in its operating frequency. Therefore the operating frequency variation was not separately investigated but naturally integrated into other experiments. From Fig. 6-31, it can be seen that the FLB-DTDCA can successfully regulate the output voltage of the prototype to the desired 5 V. Although some chattering in the output voltage has been noticed, it was due to the limitation of dSPACE output resolution.

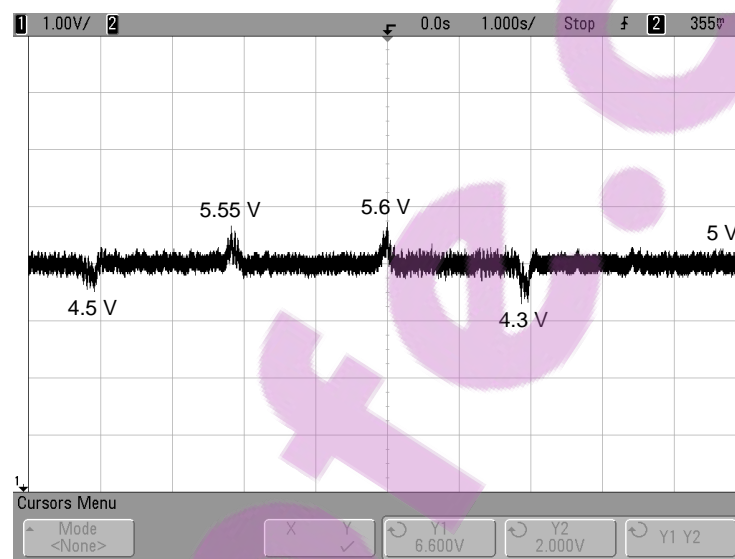
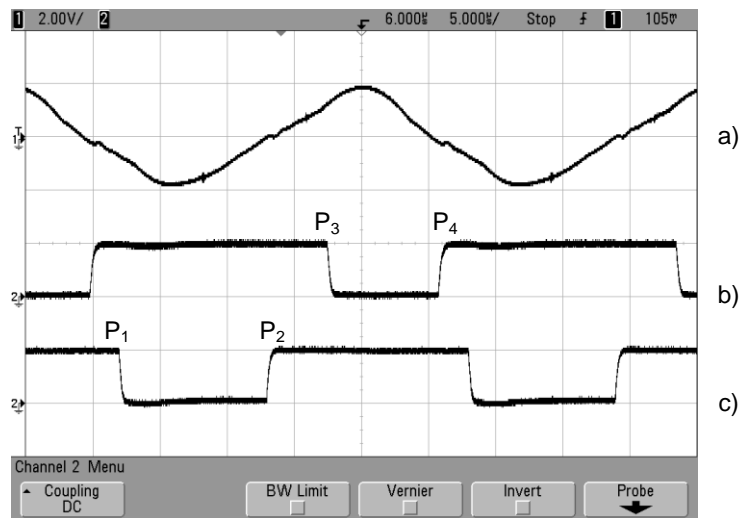


**Fig. 6-32: Output voltage waveform of FLB-DTDCA controlled LC power pickup under magnetic coupling variations**

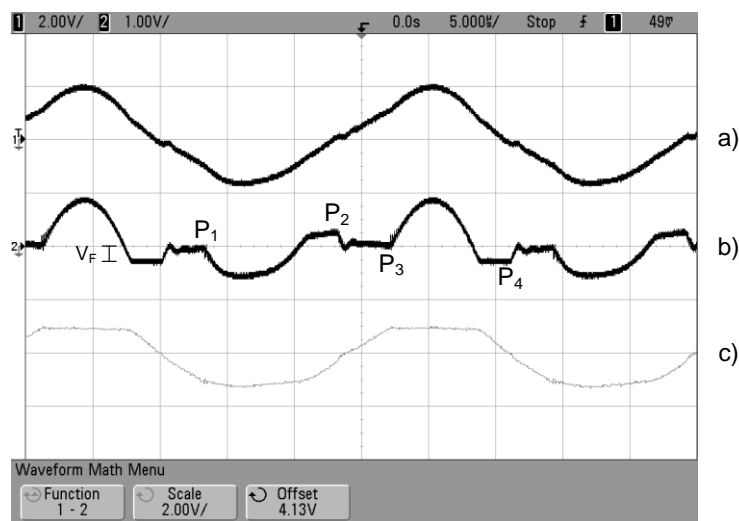
Figure 6-32 shows the controlled output voltage waveform of the pickup under the magnetic coupling variations. The experiment was carried out by changing the operating distance between the primary and the secondary side in the sequence of  $20 \rightarrow 30$  mm,  $30 \rightarrow 20$  mm,  $20 \rightarrow 10$  mm, and  $10 \rightarrow 20$  mm. And still, the output voltage of the prototype gets regulated by the FLB-DTDCA and has remained constant at 5 V.

Figure 6-33 shows the switch control signals  $V_{Ctrl-1}$  and  $V_{Ctrl-2}$  during each commutation cycle. As can be seen from the figure, position  $P_1$  and  $P_2$  are places where switch  $Q_2$  are tuned off and on respectively and position  $P_3$  and  $P_4$  are places where switch  $Q_1$  are turned off and on respectively. Each of the control signals can be varied to have duty cycles from

50 to 100%, and together, they control the equivalent capacitance of  $C_{S2}$  from zero to full capacitance.



**Fig. 6-33: Voltage waveforms of: a)  $V_{AC}$ , b) switching control signal  $V_{Ctrl-1}$ , and c) switching control signal  $V_{Ctrl-2}$**



**Fig. 6-34: Voltage waveforms of: a)  $V_{AC}$ , b) voltage across switches  $Q_1$  and  $Q_2$ , and c) voltage across  $C_{S2}$**

Measurements of the voltage across the ac switch ( $Q_1$  and  $Q_2$ ) and the variable tuning capacitor  $C_{S2}$  were taken to verify the ZVS of the switches. Figure 6-34 shows the measurement results, and the positions  $P_1$ ,  $P_2$ ,  $P_3$ , and  $P_4$  here are corresponding to the positions shown in Fig. 6-33. From the above figure, it can be seen that switches  $Q_1$  and

$Q_2$  are zero voltage switched off at  $P_1$  and  $P_3$  respectively. At positions  $P_2$  and  $P_4$ ,  $Q_1$  and  $Q_2$  are zero voltage switched on if the forward voltage drop  $V_F$  of the body diode of the switch is neglected. Hence, ZVS technique was successfully implemented on the prototype to reduce the switching losses in  $Q_1$  and  $Q_2$ .

## 6.6 Summary

In this chapter, the proposed FLB-DTDCA controller has been applied to a conventional parallel LC power pickup for the output voltage regulation. The behaviors of the LC tuning circuit including the output voltage, current and power have been investigated under variable tuning capacitor control in the resonant tank.

Effects of variations in the operating frequency, magnetic coupling and load resistance on the pickup output voltage have been analyzed, and equations for calculating the required tuning capacitance to achieve the desired output voltage under these parameter variations have been obtained. It has been found that in order to cover all the considered parameter variations, the LC power pickup has to be operated in the detuning region.

The effects of using different quality factor or  $r_k$  (ratio between the desired output voltage and the maximum output voltage under fully-tuned condition) on the relationship between the tuning capacitance and the output voltage have also been investigated. The results obtained show that the relationship between the output voltage and the magnetic coupling variation is not affected by the quality factor and  $r_k$ . However, these two factors do affect the sensitivities of the output voltage to the variations in the operating frequency and the load. It has been found that the sensitivities of the output voltage to the variations in the operating frequency and the load can be reduced by lowering  $r_k$ . However, if the output sensitivity is to be reduced through changing the design of quality factor, then by lowering the quality factor can only reduce the output sensitivity to the operating frequency variation. But this will increase the output sensitivity in the case of load variation. In addition, with a predefined constant output voltage, decreasing one of the two factors means increasing the other.

A comparison between the LC and the LCL power pickup has been carried out based on the results of the output sensitivities to the considered parameter variations. The results of

the comparison show that the LC tuning circuit is less sensitive to the parameter variations in the detuning region.

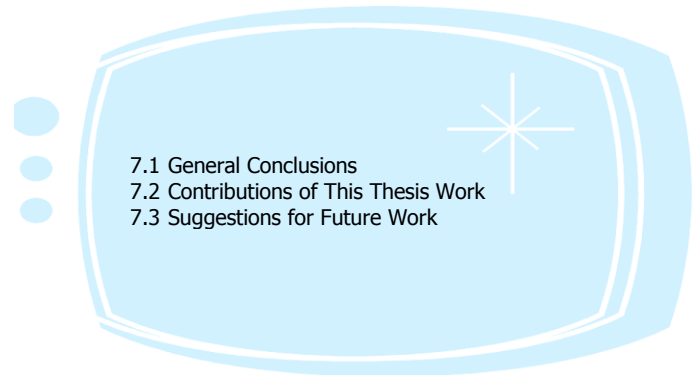
A general structure of the FLB-DTDC controlled LC power pickup has been proposed based on switch-mode variable tuning capacitor technique. The control range of the variable tuning capacitor has been determined and the relationship between the controlled duty cycle and the equivalent tuning capacitance has been obtained. A simplified model has been introduced which approximates the dc output voltage of the pickup after the application of each control action. Moreover, a general guideline for selecting the sampling frequency of the controller has been proposed based on this model.

A method for converting the original output signal of the FLB-DTDC into control signals  $V_{Ctrl-1}$  and  $V_{Ctrl-2}$  for the ac switch  $Q_1$  and  $Q_2$ , respectively, has been proposed and designed for the switches to achieve ZVS. The conversion method has been practically implemented on a prototype circuit to help reduce the switching losses during operation while achieving the desired equivalent tuning capacitances.

Both the simulation and experimental results have demonstrated the effectiveness of the proposed FLB-DTDC in regulating the output voltage of LC power pickups.

## Chapter 7

# Conclusions and Suggestions for Future Work



---

### 7.1 General Conclusions

A comprehensive investigation of full-range tuning power flow control for IPT (Inductive Power Transfer) power pickups has been undertaken in this thesis. Attention has been paid to the following four main aspects:

- New power flow control methods and algorithms for the IPT power pickups.
- Full-range control of tuning curves of IPT power pickup tuning circuits.
- Effects of variations of parameters of pickup circuit on the output voltage of the IPT power pickups.
- Performance evaluation of the output voltage regulation of the IPT power pickups.

A general introduction to contactless/wireless power transfer systems has been given in Chapter 1. It has been shown that although currently the majority of mainstream power transfer systems are based on direct power flow along the conductors, the demands of contactless/wireless power transfer systems have significantly been increased in the past decade and continues to grow due to the unique and convenient way of transferring power. Three main contactless/wireless power solutions have been discussed, which are energy harvesting, CPT (Capacitive Power Transfer), and IPT. However, since the energy harvesting systems are limited to low power applications, and practical implementation of

CPT is often difficult due to low permittivity of air, the IPT systems have become the preferable choice for many practical applications. Nevertheless, accurate power flow control of the IPT systems has been found to be challenging, particularly under variations of several circuit parameters such as variations in the operating frequency, magnetic coupling between the primary and the secondary side of the system, tuning capacitance, load resistance, etc.

In Chapter 2, the basic structure and major components of an IPT system have been systematically discussed including an overview of the power flow control methods of the IPT systems. The power flow control methods of the IPT systems are categorized into the control of primary track current and the control of secondary power pickup. Although the primary track current can be controlled to regulate the pickup output voltage, it is only suitable for single power pickup applications. On the contrary, if the power flow control is applied to the secondary power pickups, each pickup which couples to the primary power supply can have their own power regulation. Thus the power flow control of the secondary pickup is a preferable control strategy for multiple-pickups operation.

In the secondary power pickup control, there are three different methods that have been commonly used in the IPT applications. These are the adoption of simple voltage regulator, shorting-control, and the dynamic tuning/detuning control. The adoption of voltage regulator and shorting-control have several drawbacks, e.g., 1) it requires that the circuit to be fine-tuned and overdesigned to meet the output power requirement under all parameter variations, 2) significant excessive power may exist under light loading conditions, and 3) a heat sink is needed for the dissipation of excessive power. Under high  $Q$  operation, the fine tuning process can be more troublesome as the circuit tuning of the pickup becomes more sensitive to the variations of the circuit parameters. As a result,  $Q$  factor of the power pickup circuit has to be limited, and it is normally below 6 and a maximum of 10. The dynamic tuning/detuning control which is designed to dynamically change the tuning condition of the power pickup allows the secondary pickup to only take sufficient power from the primary side according to the actual load demands and hence increases the overall efficiency of the secondary pickup. Nevertheless, the adopted conventional PI (Proportional and Integral) controller is only able to achieve single-side

tuning control in either under-tuning or over-tuning region, rather than covering the entire tuning curve of the pickup circuit.

Following the overview of the IPT system and its existing power flow control methods, a novel control algorithm called as DTDCA (Directional Tuning/Detuning Control Algorithm) has been proposed in Chapter 3 for the output voltage regulation of the pickup. The concept of DTDCA is based on using the comparison result of: 1) output voltage  $V_L(t_n)$  and reference voltage  $V_{ref}(t_n)$ , 2) output voltage  $V_L(t_n)$  and output voltage of previous state  $V_L(t_{n-1})$ , and 3) the validity of the previous tuning direction signal, to determine the tuning direction signal of the next state control. Similar to other discrete controllers, the performance of DTDCA is also dependent on the selection of sampling frequency and the magnitude of control signal (tuning step-size). However these two factors can vary depending on the topology of the pickup circuit and therefore require to be examined for each individual case.

In Chapter 4, an LCL tuning configuration has been thoroughly studied as a potential alternative to the conventional LC tuning circuit. Theoretically, the LCL tuning circuit behaves as a voltage source under fully-tuned condition, which is very advantageous in most applications; since the output voltage can always remain constant regardless of the load variations. However, variations in the operating frequency, magnetic coupling, tuning capacitance, and load can exist in practical operations, and their combined effect can cause the output voltage to significantly deviate from the desired value. It has been found that the above considered parameter variations would change the magnitude of the possible maximum output voltage. In addition, the variations in the operating frequency and the tuning capacitance would also shift the tuned-point from its designated point. These facts have shown that in order to fully compensate for all the considered parameter variations, the LCL power pickup has to be operated in the detuning region, which consequently loses its voltage source property.

Both the simulation and experimental results have proven the effectiveness of the proposed DTDCA in achieving full-range tuning control, output voltage regulation, and compensation for the considered parameter variations. This enables the pickup to be fully-tuned on-line, if required, and makes the high  $Q$  operation possible. The two key factors that govern the controller performance, namely the sampling frequency and the tuning

step-size, have also been determined. The sampling frequency for the LCL power pickup has been found to have a proportional relationship with the system operating frequency and magnitude of the output voltage ripple, but it is inversely proportional to the magnitude of output voltage. As for the tuning step-size of the controller, it has been designed to vary according to the state of controller. When the controller is in the coarse tuning state, the tuning step-size is a fixed value which avoids the tracking process from traversing between the under-tuning and over-tuning regions. When the controller is in the fine tuning state, the tuning step-size is changed by an algorithm, called Simple Step-Size Adjustment (SSSA), to help the DTDCA in reducing the control signal and hence gradually reaching to the reference value. However, several issues have also been discovered in the DTDCA controlled LCL power pickup in terms of control quality. First of all, it has been found that the pickup output voltage is much more sensitive to the operating frequency and tuning capacitance variations in the over-tuning region than in the under-tuning region. This causes the LCL pickup to have poor transient output characteristic when operating in the over-tuning region, and has the possibility of generating overvoltages when the considered parameters change dramatically. Second, since the DTDCA requires a validity check for the previous control action before it can determine the next control signal, the tuning attempt performed by the DTDCA may have a 50% chance of tuning to the wrong direction with additional error to the output voltage. Third, although the tuning step-size for the coarse tuning state has been determined on the basis of avoiding the tracking process from traversing between the operating regions of the tuning curves so a more efficient control can be achieved. This feature is however only guaranteed at the initial startup of the controller but cannot be assured at any other times during the operation.

To solve the above problems, a fuzzy logic based tuning step-size control has been integrated to the DTDCA in Chapter 5. In the design of the fuzzy logic controller (FLC), the error and rate of error of the output voltage are taken as the input signals to the controller. By processing the input signals through the control rule base and defuzzification, the FLC can generate three different types of output signal, which are zero, medium and large tuning step-sizes for the corresponding conditions of the FLC input signals. The analytical structure of the proposed FLC has been analyzed and found to have 13 different analytical expressions for 28 different input combinations (ICs). The



obtained analytical expressions can also be expressed by classical forms (P, PI, PD, or PID) and has got 4 different P-like, 5 different D-like and 2 different PD-like controllers. These controllers all have nonlinear and variable proportional and derivative gains, and they can only be treated as 'local' P-, D-, or PD-like controllers as they are only valid to the corresponding ICs. A special attention has been paid to the condition of the output voltage having a large error and a large rate of error in the wrong tuning direction. Because the output signal of the FLC under such a condition may go down to zero according to the control rule base. This requires the interval  $L$  of the input signals of the FLC to be designed larger than the expected maximum rate of error, so insufficient perturbations during the control process can be avoided.

Both the simulation and experimental results have shown that the LCL power pickup using FLB-DTDCA (Fuzzy Logic Based Directional Tuning/Detuning Control Algorithm) for its output voltage regulation obtains better performance in the following aspects:

- Achieving smooth reference tracking without chattering effect in the output voltage since the tuning step-size is dynamically changed according to the conditions of error and rate of error.
- Reducing perturbation error in the output voltage when the controller performs a tuning attempt.
- Removing the steady state error that was originally existed in the SSSA-DTDCA (DTDCA using Simple Step-Size Adjustment).

In Chapter 6, the FLB-DTDCA has been applied to the conventional parallel LC power pickup. The equivalent capacitance of the tuning capacitor is switch-mode controlled by the control signals of the FLB-DTDCA so that the tuning condition of the pickup can be varied to have different pickup output powers/voltages for meeting the actual load demands. The effects of variations in the operating frequency, magnetic coupling, and load resistance on the output voltage of the LC pickup have been studied, and it has been found that the operating frequency variation causes the designated tuned-point to shift, and the variations in the magnetic coupling and load resistance both change the magnitude of the maximum output voltage. A comparison on the output voltage variation to the parameters variation between the LC and the LCL power pickups has also been carried out. The results have shown that since both the LC and LCL power pickups have to be

operated in the detuning region to fully compensate for all possible parameter variations, the higher output sensitivity possessed by the LCL power pickup (especially in the over-tuning region) makes the LC power pickup a more preferable choice in applications where tolerance of drastic output voltage variation is low.

## 7.2 Contributions of This Thesis Work

The main contributions of this thesis work include:

Proposing a full-range tuning control algorithm namely DTDCA (Directional Tuning/Detuning Control Algorithm), and using it to successfully regulate the output voltage of the secondary power pickups for the IPT systems. This enables the pickup to be fully-tuned on-line, when necessary, even under high  $Q$  or  $k_{VR}$  operation.

Analyzing the fundamental properties of the LCL and the LC power pickups, and the effects of variations in the operating frequency, magnetic coupling between the primary and the secondary side, tuning capacitance (for the LCL tuning configuration), and load resistance on the output voltage of the LCL and the LC power pickups in the steady state. The analytical method used can also be extended for analyzing other possible parameter variations of the secondary power pickup.

Determining the control range for the variable tuning inductor/capacitor of the LCL/LC power pickup to achieve full-range tuning control under all considered parameter variations.

Determining the proper sampling frequency for the DTDCA in the LCL/LC power pickups.

Proposing and developing the SSSA-DTDCA to control an LCL power pickup with a linear-mode saturable inductor.

Proposing a fuzzy logic based tuning step-size control to dynamically change the tuning step-size for the DTDCA according to the input combinations of the error and rate of error. It has been successfully used to improve the performance of the SSSA-DTDCA in the LCL and the LC power pickups. The analytical structure of the proposed fuzzy logic

controller has been developed and expressed in the classical P, D, or PD controller forms for the corresponding input combinations.

Proposing and developing a method for converting the raw control signal of the FLB-DTDCA into duty cycle controlled switching signals for the ac switch of the switch-mode variable capacitor that used in the LC power pickup. It has been used to achieve the required equivalent tuning capacitance and also to reduce the switching losses through ZVS (Zero Voltage Switching) operation.

Part of the above contributions has been published in one journal paper [118] and five conference papers [72, 119-122], and one book chapter has been accepted [123]. Another journal paper has been submitted and under review [124]. A provisional patent based on the FLB-DTDCA controlled LC power pickup has been filed.

### 7.3 Suggestions for Future Work

The work conducted in this thesis has focused on the development of full-range tuning controller for the power flow control of the IPT secondary power pickups. Various theoretical analyses, system and component level simulations, and experimental tests have been undertaken to achieve the research objectives. As a result, the controller has been successfully developed with very useful results for practical analysis and design. Further, more areas have also been opened for investigation in the future. To conclude this thesis, several areas are suggested here for future research on the topic.

#### ***Reflected effects to the primary power supply***

Unlike fully-tuned series/parallel power pickups, the proposed DTDCA tunes/detunes the secondary pickups to meet the actual load demand so the reflected impedance may have large imaginary components which may affect the primary converter operations. The actual reflected impedance on the primary side therefore needs to be further investigated. The obtained results can be very useful in designing the primary power supply of the IPT system that adopts the DTDCA control at the secondary.

#### ***Systematic design method for determining the proper $k_{VR}$ , $Q_{S_p}$ , and $r_k$***

As it has been described in Chapter 3 and Chapter 5 of this thesis, the choice of  $k_{VR}$ ,  $Q_{S_p}$  and  $r_k$  can all affect the output sensitivity of the secondary power pickups to the

considered parameter variations in different degrees. If a relationship between the choice of  $k_{VR}$ ,  $Q_{S_p}$ ,  $r_k$ , and specifications of the application can be established, the obtained result can be very useful, especially for optimizing power pickup design.

#### ***Better approximation for settling time of pickup circuits***

Two simplified models have been introduced in this thesis to separately approximate the settling time of the investigated pickup circuits. The model that has been used in modeling the CR filter with a current step change is proven by the simulations to provide valid approximation for the settling time of the LCL power pickup. However, the model that has been used in modeling the LCR filter with a voltage step change can only provide a very general guideline on how to select the sampling frequency for the LC power pickup, and caused the calculated sampling period is much slower than the actual settling time of the circuit. To obtain a better controller performance in the LC power pickup by selecting the proper sampling frequency, a better approximation of the settling time for the LC pickup needs to be provided.

#### ***Accurate secondary power pickup modeling***

Although the DTDCAs have been proven effective on the power flow control of the secondary power pickups, an accurate closed form secondary power pickup model with actual rectification circuitry and the proposed DTDCAs controller has not been obtained in this research. Difficulties in achieving such a task include the model establishment of the circuit with nonlinear components like diode rectifications, and fitting the DTDCAs into an analytical form. These two topics can be regarded as new research directions for better understanding of both the transient and steady state behaviors of the DTDCAs controlled power pickups.

# References

---

- [1] F.E. Terman: *Radio Engineering*, McGraw Hill, Inc., 3rd edition, 1947.
- [2] G.A.J. Elliott, G.A. Covic, D. Kacprzak and J.T. Boys, "A new concept: asymmetrical pick-ups for inductively coupled power transfer monorail systems," *IEEE Transactions on Magnetics*, vol. 42, no. 10, pp. 3389-3391, 2006.
- [3] A.M. Bradley, M.D. Feezor, H. Singh and F. Yates Sorrell, "Power systems for autonomous underwater vehicles," *IEEE Journal of Oceanic Engineering*, vol. 26, no. 4, pp. 526-538, 2001.
- [4] R.R. Harrison, "Designing efficient inductive power links for implantable devices," in *IEEE International Symposium on Circuits and Systems, ISCAS 2007*, 2007, pp. 2080-2083.
- [5] T. Taithongchai and E. Leelarasmee, "Adaptive electromagnetic energy harvesting circuit for wireless sensor application," in *6th International Conference on Electrical Engineering/Electronics, Computer, Telecommunications and Information Technology, ECTI-CON 2009*, 2009, pp. 278-281.
- [6] S. Dwari, R. Dayal, L. Parsa and K.N. Salama, "Efficient direct ac-to-dc converters for vibration-based low voltage energy harvesting," in *34th Annual IEEE Conference of Industrial Electronics, IECON 2008*, 2008, pp. 2320-2325.
- [7] S. Dwari and L. Parsa, "Low voltage energy harvesting systems using coil inductance of electromagnetic microgenerators," in *24th Annual IEEE Applied Power Electronics Conference and Exposition, APEC 2009*, 2009, pp. 1145-1150.
- [8] T. Becker, M. Kluge, J. Schalk, T. Otterpohl and U. Hilleringmann, "Power management for thermal energy harvesting in aircrafts," in *IEEE Sensors*, 2008, pp. 681-684.
- [9] S. Sherrit, "The physical acoustics of energy harvesting," in *IEEE Ultrasonics Symposium, IUS 2008*, 2008, pp. 1046-1055.
- [10] V. Raghunathan, A. Kansal, J. Hsu, J. Friedman and M. Srivastava, "Design considerations for solar energy harvesting wireless embedded systems," in *4th International Symposium on Information Processing in Sensor Networks, IPSN 2005*, 2005, pp. 457-462.
- [11] P. Li, Y. Wen, P. Liu, X. Li and C. Jia, "An electromagnetic energy harvesting circuits for self-powered wireless sensor network," in *10th International Conference on Control, Automation, Robotics and Vision, ICARCV 2008*, 2008, pp. 214-217.

- [12] J. Elmes, V. Gaydarzhiev, A. Mensah, K. Rustom, J. Shen and I. Batarseh, "Maximum energy harvesting control for oscillating energy harvesting systems," in *IEEE Power Electronics Specialists Conference, PESC 2007*, 2007, pp. 2792-2798.
- [13] L. Garbuio, M. Lallart, D. Guyomar, C. Richard and D. Audigier, "Mechanical energy harvester with ultralow threshold rectification based on SSHI nonlinear technique," *IEEE Transactions on Industrial Electronics*, vol. 56, no. 4, pp. 1048-1056, 2009.
- [14] J.W. Kimball, B.T. Kuhn and R.S. Balog, "A system design approach for unattended solar energy harvesting supply," *IEEE Transactions on Power Electronics*, vol. 24, no. 4, pp. 952-962, 2009.
- [15] X. Cao, W.-J. Chiang, Y.-C. King and Y.-K. Lee, "Electromagnetic energy harvesting circuit with feedforward and feedback DC-DC PWM boost converter for vibration power generator system," *IEEE Transactions on Power Electronics*, vol. 22, no. 2, pp. 679-685, 2007.
- [16] M. Lallart, L. Garbuio, L. Petit, C. Richard and D. Guyomar, "Double synchronized switch harvesting (DSSH): a new energy harvesting scheme for efficient energy extraction," *IEEE Transactions on Ultrasonics, Ferroelectrics and Frequency Control*, vol. 55, no. 10, pp. 2119-2130, 2008.
- [17] H.-P. Tan, P.W.Q. Lee, W.K.G. Seah and Z.A. Eu, "Impact of power control in wireless sensor networks powered by ambient energy harvesting (WSN-HEAP) for railroad health monitoring," in *International Conference on Advanced Information Networking and Applications Workshops, WAINA '09*, 2009, pp. 804-809.
- [18] C. Liu, A.P. Hu and N.K.C. Nair, "Coupling study of a rotary capacitive power transfer system," in *IEEE International Conference on Industrial Technology, ICIT 2009*, 2009, pp. 1-6.
- [19] A.P. Hu, C. Liu and H.L. Li, "A novel contactless battery charging system for soccer playing robot," in *15th International Conference on Mechatronics and Machine Vision in Practice, M2VIP 2008*, 2008, pp. 646-650.
- [20] J.T. Boys and A.W. Green, "Inductively coupled power transmission - concept, design and application," *IPENZ Transactions*, vol. 1, no. 22, pp. 1-9, 1995.
- [21] A.P. Hu, "Selected Resonant Converters for IPT Power Supplies," PhD thesis, the Department of Electrical and Electronic Engineering, University of Auckland, Auckland, 2001.
- [22] G.B. Joun and B.H. Cho, "An energy transmission system for an artificial heart using leakage inductance compensation of transcutaneous transformer," *IEEE Transactions on Power Electronics*, vol. 13, no. 6, pp. 1013-1022, 1998.
- [23] J.S. Mueller and R.S. Gyurcsik, "Two novel techniques for enhancing powering and control of multiple inductively-powered biomedical implants," in *Proceedings*

- of 1997 *IEEE International Symposium on Circuits and Systems, ISCAS '97*, 1997, pp. 289-292.
- [24] A.P. Hu, I.L.W. Kwan, C. Tan and Y. Li, "A wireless battery-less computer mouse with super capacitor energy buffer," in *2nd IEEE Conference on Industrial Electronics and Applications, ICIEA 2007*, 2007, pp. 2024-2029.
- [25] A.W. Guy, "History of biological effects and medical applications of microwave energy," *IEEE Transactions on Microwave Theory and Techniques*, vol. 32, no. 9, pp. 1182-1200, 1984.
- [26] Y. Hu, B. Bai and D. Xie, "The electromagnetic field distribution in the human body under the ultra-high voltage transmission lines," in *Proceedings of International Conference on Power System Technology, PowerCon 2002*, 2002, pp. 2243-2246.
- [27] S.K. Palit, "Biological effects of electromagnetic waves-an overview," in *Proceedings of 2nd International Conference on Bioelectromagnetism*, 1998, pp. 195-196.
- [28] Z. Sienkiewicz, "Biological effects of electromagnetic fields and radiation," in *9th International Conference on Electromagnetic Compatibility*, 1994, pp. 17-21.
- [29] Z. Sienkiewicz, "Biological effects of electromagnetic fields," *Power Engineering Journal*, vol. 12, no. 3, pp. 131-139, 1998.
- [30] G. Elliot, "An investigation into the biological effects of 10 kHz (VLF) electromagnetic fields," in *G. T. Murray Memorial Prize, IPENZ NZ*, 1994, pp. 1-10.
- [31] P.E. Tyler, "Overview of the biological effects of electromagnetic radiation," *IEEE Transactions on Aerospace and Electronic Systems*, vol. AES-9, no. 2, pp. 225-228, 1973.
- [32] H.H. Wu, M.Z. Feng, J.T. Boys and G.A. Covic, "A wireless multi-drop IPT security camera system," in *4th IEEE Conference on Industrial Electronics and Applications, ICIEA 2009*, 2009, pp. 70-75.
- [33] O. GIZMO! *Oral-B triumph electric toothbrush with wireless smartguide*. 2010 [cited 2009 September 10]; Available from: [http://www.ohgizmo.com/wp-content/uploads/2009/03/oralb\\_triumph\\_8.jpg](http://www.ohgizmo.com/wp-content/uploads/2009/03/oralb_triumph_8.jpg).
- [34] J. Achterberg, E.A. Lomonova and J. de Boeij, "Coil array structures compared for contactless battery charging platform," *IEEE Transactions on Magnetics*, vol. 44, no. 5, pp. 617-622, 2008.
- [35] X. Liu and S.Y.R. Hui, "Equivalent circuit modeling of a multilayer planar winding array structure for use in a universal contactless battery charging platform," *IEEE Transactions on Power Electronics*, vol. 22, no. 1, pp. 21-29, 2007.

- [36] X. Liu, P.W. Chan and S.Y.R. Hui, "Finite element simulation of a universal contactless battery charging platform," in *20th Annual IEEE Applied Power Electronics Conference and Exposition, APEC 2005*, 2005, pp. 1927-1932.
- [37] S.Y.R. Hui and W.W.C. Ho, "A new generation of universal contactless battery charging platform for portable consumer electronic equipment," *IEEE Transactions on Power Electronics*, vol. 20, no. 3, pp. 620-627, 2005.
- [38] X. Liu and S.Y. Hui, "Simulation study and experimental verification of a universal contactless battery charging platform with localized charging features," *IEEE Transactions on Power Electronics*, vol. 22, no. 6, pp. 2202-2210, 2007.
- [39] X. Liu and S.Y. Hui, "Optimal design of a hybrid winding structure for planar contactless battery charging platform," *IEEE Transactions on Power Electronics*, vol. 23, no. 1, pp. 455-463, 2008.
- [40] M. Shen and F.Z. Peng, "Control of the z-source inverter for fuel cell-battery hybrid vehicles to eliminate undesirable operation modes," in *Conference Record of 41st Annual IEEE Industry Applications Conference, IAS 2006*, 2006, pp. 1667-1673.
- [41] C.C. Chan and Y.S. Wong, "The state of the art of electric vehicles technology," in *4th International Power Electronics and Motion Control Conference, IPEMC 2004*, 2004, pp. 46-57.
- [42] J. Liu and H. Peng, "Control optimization for a power-split hybrid vehicle," in *American Control Conference*, 2006, pp. 6.
- [43] L. Egiziano, A. Giustiniani, G. Lisi, G. Petrone, G. Spagnuolo and M. Vitelli, "Experimental characterization of the photovoltaic generator for a hybrid solar vehicle," in *IEEE International Symposium on Industrial Electronics, ISIE 2007*, 2007, pp. 329-334.
- [44] M.B. Camara, F. Gustin, H. Gualous and A. Berthon, "Supercapacitors and battery power management for hybrid vehicle applications using multi boost and full bridge converters," in *European Conference on Power Electronics and Applications*, 2007, pp. 1-9.
- [45] G.A. Covic, G. Elliott, O.H. Stielau, R.M. Green and J.T. Boys, "The design of a contact-less energy transfer system for a people mover system," in *Proceedings of International Conference on Power System Technology, PowerCon 2000*, 2000, pp. 79-84.
- [46] BOMBARDIER. *Contactless power transfer – A world premiere in urban rail transport*. 2010 [cited 2009 September 11]; Available from: <http://www.bombardier.com/en/transportation/sustainability/technology/primove-catenary-free-operation>.
- [47] T.W. Altshuler, T.W. Vaneck and J.G. Bellingham, "Odyssey IIB -- towards commercialization of AUVs," *Sea Technology*, vol. 36, no. 12, pp. 15-20, 1995.



- [48] M.D. Feezor, F. Yates Sorrell and P.R. Blankinship, "An interface system for autonomous undersea vehicles," *IEEE Journal of Oceanic Engineering*, vol. 26, no. 4, pp. 522-525, 2001.
- [49] M.D. Feezor, F. Yates Sorrell, P.R. Blankinship and J.G. Bellingham, "Autonomous underwater vehicle homing/docking via electromagnetic guidance," *IEEE Journal of Oceanic Engineering*, vol. 26, no. 4, pp. 515-521, 2001.
- [50] G.E. Schubak and D.S. Scott, "A techno-economic comparison of power systems for autonomous underwater vehicles," *IEEE Journal of Oceanic Engineering*, vol. 20, no. 1, pp. 94-100, 1995.
- [51] L. Wang, M. Chen and D. Xu, "Increasing inductive power transferring efficiency for Maglev emergency power supply," in *37th IEEE Power Electronics Specialists Conference, PESC '06*, 2006, pp. 1-7.
- [52] M. Chen, D. Xu, D. Zhou and X. Wu, "Inductive power transferring in Maglev using harmonic injection method," in *Conference Proceedings of 9th Annual IEEE Applied Power Electronics Conference and Exposition, APEC '94*, 2004, pp. 1165-1170.
- [53] B.-M. Song, R. Kratz and S. Gurol, "Contactless inductive power pickup system for Maglev applications," in *37th Annual Conference of Industry Applications, IAS 2002*, 2002, pp. 1586-1591.
- [54] H. Oman, "Artificial hearts, batteries, and electric vehicles," *IEEE Aerospace and Electronic Systems Magazine*, vol. 17, no. 8, pp. 34-39, 2002.
- [55] P. Wouters, R. Puers, R. Geers and V. Goedseels, "Implantable biotelemetry devices for animal monitoring and identification," in *Proceedings of Annual IEEE International Conference of Engineering in Medicine and Biology Society*, 1992, pp. 2665-2666.
- [56] G. Yan, P. Zan, D. Ye and H. Liu, "Design of transcutaneous energy transmission system for artificial anal sphincter," in *International Conference on Mechatronics and Automation, ICMA 2007*, 2007, pp. 1434-1438.
- [57] A. Ghahary and B.H. Cho, "Design of transcutaneous energy transmission system using a series resonant converter," *IEEE Transactions on Power Electronics*, vol. 7, no. 2, pp. 261-269, 1992.
- [58] H.H. Wu, A.P. Hu, P. Si, D. Budgett, C. Tung and S. Malpas, "A push-pull resonant converter with dual coils for Transcutaneous Energy Transfer systems," in *4th IEEE Conference on Industrial Electronics and Applications, ICIEA 2009*, 2009, pp. 1051-1056.
- [59] T.D. Dissanayake, D. Budgett, H. Patrick and S. Malpas, "Experimental thermal study of a TET system for implantable biomedical devices," in *IEEE Biomedical Circuits and Systems Conference, BioCAS 2008*, 2008, pp. 113-116.

- [60] H.H. Wu, A.P. Hu, S.C. Malpas and D.M. Budgett, "Determining optimal tuning capacitor values of TET system for achieving maximum power transfer," *IEEE Electronics Letters*, vol. 45, no. 9, pp. 448-449, 2009.
- [61] T. RESEARCH. *Biomedical data acquisition sensor*. 2010 [cited 2009 September 12]; Available from: [http://www.telemetryresearch.com/index.php?option=com\\_content&task=view&id=39&Itemid=164](http://www.telemetryresearch.com/index.php?option=com_content&task=view&id=39&Itemid=164).
- [62] A.W. Kelley and W.R. Owens, "Connectorless power supply for an aircraft-passenger entertainment system," *IEEE Transactions on Power Electronics*, vol. 4, no. 3, pp. 348-354, 1989.
- [63] J. Gao, "Inductive power transmission for untethered micro-robots," in *31st Annual IEEE Conference of Industrial Electronics Society, IECON 2005*, 2005, pp. 6.
- [64] K.W. Klontz, D.M. Divan, D.W. Novotny and R.D. Lorenz, "Contactless power delivery system for mining applications," *IEEE Transactions on Industry Applications*, vol. 31, no. 1, pp. 27-35, 1995.
- [65] J. Murakami, F. Sato, T. Watanabe, H. Matsuki, S. Kikuchi, K. Harakawa and T. Satoh, "Consideration on cordless power station-contactless power transmission system," *IEEE Transactions on Magnetics*, vol. 32, no. 5, pp. 5037-5039, 1996.
- [66] P. Si, "Wireless Power Supply for Implantable Biomedical Devices," PhD thesis, the Department of Electrical and Computer Engineering, University of Auckland, Auckland, 2008.
- [67] I.L.K. Kwan, "Battery-less Wireless Computer Mouse," Master thesis, the Department of Electrical and Computer Engineering, University of Auckland, Auckland, 2004.
- [68] A.P. Hu and S. Hussmann, "Improved power flow control for contactless moving sensor applications," *IEEE Power Electronics Letters*, vol. 2, no. 4, pp. 135-138, 2004.
- [69] Y.-H. Chao, J.-J. Shieh, C.-T. Pan, W.-C. Shen and M.-P. Chen, "A primary-side control strategy for series-parallel loosely coupled inductive power transfer systems," in *2nd IEEE Conference on Industrial Electronics and Applications, ICIEA 2007*, 2007, pp. 2322-2327.
- [70] A.W. Green and J.T. Boys, "10 kHz inductively coupled power transfer-concept and control," in *5th International Conference on Power Electronics and Variable-Speed Drives*, 1994, pp. 694-699.
- [71] J. James, J. Boys and G. Covic, "A variable inductor based tuning method for ICPT pickups," in *7th International Power Engineering Conference, IPEC 2005*, 2005, pp. 1142-1146.

- [72] P. Si, A.P. Hu, J.W. Hsu, M. Chiang, Y. Wang, S. Malpas and D. Budgett, "Wireless power supply for implantable biomedical device based on primary input voltage regulation," in *2nd IEEE Conference on Industrial Electronics and Applications, ICIEA 2007*, 2007, pp. 235-239.
- [73] J.T. Boys, G.A.J. Elliott and G.A. Covic, "An appropriate magnetic coupling coefficient for the design and comparison of ICPT pickups," *IEEE Transactions on Power Electronics*, vol. 22, no. 1, pp. 333-335, 2007.
- [74] B. Choi, J. Nho, H. Cha, T. Ahn and S. Choi, "Design and implementation of low-profile contactless battery charger using planar printed circuit board windings as energy transfer device," *IEEE Transactions on Industrial Electronics*, vol. 51, no. 1, pp. 140-147, 2004.
- [75] O.H. Stielau and G.A. Covic, "Design of loosely coupled inductive power transfer systems," in *Proceedings of International Conference on Power System Technology, PowerCon 2000*, 2000, pp. 85-90.
- [76] W. Zhou and H. Ma, "Steady-state analysis of the inductively coupled power transfer system," in *32nd Annual IEEE Conference of Industrial Electronics, IECON 2006*, 2006, pp. 2438-2443.
- [77] J.T. Boys, G.A. Covic and Y. Xu, "DC analysis technique for inductive power transfer pick-ups," *IEEE Power Electronics Letters*, vol. 1, no. 2, pp. 51-53, 2003.
- [78] C.-S. Wang, G.A. Covic and O.H. Stielau, "Power transfer capability and bifurcation phenomena of loosely coupled inductive power transfer systems," *IEEE Transactions on Industrial Electronics*, vol. 51, no. 1, pp. 148-157, 2004.
- [79] S. Raabe, J.T. Boys and G.A. Covic, "A high power coaxial inductive power transfer pickup," in *IEEE Power Electronics Specialists Conference, PESC 2008*, 2008, pp. 4320-4325.
- [80] S. Raabe, G.A.J. Elliott, G.A. Covic and J.T. Boys, "A quadrature pickup for inductive power transfer systems," in *2nd IEEE Conference on Industrial Electronics and Applications, ICIEA 2007*, 2007, pp. 68-73.
- [81] H. Chen, A.P. Hu and D. Budgett, "Power loss analysis of a TET system for high power implantable devices," in *2nd IEEE Conference on Industrial Electronics and Applications, ICIEA 2007*, 2007, pp. 240-245.
- [82] S.-J. Chen and H.-C. Chang, "Analysis and implementation of low-side active clamp forward converters with synchronous rectification," in *33rd Annual IEEE Conference of Industrial Electronics Society, IECON 2007*, 2007, pp. 1506-1511.
- [83] H.K. Ji and H.J. Kim, "Active clamp forward converter with MOSFET synchronous rectification," in *25th Annual IEEE Power Electronics Specialists Conference, PESC '94*, 1994, pp. 895-901.

- [84] Y. Liu, Y. Jiang and G.C. Hua, "A self-driven synchronous rectification scheme for low output switching-mode converter," in *4th International Power Electronics and Motion Control Conference, IPEMC 2004*, 2004, pp. 1166-1169.
- [85] A. Fernandez, J. Sebastian, M.M. Hernando, P. Villegas and D.G. Lamar, "Using synchronous rectification for medium voltage applications," in *35th Annual IEEE Power Electronics Specialists Conference, PESC 04*, 2004, pp. 1487-1493.
- [86] W. Zhou and H. Ma, "Design considerations of compensation topologies in ICPT system," in *22nd Annual IEEE Applied Power Electronics Conference, APEC 2007*, 2007, pp. 985-990.
- [87] C.-S. Wang, O.H. Stielau and G.A. Covic, "Load models and their application in the design of loosely coupled inductive power transfer systems," in *Proceedings of International Conference on Power System Technology, PowerCon 2000*, 2000, pp. 1053-1058.
- [88] P. Si, A.P. Hu, S. Malpas and D. Budgett, "A frequency control method for regulating wireless power to implantable devices," *IEEE Transactions on Biomedical Circuits and Systems*, vol. 2, no. 1, pp. 22-29, 2008.
- [89] S.-H. Chiang, "'A Combined Wireless Power and Signal Transfer System for Biomedical Implants'," Report, the Department of Electrical and Computer Engineering, University of Auckland, 2006.
- [90] Y.X. Xu, J.T. Boys and G.A. Covic, "Modeling and controller design of ICPT pick-ups," in *Proceedings of International Conference on Power System Technology, PowerCon 2002*, 2002, pp. 1602-1606.
- [91] J.T. Boys, G.A. Covic and A.W. Green, "Stability and control of inductively coupled power transfer systems," *IEE Proceedings of Electric Power Applications*, vol. 147, no. 1, pp. 37-43, 2000.
- [92] N.A. Keeling, J.T. Boys and G.A. Covic, "Unity power factor inductive power transfer pick-up for high power applications," in *34th Annual IEEE Conference of Industrial Electronics, IECON 2008*, 2008, pp. 1039-1044.
- [93] S. Hussmann and P.A. Hu, "A microcomputer controlled ICPT power pick-up and its EMC considerations for moving sensor applications," in *Proceedings of International Conference on Power System Technology, PowerCon 2002*, 2002, pp. 1011-1015.
- [94] M. Eghtesadi, "Inductive power transfer to an electric vehicle-analytical model," in *40th IEEE Vehicular Technology Conference*, 1990, pp. 100-104.
- [95] P. Si, A.P. Hu, S. Malpas and D. Budgett, "Switching frequency analysis of dynamically detuned ICPT power pick-ups," in *International Conference on Power System Technology, PowerCon 2006*, 2006, pp. 1-8.

- [96] P. Sen, P. Biringer and R. Segsworth, "Thyristor-controlled single phase variable inductor," *IEEE Transactions on Magnetics*, vol. 3, no. 3, pp. 240-245, 1967.
- [97] A. Ghosh and D. Chatterjee, "Transient stability assessment of power systems containing series and shunt compensators," *IEEE Transactions on Power Systems*, vol. 22, no. 3, pp. 1210-1220, 2007.
- [98] C.C. Marouchos: *The Switching Function - Analysis of Power Electronic Circuits*, The Institution of Engineering and Technology, 1st edition, 2006.
- [99] *Basic Electricity*, Research & Education Association, 1st edition, 2004.
- [100] K.M. Smith, Jr. and K.M. Smedley, "Intelligent magnetic-amplifier-controlled soft-switching method for amplifiers and inverters," *IEEE Transactions on Power Electronics*, vol. 13, no. 1, pp. 84-92, 1998.
- [101] M. Brkovic and S. Cuk, "A novel single stage AC-to-DC full-bridge converter with magnetic amplifiers for input current shaping," in *26th Annual IEEE Power Electronics Specialists Conference, PESC '95*, 1995, pp. 990-995.
- [102] T. Koyashiki and S. Ohzora, "Control characteristics in a magnetic-amplifier-controlled DC-DC converter," in *19th Annual IEEE Power Electronics Specialists Conference, PESC '88*, 1988, pp. 390-397.
- [103] M.C. Caponet, F. Profumo and A. Tenconi, "Cost effective saturable inductor for zero voltage switching-zero current switching DC/DC power conditioning converter for fuel cells," in *38th Annual Conference of Industry Applications, IAS 2003*, 2003, pp. 1576-1581.
- [104] N. Barry and B. Daly, "Coupled magnetic amplifiers in forward converter topologies," *IEEE Transactions on Power Electronics*, vol. 14, no. 1, pp. 168-176, 1999.
- [105] V. Yaskiv, "Using of high-frequency magnetic amplifier in switch mode DC power supplies," in *35th Annual IEEE Power Electronics Specialists Conference, PESC 04*, 2004, pp. 1658-1662.
- [106] I.C. Chan, G.A. Covic and J.T. Boys, "Regulator capacitor selection for series compensated IPT pickups," in *34th Annual IEEE Conference of Industrial Electronics, IECON 2008*, 2008, pp. 932-937.
- [107] A.K. Swain, "A simple fuzzy controller for single area hydro power system considering generation rate constraints," *Institution of Engineers India Part el Electrical Engineering Division*, vol. 87, no. 1, pp. 12-17, 2006.
- [108] Y. Ding, H. Ying and S. Shao, "A fuzzy system for real-time control of tissue temperature during laser heating," in *Conference of the North American of Fuzzy Information Processing Society - NAFIPS*, 1998, pp. 5-9.

- [109] H. Ying, W. Siler and J.J. Buckley, "Fuzzy control theory: A nonlinear case," *Automatica*, vol. 26, no. 3, pp. 513-520, 1990.
- [110] A. Botta, B. Lazzerini and F. Marcelloni, "Context adaptation of Mamdani fuzzy systems through new operators tuned by a genetic algorithm," in *IEEE International Conference on Fuzzy Systems*, 2006, pp. 1641-1648.
- [111] K. Belarbi, F. Titel, W. Bourebia and K. Benmahammed, "Design of Mamdani fuzzy logic controllers with rule base minimisation using genetic algorithm," *Engineering Applications of Artificial Intelligence*, vol. 18, no. 7, pp. 875-880, 2005.
- [112] L. Chen, Y. Xu, Y.-F. Liu and R. Jin, "Small-signal analysis and simulation of fuzzy controlled buck converter," in *4th IEEE Conference on Industrial Electronics and Applications, ICIEA 2009*, 2009, pp. 816-820.
- [113] Y. Chai, L. Jia and Z. Zhang, "Mamdani model based adaptive neural fuzzy inference system and its application in traffic level of service evaluation," in *6th International Conference on Fuzzy Systems and Knowledge Discovery, FSKD '09*, 2009, pp. 555-559.
- [114] H. Ying, "Constructing nonlinear variable gain controllers via the Takagi-Sugeno fuzzy control," *IEEE Transactions on Fuzzy Systems*, vol. 6, no. 2, pp. 226-234, 1998.
- [115] H. Ying, "The simplest fuzzy controllers using different inference methods are different nonlinear proportional-integral controllers with variable gains," *Automatica*, vol. 29, no. 6, pp. 1579-1589, 1993.
- [116] P. Si and A.P. Hu, "Analyses of DC inductance used in ICPT power pick-ups for maximum power transfer," in *IEEE/PES Transmission and Distribution Conference and Exhibition: Asia and Pacific*, 2005, pp. 1-6.
- [117] D. Chattopadhyay and P.C. Rakshit: *Electronics - Fundamentals and Applications*, New Age International (P) Ltd., 7th edition, 2006.
- [118] J.-U.W. Hsu, A.P. Hu and A. Swain, "A wireless power pickup based on directional tuning control of magnetic amplifier," *IEEE Transactions on Industrial Electronics*, vol. 56, no. 7, pp. 2771-2781, 2009.
- [119] J.-U.W. Hsu, A.P. Hu, A. Swain, D. Xin and S. Yue, "A new contactless power pick-up with continuous variable inductor control using magnetic amplifier," in *International Conference on Power System Technology, PowerCon 2006*, 2006, pp. 1-8.
- [120] J.U. Hsu, A.P. Hu, P. Si and A. Swain, "Power flow control of a 3-D wireless power pick-up," in *2nd IEEE Conference on Industrial Electronics and Applications, ICIEA 2007*, 2007, pp. 2172-2177.

## References

---

- [121] J.U.W. Hsu and A.P. Hu, "Determining the variable inductance range for an LCL wireless power pick-up," in *IEEE Conference on Electron Devices and Solid-State Circuits, EDSSC 2007*, 2007, pp. 489-492.
- [122] J.U.W. Hsu, A.P. Hu and A. Swain, "Fuzzy based directional tuning controller for a wireless power pick-up," in *IEEE Region 10 Conference, TENCON 2008*, 2008, pp. 1-6.
- [123] J.U. Hsu, A.P. Hu and A. Swain, "Directional tuning control of wireless/contactless power pickup for inductive power transfer (IPT) system," in *Advances in Solid State Circuits Technologies, INTECH*, 2010, pp. 221-238.
- [124] J.-U.W. Hsu, A.P. Hu and A. Swain, "Fuzzy logic based directional tuning control for LC power pickup of inductive power transfer system," *IEEE Transactions on Industrial Electronics*, Nov 2009.





# Bibliographies

---

- [1] C.K. Alexander and M.N.O. Sadiku: *Fundamentals of Electric Circuits*, The McGraw-Hill Companies, Inc., 2nd edition, 2004.
- [2] S. Ang and A. Oliva: *Power-Switching Converters*, Taylor & Francis Group, 2nd edition, 2005.
- [3] M. Attenborough: *Engineering Mathematics*, McGRAW-HILL Book Company Europe, 1st edition, 1994.
- [4] L. Austrin, D. Ribbenfjard and G. Engdahl, "Simulation of a magnetic amplifier circuit including hysteresis," *IEEE Transactions on Magnetics*, vol. 41, no. 10, pp. 3994-3996, 2005.
- [5] J.M. Barnard, J.A. Ferreira and J.D. van Wyk, "Optimized linear contactless power transmission systems for different applications," in *Proceedings of 12th Annual Conference on Applied Power Electronics Conference and Exposition, APEC'97*, 1997, pp. 953-959.
- [6] T. Bieler, M. Perrottet, V. Nguyen and Y. Perriard, "Contactless power and information transmission," *IEEE Transactions on Industry Applications*, vol. 38, no. 5, pp. 1266-1272, 2002.
- [7] M. Borage, S. Tiwari and S. Kotaiah, "Analysis and design of an LCL-T resonant converter as a constant-current power supply," *IEEE Transactions on Industrial Electronics*, vol. 52, no. 6, pp. 1547-1554, 2005.
- [8] J.T. Boys, C.I. Chen and G.A. Covic, "Controlling inrush currents in inductively coupled power systems," in *7th International Power Engineering Conference, IPEC 2005*, 2005, pp. 1046-1051.
- [9] J.T. Boys, G.A. Covic and G.A.J. Elliott, "Pick-up transformer for ICPT applications," *IEE Electronics Letters*, vol. 38, no. 21, pp. 1276-1278, 2003.
- [10] J.T. Boys, A.P. Hu and G.A. Covic, "Critical Q analysis of a current-fed resonant converter for ICPT applications," *IEE Electronics Letters*, vol. 36, no. 17, pp. 1440-1442, 2000.
- [11] J.T. Boys, C.Y. Huang and G.A. Covic, "Single-phase unity power-factor inductive power transfer system," in *IEEE Power Electronics Specialists Conference, PESC 2008*, 2008, pp. 3701-3706.
- [12] M. Brkovic, A. Pietkiewicz and S. Cuk, "Novel soft-switching converter with magnetic amplifiers," in *Proceedings of International Conference on Industrial Electronics, Control, and Instrumentation, IECON '93*, 1993, pp. 830-835.

- [13] J. Buckley and H. Ying, "Linear fuzzy controller: It is a linear nonfuzzy controller," *Information Sciences*, vol. 51, no. 2, pp. 183-192, 1990.
- [14] D. Chattopadhyay and P.C. Rakshit: *Electronics - Fundamentals and Applications*, New Age International (P) Ltd., 7th edition, 2006.
- [15] R.W.-J. Chen, "Improvement of a dSPACE Platform for Power Electronics Control," Summer Research Report, the Department of Electrical and Computer Engineering, University of Auckland, Auckland, 2005.
- [16] S.-H. Chiang, "'A Combined Wireless Power and Signal Transfer System for Biomedical Implants'," Report, the Department of Electrical and Computer Engineering, University of Auckland, 2006.
- [17] G.A. Covic, J.T. Boys, M.L.G. Kissin and H.G. Lu, "A three-phase inductive power transfer system for roadway-powered vehicles," *IEEE Transactions on Industrial Electronics*, vol. 54, no. 6, pp. 3370-3378, 2007.
- [18] G.A. Covic, J.T. Boys, A.M.W. Tam and J.C.H. Peng, "Self tuning pick-ups for inductive power transfer," in *IEEE Power Electronics Specialists Conference, PESC 2008*, 2008, pp. 3489-3494.
- [19] *dSPACE: Real-Time Interface (RTI and RTI-MP) Implementation Guide*, dSPACE Gmgh, 1st edition, 2009.
- [20] M.G. Egan, D.L. O'Sullivan, J.G. Hayes, M.J. Willers and C.P. Henze, "Power-factor-corrected single-stage inductive charger for electric vehicle batteries," *IEEE Transactions on Industrial Electronics*, vol. 54, no. 2, pp. 1217-1226, 2007.
- [21] L. Egiziano, A. Giustiniani, G. Lisi, G. Petrone, G. Spagnuolo and M. Vitelli, "Experimental characterization of the photovoltaic generator for a hybrid solar vehicle," in *IEEE International Symposium on Industrial Electronics, ISIE 2007*, 2007, pp. 329-334.
- [22] G.A.J. Elliott, J.T. Boys and A.W. Green, "Magnetically coupled systems for power transfer to electric vehicles," in *Proceedings of International Conference on Power Electronics and Drive Systems*, 1995, pp. 797-801.
- [23] R. Esmaili, L. Xu and D.K. Nichols, "A new control method of permanent magnet generator for maximum power tracking in wind turbine application," in *IEEE Power Engineering Society General Meeting*, 2005, pp. 2090-2095.
- [24] C. Fernandez, O. Garcia, R. Prieto, J.A. Cobos and J. Uceda, "Overview of different alternatives for the contact-less transmission of energy," in *28th Annual IEEE Conference of Industrial Electronics Society, IECON 02*, 2002, pp. 1318-1323 vol.2.
- [25] G.F. Franklin and J.D. Powell: *Digital Control of Dynamic Systems*, Addison-Wesley Publishing Company, Inc., 1st edition, 1980.

- [26] D.D. Gajski: *Principles of Digital Design*, Prentice-Hall, Inc., International edition, 1997.
- [27] W. Gao and N.M. Sammes: *An Introduction to Electronic and Ionic Materials*, World Scientific Publishing Co. Pte. Ltd., 1st edition, 1999.
- [28] F.M. Gardner: *Phaselock Techniques*, John Wiley & Sons, Inc., 2nd edition, 1979.
- [29] K. Harada and T. Nabeshima, "Applications of magnetic amplifiers to high-frequency DC-to-DC converters," *IEEE Proceedings*, vol. 76, no. 4, pp. 355-361, 1988.
- [30] T. Hiyama, S. Kouzuma and T. Imakubo, "Identification of optimal operating point of PV modules using neural network for real time maximum power tracking control," *IEEE Transactions on Energy Conversion*, vol. 10, no. 2, pp. 360-367, 1995.
- [31] T. Hiyama, S. Kouzuma, T. Imakubo and T.H. Ortmeyer, "Evaluation of neural network based real time maximum power tracking controller for PV system," *IEEE Transactions on Energy Conversion*, vol. 10, no. 3, pp. 543-548, 1995.
- [32] P. Horowitz and W. Hill: *The Art of Electronics*, Cambridge University Press, 2nd edition, 1989.
- [33] C. Hua and C. Shen, "Comparative study of peak power tracking techniques for solar storage system," in *Proceedings of 13th Annual Applied Power Electronics Conference and Exposition, APEC '98*, 1998, pp. 679-685.
- [34] C. Hua and C. Shen, "Study of maximum power tracking techniques and control of DC/DC converters for photovoltaic power system," in *29th Annual IEEE Power Electronics Specialists Conference, PESC 98*, 1998, pp. 86-93.
- [35] O. Ichinokura, T. Jinzenji and K. Tajima, "A new variable inductor for VAR compensation," *IEEE Transactions on Magnetics*, vol. 29, no. 6, pp. 3225-3227, 1993.
- [36] D.K. Jackson, S.B. Leeb and S.R. Shaw, "Adaptive control of an inductive power transfer coupling for servomechanical systems," in *30th Annual IEEE Power Electronics Specialists Conference, PESC 99*, 1999, pp. 1191-1198.
- [37] D.K. Jackson, A.M. Schultz, S.B. Leeb, A.H. Mitwalli, G.C. Verghese and S.R. Shaw, "A multirate digital controller for a 1.5-kW electric vehicle battery charger," *IEEE Transactions on Power Electronics*, vol. 12, no. 6, pp. 1000-1006, 1997.
- [38] S.K. Jain and R. Sharma, "Potential of multichannel implanted underskin biotelemetry transmitter systems," in *Proceedings of 14th IEEE International Conference of Biomedical Engineering Society of India*, 1995, pp. 4/119-4/120.
- [39] C.S. John, "Powering an artificial heart: birth of the inductively coupled-radio frequency system in 1960," *Artificial Organs*, vol. 26, no. 11, pp. 909-915, 2002.

- [40] D.W. Jordan and P. Smith: *Mathematical Techniques*, Oxford University Press Inc., 2nd edition, 1997.
- [41] D. Kacprzak, G.A. Covic and J.T. Boys, "An improved magnetic design for inductively coupled power transfer system pickups," in *7th International Power Engineering Conference, IPEC 2005*, 2005, pp. 1133-1136.
- [42] S.T. Karris: *Introduction to Simulink with Engineering Applications*, Orchard Publications, 2nd edition, 2008.
- [43] C.-G. Kim, D.-H. Seo, J.-S. You, J.-H. Park and B.H. Cho, "Design of a contactless battery charger for cellular phone," *IEEE Transactions on Industrial Electronics*, vol. 48, no. 6, pp. 1238-1247, 2001.
- [44] M.L.G. Kissin, J.T. Boys and G.A. Covic, "Interphase mutual inductance in polyphase inductive power transfer systems," *IEEE Transactions on Industrial Electronics*, vol. 56, no. 7, pp. 2393-2400, 2009.
- [45] T. Koyashiki and S. Ohzora, "Control characteristics in a magnetic-amplifier-controlled DC-DC converter," in *19th Annual IEEE Power Electronics Specialists Conference, PESC '88*, 1988, pp. 390-397.
- [46] N.H. Kutkut, "A full bridge LCL resonant battery charger for an EV conductive coupler," in *29th Annual IEEE Power Electronics Specialists Conference, PESC 98*, 1998, pp. 2069-2075.
- [47] J. Lastowiecki and P. Staszewski, "Sliding transformer with long magnetic circuit for contactless electrical energy delivery to mobile receivers," *IEEE Transactions on Industrial Electronics*, vol. 53, no. 6, pp. 1943-1948, 2006.
- [48] I.J. Lee, D.Y. Chen, Y.P. Wu and C. Jamerson, "Modeling of control loop behavior of magamp post regulators," *IEEE Transactions on Power Electronics*, vol. 5, no. 4, pp. 476-484, 1990.
- [49] H.L. Li, A.P. Hu and G.A. Covic, "FPGA controlled high frequency resonant converter for contactless power transfer," in *IEEE Power Electronics Specialists Conference, PESC 2008*, 2008, pp. 3642-3647.
- [50] H.L. Li, A.P. Hu, G.A. Covic and C.S. Tang, "A new primary power regulation method for contactless power transfer," in *IEEE International Conference on Industrial Technology, ICIT 2009*, 2009, pp. 1-5.
- [51] U.K. Madawala, J. Stichbury and S. Walker, "Contactless power transfer with two-way communication," in *30th Annual IEEE Conference of Industrial Electronics Society, IECON 2004*, 2004, pp. 3071-3075.
- [52] U.K. Madawala, D. Thrimawithana and N. Kularathna, "An ICPT-supercapacitor technology for contactless power transfer with surge suppression," in *31st Annual IEEE Conference of Industrial Electronics Society, IECON 2005*, 2005, pp. 6.

- [53] H.M. Mashaly, A.M. Sharaf, M. Mansour and A.A. El-Sattar, "A photovoltaic maximum power tracking using neural networks," in *Proceedings of 3rd IEEE Conference on Control Applications*, 1994, pp. 167-172.
- [54] D. Medini and S. Ben-Yaakov, "A current-controlled variable-inductor for high frequency resonant power circuits," in *Conference Proceedings of 9th Annual IEEE Applied Power Electronics Conference and Exposition, APEC '94*, 1994, pp. 219-225.
- [55] H. Miura, S. Arai, F. Sato, H. Matsuki and T. Sato, "A synchronous rectification using a digital PLL technique for contactless power supplies," *IEEE Transactions on Magnetics*, vol. 41, no. 10, pp. 3997-3999, 2005.
- [56] N. Mohan, T.M. Undeland and W.P. Robbins: *Power Electronics*, John Wiley & Sons, Inc., 3rd edition, 2003.
- [57] I.J. Nagrath and M. Gopal: *Control Systems Engineering*, John Wiley & Sons, Inc., 2nd edition, 1982.
- [58] N.S. Nise: *Control Systems Engineering*, John Wiley & Sons, Inc., 3rd edition, 2000.
- [59] K. O'Brien, R. Teichmann and H. Gueldner, "Magnetic field generation in an inductively coupled radio-frequency power transmission system," in *37th IEEE Power Electronics Specialists Conference, PESC '06*, 2006, pp. 1-7.
- [60] O.I. Okoro and E. Chikuni: *The Essential MATLAB & Simulink for Engineers and Scientists*, Juta and Company Ltd, 1st edition, 2010.
- [61] A. Okuno, L. Gamage and M. Nakaoka, "Performance evaluations of high-frequency inverter-linked DC/DC converter with noncontact pickup coil," *IEEE Transactions on Industrial Electronics*, vol. 48, no. 2, pp. 475-477, 2001.
- [62] C.L. Phillips and H.T. Nagle: *Digital Control System - Analysis and Design*, Prentice-Hall, Inc., 2nd edition, 1989.
- [63] J.I. Rodriguez, D.K. Jackson and S.B. Leeb, "Capability analysis for an inductively coupled power transfer system," in *7th Workshop on Computers in Power Electronics, COMPEL 2000*, 2000, pp. 59-63.
- [64] J.I. Rodriguez and S.B. Leeb, "A multilevel inverter topology for inductively coupled power transfer," *IEEE Transactions on Power Electronics*, vol. 21, no. 6, pp. 1607-1617, 2006.
- [65] H. Sakamoto and S. Washimiya, "Magnetic coupled power and data transferring system with a detachable transformer," *IEEE Transactions on Magnetics*, vol. 32, no. 5, pp. 4983-4985, 1996.
- [66] A.S. Sedra and K.C. Smith: *Microelectronic Circuits*, Oxford University Press, Inc., 5th edition, 2004.

- [67] W. Siler and H. Ying, "Fuzzy control theory: The linear case," *Fuzzy Sets and Systems*, vol. 33, no. 3, pp. 275-290, 1989.
- [68] P. Silvester: *Modern Electromagnetic Fields*, Prentice-Hall, Inc., 1st edition, 1968.
- [69] K.M. Smith, Jr. and K.M. Smedley, "Intelligent magnetic-amplifier-controlled soft-switching method for amplifiers and inverters," *IEEE Transactions on Power Electronics*, vol. 13, no. 1, pp. 84-92, 1998.
- [70] H. Sugimoto and H. Dong, "A new scheme for maximum photovoltaic power tracking control," in *Proceedings of Power Conversion Conference - Nagaoka 1997*, 1997, pp. 691-696.
- [71] V.J. Thottuvelil, "Using SPICE to model the dynamic behavior of DC-to-DC converters employing magnetic amplifiers," in *Conference Proceedings of 5th Annual IEEE Applied Power Electronics Conference and Exposition, APEC '90*, 1990, pp. 750-759.
- [72] F.T. Ulaby: *Fundamentals of Applied Electromagnetics*, Pearson Education, Inc., Media edition, 2004.
- [73] E.L. Van Boheemen, J.T. Boys and G.A. Covic, "Dual-tuning IPT systems for low bandwidth communications," in *2nd IEEE Conference on Industrial Electronics and Applications, ICIEA 2007*, 2007, pp. 586-591.
- [74] K. Van Schuylenbergh and R. Puers, "Self tuning inductive powering for implantable telemetric monitoring systems," in *8th International Conference on Solid-State Sensors and Actuators*, 1995, pp. 55-58.
- [75] C.-S. Wang, G.A. Covic and O.H. Stielau, "Investigating an LCL load resonant inverter for inductive power transfer applications," *IEEE Transactions on Power Electronics*, vol. 19, no. 4, pp. 995-1002, 2004.
- [76] C.-S. Wang, O.H. Stielau and G.A. Covic, "Design considerations for a contactless electric vehicle battery charger," *IEEE Transactions on Industrial Electronics*, vol. 52, no. 5, pp. 1308-1314, 2005.
- [77] G. Wang, W. Liu, R. Bashirullah, M. Sivaprakasam, G.A. Kendir, Y. Ji, M.S. Humayun and J.D. Weiland, "A closed loop transcutaneous power transfer system for implantable devices with enhanced stability," in *Proceedings of 2004 International Symposium on Circuits and Systems, ISCAS '04*, 2004, pp. 17-20.
- [78] Y. Wu, L. Yan and S. Xu, "A new contactless power delivery system," in *6th International Conference on Electrical Machines and Systems, ICEMS 2003*, 2003, pp. 253-256.
- [79] W. Xiao, M.G.J. Lind, W.G. Dunford and A. Capel, "Real-time identification of optimal operating points in photovoltaic power systems," *IEEE Transactions on Industrial Electronics*, vol. 53, no. 4, pp. 1017-1026, 2006.

- [80] V. Yaskiv, "Using of high-frequency magnetic amplifier in switch mode DC power supplies," in *35th Annual IEEE Power Electronics Specialists Conference, PESC 04*, 2004, pp. 1658-1662.
- [81] H. Ying, "A nonlinear fuzzy controller with linear control rules is the sum of a global two-dimensional multilevel relay and a local nonlinear proportional-integral controller," *Automatica*, vol. 29, no. 2, pp. 499-505, 1993.
- [82] H. Ying, "Analytical structure of a two-input two-output fuzzy controller and its relation to PI and multilevel relay controllers," *Fuzzy Sets and Systems*, vol. 63, no. 1, pp. 21-33, 1994.
- [83] W. Zhou and H. Ma, "Dynamic analysis of a current source inductively coupled power transfer system," in *CES/IEEE 5th International Power Electronics and Motion Control Conference, IPEMC 2006*, 2006, pp. 1-5.





# Appendices

---

## Embedded Matlab Functions of SSSA-DTDCa and FLB-DTDCa Simulations

```
%-----%
```

```
function NxtS = fcn(Vo, Vprev, Vref, PrevS)
% This block supports an embeddable subset of the MATLAB language.
% See the help menu for details.

%This program is used to determine the tuning direction signal according
%to equation 3-3.

    if Vo > Vref
        S1 = 1;
    else
        S1 = 0;
    end

    if Vo > Vprev
        S2 = 1;
    else
        S2 = 0;
    end

    NxtS = or(and(PrevS, xor(S1, S2)), and(~PrevS, ~xor(S1, S2))); %S4
```

```
%-----%
```

```
function S7 = fcn(Vo, Vprev, Vref, Vpprev)
% This block supports an embeddable subset of the MATLAB language.
% See the help menu for details.

%This program is used to generate signal for determining whether the
%pickup should be coarse-tuned or fine-tuned according to equation
%3-6.
```

```
    if Vo > Vref
        S1 = 1;
    else
        S1 = 0;
    end

    if Vo > Vpprev
        S2 = 1;
    else
        S2 = 0;
    end
```

```

    if Vprev > Vref
        S5 = 1;
    else
        S5 = 0;
    end

    if Vpprev > Vref
        S6 = 1;
    else
        S6 = 0;
    End

    S7 = or(or(and(S5, and(S1, S2)), and(~S5, and(~S1, ~S2))),
            or(and(S6, and(S1, S5)), and(~S6, and(~S1, ~S5))));

%-----%

function h = fcn(S7, hprev, Vo)
% This block supports an embeddable subset of the MATLAB language.
% See the help menu for details.

%This program is used to determine tuning step-size of the DTDCA using
%Simple Step-Size Adjustment (SSSA) according to equation 3-5.

    hm = 7.01e-6;
    beta = 0.1;
    h = hprev;

    if S7 == 1 && Vo < 5.1 && Vo > 4.9
        h = 0;
    elseif S7 == 0 && Vo < 5.1 && Vo > 4.9
        h = 0;
    elseif S7 == 1
        h = hm;
    elseif S7 == 0
        h = hprev-beta*hm;
    end

%-----%

function h = fcn(err, errprev)
% This block supports an embeddable subset of the MATLAB language.
% See the help menu for details.

%This program is used to determine tuning step-size for the DTDCA using
%Fuzzy Logic Control Algorithm.

    GE = 0.6;                %Scaling factor for error
    GR = 0.37;               %Scaling factor for rate of error
    SG = 4e-6;               %Scaling factor for output signal
    L = 1;                   %Interval L
    H = 1;                   %Interval H
    e = GE*err;              %Error
    r = GR*(err - errprev);  %Rate of error

    %Fuzzification (L can be changed, depends on the design)
    %-----Membership Functions for error-----%

```

```

if e>=0
    ep = e/L;
    epz = (L-e)/L;
    enz = 0;
    en = 0;
    if e>L
        ep = 1;
        epz = 0;
    end
else
    en = ((-1)*e)/L;
    enz = (L+e)/L;
    epz = 0;
    ep = 0;
    if e<(-1)*L
        en = 1;
        enz = 0;
    end
end
end
%-----Membership Functions for rate of error-----%
if r>=0
    rp = r/L;
    rpz = (L-r)/L;
    rnz = 0;
    rn = 0;
    if r>L
        rp = 1;
        rpz = 0;
    end
else
    rn = ((-1)*r)/L;
    rnz = (L+r)/L;
    rpz = 0;
    rp = 0;
    if r<(-1)*L
        rn = 1;
        rnz = 0;
    end
end
end
%-----End of Membership Functions-----%

%-----Control Rule Base-----%
ur1 = min(ep, rp);           %Rule 1
ur2 = min(ep, rpz);         %Rule 2
ur3 = min(ep, rnz);         %Rule 3
ur4 = min(ep, rn);          %Rule 4
ur5 = min(en, rp);          %Rule 5
ur6 = min(en, rpz);         %Rule 6
ur7 = min(en, rnz);         %Rule 7
ur8 = min(en, rn);          %Rule 8
ur9 = min(1, epz+enz);      %Rule 9
%-----End of Control Rule Base-----%

%-----Defuzification-----%
ol = min(1, ur2+ur3+ur6+ur7);
om = min(1, ur4+ur5);
oz = min(1, ur1+ur8+ur9);

Sol = ol*(2-ol)*H;

```

```
Som = om*(2-om)*H;
Soz = oz*(2-oz)*H;

%Centroid Defuzzification
o = ((Sol*H)+(Som*0.5*H)+(Soz*0))/(Sol+Som+Soz);
h = SG*o;
%-----End of Defuzification-----%
%-----%

function CS = fcn(NxtS, h, CSprev)
% This block supports an embeddable subset of the MATLAB language.
% See the help menu for details.

%This program is used to determine the final output signal of the DTDCA
%using either Simple Step-Size Adjustment or Fuzzy Logic Control.

SS = NxtS*1;
CS = CSprev + h*(-1)^(SS+1);

%-----%
```